UNIVERSITÀ
DEGLI STUDI
FIRENZE

Dottorato di Ricerca in Fisica e Astronomia
Ciclo XXVII

Control of optical propagation in atomic and diffusive media

Settore Scientifico Disciplinare FIS/03

Dottorando
Tommasi Federico

Tutore
Prof. Cavalieri Stefano

Coordinatore
Prof. Livi Roberto

Anni 2012/2014

Contents

Introduction

The present thesis work has been devoted to the experimental investigation, supported by the development of theoretical and numerical models, on the propagation of light in atomic media and diffusive materials.

In the last three decades, an increasing interest in physics of optical signal propagation has been observed and insights about the light-matter interactions have lead to the development of different experimental schemes, with the the aim to tailor the properties of material systems in order to achieve a desired optical response. Large variations in group velocity can be achieved by exploring the spectral regions where the slope of the dispersion curve abruptly changes, since the group velocity depends on the derivative of the refractive index with respect to the frequency. The main part of these schemes are based on coherent effects, like electromagnetic induced transparency [1], and, besides extremely low group velocities (*slow light*), also superluminal group velocities (*fast light*) have been reported. Such exotic velocities, whose existence had been surrounded by misconceptions about their apparent violation of causality and special relativity [2–4], have been experimentally realized [5, 6]. In this field, concerning the control of propagation dynamics of optical pulses, is set the framework of the first part of the present work. The used scheme allow to achieve slow and fast light propagation without involving coherent interactions [7]. Therefore, the interaction between the control pumping beam and the probe occurs with no temporal overlap of the two pulses.

Another property linked to the refractive index comes out from the inhomogeneity that can characterize an optical medium; for example, in a turbid medium, the light interacts with a bulk material where there are small scattering particles dispersed. Such heterogeneities, due to the refractive index mismatch between the particles and the bulk material, at microscopic scale originate the phenomenon of *scattering*, that is macroscopically observed as light diffusion.

The scenario becomes more complex and interesting if amplification is added in the disordered medium, in such a way to cause the spontaneously emitted photons to experience gain during the propagation between consecutive scattering events, before they leave the material. Such an optical system does not need an optical cavity and light is amplified along random paths, leading to laser-like emission if the gain overcomes the losses [8]. Then a *random laser*-type source shares features with the conventional lasers, but manifests different properties especially in some spectral characteristics and directionality of the output emission.

In the case of modest energy amount stored in the medium, the emission spectra are broad and ruled by spontaneous emission, whereas, as the energy increases, the stimulated emission leads to a spectral narrowing. As a peculiar and interesting feature, the spectra can also show large fluctuations, whose presence is linked to the disorder level and the available gain, in the form of random spikes at random frequencies.

Since 1960s, when Letokhov suggested the pioneer idea of a disordered amplified medium

[9], many different samples, with very different scattering properties, has been proposed [10–13]. However, despite the extensive investigation, the link between theory and experiment has not been completely clarified. Therefore, in the second part of this thesis, the experimental and theoretical work has been devoted to the study of random laser systems, in the aim of characterize the spectral features in term of statistical regimes of the emission and to find a clear link between theory and experiment.

In summary, the text in divided in five chapters, that cover the above topics, which also introduce the necessary basics.

Chap. (I) is devoted to the physical background that underlies the interaction between a optical signal and an atomic medium. The fundamental concept of *group velocity* is introduced, as well as the agreement between possible superluminal speed values, that such a velocity can assume, with causality and special relativity.

Chap. (II) describes the experimental realization of an incoherent interactions scheme for the optical control of propagation of a light pulse 3 ns long in passive atomic medium, composed by hot sodium vapor at very low pressure. The dynamics of the process can be basically described by the excitation of the medium by a control pulse, whereas the probe pulse, that propagates in the material when the previous interaction is over, experiences at a successive time the arranged effects.

Chap. (III) shows the same experimental scheme to induce a *fast light* propagation, with a probe pulse that takes advance respect to the vacuum propagation.

Moreover, in this chapter the most important innovation developed during this thesis work is also described: the realization of a fast light propagation suitable for the recovering of a previously induced delay. Indeed, the results achieved with the two different configurations cited above suggested the opportunity to include both the propagation modes in the same experimental set-up.

Chap. (IV) aims to provide the basis of the scattering process and to introduce the framework and the history of random laser. Both scattering and random lasers regimes are discussed, as well as the basic description of the state of the art.

Finally, Chap. (V) describes the part of the thesis work devoted to an original theoretical and experimental investigation on random laser emission in diffusive scattering regime. In such a regime, where the scattering mean free path is much larger than the radiation wavelength, the interference conditions in light propagation can be neglected and the optical energy transport inside the medium can be described as a diffusion process. A model based on a non-resonant feedback mechanism and extended modes [14] has provided the groundwork for numerical simulations, that confirm the presence of the different statistical regimes observed in the experiments. At the end of this last chapter, an experimental and theoretical investigation about the enhancement of the directionality level of the random laser emission is also shown, as topic under development.

[1] M. Fleischhauer, A. Imamoglu, and J. P. Marangos. “Electromagnetically induced transparency: Optics in coherent media”. In: *Rev. Mod. Phys.* 77 (2005), pp. 633–673. DOI: 10.1103/RevModPhys.77.633 (cited in page 1).

[2] L. Brillouin. *Wave Propagation and Group Velocity*. New York: Academic, 1960 (cited in page 1).

[3] D. Gauthier and R. Boyd. "Fast light, slow light, and optical precursors: What does it all mean?" In: *Photonics Spectra* (2007), pp. 82–90 (cited in page 1).

[4] P. W. Milonni. *Fast Light, Slow Light and Left-Handed Light*. Series in Optics and Optoelectronics. Taylor & Francis, 2004 (cited in page 1).

[5] L. J. Wang, A. Kuzmich, and A. Dogariu. "Gain-assisted superluminar light propagation". In: *Nature* 406 (2000), pp. 277–279. DOI: http://dx.doi.org/10.1038/35018520 (cited in page 1).

[6] M. D. Stenner, D. J. Gauthier, and M. A. Neifeld. "The speed of information in a /'fast-light/' optical medium". In: *Nature* 425 (2003), pp. 695–698. DOI: http://dx.doi.org/10.1038/nature02016 (cited in page 1).

[7] M. V. Tognetti, E. Sali, S. Cavalieri, and R. Buffa. "Temporal pulse compression and retardation by incoherent all-optical control". In: *Phys. Rev. A* 81 (2010), p. 023807. DOI: 10.1103/PhysRevA.81.023807 (cited in page 1).

[8] D. S. Wiersma. "The physics and applications of random lasers". In: *Nat Phys* 4 (5) (2008), pp. 359–367 (cited in page 1).

[9] V. S. Letokhov. "Generation of light by a scattering medium with negative resonance absorption [*Zh. Eksp. Teor. Fiz.* 53, 1442-1447 (1967)]". In: *Sov. Phys. JETP* 26 (1968), pp. 835–840 (cited in page 2).

[10] N. M. Lawandy, R. M. Balachandran, A. S. L. Gomes, and E. Suvain. "Laser action in strongly scattering media". In: *Nature* 368 (1995), pp. 436–437. DOI: 10.1038/368436a0 (cited in page 2).

[11] D. Wiersma and A. Lagendijk. "Light diffusion with gain and random lasers". In: *Phys. Rev. E.* 54 (1996), pp. 4256–4265. DOI: 10.1103/PhysRevE.54.4256 (cited in page 2).

[12] H. Cao. "Lasing in random media". In: *Waves in Random Media* 13.3 (2003), R1–R39. DOI: 10.1117/3.832717.ch11 (cited in page 2).

[13] M. Noginov and V. S. Letokhov. *Solid-State Random Lasers*. Springer Series in Optical Sciences. Springer, 2005. ISBN: 9780387239132 (cited in page 2).

[14] S. Mujumdar, M. Ricci, R. Torre, and D. S. Wiersma. "Amplified Extended Modes in Random Lasers". In: *Phys. Rev. Lett.* 93 (2004), p. 053903. DOI: 10.1103/PhysRevLett.93.053903 (cited in page 2).

Chapter I

Optical Signal Propagation through Dispersive Media

The propagation of optical signals through a material system involves the knowledge about the interaction between the wave components of the pulse and the atoms. The macroscopic manifestation of such an interactions is the refractive index, with its dependence on frequency, that leads to the dispersive properties.

This chapter is devoted to provide the theoretical framework that is indispensable for the introduction to the experimental realization of a control of the propagation dynamics of optical pulses.

In the Sec. (1.1.1) the principal concepts that underlie the light-matter interaction are briefly reminded, starting with definition of electromagnetic waves Sec. (1.1.1) and then introducing the fundamental concept of dispersion Sec. (1.1.2) and phase and group velocity Sec. (1.1.3).

In Sec. (1.2) we get in the hearth of the question, by discussing the propagation of a wave packet through a rarefied vapor Sec. (1.2.1) and through two level atomic system Sec. (1.2.2).

Finally, Sec. (1.3) is dedicated to clarify the puzzling issue about interpretation of exotic group velocities in the light of the special relativity and causality constrains. The starting point is the concept of causality in the framework of signal transmission (Sec. (1.3.1)). Then the definition of velocity of the optical front and the optical forerunner is introduced (Sec. (1.3.2)). The Sec. (1.3.3) is devoted to reassure about the fact that the experimental realization of superluminal group velocities does not cause temporal paradoxes.

1.1 Interaction of electromagnetic radiation with matter

1.1.1 Electromagnetic waves

Any macroscopic electromagnetic phenomena is describable by the equations established by James Clerk Maxwell in the XIXth century, with the *Maxwell equations* [1]:

$$\nabla \wedge \mathbf{E} = -\frac{\partial \mathbf{B}}{\partial t} \tag{I.1a}$$

$$\nabla \wedge \mathbf{H} = \frac{\partial \mathbf{D}}{\partial t} + \mathbf{j} \tag{I.1b}$$

$$\nabla \cdot \mathbf{D} = \rho \tag{I.1c}$$

$$\nabla \cdot \mathbf{B} = 0 \tag{I.1d}$$

The Maxwell equations and these relations known as *material equations* or *constitutive equations* establish the connection between the *electric* **E** and *magnetic field* **H**, the *magnetic induction* **B**, the *electric displacement* **D** end the *electric density current* **j**. A first demonstration of a link between light and electricity and magnetism had been found in 1845 by Michael Faraday by the observation of the alteration of polarization of an optical beam by a strong magnetic field. If the medium is isotropic and its perturbation response linear, the material equations are the following:

$$\mathbf{j} = \sigma \mathbf{E} \tag{I.2a}$$

$$\mathbf{D} = \epsilon \mathbf{E} \tag{I.2b}$$

$$\mathbf{B} = \mu \mathbf{H} \tag{I.2c}$$

where σ is the *specific conductivity*, ϵ is the *dielectric constant* and μ is the *magnetic permeability*. In a region that contains no currents and charges, i.e. where **j**=0 end charge density ρ=0, and if the medium is homogeneous, the Maxwell equations for free space can be manipulated into two equations:

$$\nabla^2 \mathbf{E} - \epsilon\mu \ddot{\mathbf{E}} = 0 \tag{I.3a}$$

$$\nabla^2 \mathbf{B} - \epsilon\mu \ddot{\mathbf{B}} = 0 \tag{I.3b}$$

Each cartesian component ψ of the electric end magnetic field obeys to the *d'Alembert equation*, i.e. the *differential wave equation* that describes the propagation of a wave with speed v:

$$\frac{\partial^2 \psi}{\partial x^2} + \frac{\partial^2 \psi}{\partial y^2} + \frac{\partial^2 \psi}{\partial z^2} = \frac{1}{v^2} \frac{\partial^2 \psi}{\partial t^2} \tag{I.4}$$

where the speed v is given by:

$$v = \frac{1}{\sqrt{\epsilon\mu}} \tag{I.5}$$

Therefore Maxwell suggested the existence of an electromagnetic wave that propagates at a speed whose value has been evaluate by ϵ and μ[2] With ϵ_0 and μ_0 the value corresponding to

[1] Expressed in SI units.

[2] Experiment of Wilhem Weber and Rudolph Kohlrausch (Leipzig - 1856).

vacuum, the predicted theoretical value of v in vacuum, expressed by the symbol c ($\approx 3 \times 10^8$ m/s), was in good agreement with the speed of light[3] measured by Fizeau[4].

In general the measurement of the speed v that appears in the equation I.5 is not directly performed and it is indeed derived by refraction laws:

$$n = c/v = \sqrt{\epsilon_r \mu_r} \tag{I.6}$$

where $\epsilon_r = \epsilon/\epsilon_0$ and $\mu_r = \mu/\mu_0$ are the relative dielectric constant and magnetic permeability and n the *absolute refractive index*.

1.1.2 Dispersion

As mentioned in the previous section, whereas in the theory briefly shown the material response to the incoming electromagnetic wave is characterized by two macroscopic constants (ϵ and μ), in nature such phenomenon is strongly dependent on frequency. Hence the atomic nature of the medium plays a fundamental role in order to describe phenomena as dispersion, absorption and emission. No real medium with the exception of the vacuum is dispersionless.

As pictured by H. A. Lorentz in 1878, the interaction between the electric field of the wave and atoms causes a distortion of their internal charge, with production of electric dipole moment that in turn contribute to the global field. Such effect is described by the *electric polarization* **P**, i.e. the resultant dipole moment in unit volume, that in first approximation is proportional to the applied field.

According to the quantum mechanics picture, if N is the number of atoms in unit of volume and **d** is electric dipole moment:

$$\mathbf{P} = N\langle\psi|\mathbf{d}|\psi\rangle \tag{I.7}$$

where $|\psi\rangle$ is the wavefunction that is solution of the Schrödinger equation :

$$i\hbar\frac{\partial|\psi\rangle}{\partial t} = (H_0 + V)|\psi\rangle \tag{I.8}$$

where H_0 is the unperturbed Hamiltonian of the atomic system and V describes the matter-radiation interaction. In general **P** is a non-linear function of the electric field **E** and χ is a tensor. In the linear case:

$$\mathbf{P} = \epsilon_0 \int_{-\infty}^{+\infty} \chi(t - t') \cdot \mathbf{E}(\mathbf{r}', t)dt \tag{I.9}$$

where χ is the *linear electric susceptibility*. Since the effect can not precede the cause the susceptibility, that is the medium response to the incoming perturbation, is zero for $t < t'$. If the perturbation field is supplied by a monochromatic wave, the field in the frequency domain is $\mathbf{E}(\mathbf{k}, \omega) = \mathbf{E_0}(\mathbf{k}, \omega)\exp(i\mathbf{k} \cdot \mathbf{r} - i\omega t)$, the convolution theorem implies:

$$\mathbf{P}(\mathbf{k}, \omega) = \epsilon_0 \chi(\mathbf{k}, \omega)\mathbf{E} \cdot (\mathbf{k}, \omega) \tag{I.10}$$

with

$$\chi(\mathbf{k}, \omega) = \int_{-\infty}^{+\infty} \chi(\mathbf{r}, t)e^{-i\mathbf{k}\cdot\mathbf{r}+i\omega t}d\mathbf{r}'dt \tag{I.11}$$

[3] Maxwell died in 1879, eight years before the experimental confirmation of his insights by Hertz, that reported the production and detection of electromagnetic waves.

[4] Experiment with rotating toothed wheel (1849)

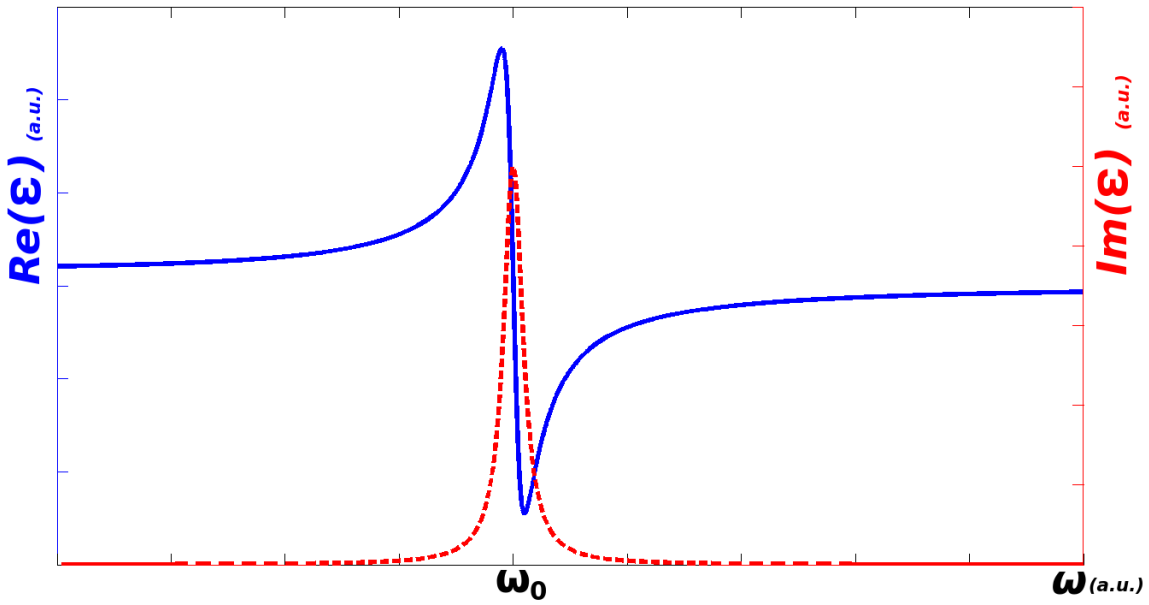

Figure I.1: Qualitative numerical simulation of equation I.17, based to the Drude-Lorentz model. The blue continuous curve is the real part of the dielectric constant, while the red dashed one is the imaginary part. The zone where ω is far away or in the wings of the resonance frequency ω_0 is called *normal dispersion zone*. The spectral region that surrounds the resonance is the *absorption band* and there is also located the *anomalous dispersion zone*, where $dn/d\omega$ is negative.

In non-magnetic materials, the susceptibility completely characterizes the optical properties of a medium and it can be calculated by a detailed knowledge of the microscopic structure or by approximate models, like the *Drude-Lorentz model*, whereby the atoms are pictured as a set of classical forced harmonic oscillators driven by an elastic-type force given by the time-varying electric field of the incoming wave. The electric dipole moment, with a charge e and a displacement vector $\mathbf{x}$:

$$\mathbf{d} = e\mathbf{x} = \alpha\mathbf{E} \tag{I.12}$$

Every atom contributes to the electric polarization with its electric dipole moment:

$$\mathbf{P} = N\mathbf{d} \tag{I.13}$$

where

$$\mathbf{P} = (\epsilon - \epsilon_0)\mathbf{E} \tag{I.14}$$

Under the Drude-Lorentz picture and if m and e denotes the mass and the electric charge of the electron respectively, the equation of motion is:

$$m\ddot{x} + \Gamma\dot{x} + m{\omega_0}^2 = eEe^{-i\omega t} \tag{I.15}$$

where $\Gamma\dot{x}$ is a damping force that represents the energy dissipation and ω and ω_0 are the frequency of the incoming wave and the *resonance frequency* of the oscillator. The stationary solution is:

$$x = \frac{eE}{m({\omega_0}^2 - \omega^2) - i\Gamma\omega} \tag{I.16}$$

If now we consider a gaseous material system ($n \sim 1$) with k different oscillator with resonance frequency ω_{0k} and weighing factors f_k [5]:

$$\epsilon(\omega) = 1 + \frac{Ne^2}{\epsilon_0} \sum_k \frac{f_k}{m({\omega_{0k}}^2 - \omega^2) - i\Gamma_k \omega} \tag{I.17}$$

As shown in Fig. (I.1), near a resonance the imaginary part of dielectric constant has a spike, while the real part, that describes the dispersive properties, is characterized by rapid variations: in spectral ranges where $(dn/d\omega > 0)$ the dispersion is called *normal*, whereas where $(dn/d\omega < 0)$ *anomalous*.

1.1.3 Phase and group velocity

From the most general point of view a wave phenomenon can be consider *a some kind of a recognizable disturbance that is transferred from one part of a medium to another with a detectable velocity of propagation* [1]. A signal may be any clearly recognizable and temporally and spatially localized feature of the disturbance. In general, such signal undergoes changes in shape, intensity and traveling speed during propagation through different media.

Before discussing the propagation of an optical signal, let us see the simpler case of a monochromatic wave of frequency ω. Let be $g(\mathbf{r})$ a scalar function of position and $E(\mathbf{r}, t)$ the electric field of the monochromatic wave whose *complex amplitude* $U(\mathbf{r})$ is a real solution of the wave equation (I.3a):

$$E(\mathbf{r}, t) = \mathcal{R}e(U(\mathbf{r})e^{-i\omega t}) \qquad \text{with} \qquad U(\mathbf{r}) = a(\mathbf{r})e^{g(\mathbf{r})} \tag{I.18}$$

The surfaces where $g(\mathbf{r})$ is constant are the *co-phasal surfaces*. Since the phase $(\omega t - g(\mathbf{r}))$ is the same for $(\mathbf{r}, t)$ and $(\mathbf{r} + d\mathbf{r}, t + dt)$:

$$\omega dt - \nabla g(\mathbf{r}) \cdot d\mathbf{r} = 0 \tag{I.19}$$

Indicating with $\hat{r}$ the versor such that $d\mathbf{r} = \hat{r} ds$:

$$\frac{ds}{dt} = \frac{\omega}{\hat{r} \nabla g(\mathbf{r})} \tag{I.20}$$

Let $\hat{r}$ normal to the co-phasal surface $g(\mathbf{r})$, the *phase velocity*:

$$v_p = \frac{\omega}{|\nabla g(\mathbf{r})|} \tag{I.21}$$

In the case of a plane wave since $g(\mathbf{r}) = \mathbf{k} \cdot \mathbf{r} - \theta$, where θ is an initial phase factor, $\nabla g(\mathbf{r}) = \mathbf{k}$ and the (I.22) gives:

$$v_p = \frac{\omega}{k(\omega)} = \frac{c}{n(\omega)} \tag{I.22}$$

The dependence of k on frequency is the *dispersion relation* determines the speed of a monochromatic wave through a dispersive medium, macroscopically described by the refractive index n.

[5] The *oscillator strength* f_k satisfies the requirement $\sum_k f_k = 1$ and it is linked to the transition probability of a atomic transition. The resonant frequency ω_{0k} is the frequency of such transition at which an atom absorb and emit radiation.

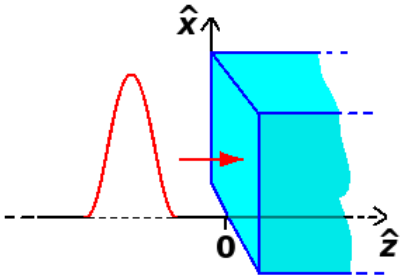

Figure I.2: An optical wave packet that propagates that propagates into a dispersive medium whose origin is localized on coordinate $z = 0$ along the direction of propagation.

A real optical signal with a finite time duration can not be composed by a single monochromatic wave. A fundamental property of the (I.4) is the linearity: if a set of functions is solution, any linear combination of them is a solution too; hence for the *principle of superposition* such property implies that a disturbance that propagates in a medium is a algebraic sum of its constituent waves. Therefore an optical pulse is a *wave packet* and the constructive and destructive interferences between its monochromatic components determine the localization of the *modulation envelope* in space and time. In a dispersive medium the refractive index depends on the frequency of each wave component, leading to a changes on the interference conditions that causes a different propagation speed of the modulation envelope and, in general, a distortion of the original shape of the pulse.

Let us consider a wave packet, propagating along a direction labeled with the coordinate z, composed by monochromatic wave of different frequencies, with the approximation of negligible Fourier amplitudes $\mathcal{L}_\omega$, except for a narrow spectral window $\delta\omega$ centered on the *carrier wave* $\bar{\omega}$. The origin of a dispersive medium is located in $z = 0$, where the functional form of every $\mathcal{L}_\omega$ is known (Fig. (I.2)). The electric field of the pulse is:

$$E = \frac{1}{2\pi}\left(\int_0^\infty \mathcal{L}_\omega \mathrm{e}^{-i(\omega t - k(\omega)z)} d\omega + c.c.\right) \qquad \text{with} \qquad \bar{\omega} - \frac{\delta\omega}{2} \leq \omega \leq \bar{\omega} + \frac{\delta\omega}{2} \tag{I.23}$$

If $\delta\omega$ is sufficiently small the linear approximation of the dispersion relation becomes justified and around the wave number $\bar{k} = n(\bar{\omega})\bar{\omega}/c$ [6]:

$$k \approx \bar{k} + \left(\frac{dk}{d\omega}\right)_{\bar{\omega}} (\omega - \bar{\omega}) \tag{I.24}$$

The (I.24) becomes:

$$E = \frac{1}{2}\left(\mathcal{E}(z,t)\exp[-i(\bar{\omega}t - \bar{k}z)] + c.c.\right) \tag{I.25}$$

where $\mathcal{E}$ is the pulse *modulation envelope*, that oscillates at the frequency $\bar{\omega}$. Calculating the integral only over the frequency window where the Fourier amplitudes are appreciably different from zero:

$$\mathcal{E} \simeq \int_{\delta\omega} \mathcal{L}_\omega \exp\left[-i(\omega - \bar{\omega})(t - \left(\frac{dk}{d\bar{\omega}}\right)_{\bar{\omega}} z)\right] d\omega \tag{I.26}$$

[6]Such an assumption is inserted in sake of simplicity in order to define the group velocity. In theoretical picture and numerical simulation discussed in Chap. (III) all terms of the expansion are included.

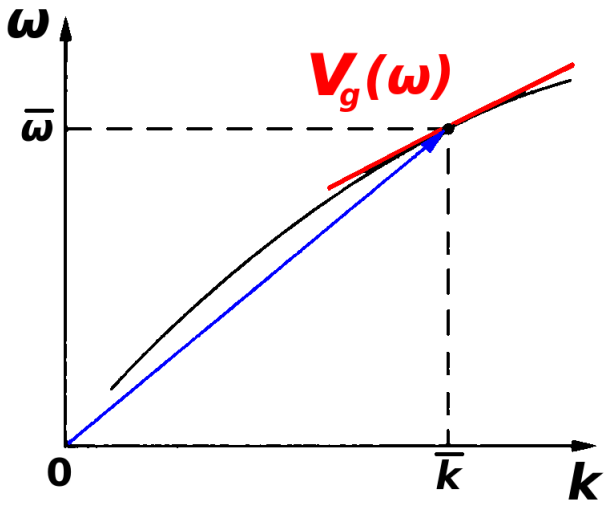

Figure I.3: The black line is the dispersion relation. The phase velocity is the slope of the blue line drawn from the origin to the point $(\bar{\omega}, \bar{k})$. The group velocity is the slope of the tangent to the curve in that point (in red).

Then, if the linear approximation (I.24) holds, the pulse propagates without distortions and the Fourier amplitudes $\mathcal{L}_\omega$ maintain their functional shape after the entrance in the dispersive medium. Then the equation (I.25) can be rewritten as follow:

$$E = \frac{1}{2}\Big(\mathcal{E}(t - z/v_g)\exp[-i(\bar{\omega}t - z/v_p)] + c.c.\Big) \tag{I.27}$$

Hence the field E can be viewed as the product of two factors:

(1) A phase factor propagating at the *phase velocity* $v_p = \bar{\omega}/\bar{k} = c/n(\bar{\omega})$

(2) A modulation envelope $\mathcal{E}$ that travels without distortions at the *group velocity* defined as follow:

$$v_g = \left(\frac{d\omega}{dk}\right)_{\bar{k}} \tag{I.28}$$

For signals composed by a superposition of harmonic components localized around a narrow bandwidth in a carrier wave, the group velocity describes the speed of the modulation envelope through a dispersive medium. Although the group velocity concept is often referred to the *speed of the signal*, such definition can be affected by misinterpretations where v_g assumes anomalous value, as observed by Sommerfeld and Brillouin [2]. In Fig. (I.3) a plot of the phase and the group velocity is shown; the group velocity is the slope of the tangent to the dispersion curve in the point $\bar{\omega}, \bar{k}$.

Hence, in an undistorted pulse, in correspondence of the peak the contributes of the spectral components tend to add up in phase for all values of the z-coordinate during the propagation through the dispersive medium. Such condition can be mathematically expressed by writing the phase as:

$$\phi = \frac{n\omega z}{c} - \omega t \tag{I.29}$$

and by imposing that, at the first order in ω:

$$\frac{d\phi}{d\omega} = \frac{dn}{d\omega}\frac{\omega z}{c} + \frac{nz}{c} - t = 0 \tag{I.30}$$

Since $k = n\omega/c$, it follows:

$$\frac{z}{t} = \frac{c}{n + \omega\left(\frac{dn}{d\omega}\right)} = \frac{d\omega}{dk} = v_g \tag{I.31}$$

In analogy with the definition of the phase velocity (I.22), the (I.31) can be written as:

$$v_g = \frac{c}{n_g} \tag{I.32}$$

where n_g is the *group refractive index*, that differs from the refractive index by a term that depends on the dispersion [3]:

$$n_g = n(\omega) + \omega\left(\frac{dn}{d\omega}\right) \tag{I.33}$$

As viewed in Fig. (I.1) and in Sec. (1.1.2), different values of $dn/d\omega$ correspond to spectral regions where the dispersion is normal or anomalous. Then also n_g can span among a large range of values, determining $v_g \ll c$ in normal dispersion zone or tending to approach more exotic *superluminal velocities* $> c$ or also *negative*.

Although the group velocity can be greater than the speed of light in vacuum, such phenomenon is not in contrast with the theory of special relativity and the principle of causality and it does not allow a superluminal velocity of the information [2]. Such a puzzling topic is discussed in Sec. (1.3).

Then, by tuning the dispersive properties of material systems, researchers have been able to control the propagation dynamics, achieving extremely slow velocities (*slow light regime*) or superluminal group velocities (*fast light regime*).

1.2 Optical pulse propagation in an atomic medium

1.2.1 Wave packet through gaseous medium

If the wave packet described by equation (I.25) propagates through a non-magnetic low-density gaseous dispersive material system, in which electric free charges and currents are not present, the approximation of a medium composed by a set of weakly interacting atomic levels is justified. In such case in the Maxwell equations the polarization act as a source term:

$$\nabla \wedge \mathbf{E} = -\mu_o \frac{\partial \mathbf{H}}{\partial t}, \tag{I.34a}$$

$$\nabla \wedge \mathbf{H} = \varepsilon_o \frac{\partial \mathbf{E}}{\partial t} + \frac{\partial \mathbf{P}}{\partial t} \tag{I.34b}$$

From which follows:

$$\nabla \wedge \nabla \wedge \mathbf{E} + \frac{1}{c^2}\frac{\partial^2 \mathbf{E}}{\partial t^2} = -\mu_o \frac{\partial^2 \mathbf{P}}{\partial t^2} \tag{I.35}$$

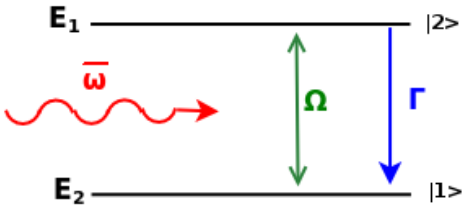

Figure I.4: Diagram of the interaction of a two levels atomic system with quasi-resontant field of frequency $\bar{\omega}$. $\Omega = d_{12}\mathcal{E}/\hbar$ is the Rabi frequency, d_{12} the electric dipole moment of the transition $|1\rangle - |2\rangle$ and $\Gamma = 1/T$, where T is the lifetime of the level $|2\rangle$.

By considering an isotropic medium, since $\nabla \cdot \mathbf{E} = 0$ $\nabla \wedge \nabla \wedge \mathbf{E} = -\nabla^2\mathbf{E}$. If the propagation develops along the coordinate $\hat{z}$ and the linearly polarized electric field lies to the perpendicular coordinate $\hat{x}$ $\mathbf{E}$(**r**,t) = $\hat{x}E(z,t)$), the equation (I.35) becomes:

$$\frac{\partial^2 E(z,t)}{\partial z^2} - \frac{1}{c^2}\frac{\partial^2 E(z,t)}{\partial t^2} = \mu_o \frac{\partial^2 P(z,t)}{\partial t^2} \tag{I.36}$$

where the polarization has the same form of the (I.25):

$$P = \frac{1}{2}\left(\mathcal{P}(z,t)e^{-i(\bar{\omega}t-\bar{k}z)} + c.c.\right) \tag{I.37}$$

By inserting the (I.25) and the (I.37) in the (I.36):

$$\frac{\partial^2 \mathcal{E}}{\partial z^2} - 2i\bar{k}\frac{\partial \mathcal{E}}{\partial z} - \frac{1}{c^2}\frac{\partial^2 \mathcal{E}}{\partial t^2} - \frac{2i\bar{\omega}}{c^2}\frac{\partial \mathcal{E}}{\partial t} = \mu_o\left(\frac{\partial^2 \mathcal{P}}{\partial t^2} + 2i\bar{\omega}\frac{\partial \mathcal{P}}{\partial t} - \bar{\omega}^2\mathcal{P}\right) \tag{I.38}$$

If the temporal variation of the electric field is slow on the temporal and the spatial scale provided by $2\pi\bar{\omega}^{-1}$ and $2\pi\bar{k}^{-1}$ respectively, the (*Slowly Varying Envelope Amplitude approximation (SVEA)* allows to rearrange the (I.38) as a first order differential equation:

$$\frac{\partial^2}{\partial z^2} \ll \bar{k}\frac{\partial}{\partial z} \qquad \frac{\partial^2}{\partial t^2} \ll \bar{\omega}\frac{\partial}{\partial t} \ll \bar{\omega}^2 \tag{I.39}$$

$$\frac{\partial \mathcal{E}}{\partial z} + \frac{1}{c}\frac{\partial \mathcal{E}}{\partial t} = -\frac{i\bar{\omega}\mathcal{P}}{2c\varepsilon_o} \tag{I.40}$$

1.2.2 Two levels atomic system

Let us consider a two levels atomic system (with energy E_1 e E_2) in Fig. (I.4) that interacts with a probe field quasi-resonant with the transition $|1\rangle - |2\rangle$. The equation of the field is:

$$E(z,t) = [\mathcal{E}(z,t)e^{i(\bar{\omega}t-z/c)} + c.c.]/2 \qquad \text{with} \qquad \bar{\omega} \approx (E_2 - E_1)/\hbar = \omega_{12} \tag{I.41}$$

The state wave function can be expanded on the basis given by the unperturbed states:

$$|\Psi\rangle = c_1 e^{-i\omega_1 t}|1\rangle + c_2 e^{-i\omega_2 t}|2\rangle \tag{I.42}$$

where $\omega_{1,2} = E_{1,2}/\hbar$. The evolution is given by the time-dependent Schrödinger equation

$$i\hbar\frac{\partial|\Psi\rangle}{\partial t} = H|\Psi\rangle \qquad H = H_o + H_{int} + H_r \tag{I.43}$$

where H_o is the unperturbed Hamiltonian, H_{int} is the field-atom interaction and the phenomenological term H_r is added to take into account the relaxation of the system. $\mathbf{d_{12}}$ is the electric dipole moment of the transition $|1\rangle - |2\rangle$, $H_{int} = -\mathbf{d_{12}} \cdot \mathbf{E}$ and with the electric dipole approximation the spatial variations of $\mathbf{E}$ can be neglected on the atomic dimension scale. In the expression for the temporal evolution of the coefficients c_1 and c_2 of the equation (I.42) the fast oscillating term $\exp[\pm i(\bar{\omega} + \omega_{12})]$ becomes negligible respect the quasi-resonant term $\exp[\pm i(\bar{\omega} - \omega_{12})]$, because in the timescale during which the coefficients change appreciably it is averaged to a much small value. Then in the resolution of the (I.43) the *Rotating Wave Approximation (RWA)* can be applied at optical frequencies:

$$\dot{c_1} = \frac{i\Omega}{2}c_2 e^{i(\bar{\omega}-\omega_{12})t} \tag{I.44a}$$

$$\dot{c_2} = \frac{-i\Omega}{2}c_1 e^{i(\bar{\omega}-\omega_{12})t} \tag{I.44b}$$

where $\Omega = d_{12}\mathcal{E}/\hbar$ is the *Rabi frequency*.

Under the formalism of the *density matrix* the polarization can be expressed as a function of the coherence terms. Indicating with N the number of atoms per volume units, it follows:

$$\langle\mathbf{P}\rangle = Tr(\rho\mathbf{P}) = N\sum_{mn}\rho_{nm}\langle\Psi|\mathbf{d_{12}}|\Psi\rangle \tag{I.45}$$

As the electric field expression, the polarization can be written in the following form:

$$P(z,t) = \mathcal{P}(z,t)e^{i\bar{\omega}(t-z/c)} + c.c. \tag{I.46}$$

with, from I.45:

$$\mathcal{P}(z,t) = Nd_{12}\rho_{12} \tag{I.47}$$

With the SVEA approximation and the (I.47), the propagation equation is the following:

$$\left(\frac{\partial}{\partial z} + \frac{1}{c}\frac{\partial}{\partial t}\right)\mathcal{E} = i\frac{N\bar{\omega}d_{12}}{2\varepsilon_o c}\rho_{12} \tag{I.48}$$

Let $\Gamma = 1/T_L$ and $\gamma = 1/T_T$ the decaying rates, where T_L and T_T are the decaying times, and with Δ the *detuning* $(\bar{\omega} - \omega_{12})$, the *Maxwell-Bloch equation* for a two levels system populations are derived:

$$\dot{\rho_{11}} = i\frac{\Omega}{2}(\rho^*{}_{12} - \rho_{12}) + \Gamma\rho_{22} \tag{I.49a}$$

$$\dot{\rho_{22}} = i\frac{\Omega}{2}(\rho_{12} - \rho^*{}_{12}) - \Gamma\rho_{22} \tag{I.49b}$$

$$\dot{\rho_{12}} = i\frac{\Omega}{2}(\rho_{22} - \rho_{11}) - (i\Delta + \gamma)\rho_{12} \tag{I.49c}$$

Under the assumption that only radiative channels are allowed, $2T_T \cong T_L$ is justified. Now let the amplitude of the probe electric field be low enough to leave the levels populations unperturbed (*weak field approximation*) and let, for the sake of simplicity, the initial populations be $\rho_{11} = 1$ e $\rho_{22} = 0$, in the case of a *passive medium*, or $\rho_{11} = 0$ e $\rho_{22} = 1$, if the system is an *active medium*. It is worth to note that the relations holds unchanged their validity even if both levels are populated, i.e. if $(\rho_{11} - \rho_{22}) = \xi$, where ξ is a constant that assumes values between 1 and -1. In this more general case the product $N \cdot \xi$ is identifiable with the definition of *population difference* which in turn, if $\xi < 0$, coincides with the *population inversion*. In the following the treatment of the case of a passive medium with $\xi = 1$, while other cases can be derived by the substitution $N \longrightarrow N \cdot \xi$.

As in Sec. (1.1.3), the field is expressed as sum of Fourier components, whose functional form is known at the entrance into the medium ($z = 0$):

$$\mathcal{E}(z,t) = \int_{-\infty}^{\infty} \mathcal{L}(\omega, z) e^{-i\omega t} d\omega \tag{I.50}$$

The equation for $\rho_{12}(z,t)$ becomes:

$$\rho_{12}(z,t) = -\frac{d_{12}}{2\hbar} \int_{-\infty}^{\infty} \mathcal{L}(\omega, z) f_{12} e^{-i\omega t} d\omega \tag{I.51}$$

where the function $f_{12} = f_{12}(\omega)$ has Δ and γ as parameters that depend on the characteristics of the probe beam and the medium:

$$f_{12}(\omega) = \frac{1}{[i\gamma + (\omega + \Delta)]} \tag{I.52}$$

With the (I.48) and the (I.51) the propagation equation of $\mathcal{S}(\omega, z)$ is the following:

$$\frac{\partial}{\partial z}\mathcal{L} = -ik(\omega)\mathcal{L} \tag{I.53}$$

with a dispersion relation for $k(\omega)$:

$$k(\omega) = \frac{\omega}{c} + \frac{N\bar{\omega}{d_{12}}^2}{4\hbar\varepsilon_o c} f_{12}(\omega) \tag{I.54}$$

As in Sec. (1.1.2), let consider a narrow bandwidth pulse. In particular:

$$\delta\omega \ll \sqrt{\Delta^2 + \gamma^2} \tag{I.55}$$

If the above condition is satisfied f_{12} can be expanded in series:

$$f_{12}(\omega) \approx f_{12}(0) + f'_{12}(0)\omega \qquad \text{with} \quad f'_{12}(0) = \left.\frac{df_{12}(\omega)}{d\omega}\right|_{\omega=0} \tag{I.56}$$

where

$$f_{12}(0) = -\frac{\Delta + i\gamma}{[\Delta^2 + \gamma^2]} \tag{I.57a}$$

$$f'_{12}(0) = -\frac{\Delta^2 - \gamma^2 + 2i\Delta\gamma}{[\Delta^2 + \gamma^2]^2} \tag{I.57b}$$

Hence, with these approximations, the dispersion relation I.54 can be written as follows around $\bar{\omega}$:

$$k(\omega) = \frac{\omega}{c} + \frac{N\bar{\omega}{d_{12}}^2}{4\hbar\varepsilon_o c}(f_{12}(0) + {f'}_{12}(0)\omega) \tag{I.58a}$$

$$= \frac{N\bar{\omega}{d_{12}}^2}{4\hbar\varepsilon_o c}\Big(\mathcal{R}e[f_{12}(0)] + i\mathcal{I}m[f_{12}(0)]\Big) + \left(\frac{1}{c} + \Big(\frac{N\bar{\omega}{d_{12}}^2}{4\hbar\varepsilon_o c}\Big)\Big(\mathcal{R}e[{f'}_{12}(0)] + i\mathcal{I}m[{f'}_{12}(0)]\Big)\right)\omega \tag{I.58b}$$

From I.55 it follows:

$$\mathcal{I}m[{f'}_{12}(0)]\delta\omega \ll \mathcal{I}m[f_{12}(0)] \tag{I.59}$$

Therefore the contribute supplied by the imaginary part of $k(\omega)$ given by ${f'}_{12}(0)$ can be neglected in the expression of I.58b. Within the medium ($z > 0$), the I.50 becomes:

$$\mathcal{E}(z,t) = \int_{-\infty}^{\infty} \mathcal{L}(\omega, 0)e^{-i(\omega t - k(\omega)z)}d\omega \tag{I.60}$$

As the classic case I.27, the expression for the field of the probe pulse that propagates in a two levels atomic system is the following:

$$E(z,t) = \mathcal{E}(t - z/v_g)\exp[i\bar{\omega}(t - z/v_f) - \beta z] \tag{I.61}$$

where, besides the phase and group velocity, it is also present a term β due to the absorption:

Phase Velocity:
$$\frac{1}{v_f} = \frac{1}{c} + \frac{N\bar{\omega}{d_{12}}^2}{4\hbar\varepsilon_o c}\mathcal{R}e[f_{12}(0)] = \frac{1}{c} - \frac{N\bar{\omega}{d_{12}}^2}{4\hbar\varepsilon_o c}\frac{\Delta}{[\Delta^2 + \gamma^2]} \tag{I.62a}$$

Group Velocity:
$$\frac{1}{v_g} = \frac{1}{c} + \frac{N\bar{\omega}{d_{12}}^2}{4\hbar\varepsilon_o c}\mathcal{R}e[{f'}_{12}(0)] = \frac{1}{c} + \frac{N\bar{\omega}{d_{12}}^2}{4\hbar\varepsilon_o c}\frac{\Delta^2 - \gamma^2}{[\Delta^2 + \gamma^2]^2} \tag{I.62b}$$

Absorption:
$$\beta = -\frac{N\bar{\omega}{d_{12}}^2}{4\hbar\varepsilon_o c}\mathcal{I}m[f_{12}(0)] = \frac{N\bar{\omega}{d_{12}}^2}{4\hbar\varepsilon_o c}\frac{\gamma}{[\Delta^2 + \gamma^2]} \tag{I.62c}$$

The zero-order terms $\mathcal{R}e[f_{12}(0)]$ and $\mathcal{I}m[f_{12}(0)]$determine the phase velocity and the absorption coefficient for a wave that propagates within a dispersive medium, whereas the real part of the first-order term $\mathcal{R}e[{f'}_{12}(0)]\omega$ describes the speed of a non-distorted modulation envelope, i.e. the group velocity. Now these quantities are expressed as a function of the atomic parameters and the probe field characteristics. Changing the sign of N the β parameter becomes an amplification factor within an inverted medium.

If the frequency of the field is resonant with the atomic transition ($\Delta = 0$), in a absorbing medium the probed dispersion zone is anomalous, and the I.62b and I.62c become:

$$\frac{1}{v_g} = \frac{1}{c} - \frac{N\bar{\omega}{d_{12}}^2}{4\hbar\varepsilon_o c\gamma^2} \tag{I.63a}$$

$$\beta = \frac{N\bar{\omega}{d_{12}}^2}{4\hbar\varepsilon_o c\gamma} \tag{I.63b}$$

In such case the group velocity assumes "exotic" values, exceeding the speed of light in vacuum or becoming negative:

$$v_g = \frac{c}{1 - \frac{N\bar{\omega}{d_{12}}^2}{4\hbar\varepsilon_o\gamma^2}} \quad > c \quad \text{or} \quad < 0 \tag{I.64}$$

In the matter of the distortion, the narrow bandwidth approximation becomes more critical with respect the I.55; the second-order term $k^{(2)}$ in the expansion of $k(\omega)$ describes the distortion. Since $k(\omega)$ appears as a phase factor in the expression I.60 of the field, in order to neglect its contribute, $k^{(2)} \cdot L$, where L is the length of the medium, has to be much smaller than 2π:

$$\frac{N\bar{\omega}d_{12}^2}{4\hbar\varepsilon_o c} f''_{12}(0) \cdot L \ll 2\pi \qquad \text{where} \quad f''_{12}(0) = \left.\frac{d^2 f_{12}(\omega^2)}{d\omega^2}\right|_{\omega=0} \tag{I.65}$$

1.3 Physical interpretation

1.3.1 Causality

The most intuitive and basic form of *causality* consists in the requirement that "the effect can not precede the cause" [4]. Let us consider a inertial reference frame and an event at (x, t) that causes another event at $(x + \Delta x, t + \Delta t)$ by means of an optical signal with speed u. In an another inertial reference frame, with relative velocity $v < c$, the time interval between the events becomes:

$$\Delta t' = \frac{\Delta t - (v/c^2)\Delta x}{\sqrt{1 - v^2/c^2}} = \frac{\Delta t(1 - uv/c^2)}{\sqrt{1 - v^2/c^2}} \tag{I.66}$$

If the velocity of the signal were superluminal ($u > c$) there are relative velocities v for the reference frame for which Δt and $\Delta t'$ have different sign. In other words, if an Universe where the superluminal communication is possible, there also always exist some inertial reference frames in which the temporal sequence of the events of cause and effect is reversed, i.e. a signal reaches the receiver before it leaves the sender, creating a sort of *grandfather paradox* [7] [5]. Then, since the causality is considered a fundamental principle of nature, the special relativity makes the superluminal transfer of information impossible.

So, since the existence of superluminal, infinite or negative group velocities is well experimentally verified, how do these exotic propagations satisfy the causality requirement? The solution of this apparent paradox lies in the distinction between the values that a certain velocity can assume and the maximum speed of information transfer, that is limited by the unsurmountable barrier of the speed of light in vacuum c.

As previously claimed in Sec. (1.1.3), the group velocity has been often confused as the signal velocity, since in many practical cases these velocities coincide. Despite the pioneer and extensive work of Sommerfeld and Brillouin [2, 6, 7], the confusion about the concept of group velocity has lasted. Indeed, there are classic and good text of electromagnetism where it is incorrectly claimed that superluminal group velocity is a meaningless concept, due to severe distortion that should affect the pulse [8]. On the contrary, in this work and as in previous works, superluminal group velocity have been achieved, with a pulse peak that advances in propagation

[7] This famous paradox about time travel has been described for the first time in a science fiction short story in 1933. The story is about a time traveller that attempts to kill his grandfather before his grandfather meets his grandmother.

the vacuum propagation. An infinite group velocity means that the peak instantaneously exits from the medium as soon as it enters. A negative group velocity means that the peak of pulse leaves the medium in an earlier time its entrance. The distortion of the pulse in fast light propagation experimentally verified is not severe and often negligible.

The effect that allows researchers to achieve these group velocities is linked to the optical response of a medium, arranged in such a way to produce the desired effects. Albeit such an arrangement can occur before the pulse propagation, the optical response of the medium needs that the disturbance, that belongs to the pulse, is already present. The Kramers-Kronig relations, that relate the real part to the imaginary part of a response functions in physical systems (as the susceptibility is) strictly needs that the causality is satisfied [9].

1.3.2 Optical front and forerunners

As discussed in Sec. (1.1.3), a signal definition involves new information transfer by means of a recognizable feature or element of discontinuity that could not have been predicted from the motion of the wave packet, that composes the signal, at an earlier time [10]. Sommerfeld and Brillouin [2, 6, 7] suggested that the velocity of signal is different from the group velocity, albeit in many practical cases such velocities coincide. They considered as signal of electromagnetic nature a wave motion of the form of step-modulated pulse, that is 0 before a time instant and a series of waves of finite value after a sudden turn-on:

$$f(t) = \theta(t) \sin \omega t \tag{I.67}$$

where $\theta(t)$ is the Heaviside step function. The *front* of the pulse is the propagated field for time immediately following the turning on. They predict that the electrons of a material cannot react instantaneously when the arrives and then the induced polarization must have a finite response time, before which the wave propagates undisturbed.

Considering again the electric field expressed as sum of Fourier components of equation (I.50) in entrance (coordinate $z = 0$) at time t into a dispersive medium of refractive index $n(x)$:

$$\mathcal{E}(0, t) = \int_{-\infty}^{\infty} d\omega \mathcal{L}(\omega) e^{-i\omega t} \tag{I.68}$$

After a distance z inside the medium, the effect on propagation implies the multiplication of each Fourier component by a phase factor:

$$\mathcal{E}(z, t) = \int_{-\infty}^{\infty} d\omega \mathcal{L}(\omega, z) e^{-i\omega t} e^{i\omega n(\omega) z/c} \tag{I.69}$$

Using the Fourier transform of the (I.68):

$$\mathcal{E}(z, t) = \int_{-\infty}^{\infty} d\omega \mathcal{L}(\omega, z) e^{-i\omega t} e^{i\omega n(\omega) z/c} \frac{1}{2\pi} \int_{-\infty}^{\infty} dt' \mathcal{E}(0, t') e^{i\omega t'} = \int_{-\infty}^{\infty} dt \mathcal{G}(z, t - t') \mathcal{E}(0, t') \tag{I.70}$$

where

$$\mathcal{G}(z, t) = \frac{1}{2\pi} \int_{-\infty}^{\infty} d\omega e^{-i\omega\tau} e^{i\omega n(\omega) z/c} \tag{I.71}$$

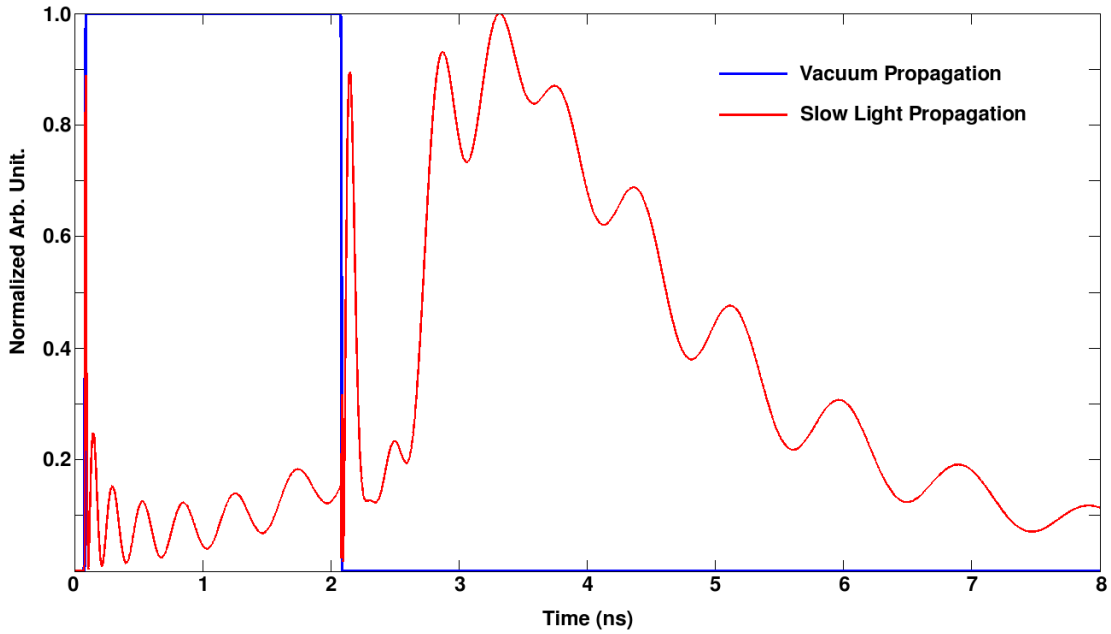

Figure I.5: Numerical simulation (see Sec. (3.1.2)) of a step pulse through a slow light medium. The components with frequency far from resonance remain unaffected.

For very large frequencies, far away from any resonance, one can assume that $n(\omega) \to 1$ as $\omega \to \infty$ and then in such a limit the integrand in (I.71) becomes $\exp(i\omega(z/c - \tau))$. Therefore, for distances larger than the distance covered at speed c, i.e. for $z > c\tau$, the integral can be replaced by a closed contour integral in the upper complex ω plane. No effect (polarization of atoms) can precede the cause (the incoming electric field) and the causality implies that the refractive index $n(\omega)$ be analytic in the upper half of the complex plane [4, 10]. Then, for $z > c\tau$, the (I.71) becomes 0, i.e. the medium can not respond:

$$\mathcal{G}(z,t) = 0 \qquad \text{for} \quad \tau < z/c \tag{I.72}$$

It follows that for a signal with a sharp wavefront, as the Sommerfeld and Brillouin-signal (I.67), the front propagates in any case at a speed that is exactly c (Fig. (I.5)). If the electric field (I.68) is 0 for all $t < 0$, then the field $E(z,t)$ is 0 for all $t > z/c$. The important consequences are:

(1) *no component of the pulse can advance the pulse front, whatever the propagation regime*

(2) *possible effects induced by the medium, included superluminal propagation, occur after the front propagation*

After the passage of the front, a mathematical prediction on the transformation of the wave packet shape is more difficult. Sommerfeld and Brillouin [2] found that the front is followed in propagation by two types of *optical forerunners*, with a very small and difficult detectability, that

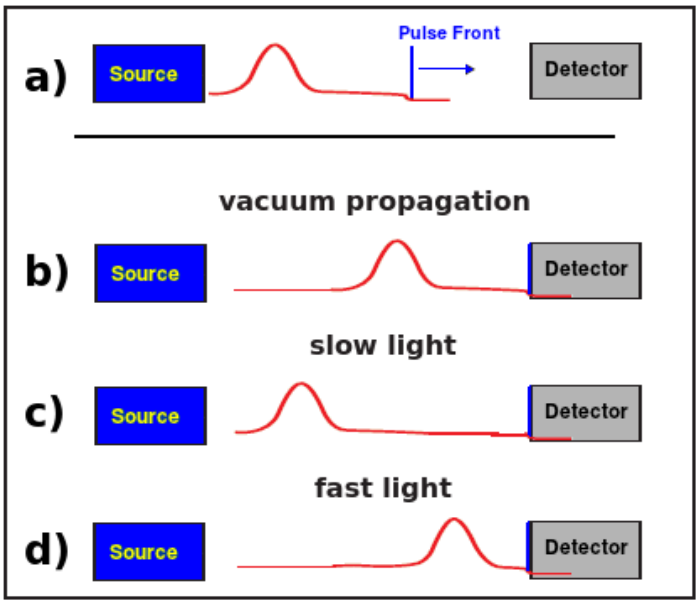

Figure I.6: In the figure a) the pulse has been emitted by a source and the front does not yet reach the detector. In the next figure the detector is reached by the front. In b) the pulse propagates in vacuum, in c) in slow light regime and in d) in fast light regime. Since the front speed is exactly c, in all cases the front reaches the detector in the same time instant. In d) the pulse peak is in advance respect the vaccum propagation, but not respect the front (Adapted from Reference [11]).

precedes the main part of the pulse. The first forerunner is associated to the large frequencies far above resonance, whereas the second forerunner to low ones far below resonances.

The predictions of the two scientists about the front propagation have been then verified in microwave frequency range [12]. Then in optical ranges, optical forerunners have been observed [13–17] and theoretically investigated [18].

1.3.3 Relativistic causality of superluminal propagation

In the previous section it has been discussed how the speed of the main part of the pulse is limited by the propagation velocity of the front and the optical forerunners.

In Sec. (1.1.3) it has been described the optical pulse as wave packet whose components are in phase in correspondence of the spatial coordinate where, at in a given time instant, the peak is located, whereas the destructive interference creates the wings of the pulse. It is important to stress that, whatever position in the pulse tail is considered, they are present the same amount of wave components of the main bulge. From information transmission point of view, each point of the pulse carries the same amount of information.

The role of the dispersive medium is connected to the variation of the phase of the components and then to a modification of the conditions of interference that create the pulse peak [19].

Fig. (I.6) gives a pictured and intuitive vision of the process. In the figure a) a pulse is created by a source; in the time instant when the switch that drives the source is turned-on the front of the pulse begins its propagation at c-speed. Then, one needs to wait a finite time to see the pulse grow to the peak value. What happens next depends on the type of medium that

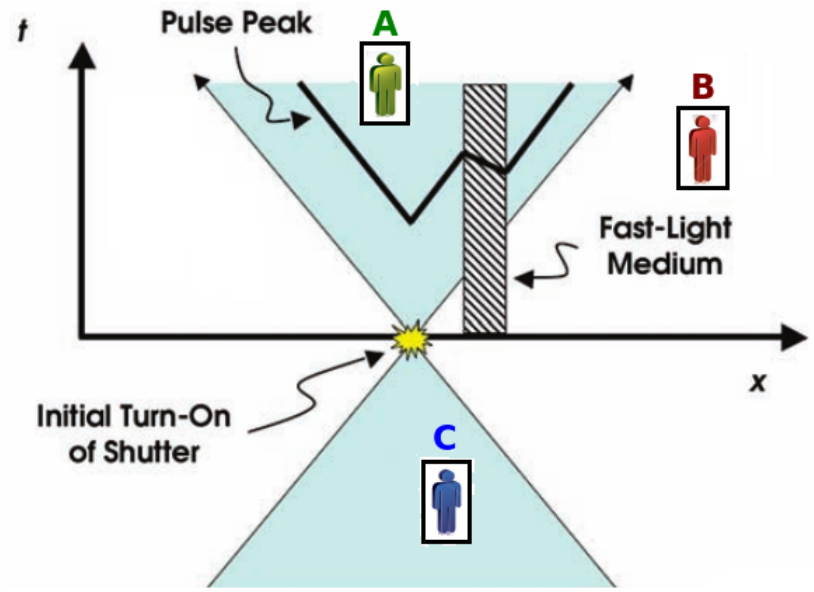

Figure I.7: Propagation of a light pulse (the front is the border of the cone) in a fast light medium. The border of the cone remain unaffected, whereas the peak is advanced towards the border. An observer in A sees the event of the pulse generation, whereas B does not. If the relativistic causality could be violated, the observer A could observe the pulse and transmit the information through a superluminal channel to C, that could inhibit the pulse generation (Adapted from Reference [11]).

stands between the source and the detector. The cases b), c), d) and e) concerns to the time instant when the front reaches the detector. In case b) the pulse propagates in vacuum, in c) in slow light regime and in d) in fast light regime. In slow light regime the pulse peak has a delay in propagation respect to the vacuum case. In case d) the superluminal propagation leads to an advance respect to the vacuum case, but not respect to the optical front [10, 11, 20–22].

In the case of negative group velocity, it occurs the extreme and counterintuitive situation in which the medium creates a "clone" of the pulse using the wave components that have yet reached the medium before the entrance of the main part of the "original" pulse, that, once it penetrates into the medium, vanishes in the material.

The information encoded in the tail of the pulse, that is often below the detectability threshold of the detectors, is the same of the pulse bulge: the detection of the information stored in the front would it makes possible the transmission of information at c speed. The transmission of information a c is not possible even for a signal that propagates in vacuum. Indeed, also in the vacuum propagation there is a finite time among the begin of front propagation and the growing of the pulse to its peak value. Such a delay can be recover (as discussed in Chap. (III)) by means of a fast light propagation and the aim of the experimental research in this field is not to realize an impossible information communication channel, but to approach the limit velocity c for information transmission.

In the space-time diagram showed in Fig. (I.7), the boundary of the light cone coincides with the front propagation at speed c. The observer in the space-time point A can see the event of pulse generation, whereas for the observer B the observation is impossible. The presence of the fast light medium causes a superluminal group velocity that makes the peak advance, whereas

the front (cone border) remains unaffected. Then the peak advances towards the cone border, but the approaching of the border is a limit condition. Therefore, with the fast light medium is not possible to realize a superluminal communication channel, whereby the observer A could communicate the event information to the observer C, that may change the event, creating a temporal paradox.

In summary, in pulse propagation theory one can distinguish seven different involved velocities [10]:

(1) Speed of Light in Vacuum c
the limit velocity of any kind of information transmission

(2) Phase Velocity $v_p = \omega/k$
the rate at which the phase of a single wave propagates in space. It can be grater than c without violate the special relativity

(3) Group Velocity $v_g = d\omega/dk$
the rate at which an undistorted modulation envelope of the wave packet propagates and can be greater or smaller then c or even negative without violate the special relativity

(4) Front Velocity
the velocity of a suddenly discontinuity that begins with the pulse creation. It is exactly c in any medium.

(5) Optical Forerunners Velocity
the speed of the frequency components of the wave packet that are far away from the resonances of the material. The forerunner follows the optical front in propagation and precede the main part of the pulse

(6) Signal Velocity
the speed at which the available and detectable information is transferred by a pulse. It cannot exceed c

(7) Energy Transport Velocity
It is linked to the signal velocity and is in general equal to the group velocity in the case of vacuum or slow light propagation, but not in the fast light case

For the energy transport speed, one can argue that, in the fast light case and when a amplifying medium is used, a large amount of energy reaches the detector in a such a way that seems to violate the special relativity, since a large amount energy of the pulse does not yet reach the medium. However, the energy “used” by the active medium has been previously stored in the medium, by means of the population inversion provided by a pumping system.

References

[1] G. B. Whitham. *Linear and Nonlinear Waves*. A Wiley-Interscience publication. Wiley, 1974 (cited in page 9).

[2] L. Brillouin. *Wave Propagation and Group Velocity*. New York: Academic, 1960 (cited in pages 11, 12, 17–19).

[3] R. W. Boyd and D. J. Gauthier. "Chapter 6 "Slow" and "fast" light". In: ed. by E. Wolf. Vol. 43. Progress in Optics. Elsevier, 2002, pp. 497 –530 (cited in page 12).

[4] P. W. Milonni. "Controlling the speed of light pulses". In: *J. Phys. B: At. Mol. Opt. Phys.* 35.6 (2002), R31 (cited in pages 17, 19).

[5] N. Schachner. "Ancestral Voices". In: *Astounding Stories* XII.4 (1933), pp. 26–30 (cited in page 17).

[6] A. Sommerfeld. "Ein Einwand gegen die Relativtheorie der Elektrodynamik und seine Beseitigung". In: *Phys. Zeitschr.* 8 (1907), p. 841 (cited in pages 17, 18).

[7] L. Brillouin. "Über die Fortpflanzung des Lichtes in dispergierenden Meddien". In: *Ann. Phys.* 22.22 (1914), pp. 1201–1204 (cited in pages 17, 18).

[8] R. Y. Chiao and P. W. Milonni. "Fast Light, Slow Light". In: *Opt. Photon. News* 13.6 (2002), pp. 26–30. DOI: 10.1364/OPN.13.6.000026 (cited in page 17).

[9] J. S. Toll. "Causality and the Dispersion Relation: Logical Foundations". In: *Phys. Rev.* 104 (1956), pp. 1760–1770. DOI: 10.1103/PhysRev.104.1760 (cited in page 18).

[10] P. W. Milonni. *Fast Light, Slow Light and Left-Handed Light*. Series in Optics and Optoelectronics. Taylor & Francis, 2004 (cited in pages 18, 19, 21, 22).

[11] D. Gauthier and R. Boyd. "Fast light, slow light, and optical precursors: What does it all mean?" In: *Photonics Spectra* (2007), pp. 82–90 (cited in pages 20, 21).

[12] P. Pleshko and I. Palócz. "Experimental Observation of Sommerfeld and Brillouin Precursors in the Microwave Domain". In: *Phys. Rev. Lett.* 22 (1969), pp. 1201–1204. DOI: 10.1103/PhysRevLett.22.1201 (cited in page 20).

[13] J. Aaviksoo, J. Kuhl, and K. Ploog. "Observation of optical precursors at pulse propagation in GaAs". In: *Phys. Rev. A* 44 (1991), R5353–R5356. DOI: 10.1103/PhysRevA.44.R5353 (cited in page 20).

[14] S. Zhang, J. F. Chen, C. Liu, M. M. T. Loy, G. K. L. Wong, and S. Du. "Optical Precursor of a Single Photon". In: *Phys. Rev. Lett.* 106 (2011), p. 243602. DOI: 10.1103/PhysRevLett.106.243602 (cited in page 20).

[15] H. Jeong, A. M. C. Dawes, and D. J. Gauthier. "Direct Observation of Optical Precursors in a Region of Anomalous Dispersion". In: *Phys. Rev. Lett.* 96 (2006), p. 143901. DOI: 10.1103/PhysRevLett.96.143901 (cited in page 20).

[16] K. E. Oughstun, N. A. Cartwright, D. J. Gauthier, and H. Jeong. "Optical precursors in the singular and weak dispersion limits". In: *J. Opt. Soc. Am. B* 27.8 (2010), pp. 1664–1670. DOI: 10.1364/JOSAB.27.001664 (cited in page 20).

[17] J. F. Chen, M. M. T. Loy, G. K. L. Wong, and S. Du. "Optical precursors with finite rise and fall time". In: *Journal of Optics* 12.10 (2010), p. 104010. DOI: doi:10.1088/2040-8978/12/10/104010 (cited in page 20).

[18] R. Safian, M. Mojahedi, and C. D. Sarris. "Asymptotic description of wave propagation in an active Lorentzian medium". In: *Phys. Rev. E* 75 (2007), p. 066611. DOI: 10.1103/PhysRevE.75.066611 (cited in page 20).

[19] W. Guo. "Understanding subluminal and superluminal propagation through superposition of frequency components". In: *Phys. Rev. E* 73 (2006), p. 016605. DOI: 10.1103/PhysRevE.73.016605 (cited in page 20).

[20] J. Marangos. "Faster than a speeding photon". In: *Phys. Rev.* 406 (2000), pp. 243–244. DOI: http://dx.doi.org/10.1038/35018657 (cited in page 21).

[21] R. Y. Chiao and P. W. Milonni. "Fast Light, Slow Light". In: *Opt. Photon. News* 13.6 (2002), pp. 26–30. DOI: 10.1364/OPN.13.6.000026 (cited in page 21).

[22] W. Withayachumnankul, B. M. Fischer, B. Ferguson, B. Davis, and D. Abbott. "A Systemized View of Superluminal Wave Propagation". In: *Proceedings of the IEEE* 98.10 (2010), pp. 1775–1786. DOI: 10.1109/JPROC.2010.2052910 (cited in page 21).

Further reading

[23] M. Born and E. Wolf. *Principles of Optics*. 7th ed. Cambridge University Press, 1999.

[24] E. Hecht. *Optics*. 4th ed. Addison Wesley, 1998.

[25] Y. Shen. *The principles of nonlinear optics*. Wiley classics library. Wiley-Interscience, 2003.

[26] R. Menzel. *Photonics: Linear and Nonlinear Interactions of Laser Light and Matter*. Springer, 2007.

[27] G. T. Di Francia and P. Bruscaglioni. *Onde elettromagnetiche*. Collana di fisica. Testi e manuali. Zanichelli, 1988.

[28] G. Franceschetti. *Campi Elettromagnetici*. 2nd ed. Bollati Boringhieri, 1998.

[29] P. Milonni and J. Eberly. *Lasers*. Wiley Series in Pure and Applied Optics. Wiley, 1988.

Chapter II

Slow-Light with an Incoherent Interactions Scheme

The control of propagation dynamics of optical pulses has been an important topic and an experimental challenge in optics. In literature, the larger part of the published works are based on coherent effects, meanwhile a control beam modulates the desired characteristics of a medium during the propagation of the probe pulse.

This chapter describes the part of this thesis work devoted to the realization of slow light propagation by using an interactions scheme that does not involve and request coherent interactions [1].

Sec. (2.1) is devoted to the theoretical topic of the slow light schemes proposed in literature (Sec. (2.1.1)) and then to in the introduction of the incoherent interaction scheme realized in the present work Sec. (2.1.2) and to the in a analytic model developed to to explain the experimental data (Sec. (2.1.3).)

In Sec. (2.2) the experimental part of the work is reported, starting with the description of the laser sources used (Sec. (2.2.1) and Sec. (2.2.2)) and the hot sodium vapor that acts as atomic medium (Sec. (2.2.3)). Finally the experimental set-up (Sec. (2.2.4)) and the strategy of measurement and data analysis is described Sec. (2.2.5)).

In conclusion, the experimental results are reported in Sec. (2.3), showing the experimental temporal profiles (Sec. (2.3.1)) and the complete characterization of the control of the slow light propagation (Sec. (2.3.2)). The analytic model and the experimental results discussed in this chapter has been published as an article on Physical Review A *[2].*

In the realization of this experiment I worked in the experimental set-up arrangement and method and I wrote the software of data analysis and fitting. I also contributed to the analytical model and in writing the scientific paper.

2.1 Slow-Light Group Velocity

2.1.1 Experimental Methods

One of the first demonstrations of slow light propagation, with $v_g < c/2.5$, has been reported in 1971 with mode-locked pulses in an amplifying medium in which the high gain and the narrow resonance lead to a large value of n_g [3]. Then, in the wing of a strong absorption resonance in rubudium vapor $v_g \sim c/14$ has been achieved [4].

Many published works reported experimental procedures that make use of non-linear interactions between light and matter, in such a way to circumvent the problem of absorption. With the *self induced transparency (SIT)* [5, 6] a group velocity of about $c/1000$ [7] and even smaller has been achieved. An optical pulse, even though its field is resonantly coupled to atoms of a medium, can travel, without being absorbed, inside a normally opaque material if it is tailored so that each atom, once excited by the pulse re-emits photons coherently in forward direction. Boyd's group also demonstrated that the dynamics of the SIT can be controlled by an additional field, leading to very low group velocities [8].

A typical scheme of coherent non-linear interactions for producing slow light is the *electromagneticly induced transparency (EIT)* [9], introduced by Imamoglu and Harris in 1990 [10, 11]. A closely related phenomenon to the EIT is the *coherent population trapping (CPT)* [12, 13], observed for the first time by Alzetta *et al.* in 1976, that reported a three levels scheme where two states were driven into a coherent superposition state such that the emission from the third state is eliminated (*dark state*). In EIT, the presence of an intense auxiliary electromagnetic field modifies the optical response of the material by means of an induced coherence of atomic states, which leads to quantum interferences between the possible interactions. Such a technique, besides the creation of a "transparent window", provides a rapidly variation of the refractive index near an absorption resonance (Fig. (II.1)). Many works concerning slow light have been realized by using EIT, controlling various properties of the propagation dynamics, such as the group velocity [14, 15], temporal shape [16], central frequency [17] and spectral distribution [18]. The extreme low value of $v_g = 17$ m/s has been achieved in Bose-Einstein condensate [19, 20].

In room temperature solids an alternative approach is based on *coherent population oscillation (CPO)* [21–23], exploiting a saturable absorption [24]. In these materials two optical fields are present: a strong pump beam, resonant with the transition of the material, and a weak probe beam, with a detuning from the same resonance. If such a detuning is smaller than the transition decay rate, the interference of the two beams leads to an oscillation at the beat frequency of the population, that creates a temporal modulation of the transmission, with a creation of a spectral hole in the absorption spectrum and then a rapid variation of the refractive index.

In optical fibers, *stimulated Brillouin scattering (SBS)* provides an alternative way to control the group velocity [25–28]. According to the typical scheme a pump beam is launched into the fiber in a counter-propagating way respect to the signal, inducing a dynamic Bragg grating in the core. If the frequency difference between the two optical wave is resonant with the acoustic wave, interaction occurs, generating spectral resonances.

Other systems to generate slow light involve *Raman scattering* [29, 30], *photonic crystals* [31, 32], spectral hole burning [33] and double absorbing resonances [34].

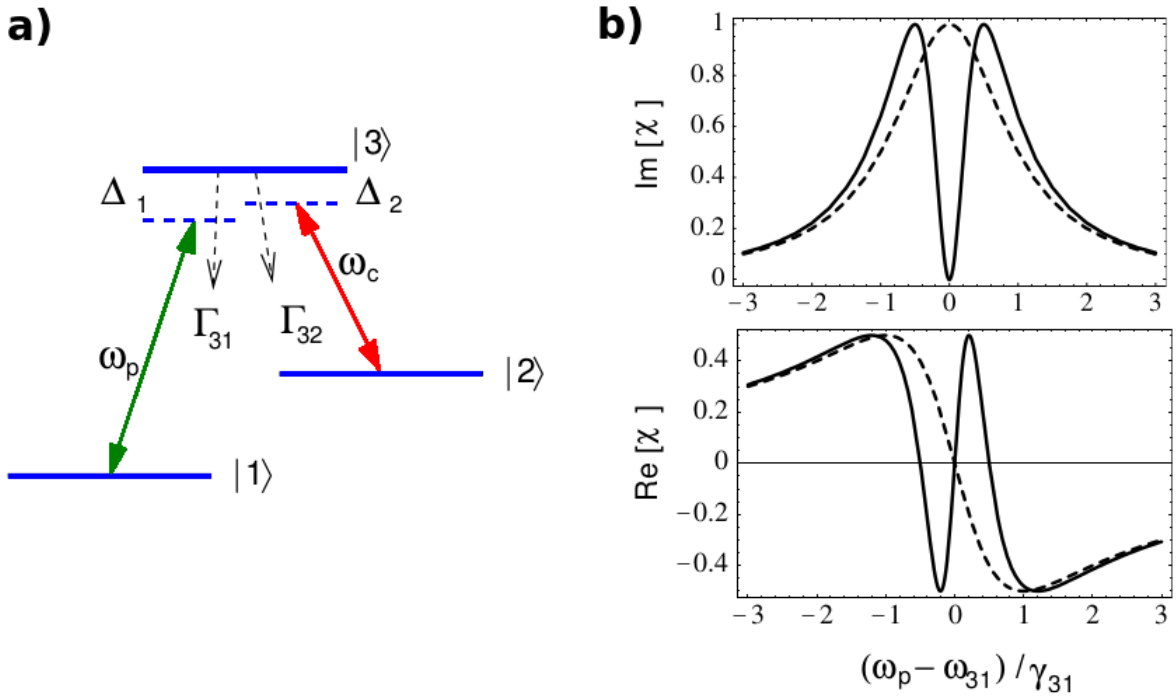

Figure II.1: a) Generic Λ-type three level system driven by a coherent coupling field of frequency ω_c and with a probe field of frequency ω_p. $\Delta_1 = \omega_{31} - \omega_p$ and $\Delta_2 = \omega_{32} - \omega_c$ are the detuning of the field from atomic resonances and Γ are the radiative decay rates.
b) Real and Imaginary part of the susceptibility as a function of frequency ω_p relative to the atomic resonance frequency $\omega_3 1$ with width γ_{31} (dashed line) and in EIT system (continuous line), when the coupled field is turned on [9].

2.1.2 Incoherent Interaction Schemes

In 2010 a new scheme to control the propagation dynamics, i.e. the group velocity and the temporal compression factor has been proposed [1]. Then, during this thesis work, the model has been theoretically improved and experimentally realized [2].

Such a scheme is based on the utilization of an *incoherent interactions*, where the term "incoherent" means that the interaction between the control light pulse and the probe light pulse is not direct: the control pulse excites the atoms of a material system and then, once such an interaction is over, the probe interacts with the medium. The tuning of the characteristics of the control pulse allow to provide the desired dispersion properties to the medium, in order to control the propagation dynamics of the probe. As discussed in Sec. (1.2.1) the probe pulse has to be *weak*, i.e. with an intensity low enough to leave the excited states unperturbed. If the latter condition is satisfied, the evolution of the population of excited atoms is solely ruled by the spontaneous emission process and by radiation absorption-reemission mechanisms (*radiation trapping*) [35].

Let us consider the three-level atomic scheme for a very rarefied sodium vapor showed in Fig. (II.2); the involved atomic levels are $|0\rangle = {}^2S_{1/2}$, $|1\rangle = {}^2P_{3/2}$ and the doublet of closely spaced resonances $|2\rangle = {}^2D$ (${}^2D_{5/2}$ and ${}^2D_{3/2}$. The control pulse central frequency ω_c is resonant with the transition $|0\rangle \rightarrow |1\rangle$, whereas the probe pulse frequency ω_p is detuned of a

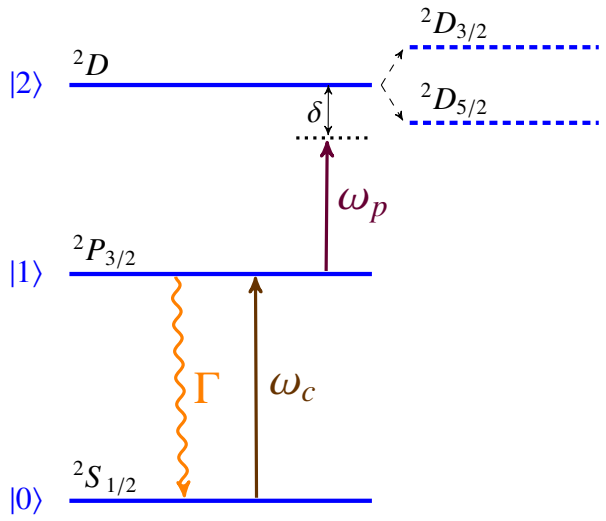

Figure II.2: Schematic diagram of the involved transitions and sodium atomic levels. The control pulse central frequency ω_c is resonant with the transition $|0\rangle \rightarrow |1\rangle$, whereas the frequency ω_p of the probe pulse is detuned by a quantity δ from the $|2\rangle \rightarrow |1\rangle$ transition frequency. Γ is the decay rate by spontaneous emission of the level $|1\rangle$.

quantity $\delta = (\omega_{D5/2,P3/2} + \omega_{D3/2,P3/2})/2 - \omega_P$ larger than the doublet fine structure separation we can consider the ^2D as a single state and neglect Doppler broadening. Once the interaction between the control pulse and the sodium vapor is over and after a temporal delay, the probe pulse propagates within a medium, that, due to the population of the level $|1\rangle$, has absorptive properties. Then, by varying δ, different dispersive zones are explored, within spectral regions near to the resonance frequency of the transition. Therefore, besides the frequency ω_p, other tuning parameters arise from the possibility to modulate the medium dispersion curve itself; indeed these parameters can be easily identified in the control pulse energy E_c, that affects the number of excited atoms, and the temporal separation Δt among the entrance time of the two pulses into the material. The latter involves the capacity of the system in storing energy in the form of the level $|1\rangle$ population, that begins to decay by spontaneous emission once it is established, albeit the radiation trapping acts as retarder for the complete depopulation. Meanwhile the population decreases during the propagation time of the pulse inside the medium, another effect on the propagation characteristics takes place, besides the lowering of the group velocity: the *temporal compression*. Indeed, due to the temporal variation of population, the leading edge of the pulse encounters a larger population than the trailing one, meaning that the two temporal wings of the pulses have different speed. In a heuristic picture, one can imagine that the leading edge is slowed down of a larger amount, the trailing edge recovers its propagation delay and "clamps" towards the pulse peak.

The final, and obvious, effect of the population in a passive medium concerns the absorption of the probe pulse photons; hence a too large number of excited atoms is to be avoided, in order to not destroy the pulse during its propagation or introduce severe distortion.

Finally, it is worth to stress further implications in using an incoherent interactions scheme. In the theoretical picture, under the matrix density formalism, the scheme implies that the co-

herence ρ_{01} of the $|0\rangle \rightarrow |1\rangle$ transition is 0 and then it does not play a role in determining the propagation. From an experimentally point of view, the system lends itself to be more easily realized in practice, since the control beam is solely used in order to populate the medium.

2.1.3 Analytic model of propagation dynamics

A theoretical model has been studied, in order to theoretically investigate the physical process that underlies the experimental proposal and to achieve an analytic expression of the propagation dynamics to compare with the experimental results. Let us start, using the density matrix formalism, with the propagation equation for the electric field E_p of the probe pulse, by means of the following coupled Maxwell-Liouville equations:

$$\frac{\partial E_p}{\partial z} + \frac{1}{c}\frac{\partial E_p}{\partial t} = -i\frac{N\omega_p}{\epsilon_0 c} d_{12}\rho_{12} \tag{II.1a}$$

$$\frac{\partial \rho_{12}}{\partial t} = -i\Omega_p \rho_{11} + [i\delta - \gamma_{12}]\rho_{12} \tag{II.1b}$$

where N is the atomic density, d_{12} the electric-dipole moment that corresponds to the transition $|1\rangle \rightarrow |2\rangle$ and γ_{12} represents all kinds of dephasing rate. The Rabi frequency Ω_p of the probe field - atom interaction is:

$$\Omega_p = \frac{d_{12}E_p}{2\hbar} \tag{II.2}$$

Notably, as discussed in Sec. (2.1.2), the coherence ρ_{01} does not appears in the (II.1b) and the population ρ_{11} evolution is solely due to incoherent decaying processes.

Considering the following conditions:

$$\delta \gg \gamma_{12} \tag{II.3}$$

$$\delta \cdot T \gg 1 \tag{II.4}$$

where T is the temporal duration of the probe, the approximated solution of the (II.1b) is the following:

$$\rho_{12} = \left[-\frac{i}{\delta^2}\frac{d}{dt} + \frac{1}{\delta} - \frac{i\gamma_{12}}{\delta^2}\right](\Omega_p \rho_{11}) \tag{II.5}$$

and equation (II.1a) can be written as:

$$\frac{\partial E_p}{\partial z} + \frac{1}{c}\frac{\partial E_p}{\partial t} = -\kappa\left[\frac{1}{\delta^2}\frac{d}{dt} + i\frac{1}{\delta} + \frac{\gamma_{12}}{\delta^2}\right](E_p \rho_{11}) \tag{II.6}$$

with

$$\kappa = \frac{\omega_p d_{12}^2}{2\hbar\epsilon_0 c} N \tag{II.7}$$

In the medium used in the experiment γ_{12} can be estimated of the order of 10^8 Hz and the condition (II.3) and (II.4), for probe pulses a few nanoseconds long, by setting values of detuning δ at least few tens of GHz.

The spontaneous emission lifetime of the level $|1\rangle$ is of the order of 20 ns, whereas the long-living phenomenon of the radiation trapping cause an effective prolongation of the population

in such a level. In the limit of pulses short compared to the temporal decay of ρ_{11} and assuming a spatiotemporal evolution of the population is given by $\rho_{11}(z,t) = \rho_{11}(t - z/c)$:

$$\rho_{11}(t - z/c) = \rho_{11}^0[A + (1 - A)e^{-\Gamma(\Delta t + t - z/c)}] \tag{II.8}$$

where z is the coordinate of the medium along the propagation direction, Δt is the time counted from the entrance of the probe pulse into the cell, A is the parameter that weighs the effect of the radiation trapping. More precisely, Δt is here defined as the time difference from the end of the control pulse and the beginning of the probe pulse at the cell entrance. The ρ_{11}^0 is the initial population after the control pulse passage.

The solution of the II.6 is the following:

$$E_p(z,t) = \frac{\rho_{11}(0,t')}{\rho_{11}(z,t)} e^{-(i\delta + \gamma_{12})(t - z/c - t')} E_p(0,t') \tag{II.9}$$

with

$$t' = \frac{\rho_{11}(0)}{\rho_{11}(t_0 - z/c)}(t - t_0) \tag{II.10}$$

and where t_0 is obtained by the solution of

$$\int_0^{t_0 - z/c} \frac{d\eta}{\rho_{11}(\eta)} - \frac{z\kappa}{\delta^2} = 0 \tag{II.11}$$

The equations (II.9) and (II.10) shows clearly that, upon propagation in the cell, the probe pulse is temporally delayed by the quantity t_0 and temporally compressed by the factor

$$n = \frac{\rho_{11}(0)}{\rho_{11}(t_0 - z/c)} \tag{II.12}$$

Then the expression (II.8) allows the analytic integration of the (II.11) to find an expression for the *induced delay* τ:

$$\tau = t_0 - \frac{L}{c} = \frac{1}{\Gamma_1} \ln\left[\frac{(1 - A)}{A}[\exp(A\Gamma_1 \frac{\kappa}{\delta^2} L\rho_{11}^0) - 1] + \exp[\Gamma_1(\Delta t + A\frac{\kappa}{\delta^2} L\rho_{11}^0)]\right] - \Delta t \tag{II.13}$$

From the insertion of (II.8) in the (II.12) it follows:

$$n = \frac{[A + (1 - A)e^{-\Gamma_1 \Delta t}]}{(1 - A)\{e^{A\Gamma_1 \frac{\kappa}{\delta^2} L\rho_{11}^0} + Ae^{\Gamma_1(\Delta t + A\frac{\kappa}{\delta^2} L\rho_{11}^0)}\}}\left[\frac{1 - A}{A}(e^{A\Gamma_1 \frac{\kappa}{\delta^2} L\rho_{11}^0} - 1) + e^{\Gamma_1 \Delta t + A\frac{\kappa}{\delta^2} L\rho_{11}^0}\right] \tag{II.14}$$

The peak intensity transmission (PIT) is the ratio between the square modulus of the field in entrance in the medium and after the propagation through the passive medium:

$$PIT = n^2 \exp[-2\gamma_{12}\tau] \tag{II.15}$$

In order to control the validity of these above equations, it can be useful to calculate their limit values in the case of constant population (no radiative decay):

$$\tau' = \frac{\kappa}{\delta^2} L\rho_{11}^0 \tag{II.16a}$$

$$n' = 1 \tag{II.16b}$$

and in the case of pure radiative decay:

$$\tau'' = \frac{1}{\Gamma} \ln[1 + \Gamma \frac{\kappa}{\delta^2} L\rho_{11}^0 exp[-\Gamma\Delta t] \tag{II.17a}$$

$$n'' = 1 + \Gamma \frac{\kappa}{\delta^2} L\rho_{11}^0 \exp[-\Gamma\Delta t] = e^{\Gamma\tau} \tag{II.17b}$$

Therefore, the induced delay τ and the other characteristics of the pulse depend on the following tuning parameters:

CONTROL PARAMETERS

(1) *the detuning δ of the central frequency of the probe pulse from resonance*

(2) *the control pulse intensity at the that determines the population of the level ρ_{11}*

(3) *delay Δt between the control pulse and the probe pulse at the entrance of the medium*

2.2 Experimental set-up

2.2.1 Probe pulse

The probe pulse is obtained from a single-mode cw extended-cavity diode laser (ECDL), whose model is Toptica DL100. In Fig. (II.4) the photo of the model used in the experiment and and the picture of the extended cavity are shown.

The laser diode operates in a single longitudinal mode with a bandwidth of the order of 1 MHz and has an external cavity with a Littrow mount grating whose rotation allows a first tuning mechanism of the emission wavelength. The Littrow grating acts as a wavelength-selective reflector, whereby the incident light is reflected back to the diode at the first order blaze wavelength [36]. The output beam consists in the 0^{th}-order.

To the laser diode is thermically connected a peltier cell, driven by a control unit (DTC100), whose function is to keep the temperature fixed around a selected value with a precision of 0.1°C. The threshold current is about 30 mA and the slope-efficiency about 1 W/A, with an output power that approaches 90 mW with a supplied current of 140 mA at the temperature of 20°C. The emission wavelength can range from ~815 to ~830 nm and its tuning and stabilization are a critical operative issue. Indeed it is very important that, during the measurement, the wavelength of the beam keeps its selected value within the tolerance of the lambda meter, that has a resolution of 1 pm. A variation of 1 pm in the wavelength can cause an abrupt change in the propagation dynamics of the probe pulse, especially if the wavelength close to the atomic resonances. In addition to the Littrow grating rotation, that act as an initial selector, the fine tuning of the wavelength is performed by tuning the supplied current and the working temperature. The dependence of the output wavelength on current and temperature is not obvious and rather unpredictable. A better stability of the system is generally achieved by selecting a working temperature close to the the room temperature of the laboratory. As an additional instrument

of tuning, a piezoelectric crystal is placed behind the grating and the variation of the applied voltage (from 0 to 60 V) causes small variations on the length of the cavity and then on the selected longitudinal mode .

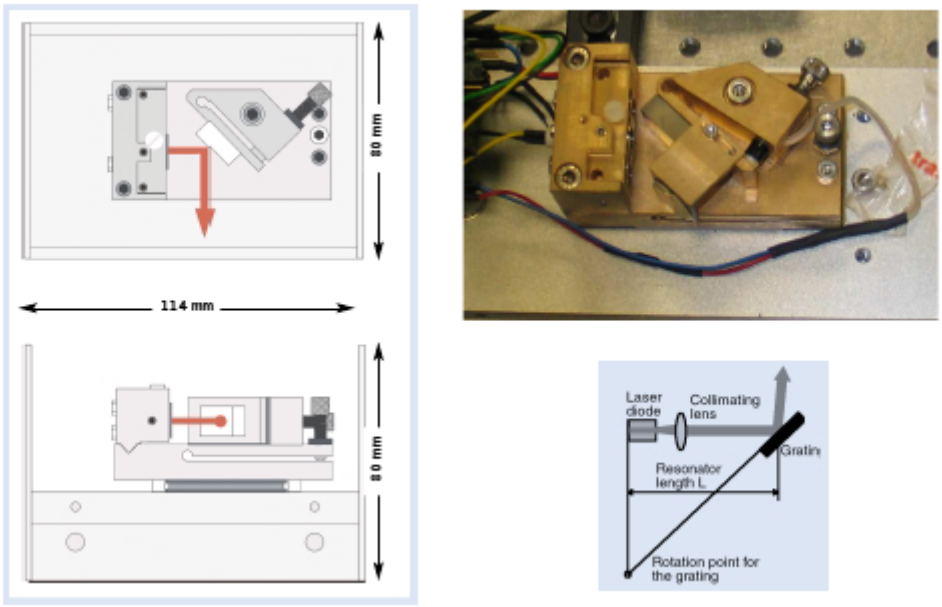

Figure II.3: Photo and internal structure of the extended-cavity laser diode Toptica DL100.

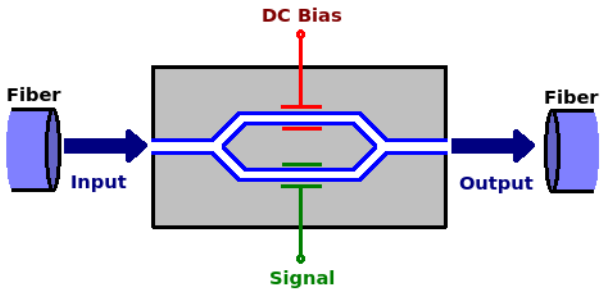

Figure II.4: Dyagram of the electro-optic modulator with Mach-Zehnder interferometer configuration.

The cw laser beam output is sent to a single-mode polarization preserving optical fiber, whose coupling is optimized by the rotation of a $\lambda/2$ plate. In order to create a light pulse of the desired duration the optical fiber is connected to an electro-optic modulator (EOSPACE AZ-0K5-10-PFU-SFU-795) with Mach-Zehnder interferometer configuration. In the modulator, made of $LiNbO_3$ birefringent negative uniaxial crystal, the input light splits up into two different paths, experiencing different phase shifts. In a path a DC bias voltage is applied in such a way to induce a refractive index variation, controlling the phase shift of the radiation. The DC voltage is tuned in order to set a destructive interference for the waves, that recombine at the output. The advantage of such kind of configuration is that the DC voltage does not exceed few tens of V. Another electric signal, in the form of a short electric pulse, is applied to the other path to create a rapid variation of the condition of destructive interference. Hence, a light signal, “cut”

from the continuous time beam, is then extracted from the output fiber. In optimal condition, the light pulse has the same temporal features of the applied electric signal. The bandwidth of the electro-optic modulator is 10 GHz and the rise time less than 100 ps.

The electric pulse generator is a Stanford Digital Delay Generator DG535, that allows to generate electric pulses after a selectable delay, with a resolution of 5 ps, from the trigger signal up to few ns long, albeit a temporal jitter about 50 ps is present. The output voltage is selected with a resolution of 50 mV±3% and can be affected by overshoot up to 100 mV±10%. Both the undesirable defects of the temporal and intensity uncertain must be reduced by means of experimental set-up expedients and suitable data acquisition mode and analysis, as discussed further in the text.

2.2.2 Control Pulse

The control pulse is generated by a frequency tunable dye laser (TDL50 Quantel Dye Laser) pumped by a frequency-doubled (532 nm) Q-switched Nd:YAG lases at a repetition rate of 10 Hz, whose pulses have about 150 mJ of energy and about 6 ns of temporal duration. A signal generated by the control unit of the Nd:YAG provides the trigger signal for the electric pulse generator, in such a way to synchronize the pulses generations and data acquiring process shot-to-shot. The variability in build-up time of the pulse inside the Nd:YAG causes a temporal jitter between the trigger signal and the effective arrival time of the pulse of about 1 ns.

The dye laser [37, 38] use as active medium Rhodamine 6G dissolved in methanol and it is provided of a reflective diffraction grating of 2400 lines per mm and fixed inclination. A rotating mirror, driven by a DC motor, reflects the first order diffraction of the grating and closes the optical cavity together with the semi-reflective output mirror. The control pulse operates in a broadband mode (30 GHz of FWHM), albeit some energy becomes wasted, in order to reduce the population fluctuations due to possible instabilities of the emission wavelength. Although the broad band, if not attenuated the control pulse is able to completely saturate the $|0\rangle \rightarrow |1\rangle$ transition. After the output mirror a $\lambda/2$ plate ensures that the control pulse has the same vertical polarization of the probe pulse. A small portion of the control beam is extracted, by a reflection on a glass plate, and sent to a photodiode, to monitor the pulse energy shot-to-shot (the output control beam has an average diameter (about 4 mm) grater than the probe beam one).

2.2.3 The Atomic Medium

The medium is composed by hot sodium vapor at very low pressure, enclosed in a metallic cell of 1.5 m total length and 1.0 m of effective length. The cell is heated by a resistance turned around its central part and the temperature is maintained stable around the selected value by means of a driving current feedback circuit. At a distance of about 20 cm from the quartz windows, the cell is cooled by water at room temperature; then the cell is produced in a gradient from the room temperature near the windows to the value detected by the thermocouple placed in the central part.

The vapor pressure is low enough to consider the probe beam propagation as in vacuum when the medium is not excited and the radiation wavelength is far from atomic resonances. The density N_{at} of sodium atoms inside the cell can be estimated by the vapor pressure, that can

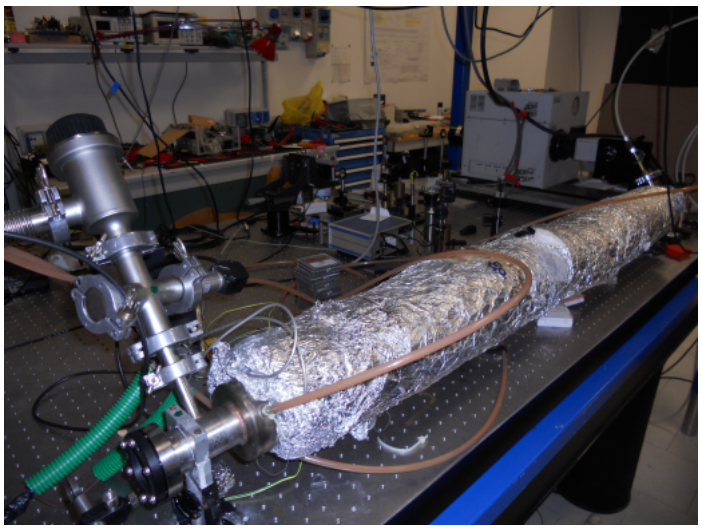

Figure II.5: The sodium cell.

be calculated as follows [39–41]:

$$\ln[P_{Na}] = a - \frac{b}{T} - c \ln T \tag{II.18}$$

where P_{Na} is the vapor pressure in MPa, T the temperature in °K and a, b and c component specific constants ($a = 11.9463, b = 12633.73, c = 0.4672$ for sodium). Then the number density N_{at} in the sodium vapor (atoms/m^3) can be estimated by means of the *ideal gas law*:

$$N_{at} = \frac{P_{Na}}{k_B T} \tag{II.19}$$

where k_B is the Boltzmann constant, T is in °K and P_{Na} in Pa.

2.2.4 Experimental set-up description

In Fig. (II.7) the schematic diagram of the experimental set-up is shown. The two laser beams are co-propagating, along the same path within the cell overlapped by means of a dichroic mirror and aligned with help of two diaphragms, one before the entrance window of the cell and one after the the exit window. The larger diameter of the control beam ensures a excited medium along a path of the probe inside the cell. The monitor of the probe pulse central frequency is performed by a lambda meter with a precision of 1 pm, that analyzes a reflection of the beam from a glass plate before the entrance in the electro-optic modulator.

At the exit of the cell the control beam is attenuated by an optical fiber (not showed in the figure) and separated from the probe beam by a dispersion prism, that prevents this beam from reaching the photodiode. Such a detector consists in an amplified GaAs (New Focus 1580-B) in transimpedance mode with a gain of -10^3 V/A. It is characterized by a bandwidth of 12 GHz, a rise time of 30 ps and it detects radiation wavelength among 400 and 870 nm. The dimension of the small sensible area is about few tens of μm^2. The resulting signal is then analyzed shot-to-shot by a 7 GHz-bandwidth oscilloscope (Tektronix TDS7704B) and sent to a PC.

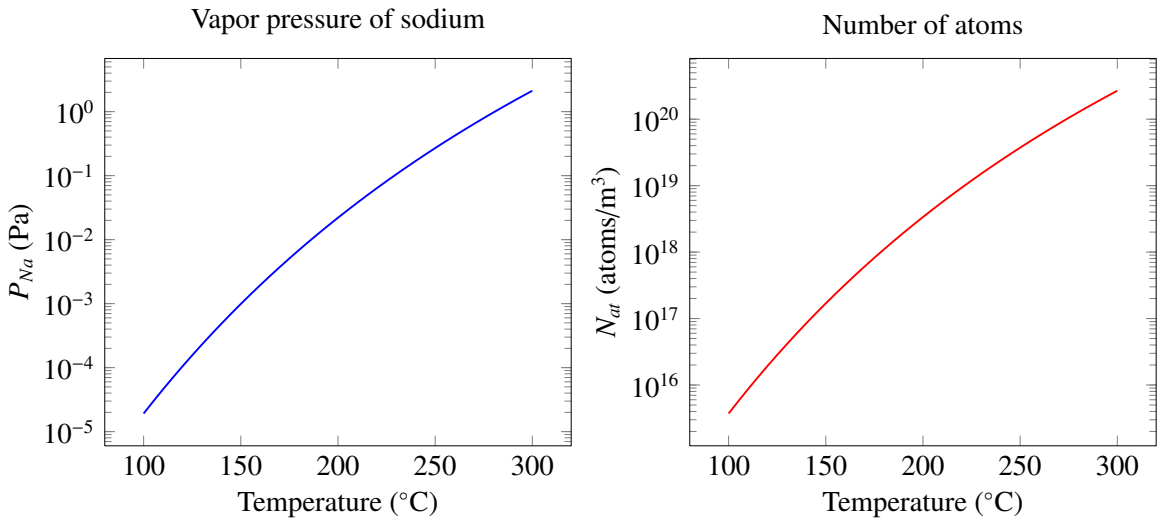

Figure II.6: Estimation of vapor pressure P_{Na} and number of atoms per volume unit N. The temperature is reported in °C.

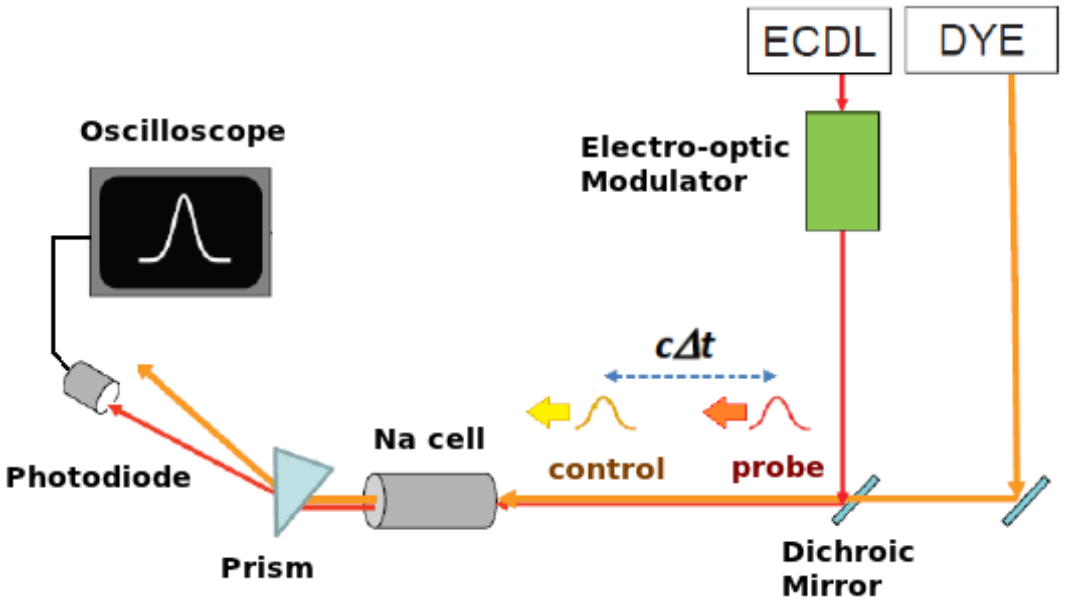

Figure II.7: Schematic diagram of the experimental set-up.

The synchronization of the whole system of generation and detection of signals starts (as anticipated in the Sec. (2.2.2)) with a trigger signal that is sent from the control unit of the Nd:YAG to the electric pulse generator, that in turn sends a trigger signal to the oscilloscope. Especially for the instability of the generation times of pulses, the measurement cannot be performed with a time average of the probe pulse signal, but acquired in shot-to-shot mode and then later analyzed. The synchronization of the overall process allows to record many hundreds of consecutive measurements.

2.2.5 Double-Pulse method

In order to eliminate the effect of fluctuations in probe pulse energy and generation time, we generated two probe pulses at a fixed delay for each trigger pulse. The first propagates in the cell before the control pulse and the second (the "true" probe) after. The schematic diagram of this "double pulse method" is showed in Fig. (II.8) and Fig. (II.9). Fig. (II.8) shows the temporal steps that lead to the generation of the two pulses:

(A) the trigger signal from the Nd:YAG control unit reaches the electric pulse generator.

(B) after a selectable delay T_D (of the order of same ns) an electric pulse is created. Another trigger signal is sent to the oscilloscope to prepare the next acquisition.

(C) the electric signal propagates through a cable that is split in two different paths of different lengths.

(D) once recombined, in the cable two different electric signals propagate, with a temporal separation T_R that depends by the difference in length between the two different paths during the step (C). Considering an electric signal in a coaxial cable about $\sim 2 \cdot 10^8$ m/s, ~4 m in paths difference lengths are needed in order to achieve T_R of order of 20 ns.

(E) the two signals reaches the electro-optic modulator and two light pulses are created

Such a system ensures that eventual intensity variation in electric pulse amplitude in electric signal does not lead to misinterpretation in absorption of the light probe pulse in the passive medium. T_D is modulated in such a way to enable the condition according which the control pulse propagates into the cell in the time that elapses between the entrance of the probe pulses (Fig. (II.9)). Moreover, a tuning of T_D also allows tuning of the time Δt, introduced in the Sec. (2.1.2) as a control parameter. Since the very low pressure of the sodium vapor, without excitation by the control pulse, the reference always propagates in vacuum; indeed the temporal separation between two successive measures (100 ms) is much greater than the spontaneous emission lifetime and the radiation trapping time. The limitations of T_R are that it must be short enough to avoid temporal superposition between the control pulse and the reference and not large to cause that the reference does not appear in the acquired trace of the oscilloscope.

Once T_D is tuned in order to achieve the desired Δt and the frequency of the probe beam is selected for a certain detuning δ, two different sets of measurement are made for each measurement campaign (Fig. (II.10)):

(1) *reference measurement*
a number of measurements are performed while the control pulse is inhibited

(2) *slow light measurement*
a control pulse excites the medium (with an energy tuned with a polarizer rotation and recorded shot-to-shot)

In the former, all the information of the two probe pulses are collected (difference in amplitude due to different resistances experienced by the electric pulse through paths with different length and temporal separation). The latter is the measurement set in which the probe pulse experience absorption and slow light propagation, while the reference remains unaffected again.

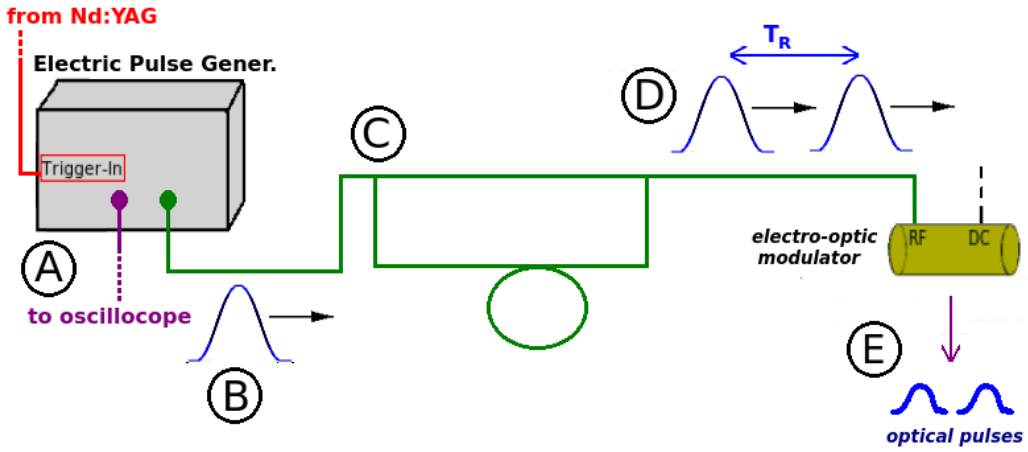

Figure II.8: Schematic diagram of the "double pulse method".

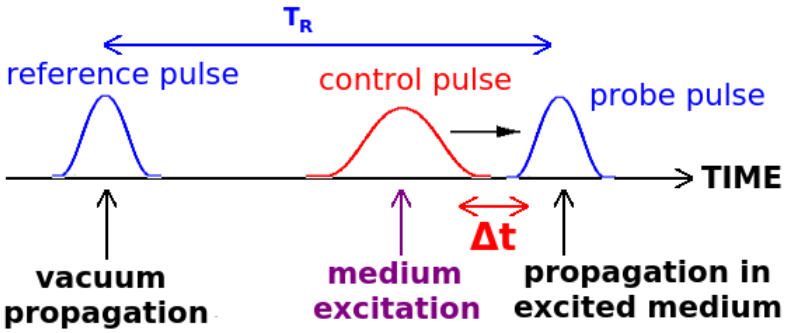

Figure II.9: Schematic diagram of the propagation of the pulses. The control pulse propagates (and then excites the atoms) after the reference probe pulse entrance and with an advance Δt respect to the probe pulse.

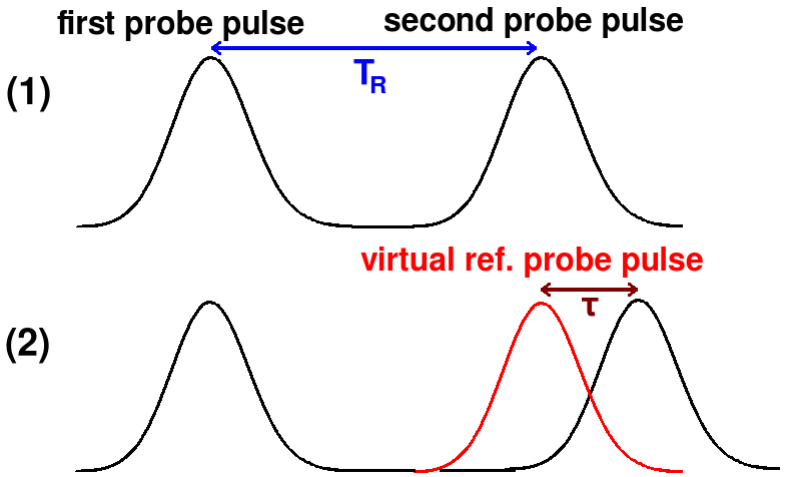

Figure II.10: (1) *reference measurement* and (2) *slow light measurement*, with the virtual probe pulse.

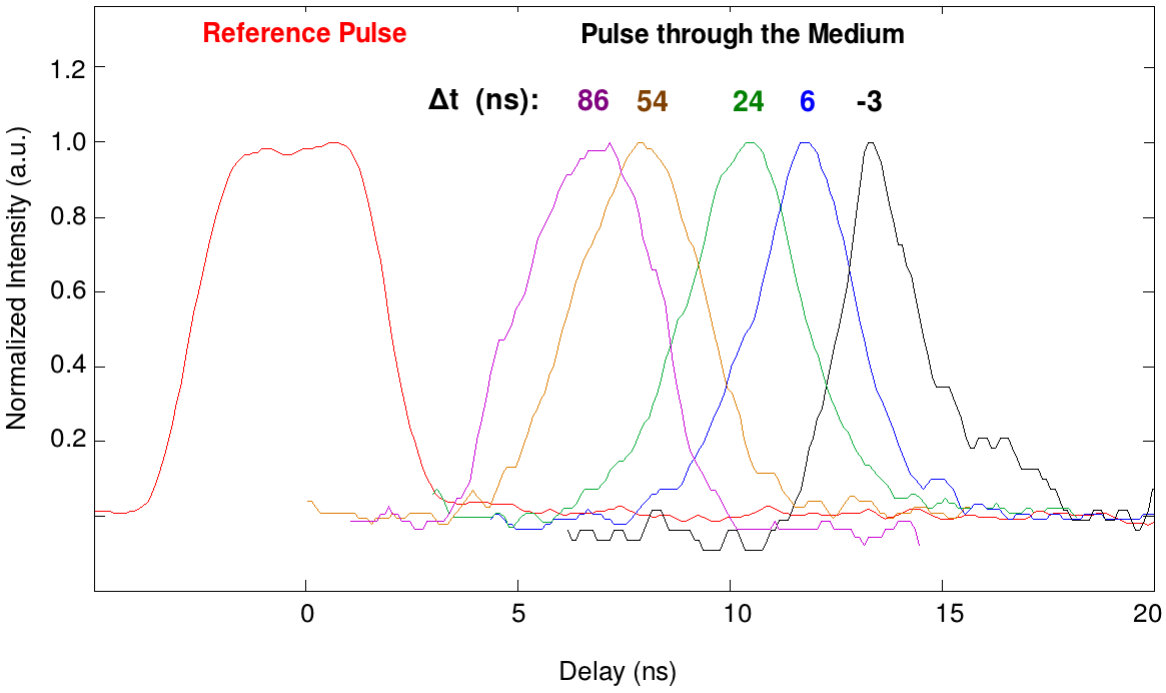

Figure II.11: Typical temporal profiles of the probe pulse after traveling through the cell for different Δt.

Once each set of measurement described in the latter part of the previous section are performed, the data stored to the PC through the oscilloscope are subjected to data analysis.

The data analysis performed by a software written in Matlab® code and, as the measurement procedure, consists of two steps. In the first one, the data collected during the *reference measurement* are used to obtain information about the two probe pulses. In the second step, that analyze the *slow light measurement*, the collected information allow to a "re-build" all features, computationally elaborated, that the probe pulse would have in vacuum propagation rather than in an excited medium. The software takes into account the shot-to-shot variation on intensity of the pulse. The new probe pulse reference becomes such a virtual pulse and the peak intensity transmission PIT, the compression n and extra delay τ are measured in reference to it. The value of τ are calculated as time difference in the time of half-peak value between the reference virtual pulse and the measured probe pulse. In a similar way PIT and n are measured for each shot.

The results showed in Sec. (2.3) takes advantage of the large number of temporal profiles acquired and the data are binned and mediated within small intervals of control pulse energies, with an improving of the measurement accuracy.

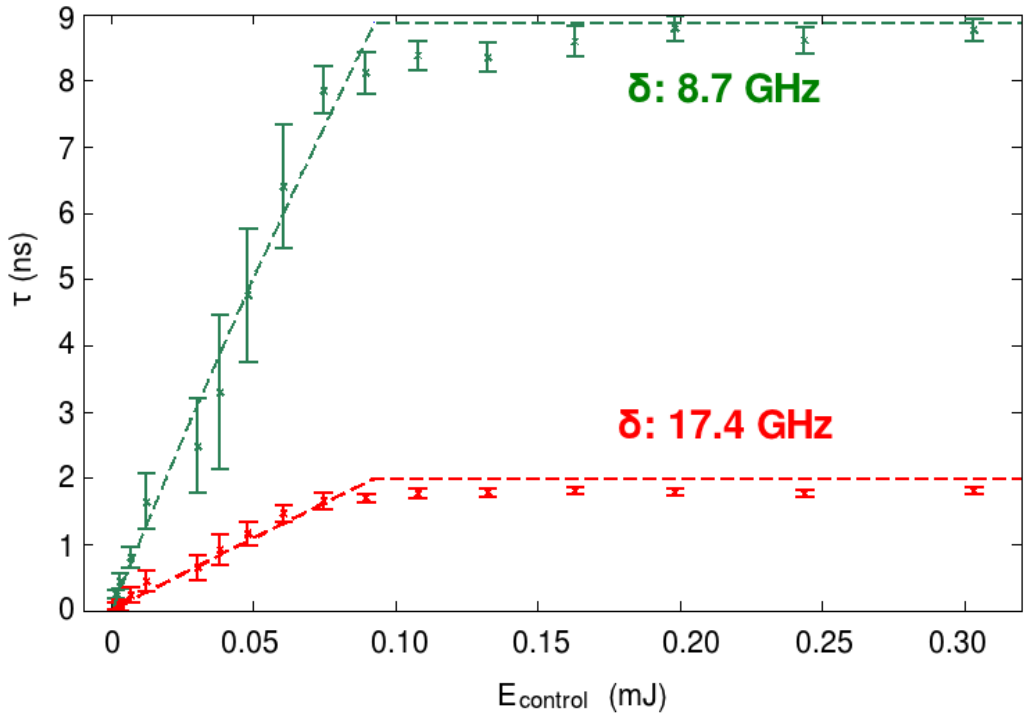

Figure II.12: Induced extra delay τ as a function of the control pulse energy for two detuning δ (8.7 GHz, in green, and 17.4 GHz, in red) and Δt=3 ns. The fits of the experimental data are presented as shaded lines.

2.3 Results

2.3.1 Temporal profiles

The sets of performed measurements can be showed highlighting the possibility of control with the three selected optical external parameters and showing the comparison with the analytic model described in Sec. (2.1.3).

Fig. (II.11) shows temporal profiles of probe pulses, with an initial temporal width of 3 ns, in vacuum propagation (in red) and in slow light for several control-probe time separations Δt: a = -3 ns, b = 6 ns, c = 24 ns, d = 54 ns, and e = 86 ns. A negative value of Δt means a partial temporal overlapping between the probe pulse and the control pulse. As expected, the probe pulses undergo to a larger extra induced delay in propagation and a compression as Δt becomes smaller. The absorption is not large enough to cause severe distortion of the probe pulse shape profile. From the results shown in this figure, it is evident that the population of the $|1\rangle$ state is still not negligible even after many times the natural lifetime (about ~16 ns). In fact for Δt greater than 80 ns, τ greater than 5 ns are still measured, whereas the transmission peak, due to absorption, is still around 40%. This is consistent with the picture of a fast spontaneous emission of a single atom combined with the long-living phenomenon of radiation trapping, as discussed in Sec. (2.1.3).

The (II.13), (II.14) and (II.15) can be evaluated with experimental and atomic parameter and

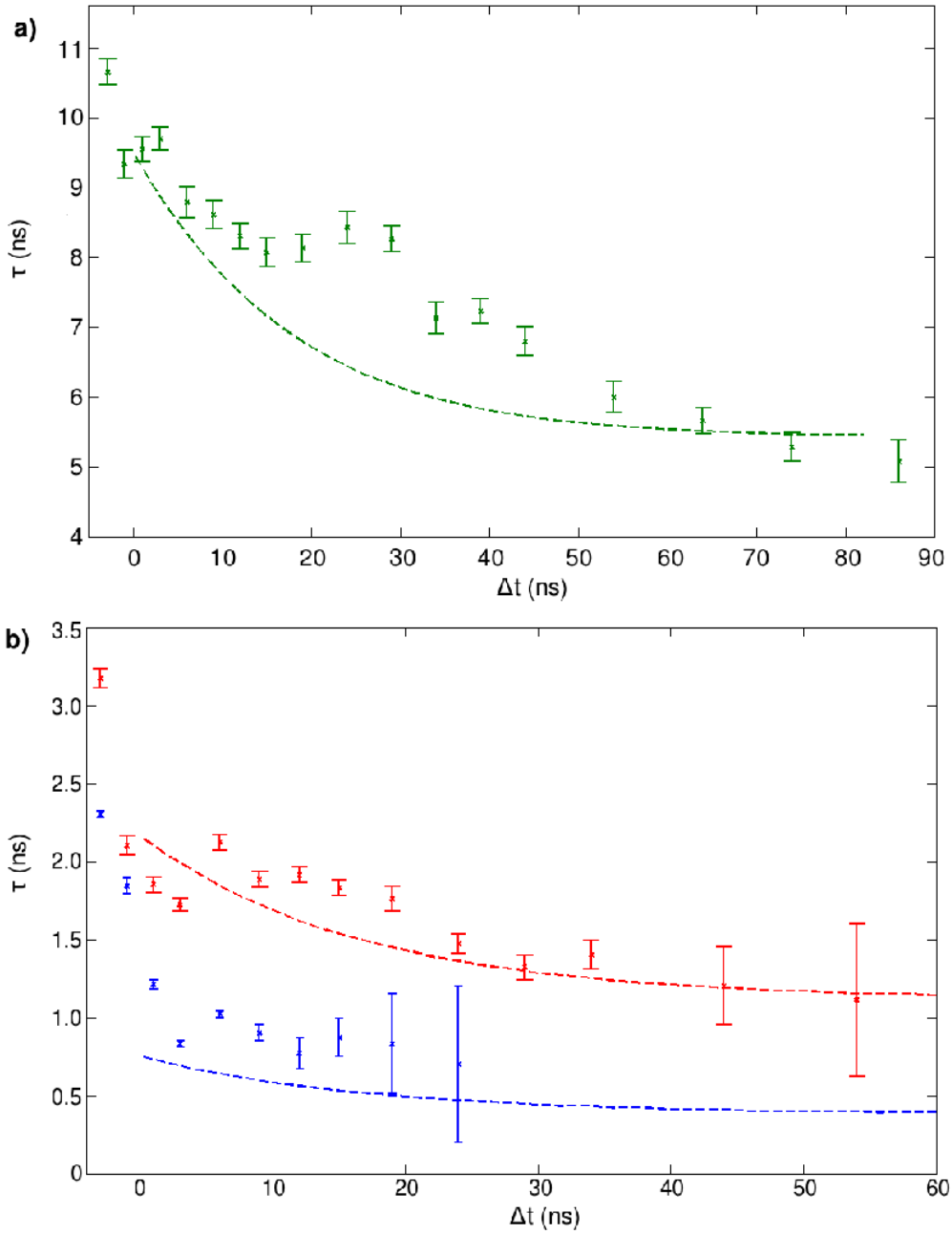

Figure II.13: Induced extra delay τ as a function of the temporal separation control-probe Δt for the detuning δ =8.7 GHz (Fig. (a), in green) and, in Fig. (b), δ of 17.4 GHz (in red) and 28.7 GHz (in blue) in condition of complete saturation of the medium. The fits of the experimental data are presented as shaded lines.

used to fit the experimental results.

$$L = \begin{cases} l\frac{E_c}{E_{sat}} & \text{for} \quad E_c < E_{sat} \\ l & \text{for} \quad E_c > E_{sat} \end{cases} \tag{II.20}$$

E_{sat} becomes a fit parameter to include in the expression (II.8) of the analytic model, in such

a way to express the population as a function of the energy of the control pulse. Another fit parameters are A, that weights the effect of the probe pulse into the cell. and N, that are varied around the value estimated by the (II.18) for the set temperature in the experiment (220°).

Table (II.1) shows the theoretical and experimental values for the transmission peak intensity for all the cases in Fig. (II.11), but the -3 ns-case, that can not be calculated in the analytic model due the temporal superposition between the control pulse and the probe pulse, as the hypothesis of incoherent interaction scheme requires. Hence, in the case of Δt=-3 ns, such a request is only partially satisfied and the equations of the analytic model cannot be rigorously applied.

Table II.1: Peak Intensity Transmission (*PIT*)

Δt (ns)	Theory (%)	Experim. (%)
6	29	30±3
24	38	39±4
54	36	32±3
86	36	39±4

2.3.2 Characterization and optical control

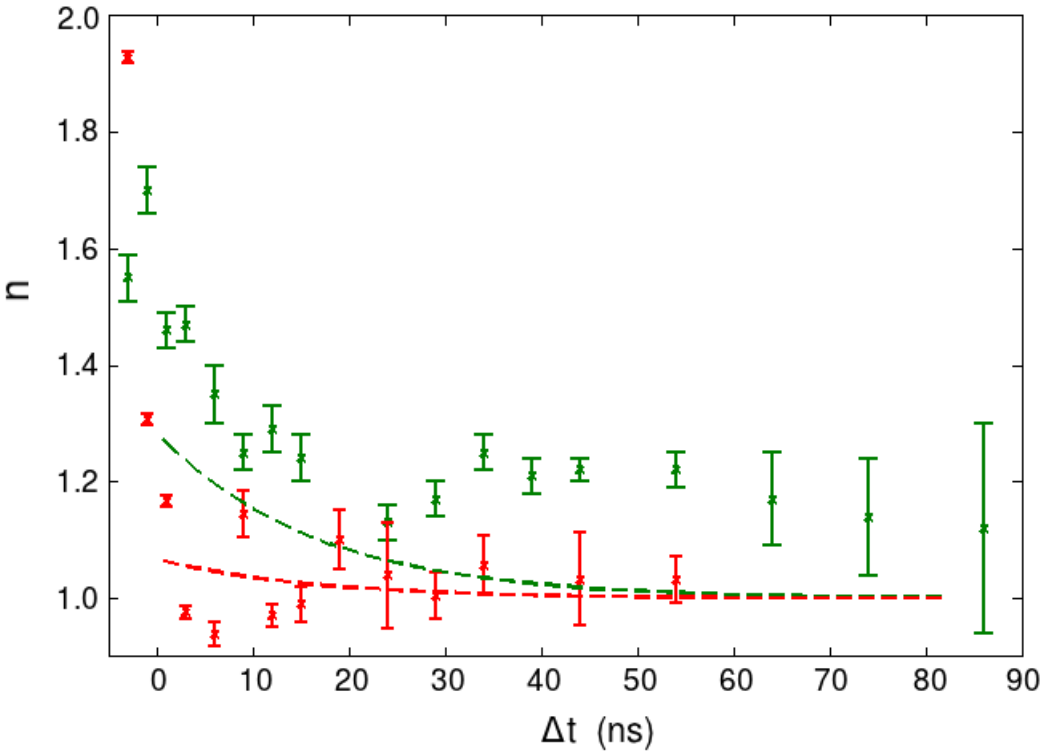

Figure II.14: Compression factor n as a function of the control-probe delay Δt for detuning δ of 17.4 GHz (in red) and 8.7 GHz (in green). The fits of the experimental data are presented as shaded lines.

Fig. (II.12) shows the extra induced delay as a function of the control pulse energy, that is one of the control parameter. The results are also dependent on the detuning δ, another parameter, whereas the temporal separation control-probe Δt is set to 3 ns. τ has a monotone behavior that approaches a constant value in correspondence of control pulse energies that lead to a complete saturation on the medium. In addition to demonstrate that the control pulse energy is a suitable control parameter, besides the detuning of the probe pulse frequency from resonance, these results are also in discrete agreement with the theoretical predictions.

In Fig. (II.13) the extra delay as a function of the control-probe separation is reported for three different values of the detuning and an energy of the control pulse (0.3 mJ) that ensures the saturation regime. In Fig. (II.14) the compression factor as a function of Δt is shown for two values of detuning. Therefore Δt is an external optical parameter that can be used to control the propagation dynamics of the probe pulse, in particular the extra induced delay and the compression factor. The compression factor n falls rapidly to 1 in a time comparable with the spontaneous emission lifetime of the atomic transition ($\sim$ 16 ns), because, when the radiation trapping becomes predominant, the population remains approximately constant during the probe pulse temporal duration (3 ns).

In conclusion, an experimental realization of a slow light propagation for optical probe pulse with a temporal duration of 3 ns has been realized and extra induced delays respect to the vacuum propagation up to $\sim$13 ns have been achieved, besides a compression factor up to $\sim$2. Three external optical parameters have been identified: the control pulse energy, the temporal separation between control pulse and probe pulse of the probe beam and the detuning from the transition atomic resonance frequency. Moreover, the originality of this work resides in the realization of such control on propagation dynamics by using an incoherent interaction scheme, that requests less critical constrains respect to other methods proposed in literature.

References

[1] M. V. Tognetti, E. Sali, S. Cavalieri, and R. Buffa. "Temporal pulse compression and retardation by incoherent all-optical control". In: *Phys. Rev. A* 81 (2010), p. 023807. DOI: 10.1103/PhysRevA.81.023807 (cited in pages 25, 27).

[2] E. Ignesti, F. Tommasi, R. Buffa, L. Fini, E. Sali, M. V. Tognetti, and S. Cavalieri. "Incoherent optical control of pulse propagation and compression". In: *Phys. Rev. A* 86 (2012), p. 063818. DOI: 10.1103/PhysRevA.86.063818 (cited in pages 25, 27).

[3] L. Casperson and A. Yariv. "Pulse Propagation in a High-Gain Medium". In: *Phys. Rev. Lett.* 26 (1971), pp. 293–295. DOI: 10.1103/PhysRevLett.26.293 (cited in page 26).

[4] D. Grischkowsky. "Adiabatic Following and Slow Optical Pulse Propagation in Rubidium Vapor". In: *Phys. Rev. A* 7 (1973), pp. 2096–2102. DOI: 10.1103/PhysRevA.7.2096 (cited in page 26).

[5] S. L. McCall and E. L. Hahn. "Self-Induced Transparency by Pulsed Coherent Light". In: *Phys. Rev. Lett.* 18 (1967), pp. 908–911. DOI: 10.1103/PhysRevLett.18.908 (cited in page 26).

[6] S. L. McCall and E. L. Hahn. "Self-Induced Transparency". In: *Phys. Rev.* 183 (1969), pp. 457–485. DOI: 10.1103/PhysRev.183.457 (cited in page 26).

[7] R. E. Slusher and H. M. Gibbs. "Self-Induced Transparency in Atomic Rubidium". In: *Phys. Rev. A* 5 (1972), pp. 1634–1659. DOI: 10.1103/PhysRevA.5.1634 (cited in page 26).

[8] Q.-H. Park and R. W. Boyd. "Modification of Self-Induced Transparency by a Coherent Control Field". In: *Phys. Rev. Lett.* 86 (2001), pp. 2774–2777. DOI: 10.1103/PhysRevLett.86.2774 (cited in page 26).

[9] M. Fleischhauer, A. Imamoglu, and J. P. Marangos. "Electromagnetically induced transparency: Optics in coherent media". In: *Rev. Mod. Phys.* 77 (2005), pp. 633–673. DOI: 10.1103/RevModPhys.77.633 (cited in pages 26, 27).

[10] K.-J. Boller, A. Imamoglu, and S. E. Harris. "Observation of electromagnetically induced transparency". In: *Phys. Rev. Lett.* 66 (1991), pp. 2593–2596. DOI: 10.1103/PhysRevLett.66.2593 (cited in page 26).

[11] S. E. Harris, J. E. Field, and A. Kasapi. "Dispersive properties of electromagnetically induced transparency". In: *Phys. Rev. A* 46 (1992), R29–R32. DOI: 10.1103/PhysRevA.46.R29 (cited in page 26).

[12] G. Alzetta, A. L. Gozzini, L. Moi, and O. G. "An experimental method for the observation of R.F. transitions of laser beat resonances in oriented Na vapor". In: *Il Nuovo Cimento B* 36 (1) (1976), p. 5 (cited in page 26).

[13] O. Kocharovskaya and Y. Khanin. "Population trapping and coherent bleaching of a three-level medium by a periodic train of ultrashort pulses [*Zh. Eksp. Teor. Fiz.* 90, 1610-1618 (1986)]". In: *Sov. Phys. JETP* 63 (1986), p. 945 (cited in page 26).

[14] A. Kasapi, M. Jain, G. Y. Yin, and S. E. Harris. "Electromagnetically Induced Transparency: Propagation Dynamics". In: *Phys. Rev. Lett.* 74 (1995), pp. 2447–2450. DOI: 10.1103/PhysRevLett.74.2447 (cited in page 26).

[15] D. F. Phillips, A. Fleischhauer, A. Mair, R. L. Walsworth, and M. D. Lukin. "Storage of Light in Atomic Vapor". In: *Phys. Rev. Lett.* 86 (2001), pp. 783–786. DOI: 10.1103/PhysRevLett.86.783 (cited in page 26).

[16] R. Buffa, S. Cavalieri, and M. V. Tognetti. "Coherent control of temporal pulse shaping by electromagnetically induced transparency". In: *Phys. Rev. A* 69 (2004), p. 033815. DOI: 10.1103/PhysRevA.69.033815 (cited in page 26).

[17] M. V. Tognetti, E. Sali, S. Cavalieri, and R. Buffa. "Temporal pulse compression and retardation by incoherent all-optical control". In: *Phys. Rev. A* 81 (2010), p. 023807. DOI: 10.1103/PhysRevA.81.023807 (cited in page 26).

[18] E. Ignesti, R. Buffa, L. Fini, E. Sali, M. V. Tognetti, and S. Cavalieri. "Controlling the spectrum of light pulses by dynamical electromagnetically induced transparency". In: *Phys. Rev. A* 83 (2011), p. 053411. DOI: 10.1103/PhysRevA.83.053411 (cited in page 26).

[19] L. V. Hau, S. E. Harris, Z. Dutton, and C. H. Behroozi. "Light speed reduction to 17 metres per second in an ultracold atomic". In: *Nature* 397 (1999), pp. 594 –598. DOI: http://dx.doi.org/10.1038/17561 (cited in page 26).

[20] C. Liu, Z. Dutton, C. H. Behroozi, and L. V. Hau. "Observation of coherent optical information storage in an atomic medium". In: *Nature* 409 (2001), pp. 490 –493. DOI: http://dx.doi.org/10.1038/35054017 (cited in page 26).

[21] M. S. Bigelow, N. N. Lepeshkin, and R. W. Boyd. "Observation of Ultraslow Light Propagation in a Ruby Crystal at Room Temperature". In: *Phys. Rev. Lett.* 90 (2003), p. 113903. DOI: 10.1103/PhysRevLett.90.113903 (cited in page 26).

[22] M. S. Bigelow, N. N. Lepeshkin, and R. W. Boyd. "Superluminal and Slow Light Propagation in a Room-Temperature Solid". In: *Science* 301.5630 (2003), pp. 200–202. DOI: 10.1126/science.1084429 (cited in page 26).

[23] F. Arrieta-Yánez, O. G. Calderón, and S. Melle. "Slow and fast light based on coherent population oscillations in erbium-doped fibres". In: *Journal of Optics* 12.10 (2010), p. 104002 (cited in page 26).

[24] S. E. Schwarz and T. Y. Tan. "Wave interactions in saturable absorber". In: *Appl. Phys. Lett.* 10.1 (1967), pp. 4–7. DOI: http://dx.doi.org/10.1063/1.1754798 (cited in page 26).

[25] L. Thévenaz. "Slow and fast light in optical fibres". In: *Nat. Photon.* 2.8 (2008), pp. 1749–4885. DOI: http://dx.doi.org/10.1038/nphoton.2008.147 (cited in page 26).

[26] K. Y. Song, M. G. Herráez, and L. Thévenaz. "Long optically controlled delays in optical fibers". In: *Opt. Lett.* 30.14 (2005), pp. 1782–1784. DOI: 10.1364/OL.30.001782 (cited in page 26).

[27] R. Pant, M. D. Stenner, M. A. Neifeld, and D. J. Gauthier. "Optimal pump profile designs for broadband SBS slow-light systems". In: *Opt. Express* 16.4 (2008), pp. 2764–2777. DOI: 10.1364/OE.16.002764 (cited in page 26).

[28] Y. Okawachi, M. S. Bigelow, J. E. Sharping, Z. Zhu, A. Schweinsberg, D. J. Gauthier, R. W. Boyd, and A. L. Gaeta. "Tunable All-Optical Delays via Brillouin Slow Light in an Optical Fiber". In: *Phys. Rev. Lett.* 94 (2005), p. 153902. DOI: 10.1103/PhysRevLett.94.153902 (cited in page 26).

[29] J. Sharping, Y. Okawachi, and A. Gaeta. "Wide bandwidth slow light using a Raman fiber amplifier". In: *Opt. Express* 13.16 (2005), pp. 6092–6098. DOI: 10.1364/OPEX.13.006092 (cited in page 26).

[30] G. Fanjou and S. Thibaut. "All-optical tunable pulse frequency chirp via slow light". In: *Opt. Lett.* 34.24 (2009), pp. 3824–3826. DOI: 10.1364/OL.34.003824 (cited in page 26).

[31] T. Baba. "Slow light in photonic crystals". In: *Nat. Photon.* 2.8 (2008), pp. 465–473. DOI: http://dx.doi.org/10.1038/nphoton.2008.146 (cited in page 26).

[32] T. Krauss. "Slow light in photonic crystal waveguides". In: *Journal of Physics D Applied Physics* 40.9 (2007), p. 2666. DOI: doi:10.1088/0022-3727/40/9/S07 (cited in page 26).

[33] R. M. Camacho, M. V. Pack, and J. C. Howell. "Slow light with large fractional delays by spectral hole-burning in rubidium vapor". In: *Phys. Rev. A* 74 (2006), p. 033801. DOI: 10.1103/PhysRevA.74.033801 (cited in page 26).

[34] R. M. Camacho, M. V. Pack, J. C. Howell, A. Schweinsberg, and R. W. Boyd. "Wide-Bandwidth, Tunable, Multiple-Pulse-Width Optical Delays Using Slow Light in Cesium Vapor". In: *Phys. Rev. Lett.* 98 (2007), p. 153601. DOI: 10.1103/PhysRevLett.98.153601 (cited in page 26).

[35] T. Holstein. "Imprisonment of Resonance Radiation in Gases". In: *Phys. Rev.* 72 (1947), pp. 1212–1233. DOI: 10.1103/PhysRev.72.1212 (cited in page 27).

[36] W. Demtröder. *Laser Spectroscopy: Basic Concepts and Instrumentation*. Advanced texts in physics. Springer, 2003. ISBN: 9783540652250 (cited in page 31).

[37] O. Svelto. *Principles of Lasers*. Springer, 2010. ISBN: 9781441913029 (cited in page 33).

[38] C. Davis. *Lasers and Electro-optics: Fundamentals and Engineering*. Cambridge University Press, 1996. ISBN: 9780521484039 (cited in page 33).

[39] P. Browning and P. Potter. "An assessment of the experimental determined vapour pressures of the liquid alkali metals". In: *Ohse R.W. (ed.) Handbook of Thermodynamic and Transport Properties of Alkali Metals* (1985), pp. 349–358 (cited in page 34).

[40] J. Fink and L. Leibowitz. "Enthalpy, entropy and specific heat-data assessment". In: *Ohse R.W. (ed.) Handbook of Thermodynamic and Transport Properties of Alkali Metals* (1985), pp. 441–434 (cited in page 34).

[41] V. Sobolev. "Database of thermophysical properties of liquid metal coolants for GEN-IV". In: *2 ed.- Mol, Belgium: SCK•CEN (Open Report of the Belgian Nuclear Research Centre; BLG-1069)* (2011) (cited in page 34).

Further reading

[42] R. W. Boyd and D. J. Gauthier. “Controlling the Velocity of Light Pulses”. In: *Science* 326.5956 (2009), pp. 1074–1077. DOI: 10.1126/science.1170885.

[43] R. W. Boyd and D. J. Gauthier. “Chapter 6 “Slow” and “fast” light”. In: ed. by E. Wolf. Vol. 43. Progress in Optics. Elsevier, 2002, pp. 497 –530. DOI: http://dx.doi.org/10.1016/S0079-6638(02)80030-0.

[44] P. W. Milonni. *Fast Light, Slow Light and Left-Handed Light*. Series in Optics and Optoelectronics. Taylor & Francis, 2004.

[45] S. E. Harris. “Electromagnetically Induced Transparency”. In: *Physics Today* 50 (1997), pp. 36–42. DOI: http://dx.doi.org/10.1063/1.881806.

Chapter III

Fast-Light and Recovering the Propagation Delay

In this chapter the experimental realization of fast light propagation by using an incoherent interactions scheme is presented (Sec. (3.1)). Then, in Sec. (3.3) the possibility of recovering a previously induced delay with a superluminal propagation is described.

Sec. (3.1.1) is devoted to summarize the experimental methods for achieving fast light propagation. In Sec. (3.1.2) and Sec. (3.2) is described how the incoherent interaction scheme can be arranged in order to induce superluminal group velocities. In Sec. (3.3.2) results, published in Physical Review A *[1], are presented.*

Sec. (3.3.1) is devoted to the possibility to include the slow and fast propagation modes in the same experimental set-up and Sec. (3.3.2) describes as this proposal has been realized. Finally, Sec. (3.3.3) shows that the recover of a delay is possible and that the "true" c-velocity, i.e. a traveling speed for a signal that reaches the optical front in propagation, can be approached. The results have been published in Optics Express *[2].*

In the realization of this experiment I worked in the experimental set-up arrangement and method and I wrote the software of data analysis. I also contributed in the numerical model and in the the scientific papers.

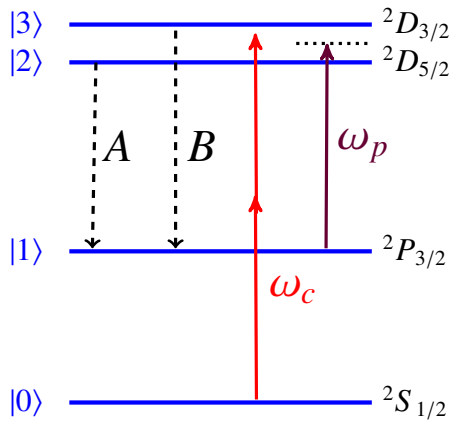

Figure III.1: Schematic diagram of the involved transitions and sodium atomic levels. The control pulse central frequency ω_c is resonant with the two-photons transition between the level $|0\rangle$ and the D-doublet, whereas the frequency ω_p of the probe pulse is detuned by a variable quantity from the transitions $|2\rangle \rightarrow |1\rangle$ and $3\rangle \rightarrow |1\rangle$. The transitions A and B are also shown.

3.1 Fast light group velocity

3.1.1 Experimental methods

As discussed in Sec. (1.3.3), the fast light group velocity has been affected by misunderstanding, but is completely meaningful as a definition of speed of a modulation envelope of an optical pulse [3–10].

In 1970, the first analytic estimation of superluminal group velocity, without distortion, in anomalous dispersion zone of an absorbing medium for Gaussian pulse has been reported [11]. Later, a confirmation of such an analysis has been presented, measuring the phase information of a laser beam that propagates within an A-exciton line of GaP:N [12].

The possibility of achieve superluminal propagation when the limited-bandwidth wave packet travels in a gain medium has been proposed in 1990s by R. Y. Chiao[13, 14]. A gain doublet exhibits larger anomalous dispersion zones, due the closely spaced resonances, that make the dispersion curve much smoother. A large anomalous dispersion zone allows to reduce the distortion, due to the derivative with respect to frequency of order higher than one of the dispersion curve.

Table III.1: Radiative transition between the levels of the doublet ($|2\rangle =^2 D_{5/2}$ and $|3\rangle =^2 D_{3/2}$) and the level $^2P_{3/2}$.

	Transition	Wavelength (pm)	Lifetime (ns)
A	$\|2\rangle \rightarrow \|1\rangle$	819707.7	19.5
B	$\|3\rangle \rightarrow \|1\rangle$	819704.3	117

The first clear fast light propagation with low distortion and with small change in amplitude has been reported in 2000 [15] by Wang, Kuzmich and Dogariu. The scheme was based on a

gain doublet in Cesium vapor excited by two cw Raman pump beams. For a Gaussian pulse of temporal duration of 3.7 μs an advance respect to the vacuum propagation of 62 ns has been measured, with a negative group velocity $v_g = -c/300$.

In 2003, Stenner, Gauthier and Neifeld measured an advance of 27.4 ns for a pulse with temporal duration of 263.4 ns, using a gain doublet in potassium vapor [16].

In this work, as a remarkable difference, in addition to the different proposed interactions scheme, the optical pulse (3 ns long) is almost of one magnitude shorter than the previous cases reported in literature.

3.1.2 Interactions scheme and numerical simulation

The interaction scheme used for the realization of fast light propagation is based on incoherent interactions [17, 18] discussed in the previous chapter (Sec. (2.1.2)). Hence the desired dispersive properties in the medium are provided by a control pulse and, once such an interaction is over, a subsequent co-propagating probe pulse experiences modification in propagation.

A schematic diagram of the involved interactions is reported in Fig. (III.1): The control pulse frequency is tuned in such a way to populate, from the ground level $|0\rangle = {}^2P_{3/2}$ by a two photons transition both levels of the D-doublet of sodium $|2\rangle =^2 D_{5/2}$ and $|3\rangle =^2 D_{3/2}$, thanks broad band (30-GHz FWHM). A population inversion is then established between the levels of the doublet and the level $|1\rangle^2P_{3/2}$ (Table (III.1)).

The probe pulse has an intensity weak enough to leave the population unaffected by its propagation. The presence of the doublet guaranties two large bandwidth anomalous dispersion zones, that are localized in the center of the doublet ($\sim$ 819706 pm) and around 819710 pm. The frequency of the control pulse in tuned to explore such spectral zones. The different radiative lifetimes of the two atomic transitions cause an asymmetry in gain and refractive index curve respect to the center of the doublet, with a larger weight played by the transition A.

In order to compare the experimental data with the theoretical predictions, a numerical model based on propagation equation in an inverted medium has been realized.

The numerical simulation, in order to considerably reduce the computational times, works in the frequency domain; as a consequence the population of the medium during the temporal width of the pulse is considered as "frozen", i.e. the decay of the population during this time ($\sim$ 3 ns) is neglected. Then, the calculation is not able to take into account the eventual temporal compression or broadening of the pulse. Then the population is considered as constant and determined by the decay time during the time delay Δt between the control pulse and the probe pulse. In the matrix density formalism, the population found by the probe pulse is the following:

$$\rho_{ii} = \rho^0 \exp \Gamma_i(\Delta t - z/c) \tag{III.1}$$

where the index i assumes value equal to 2 and 3 for the level $|2\rangle$ and $|3\rangle$ respectively, Γ_i is the radiative decay time of the level i and z the coordinate inside the medium.

The field of the probe pulse in correspondence of the entrance in medium ($z = 0$) is:

$$E(z = 0, t) = \mathcal{E}(z = 0, t) \exp(-\mathrm{i}\omega_p t) \tag{III.2}$$

where $\mathcal{E}$ is the time dependent functional form of the field amplitude in $z = 0$. Once propagated for a length z:

$$E(z, t) = e^{-\mathrm{i}\omega_p t} \int_{-\infty}^{+\infty} d\omega' \tilde{\mathcal{E}}(0, \omega') \mathrm{e}^{\mathrm{i}(kz - \omega' t)} \tag{III.3}$$

where $\tilde{\mathcal{E}}$ is the Fourier transform of the field amplitude. The wave vector k in a medium with atomic density N is the following:

$$\kappa(\omega = \omega_p + \omega') = \frac{\omega_p + \omega'}{c} + \sum_{j=2}^{3} \frac{N\omega}{4\hbar\epsilon_0 c} \left\langle \frac{{d_{1j}}^2 \rho_{jj}}{i\gamma_j - (\omega_p v/c + \omega' + \delta_j)} \right\rangle_v \tag{III.4}$$

where γ_i and δ_i represent, respectively, all kinds of dephasing rates and the detuning of ω_p from the $|i\rangle \rightarrow 1$ transition, whereas the d_{1i} are the electric dipole moments. The brackets represent the average over the Doppler velocity distribution, based on experimental parameters. Fig. (III.2) shows an example of the dispersion and gain profile calculated numerically and after

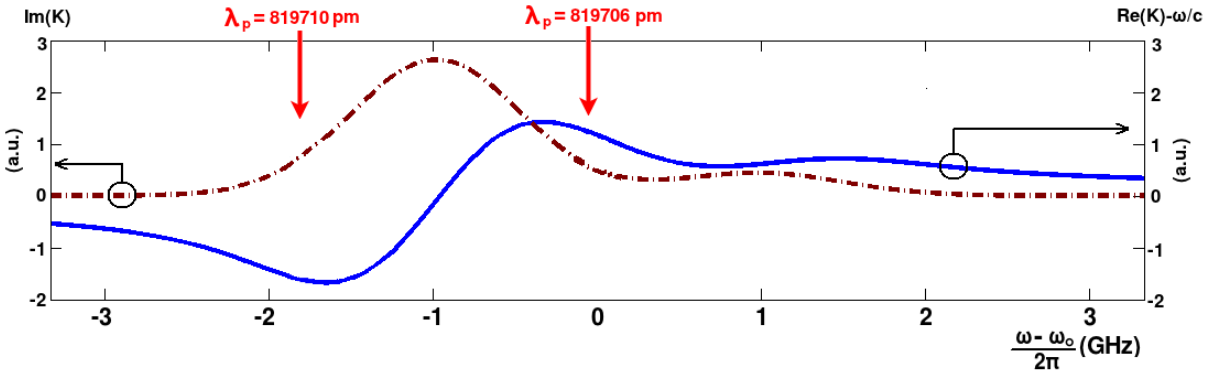

Figure III.2: Profile of real and imaginary part of k evaluated by equation (III.4). The Doppler effect is taken into account.

averaging over the Doppler velocity distribution, using experimental parameters. The atomic density at a given temperature is evaluated using the (II.18) (see Sec. (2.2.3)).

The numerical solution of the (III.3) is based on a Discrete Fourier Transform (DFT) technique , computed by a Fast Fourier Transform (FFT) algorithm.

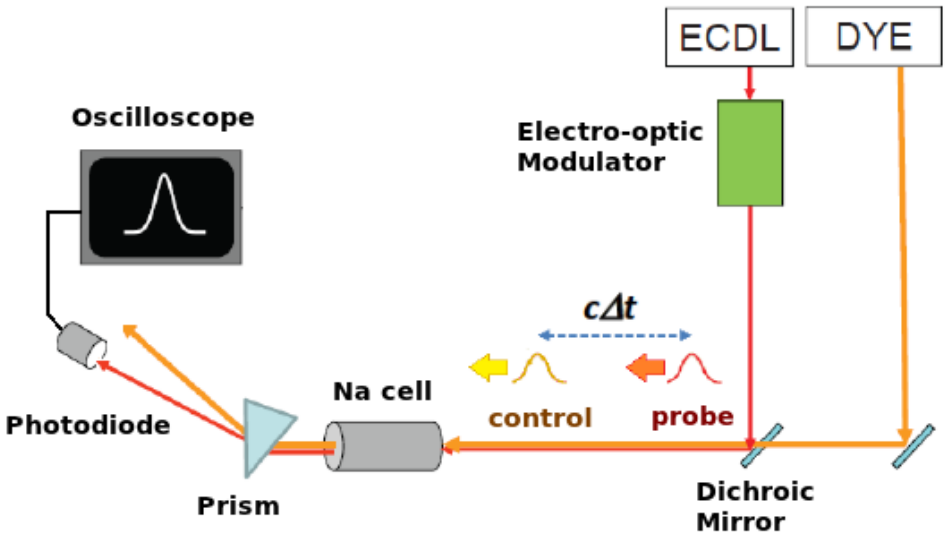

Figure III.3: Schematic diagram of the experimental set-up.

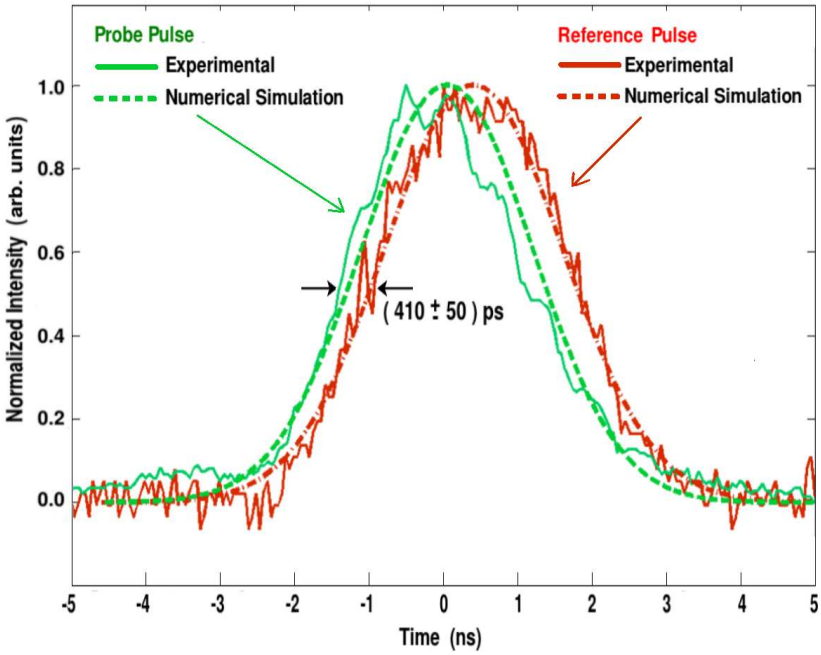

Figure III.4: Typical normalized temporal profiles of the probe pulse (in green) and the reference pulse (propagation in vacuum) in red. The continuous lines are the experimental pulses and the dashed ones the numerical simulation. The wavelength of the probe pulse is 819710 pm. The advance respect the vacuum propagation experimentally is 410±50 ps and the amplification factor 5.4.

The knowledge of ρ^0 in the (III.1) and (III.4) is not directly obtainable with a sufficient accuracy by the knowledge of the experimental parameters. Therefore, an indirect way to estimate such a parameter consists in looking at the advance as a function of amplification: ρ^0 as a function of pulse control energy can be estimated as the value that in the simulations determine an amplification factor of the signal equal to the measured one for a given energy.

3.2 Experimental set-up and methods

The experimental set-up (Fig. (III.3)) is the same described in Sec. (2.2), with some differences due to the different atomic involved interactions . The control pulse (Sec. (2.2.2)) of 4 ns duration is provided by a dye laser pumped by a Q-switched Nd:YAG at a repetition rate of 10 Hz. In order to tune the central frequency at the desired two photons resonance, the used dye is Blue Nile dissolved in methanol.

The probe pulse is derived by a single-mode extended cavity cw diode laser (Sec. (2.2.1)) tuned at quasi resonance with the transitions A and B described in the previous section. The electro-optic modulator driven by the electric pulse generator create a pulse of duration of 3 ns. The path is collinear to that of the control pulse and the systems of generation and acquisition of signals are the same described in the section Sec. (2.2.4) and Sec. (2.2.5) respectively. The temporal profiles are acquired shot-to-shot to collect a large number of data is collected for the same Δt and detuning δ of the probe pulse frequency from the center of the D-doublet. The temperature of the sodium cell (Sec. (2.2.3)) is set to 220°C.

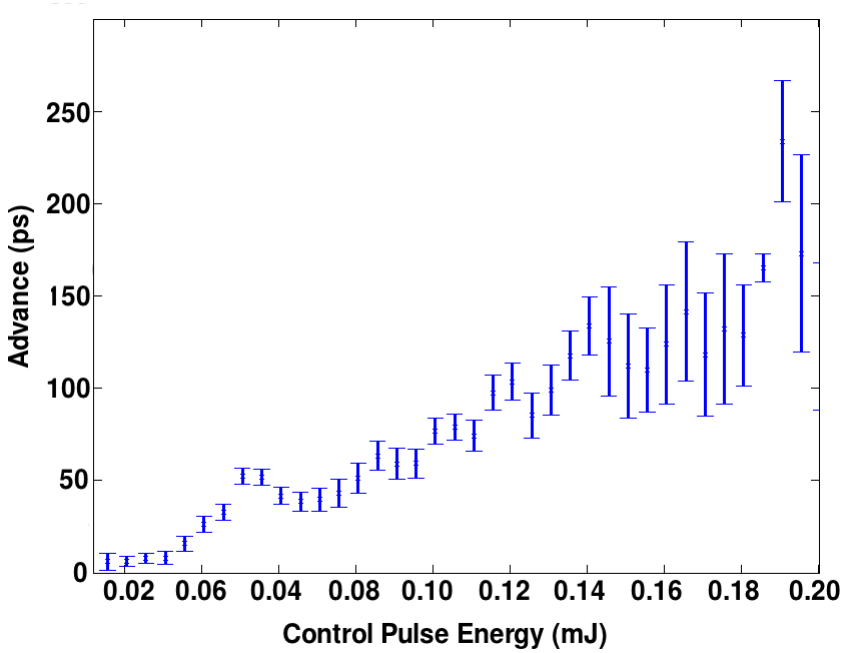

Figure III.5: Probe pulse advance respect the vacuum propagation as a function of the control pulse energy for λ_p=819706 pm.

The double pulse method is used again (Sec. (2.2.5)). Then, the reference pulse (propagation in vacuum) is the virtual reference pulse re-build via software shot-to-shot.

A remarkable difference respect to the slow light case consists in the impossibility to reach a large population inversion or a saturation condition. Indeed, in an inverted medium *amplified spontaneous emission (ASE)* [1] can occurs if a large population inversion and a preferential path of emission is provided. When the control pulse excites the medium some photons are spontaneously emitted near the entrance window of the cell; those emitted along the direction that coincides with the probe pulse can experience a large amplification. Such laser-like emission emission cause a depopulation of the medium and an emission that temporally and spectrally is overlapped to the signal. Then, ASE is a undesired effect that can mask the probe pulse profile and tends to be much frequent as the energy stored in the medium increases.

The found solution involves a limit in energy of the control pulse and required an *a posteriori* discrimination of the data acquired. Such a discrimination consists in algorithms in the automatic temporal profiles analysis that are based on the temporal form of the signal and in the time of arrival to the detector. Indeed the ASE radiation is triggered soon after the propagation of the control pulse, it is in general more energetic than the probe pulse, it has a larger temporal duration and it exhibits large oscillation.

3.2.1 Results

Fig. (III.4) shows typical normalized temporal profiles of a probe pulse and the reference for a central wavelength of λ_p=819710 pm. The continuous lines are experimental pulses, whereas the dashed ones are calculated by the numerical simulation by using the experimental parameters. The advance reported in this case is 410±50 ps respect the vacuum propagation,

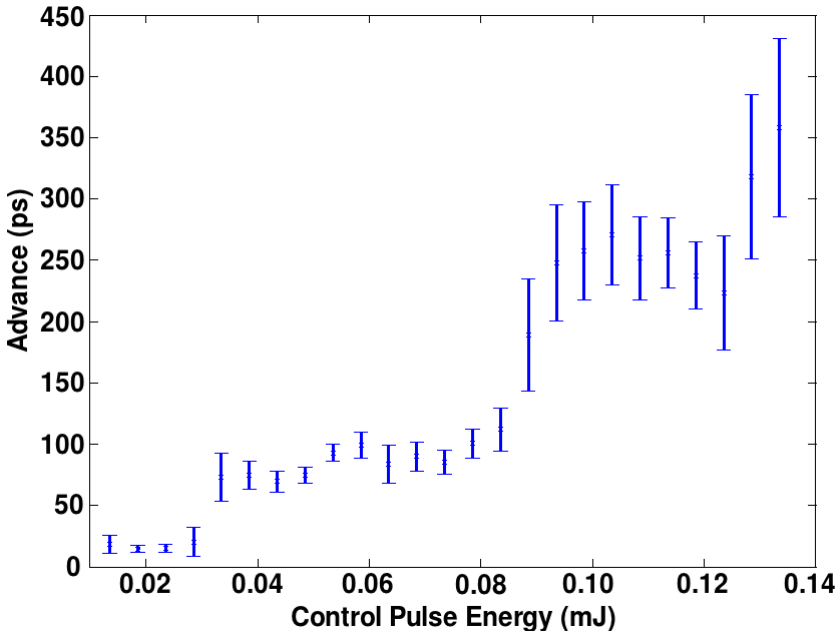

Figure III.6: Probe pulse advance respect the vacuum propagation as a function of the control pulse energy for λ_p=819710 pm.

with a factor of amplification of 5.4. The advance measurement is based on the time at which the signal intensity reaches the half of its peak value and the error comes from the average within the pulses that correspond to a certain interval in the control pulse energy binning.

In Fig. (III.5) and Fig. (III.6) the advance is reported as a function of control pulse energy for probe wavelength of 819706 pm and 819710 pm respectively. The discrimination during data analysis leads to reject a larger number of data as the energy of the control pulse increases, i.e. when ASE emission becomes more probable, leading to a lower accuracy in measurements that correspond to these ranges of energies. However, the monotone increment of the advance as the control pulse increases is evident, as the dependence on the detuning of the probe pulse frequency from the center of the *D*-doublet.

In Fig. (III.7) the advance as a function of energy is shown again for λ_p=819706 pm and different delay between probe and control pulse in entrance into the sodium cell. The monotone increment with control pulse energy decreases its slope as Δt increases. Indeed, as Δt increases the population of the *D*-doublet decays and the level $^2P_{3/2}$ becomes much populated causing that the population inversion rapidly decreases. Therefore, in addition to the control pulse energy, Δt represents, as in the slow light case, a second optical parameter of control on the group velocity.

Finally Fig. (III.8) shows the comparison between the numerical simulation and experimental data for λ_p=819710 pm. The numerical simulation, that are calculated using the experimental parameters, are in good agreement with data.

In conclusions, fast light propagation has been achieved by means of an incoherent interactions scheme and advances of the 3 ns long probe pulse respect the vacuum propagation up to 400 ps have been measured. The temporal duration used of the probe pulse is at least one order of magnitude smaller than in the cases previously reported in literature at our knowledge.

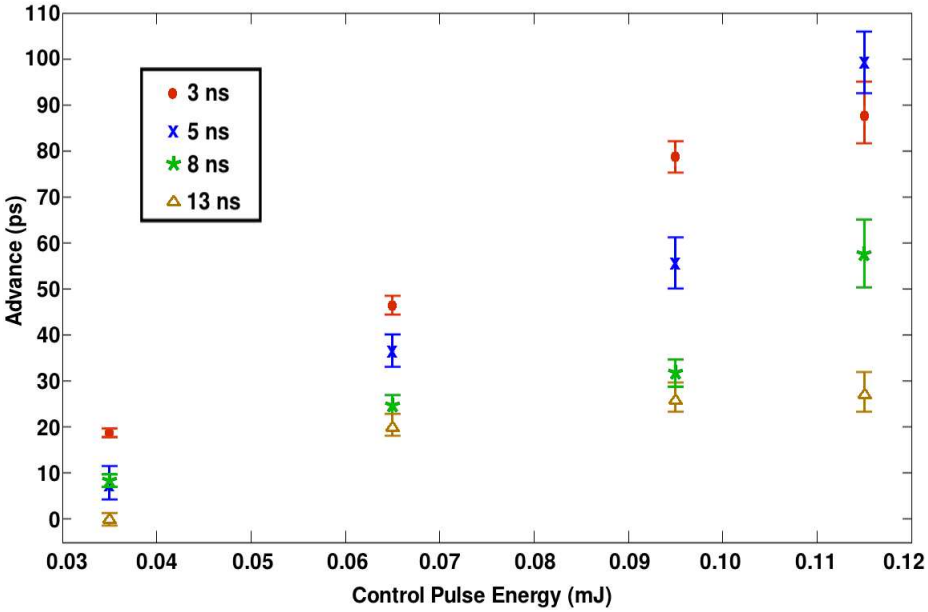

Figure III.7: Probe pulse advance respect to the vacuum propagation as a function of the control pulse energy for λ_p=819706 pm and for different values of probe-control temporal separation Δt.

3.3 Recovering the delay of a optical pulse

3.3.1 Fast and slow light propagation

In Chap. (II) and in Sec. (3.1) d the experimental realization of slow light and fast light respectively with an incoherent interaction scheme have been described. A first question that can arise from these results can be to which extent a propagation delay of an optical pulse can be recovered by means of a fast light stage.

Moreover, an intriguing question arise from experimental results on slow and fast light propagation: how does the group velocity depend on the propagation history of the pulse? And what about the limit in advance respect to the vacuum propagation? In Sec. (1.3) it has been discussed how the causality establishes a limit to the group velocity that a pulse can exhibit, by means of the optical front propagation speed. As a simplified picture, one can image that a pulse in superluminal propagation "piles-up" to the front as the modulation envelope speed increases. Does exist a method that allow to circumvent such a "cruise control" on the group velocity? Then the answer can be provided if an extra delay is induced to a pulse before its entrance in the fast light stage. Since the propagation of the optical front does not depend on the traversed media, one can suggest that in this case the group pulse has a larger delay to recover before it is limited in speed by causality reasons.

In literature, researchers reported experimental schemes that are able to achieve both fast and slow light propagation. Slow or fast light propagation in the same medium has been obtained in a waveguide overcoupled to microring resonators [19, 20], by coherent population oscillations in chromium ions in an alexandrite crystal at room temperature [21], coherent population oscillation in erbium-doped fibers [22] in a $Er3^+$ /$Yb3^+$ co-doped single-mode phosphate glass fiber [23] and by optically controlled stimulated Brillouin scattering [24].

Something similar to the inclusion of fast and slow propagation in the same experimental

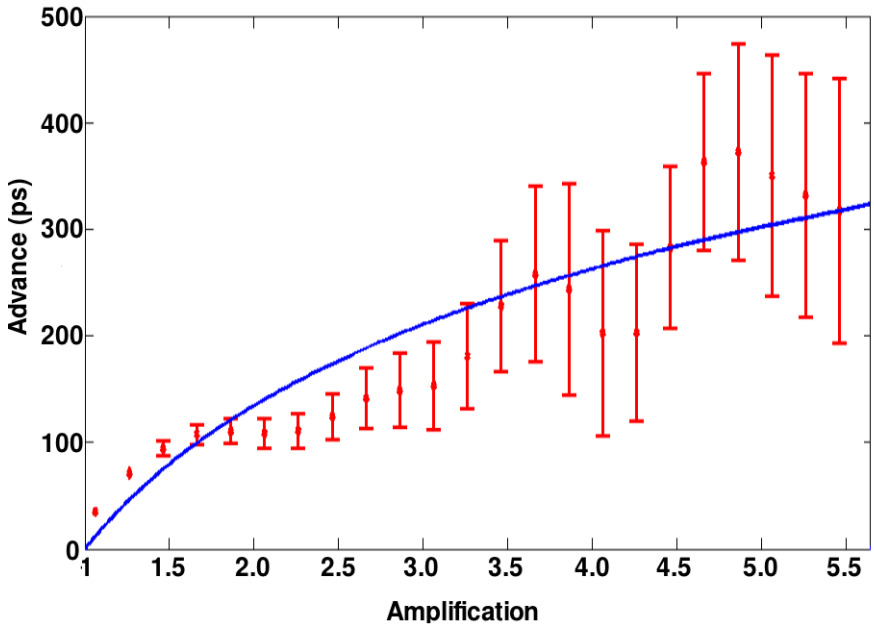

Figure III.8: Comparison between numerical simulation and experimental data for λ_p=819710 pm.

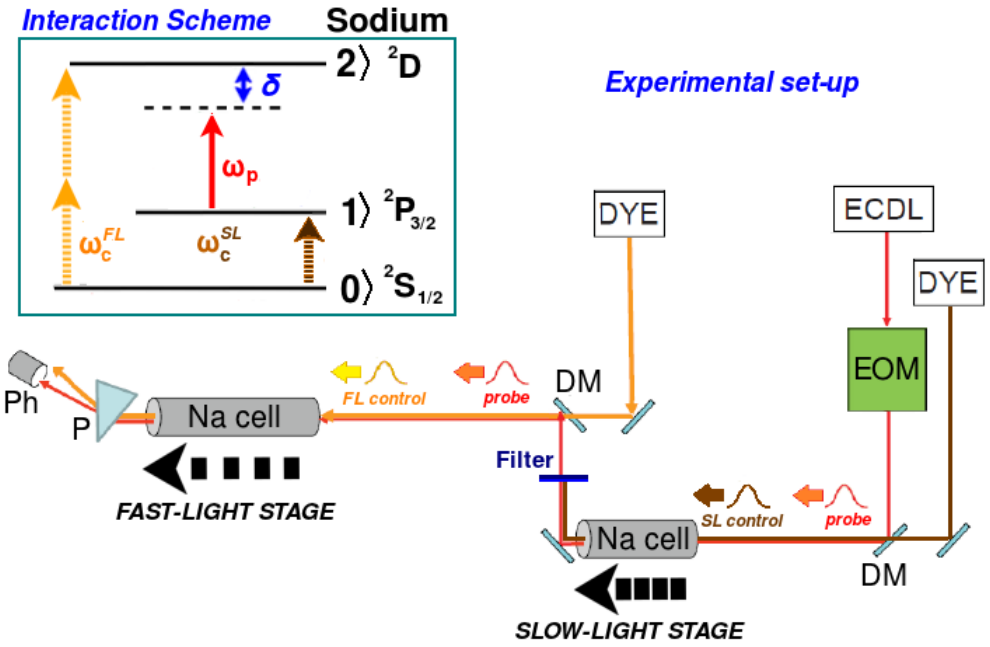

Figure III.9: Experimental set-up for recovering the delay of a optical pulse. In the upper-left of the figures the interactions scheme diagram is reported.

setup has been reported since 2012 and concerns a fascinating correlated topic and research line; nonlinear process of Bragg scattering via four-wave mixing has been used to achieve a first experimental realization of a *temporal cloaking device*, consisting in a temporal gap of 50 ps that is able to cancel detectability of a event, consisting in a nonlinear generation of new frequencies due interaction between a probe beam and a short pump pulse via four-wave mixing

[25] (see also [26]). Similar effects have been reported in the aim of find applicability in data transmission and cryptography [27, 28].

3.3.2 Experimental setup and scheme

Concerning the works reported in this thesis, a rearrangement of the experimental set-up, shown in Fig. (III.9) allowed to achieve both the propagation modes for the same probe pulse. In the following text, the abbreviations FL and SL are used to label experimental stages for fast light and slow light propagation respectively. The term "stage" means a part of the experimental set-up composed by a cell filled by the sodium vapor and a control pulse, whose frequency is tuned in such a way to realize the desired effect. Hence, an inhibition of a control pulse causes to switch-off the corresponding stage.

With reference to Fig. (III.9), two sodium cells are used besides two different dye lasers, Rhodamine 6G for the laser with frequency ω_c^{SL} and Blue Nile for the one of frequency ω_c^{fL}, pumped by the same frequency-doublet Q-switched Nd:YAG. The probe pulse path is arranged in such a way to propagate inside the volume of the media excited by the control pulses. A dichroic filter is set after the SL stage and before the FL stage, in order to prevent to the remnant of the control pulse of frequency ω_c^{SL} to reach the next stage, leaving the probe pulse unaffected. At the output of the FL stage, a prism prevents the control pulse of frequency ω_c^{FL} to reach the detector. The energy of the control pulse for the SL stage is set to a constant value to maintain the cell population stable and fixed shot-to-shot. On the contrary, the energy of the other control pulse is tuned during the measurement and the energy of each shot is collect by means of a semi-transparent plate and a photo-diode. This photo-diode is connected to the oscilloscope, that measures the temporal profile to estimate the energy by calculation of the integral and by the knowledge of the reflection coefficient of the semi-transparent plate.

From temporal point of view, each single shot is started by the control unit of the Nd:YAG, that sends a trigger signal to the electric pulse generator for the generation of the control pulse, using the double-pulse method and contemporaneously generate the pump pulse for the dye laser systems. The path of the control pulses is conveniently extended in order to send them into each stage with a desired temporal advance respect the entrance in the medium of the probe pulse. The synchronization of the experiment remains similar to that discussed in Sec. (2.2.4) and Sec. (3.2). The temperature of the cell of the SL stage is set to 165°C, whereas in the FL stage is set to The waveforms were acquired by an Agilent digital storage oscilloscope (DSO90804A) of 8 GHz of bandwidth and 40 Gsamples/s.

In Fig. (III.12) is reported the logic diagram scheme of two possible modes of propagation:

(a) *SL stage* OFF - *FL stage* ON
The control pulse for the SL stage is prevented to enter in the cell. The control pulse for the FL stage excited the medium, creating the population inversion described in Sec. (3.1.2). The probe pulse propagates in vacuum in the first cell and in a fast light medium in the second one.

(b) *SL stage* ON - *FL stage* ON
Both control pulses excite the corresponding medium; then a passive medium (Sec. (2.1.2)) in the SL stage and an active medium in the FL stage (Sec. (3.1.2)) are establish. The

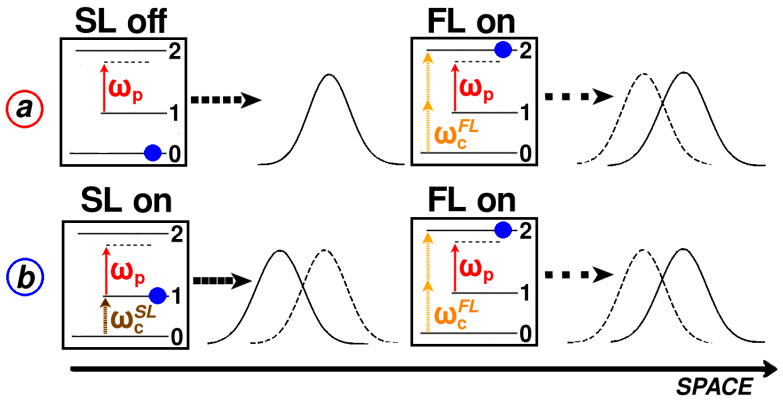

Figure III.10: Logical diagram of the experimental procedure with the corresponding atomic interactions schemes. In the case a) the pulse propagated in vacuum and then is advanced by the fast light (FL) stage. In b) the pulse is previously delayed in the slow light (SL) stage and then advanced.

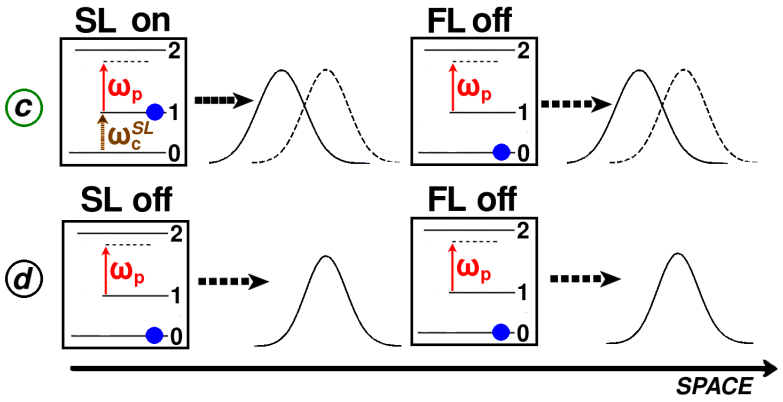

Figure III.11: Complementary cases of the ones shown in Fig. (III.10) for reference. In the case c) the pulse propagated in slow light stage and then in vacuum. In d) the pulse propagates in vacuum in both stages.

probe pulse experiences a delay in the first stage and in the second one can recover this delay or also experience an extra advance respect to the vacuum propagation.

The two complementary modes, that acts only for reference and reported in Fig. (III.11) are:

(c) *SL stage* ON - *FL stage* OFF
Only the control pulse for the SL stage is sent into the medium. Then pulse is delayed and then propagates in vacuum.

(d) *SL stage* OFF - *FL stage* OFF
Both stages are switched off and the reference probe pulse propagates in vacuum in both stages.

3.3.3 Results

In Fig. (III.12) typical normalized temporal profiles of the probe pulse in different cases, with a pump energy of the FL stages (when ON) of 80 mJ are shown. Above, the probe pulse

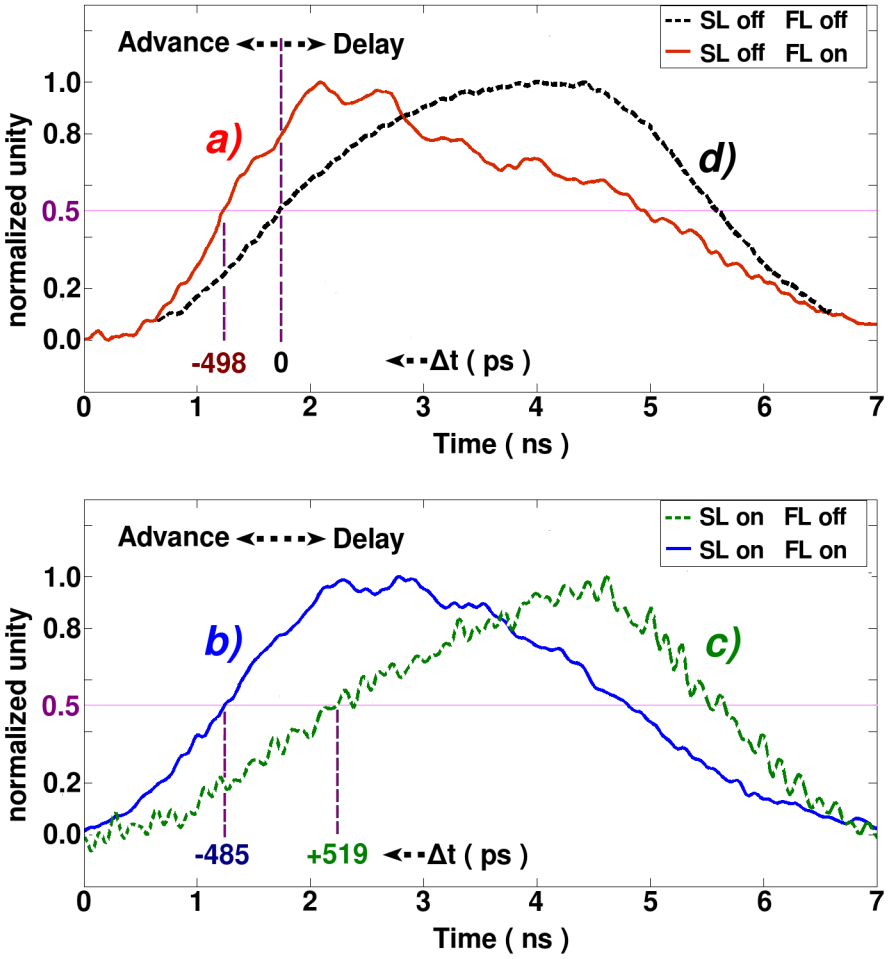

Figure III.12: Temporal profiles of the probe pulse after propagation through the SL and the FL stages. The red and blue curves refer respectively to the case a) and b) in Fig. (III.10). The black curve is propagation in vacuum (case (c) - averaged over the 10% of the signal peak) when both stages are switched off (case (d)). The greed dashed curve refers to the pulse that is delayed by the SL stage and then propagates in vacuum.

that propagates in the case a) is reported in red and the dashed black is the reference (averaged above the 10% of the peak value) that propagates through both stages in vacuum. The probe pulse experiences an advance respect to the vacuum propagation of 500 ps. Below, the blue profile is the probe pulse that propagates when both stages are switched on (case b)); then it is delayed and then advanced of ~500 ps. The green profile is the reference pulse in the case c), when it is solely delayed in the SL stage. Therefore, the FL stage is able to complete recover by the delay induced by the previous SL stage and then produce an advance respect to the vacuum propagation of the same mount than in the case a).

These results suggest that, with only the FL stage ON, the trailing edge of the pulse travels very close to the optical front, thus the causality limits the maximum possible advance. Since in the case b) the SL stage induces a delay of about 520 ps, the overall advance of about 1 ns is experienced in this case: the acquired delay with respect the optical front makes the subsequent

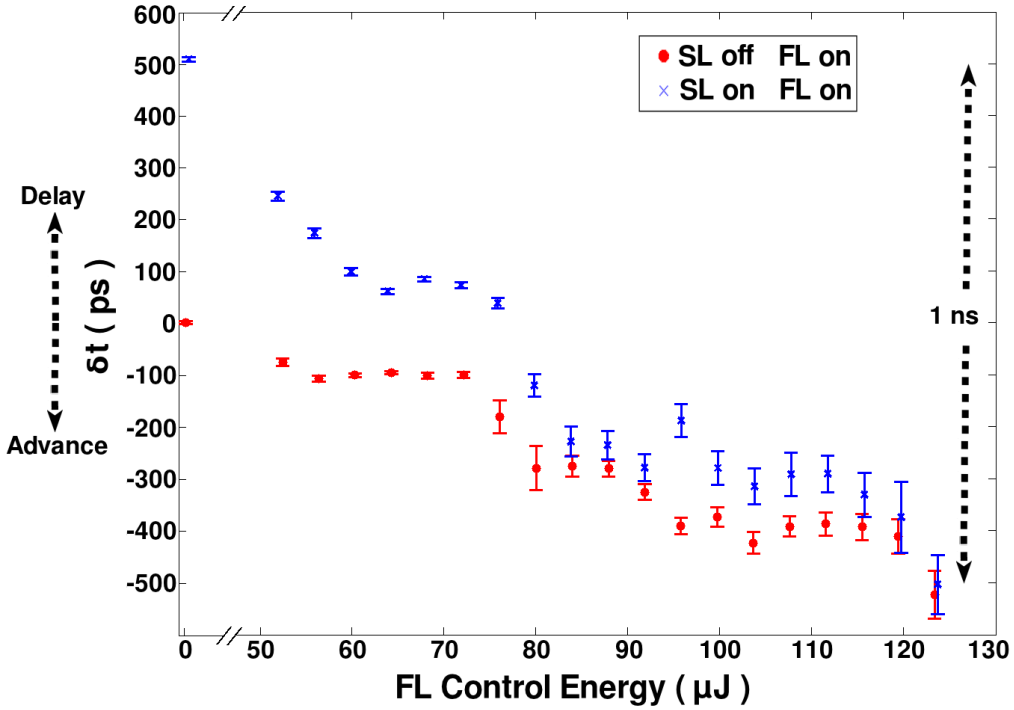

Figure III.13: Temporal shift δt in propagation as a function of the FL energy. Positive values are delays and negatives are advances. Red point are the results relative for the case a) in Fig. (III.10) and the blue ones for the case b).

fast light propagation more efficient. *The pulse moves faster if it is previously delayed.*

The pump energy of the both FL and SL stages (when are ON) are the same in all cases: the difference between the pulse in the case a) and b) can be found only in the total final energy of the pulse (in the case b) the pulse is also affected by absorption due the SL stage, but not in the arrival time. Thus, after traversing both stages, from the time of arrival to the detector, it is impossible to distinguish if the probe pulse had been previously delayed or not.

Fig. (III.13) shows the value of the shift δt in arrival time of the probe pulse in the cases a) (red) and b) (blue) as a function of the control pulse energy of the FL stage. An energy 0 corresponds to switching OFF the FL stage, in order to investigate the cases c) and d). Clearly, the control by FL energy of the delay recover demonstrated in the case b). As the energy increases the advance with respect the vacuum propagation approaches the same limit value of 500 ps in both cases. Therefore, for high energy, a complete cancellation of propagation history of the pulse is approached. In such a limit case, by a temporal measurement an observer is not able to distinguish if the probe pulse has been delayed in a passive medium or not. In the experiment only the final intensity of the pulse can give indication about the history of the pulse. However such a indication can be circumvented by introduction of an additional passive or gain medium that does not alter the propagation speed.

In conclusions, the possibility of recovering an induced delay with a fast light propagation is demonstrated and optically controlled by means of the energy of the control pulse. The medium has been tailored in such a way to achieve an approaching to the limit speed for the propagation of the optical signal. Finally, these results suggest possible future practical applications; indeed,

in telecommunication any transmission line is affected by unavoidable losses, that are corrected by means of amplification stages, to which a fast light stage could be added. Hence this experiment is also a proof of principle demonstration showing this, up to now, uncovered possibility that can lead to an actual propagation at the maximum reachable velocity for a signal.

References

[1] E. Ignesti, F. Tommasi, R. Buffa, L. Fini, E. Sali, and S. Cavalieri. "Optical control of superluminal propagation of nanosecond laser pulses". In: *Phys. Rev. A* 87 (2013), p. 033828. DOI: 10.1103/PhysRevA.87.033828 (cited in page 47).

[2] F. Tommasi, E. Ignesti, L. Fini, and S. Cavalieri. "Recovering the propagation delay of an optical pulse". In: *Opt. Express* 22.23 (2014), pp. 28566–28571. DOI: 10.1364/OE.22.028566 (cited in page 47).

[3] J. Marangos. "Faster than a speeding photon". In: *Phys. Rev.* 406 (2000), pp. 243–244. DOI: http://dx.doi.org/10.1038/35018657 (cited in page 48).

[4] A. Dogariu, A. Kuzmich, and L. J. Wang. "Transparent anomalous dispersion and superluminal light-pulse propagation at a negative group velocity". In: *Phys. Rev. A* 63 (2001), p. 053806. DOI: 10.1103/PhysRevA.63.053806 (cited in page 48).

[5] D. Gauthier and R. Boyd. "Fast light, slow light, and optical precursors: What does it all mean?" In: *Photonics Spectra* (2007), pp. 82–90 (cited in page 48).

[6] W. Withayachumnankul, B. M. Fischer, B. Ferguson, B. Davis, and D. Abbott. "A Systemized View of Superluminal Wave Propagation". In: *Proceedings of the IEEE* 98.10 (2010), pp. 1775–1786. DOI: 10.1109/JPROC.2010.2052910 (cited in page 48).

[7] R. W. Boyd and D. J. Gauthier. "Controlling the Velocity of Light Pulses". In: *Science* 326.5956 (2009), pp. 1074–1077. DOI: 10.1126/science.1170885 (cited in page 48).

[8] R. W. Boyd and D. J. Gauthier. "Chapter 6 "Slow" and "fast" light". In: ed. by E. Wolf. Vol. 43. Progress in Optics. Elsevier, 2002, pp. 497 –530. DOI: http://dx.doi.org/10.1016/S0079-6638(02)80030-0 (cited in page 48).

[9] P. W. Milonni. *Fast Light, Slow Light and Left-Handed Light*. Series in Optics and Optoelectronics. Taylor & Francis, 2004 (cited in page 48).

[10] P. W. Milonni. "Controlling the speed of light pulses". In: *J. Phys. B: At. Mol. Opt. Phys.* 35.6 (2002), R31 (cited in page 48).

[11] C. G. B. Garrett and D. E. McCumber. "Propagation of a Gaussian Light Pulse through an Anomalous Dispersion Medium". In: *Phys. Rev. A* 1 (1970), pp. 305–313. DOI: 10.1103/PhysRevA.1.305 (cited in page 48).

[12] S. Chu and S. Wong. "Linear Pulse Propagation in an Absorbing Medium". In: *Phys. Rev. Lett.* 48 (1982), pp. 738–741. DOI: 10.1103/PhysRevLett.48.738 (cited in page 48).

[13] R. Y. Chiao. "Superluminal (but causal) propagation of wave packets in transparent media with inverted atomic populations". In: *Phys. Rev. A* 48 (1993), R34–R37. DOI: 10.1103/PhysRevA.48.R34 (cited in page 48).

[14] E. L. Bolda, J. C. Garrison, and R. Y. Chiao. "Optical pulse propagation at negative group velocities due to a nearby gain line". In: *Phys. Rev. A* 49 (1994), pp. 2938–2947. DOI: 10.1103/PhysRevA.49.2938 (cited in page 48).

[15] L. J. Wang, A. Kuzmich, and A. Dogariu. "Gain-assisted superluminar light propagation". In: *Nature* 406 (2000), pp. 277–279. DOI: http://dx.doi.org/10.1038/35018520 (cited in page 48).

[16] M. D. Stenner, D. J. Gauthier, and M. A. Neifeld. "The speed of information in a /'fast-light/' optical medium". In: *Nature* 425 (2003), pp. 695–698. DOI: http://dx.doi.org/10.1038/nature02016 (cited in page 49).

[17] M. V. Tognetti, E. Sali, S. Cavalieri, and R. Buffa. "Temporal pulse compression and retardation by incoherent all-optical control". In: *Phys. Rev. A* 81 (2010), p. 023807. DOI: 10.1103/PhysRevA.81.023807 (cited in page 49).

[18] E. Ignesti, F. Tommasi, R. Buffa, L. Fini, E. Sali, M. V. Tognetti, and S. Cavalieri. "Incoherent optical control of pulse propagation and compression". In: *Phys. Rev. A* 86 (2012), p. 063818. DOI: 10.1103/PhysRevA.86.063818 (cited in page 49).

[19] C. Fietz and G. Shvets. "Simultaneous fast and slow light in microring resonators". In: *Opt. Lett.* 32.24 (2007), pp. 3480–3482. DOI: 10.1364/OL.32.003480 (cited in page 54).

[20] C. Fietz and G. Shvets. "Simultaneous Fast and Slow Light on a Chip Using Microring Resonators". In: *Integrated Photonics and Nanophotonics Research and Applications / Slow and Fast Light*. Optical Society of America, 2007, STuB4. DOI: 10.1364/SL.2007.STuB4 (cited in page 54).

[21] M. S. Bigelow, N. N. Lepeshkin, and R. W. Boyd. "Superluminal and Slow Light Propagation in a Room-Temperature Solid". In: *Science* 301.5630 (2003), pp. 200–202. DOI: 10.1126/science.1084429 (cited in page 54).

[22] F. Arrieta-Yáñez, O. G. Calderón, and S. Melle. "Slow and fast light based on coherent population oscillations in erbium-doped fibres". In: *Journal of Optics* 12.10 (2010), p. 104002. DOI: doi:10.1088/2040-8978/12/10/104002 (cited in page 54).

[23] J. Gan, J. Chen, S. Xu, Z. Yang, and Z. Jiang. "Slow/fast light using a very short $Er3^{+}/Yb3^{+}$ co-doped fiber". In: *Opt. Lett.* 38.5 (2013), pp. 670–672. DOI: 10.1364/OL.38.000670 (cited in page 54).

[24] M. González-Herráez, K.-Y. Song, and L. Thévenaz. "Optically controlled slow and fast light in optical fibers using stimulated Brillouin scattering". In: *Appl. Phys. Lett.* 87.8 (2005). DOI: http://dx.doi.org/10.1063/1.2033147 (cited in page 54).

[25] M. Fridman, A. Farsi, Y. Okawachi, and A. L. Gaeta. "Demonstration of temporal cloaking". In: *Nature* 481 (2012), pp. 62–65. DOI: http://dx.doi.org/10.1038/nature10695 (cited in page 56).

[26] R. W. Boyd and Z. Shi. "Optical physics: How to hide in time". In: *Nature* 481 (2012), pp. 35–36. DOI: http://dx.doi.org/10.1038/481035a (cited in page 56).

[27] J. M. Lukens, D. E. Leaird, and A. M. Weiner. "A temporal cloak at telecommunication data rate". In: *Nature* 498 (2013), pp. 205–208. DOI: http://dx.doi.org/10.1038/nature12224 (cited in page 56).

[28] P. Bony, M. Guasoni, P. Morin, D. Sugny, A. Picozzi, H. Jauslin, S. Pitois, and J. Fatome. “Temporal spying and concealing process in fibre-optic data transmission systems through polarization bypass”. In: *Nat. Commun.* 5 (2014). DOI: http://dx.doi.org/10.1038/ncomms5678 (cited in page 56).

Chapter IV

Light Propagation and Amplification in Disordered Active Media

This chapter concerns the propagation of light in a diffusive medium where gain is added. The purpose is to provide the theoretical background that underlies the original work discussed in the next chapter (Chap. (V)).

The first section (Sec. (4.4)) is devoted to the fundamentals of scattering and turbid media and to the investigation of the different behavior of light as the mean free path changes.

Then, in the second section (Sec. (4.5)) the propagation in a disordered medium is discussed. The starting point involves the historic of the development of the random laser systems, with the introduction of the non-resonant feedback mechanism (Sec. (4.5.1)), that leaded to the Letokhov's idea of disordered medium with gain (Sec. (4.5.2)). Then the first experimental evidences of random laser emission in "powder-lasers" and "laser paints" are presented in the next section (Sec. (4.5.3)). Finally the modern theoretical and experimental scenario is discussed in the next sections, paying attentions to the link between the random laser characteristics and the disorder degree of the turbid medium (Sec. (4.5.4)), the conditions of threshold (Sec. (4.5.5)) and the concept of "mode" (Sec. (4.5.6)).

4.4 Propagation in a Diffusive Medium

4.4.1 Turbid Media

The scattering process involves the interaction between photons and material elements on a wavelength scale wich causes a deviation from their initial paths. If the photons that sail off from the original optical beam preserve their energy, the scattering is elastic, as in the Rayleigh scattering case , otherwise the process is inelastic, as in the Raman scattering, and the wavelength of the radiation results greater than before the diffusion event. This diffusive behavior is observed within a medium characterized by the presence of optical nonuniformities and abrupt refractive produced by index mismatch. In such a medium, called *turbid medium*, these heterogeneities can be small particles or impurity dispersed in a homogeneous liquid, solid or gaseous material.

Whereas the absorption properties of a medium mainly depend on the chemical composition, the diffusive ones are linked to the microphysical characteristics of the particles, in particular dimension, shape and the relative refractive index n_r with respect the background medium.

Typical examples of well characterized turbid media are materials where small particles of inorganic compounds, like ZnO, TiO_2, or fat emulsion droplets, like soy bean oil or egg lipid, are dispersed. In general the bulk materials consist in transparent liquids, that can be water or alcoholic solvent like methanol, ethanol and diethylene glycol, or solid dielectric samples of crystalline or amorphous nature. It is very common to observe in air the light scattered by impurities, fogs and clouds; both the bluish color of the sky and reddening of sunlight during dusk or dawn are primarily due to the strong dependence on wavelength of the light scattering by molecules and small suspended particles in atmosphere. On the contrary, at optical frequencies, the dimensions of the cloud droplets are large enough to diffuse light whatever the wavelength, causing the white appearance.

A pure material becomes a turbid medium if local random variations of isotropy or homogeneity are induced which causes fluctuations from the mean refractive index [1]

In photonic solids, disorder can be added by means of the introduction of defects or air holes. Another important turbid medium is the biological tissue; for instance in the human eye the Rayleigh scattering of light in the stroma of the iris, as well as the concentration of melanin, determines the color, in particular in the blue or green colorations. In medicine, the light scattering properties, in addition to the absorptive ones, are particularly studied and applied for diagnostic purposes.

4.4.2 The Scattering Process

The scattering process is a phenomenon that is strongly dependent upon the size of the scatterers, the refractive index mismatch from the bulk material and the wavelength λ of the radiation.

[1] Random modifications in air density, due to the atmospheric turbulence, cause the random refractive-index fluctuations leading to the twinkling of the stars. Unlike the planets, the stars (with the obvious exception of the Sun) are far enough to represent a light point sources, whose emitted light is spatially coherent and planar when it reaches the Earth atmosphere. Hence such optical effect, just described by Aristotle, arises from interference effects that cause random atmospheric induced speckles in coherent light.

The fundamental parameter that characterizes the optical properties of a diffusive medium is the *mean free path* ℓ_s, i.e. the average of the traveling lengths between two successive scattering events. Such characteristic length scale can be derived from the *scattering coefficient* μ_s: let us consider a medium without absorbing properties and with a concentration of scatterers sufficiently low to neglect interference effects (*independent scattering approximation*) and let the $\hat{z}$-axis be the penetration direction of a light beam. After a distance z, the intensity $I(z)$ of the ballistic beam, i.e. the fraction of the beam that has not yet experienced scattering events, is given by the *Lambert-Beer Law*:

$$I(z) = I(0) \exp\left[- \int_0^z \mu_s(z')dz \right] \tag{IV.1}$$

If the medium is homogeneous μ_s does not depend on z and the ballistic beam is exponentially attenuated. Within the independent scattering approximation, the scattered power can be derived by the sum of the contribute due to each particle and expressed in term of the *scattering cross section* σ_s. Considering a volume numerical density ρ_s of identical spherical scatterers or identical randomly oriented non-spherical particle, the scattering coefficient can be expressed as following:

$$\mu_s = \rho_s \sigma_s \tag{IV.2}$$

In general experimental case, the diffusive sample consists in a mixture of scatterers of different radius and μ_s are averaged on the size distribution, since the scattering depends on the dimensions of the particles [2].

By means of σ_s and the *geometric cross section* it is then possible to define the *scattering efficiency* Q_s of the scattering event:

$$Q_s = \frac{\sigma_s}{\pi r^2} \tag{IV.3}$$

where r is the radius of the particle. Then, from (IV.2) and (IV.3) it follows:

$$\mu_s = \rho_s \pi r^2 Q_s \tag{IV.4}$$

From a statistical point of view, the probability density function can be derived from the Lambert-Beer law IV.1, since, in a homogeneous medium, $\mu_s \exp[-\mu_s z]dz$ represents the probability for a photon of the ballistic beam to undergo a scattering event within an element length between the coordinate z and $z + dz$. Then, inside a purely diffusive infinite medium (or a medium with depth much larger than the length scale provided by $1/\mu_s$), the scattering mean free path can be statistically calculated as:

$$\ell_s = \int_0^\infty z \mu_s \exp[-\mu_s z]dz = \frac{1}{\mu_s} \tag{IV.5}$$

In order to completely characterize the process, the other important parameter is the *scattering phase function* $p(\hat{s}, \hat{s}')$, defined as the probability that a photon traveling in direction $\hat{s}$ is scattered within the unit solid angle $\hat{s}'$. For unpolarized light and spherical or randomly oriented spherical particles as diffusive centers, the scattering phase function depends only on the azimuthal angle θ, i.e. the angle between $\hat{s}$ and $\hat{s}'$. As for μ_s, $p(\theta)$ depends on the particle size

[2] If r is the particle radius and $f(r)$ is the probability distribution, $\mu_s = \rho_s \int_0^\infty \sigma_s(r) f(r) dr$

and in the general case is averaged of the distribution over the scatterer radius of the sample. The *asymmetry factor* g is defined as the average cosine of the scattering angle:

$$g = \langle \cos\theta \rangle = 2\pi \int_0^{\pi} \cos\theta p(\theta) \sin\theta d\theta \tag{IV.6}$$

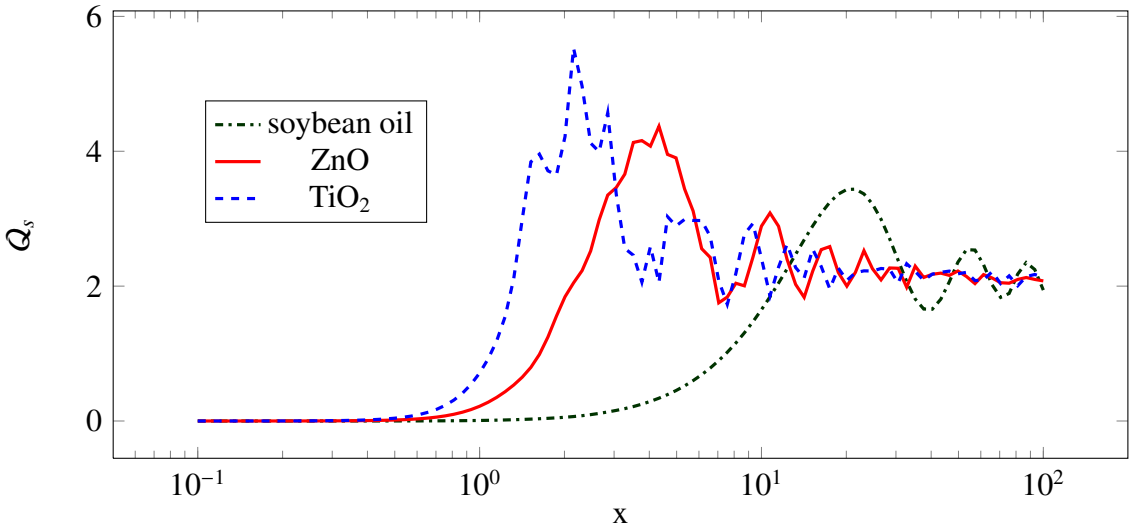

Figure IV.1: Numerical calculation of scattering efficiency Q_s as a function of the size parameter for λ =633 nm, water as bulk medium (n=1.33) and monodispersion of identical particles of: soybean oil (n=1.46), ZnO (n=2.00) and TiO_2 (n=2.58).

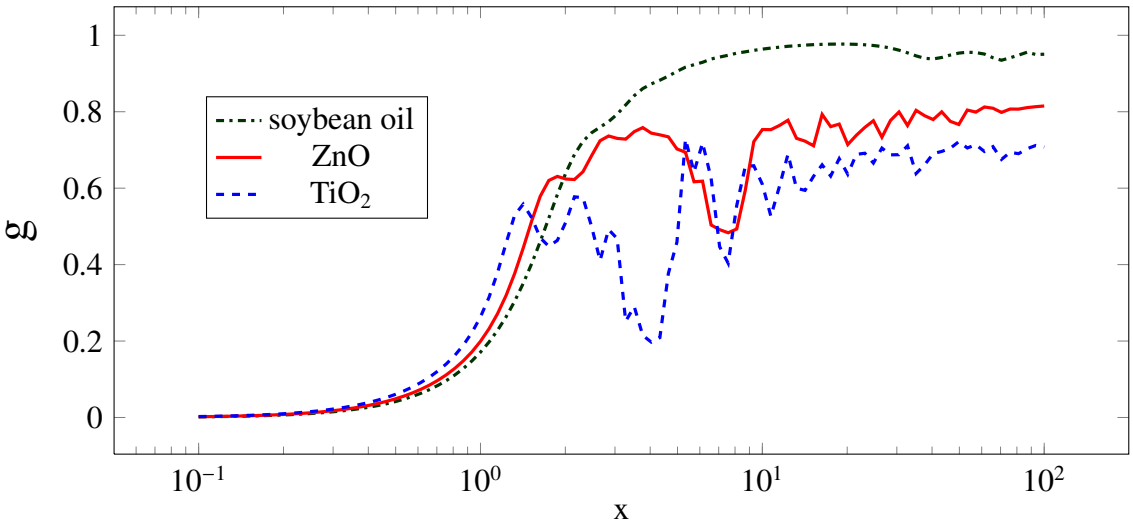

Figure IV.2: Numerical calculation of asymmetry factor g as a function of the size parameter for λ =633 nm, water as bulk medium (n=1.33) and monodispersion of identical particles of: soybean oil (n=1.46), ZnO (n=2.00) and TiO_2 (n=2.58).

When the scattering function is anisotropic the scattering phenomenon is better described by the *reduced scattering coefficient* μ_t. It can be shown [2] that after i scattering events the

average z-coordinate reached by a scattered photon is the following:

$$\langle z_i \rangle = \frac{1}{\mu_s} \sum_{i=0}^{i-1} g^i = \frac{1}{\mu_s} \frac{1-g^i}{1-g} \tag{IV.7}$$

If the number of the events becomes large, from the IV.7 follows:

$$\frac{1}{\mu_t} = \lim_{i \to \infty} \langle z_i \rangle = \frac{1}{\mu_s (1-g)} \tag{IV.8}$$

Then, as for ℓ_s (equation IV.5), it is possible to define statistically the *transport mean free path* (or *reduced scattering mean free path*) ℓ_t:

$$\ell_t = \frac{1}{\mu_t} = \frac{\ell}{1-g} \tag{IV.9}$$

It represents the average distance beyond which the propagation direction is completely randomized and it becomes the fundamental parameter in those cases where the scattering is strongly anisotropic ($g \to 1$). ℓ_t can be expressed as:

$$\ell_t = (\rho_s \sigma_t)^{-1} \tag{IV.10}$$

where the *cross section for radiation pressure*, that describes the average momentum transfer between photon and scatter, is defined as $\sigma_t = \sigma_s(1-g)$.

The dependence on the wavelength and the diameter d of the scatterers is defined by the dimensionless *size parameter* x :

$$x = \frac{\pi d}{\lambda} \tag{IV.11}$$

The condition of *small particles* typically holds for a scattering center that interacts with a electromagnetic radiation if $x < \pi/10$ [3]. In such a case the process is described by the Rayleigh scattering and σ_s decreases with the fourth power of the wavelength:

$$\sigma_s = \frac{2\pi^5}{3} \frac{d^6}{\lambda^4} \left(\frac{n^2-1}{n^2+2} \right)^2 \tag{IV.12}$$

where d is the diameter of ideally identical spherical particles. The scattering due to small particle has a low efficiency ($Q_s \propto x^4$) and an angular isotropy $g = 0$. On the contrary, for $x \gg 1$ the scattering becomes independent on the size of the particle ($Q_s \simeq 2$), while the scattering function strongly depends on it. General results for each size parameter and refractive index of spherical scatterers can be numerically calculated by the Mie solution of the Maxwell equations [4]. In Fig. (IV.1) and Fig. (IV.2) are shown numerical calculations of Q_s and g respectively for a monodispersion of identical spherical particles in water (n=1.33), for a radiation wavelength of 633 nm. The material of the particles are: soybean oil (n=1.46) [5], ZnO (n=2.00) [6] and TiO_2 (n=2.58) [7]. The values are generated with a Matlab® code based on the algorithm reported by Bohren and Huffman [8].

If x becomes large enough to consider the wavelength completely negligible, the propagation of radiation zones with different refractive index is describable in terms of the light rays of geometric optics.

Varying the concentration of the scatterers, three different scattering regimes can be identified by means of the optical thickness $\tau = \mu_s Z$ (where Z is the total depth of the diffusive medium), the wavelength of the radiation λ and ℓ_t:

SCATTERING REGIMES

(1) *quasi-ballistic regime* ($\tau \lesssim 1$)
A weakly scattering material where in average photons undergo at most one scattering event or none. The medium approaches the condition of transparency from the scattering point of view.

(2) *light diffusion regime* ($\tau \gg 1$ and $\ell_t \gg \lambda$))
With increasing the optical thickness of the sample, the ballistic beam is affected by a strong attenuation and the direction of the radiation tends to approach a complete randomization. The energy transport is similar to that of a classical particle in Brownian motion.

(3) *localized regime* ($\tau \gg 1$ and $\ell_t \sim \lambda$)
If the scattering strength is large enough to cause that the electric field of the radiation is not able to realize just one oscillation between to consecutive scattering events.

In *light diffusion regime* the treatment of the photons as random walkers is justified and the energy transport can be described by the *diffusion equation*:

$$\frac{\partial \Phi(\mathbf{r}, t))}{\partial t} = D\Delta\Phi(\mathbf{r}, t)) + \mathcal{S} \tag{IV.13}$$

where $\Phi(\mathbf{r}, t)$ is the energy density, D the *diffusion coefficient* and $\mathcal{S}$ a source term, as the incident beam.

In both light diffusion and in localized regime , the regimes are governed by a large number of scattering events before leaving the medium; the distinction among them arises from the fact that the light diffusion regime is considered as a simplified picture where the interference terms can be neglected (*single scattering approximation*) in order to describe the propagation of the radiation [9]. Such a regime represents the critical requirement for the *Anderson localization*, predicted in 1958 by P.W. Anderson for electron diffusion inside disordered material systems, like a semiconductor with impurities and defects [10]. In such a case the phenomenon has been described as a disordered-induced phase transition from the classical diffusion regime, governed by the Ohm's law, to a localized state. Under such a condition the wave-interference effects between multiple scattering events leads to an insulating behavior of the disordered semiconductor.

The critical parameter that leads to approach the localized state is known as the *Ioffe-Regel Criterion* [11, 12] and consists in the product between the wave number of the radiation k and the scattering mean free path l_s [3] :

$$k\ell_s \leq 1 \tag{IV.14}$$

[3] In the optical case the scattering mean free path ℓ_s is substituted by the transport mean free path ℓ_t.

In principle such transition from diffusive transport to localized state should occur in any material system, once the scattering strength is increased to the critical value, but at the optical frequencies is experimentally difficult because of the very small inter-particles distances required. Moreover, unlike the electrons case where the Coulomb interaction between particles occurs, in optics the photon-photon interaction can be neglected. The first experimental evidence of such phenomenon at optical frequencies has been reported in 1997 using GaAs powder suspended in methanol [13].

4.5 Random Laser System: Disordered Medium with Gain

4.5.1 Non-resonant feedback

The concept of laser source is founded on two fundamental ingredients: an *active medium* and an *optical cavity*. The first one consists in a material in which a population inversion among its atoms or molecules is established by a pumping system. Such a condition allows the light amplification via stimulated emission triggered by prior spontaneously emitted photons. An optical cavity, generally constituted by at least two reflecting surfaces, provides the necessary feedback mechanism that can allow the laser-type emission, that appears if the experienced gain overcomes the losses. Then the output radiation is characterized by a high degree of directionality, mathematically described by Gaussian beam, and high temporal and spatial coherence. The spectral behavior is dominated by the oscillation modes allowed by the optical cavity.

Since the 1960s, then very early in the history of development of the laser technology, the material scattering properties have not been considered solely a loss factor causing photons removal from the modes of the optical cavity. In order to reduce the sensibility of the laser emission upon small mechanical alteration and to smooth the speckle distribution on the intensity pattern, due to the high coherence properties, a new type of feedback mechanism was proposed by Ambartsumyan *et al*. in 1966 [14, 15]. They suggested to replace a mirror of the optical cavity with a surface or volume light scatterer, providing a *non-resonant* or *intensity feedback* mechanism. They reported, as the most relevant fact, that, unlike a conventional laser, the line narrowing around the central frequency of the emission is determined, with a much slower temporal dynamics, by the resonant frequency of the active medium rather than by the resonator modes. The direction of photons scattered back to the gain medium changed case-by-case, with light paths that in general do not overlap after round trips inside the cavity. Narrow emission line around the center of the atomic resonance, regardless the stability of geometric dimensions of the cavity, was reported in a He-Xe non-resonant feedback laser, using scatterers and mirror systems [16].

Ambartsumyan *et al*. also identified in the statistical properties of the emission, in a way similar to the ones that characterize the black body radiation, an important topic of investigation [17].

4.5.2 Photonic bomb

In 1960s decade, in order to explain anomalies that had been observed in cosmic microwave emission of the OH molecule, coherent amplification mechanism in interstellar medium with population inversion had been proposed and considered [18–20] and Vladilen S. Letokhov sug-

gested that such amplification could be the result of the feedback provided by the scattering by free electrons and dust particles in the interstellar medium [21].

Hence in 1967 the scenario was open for the next step towards a medium where the conditions of light generation, amplification and scattering are all satisfied. In his pioneer work Letokhov claims [22]:

> " The purpose of this letter is to demonstrate the possibility of generating light by means of of an aggregate of scattering particles with negative absorption in the case when the mean free path of the photon due to scattering is much smaller than the dimensions of the system, i.e. when the motion of the photons is diffuse. "

In analogy with the multiplication of neutrons in a homogeneous nuclear reactor without a reflector, he intended to find the critical condition for a new optical source, that is spatially incoherent as thermal or luminescence sources, but with an high monochromaticity, whose stability only depends on that of the frequency of the atomic resonance:

> " When the threshold condition is satisfied, such a generator emits in all directions with an exceedingly narrow spectrum."

Instead of the active and diffusive interstellar medium (essentially optically homogeneous), where ℓ_s is much larger than the dimensions of the generator, Letokhov considered a spatial region where the diffusive regime holds (see Sec. (4.4.2)) containing a set of identical particles larger than λ. Since now light moves inside an active medium where scattering properties have been added, other two characteristic length scales are to be considered. The former is the *gain length* ℓ_g, that describes the amplification due to the stimulated emission process. Let I_0 the initially spontaneously emitted energy and $I(z)$ the energy after a traveling distance z within an active medium:

$$I(z) = I_0 e^{z/\ell_g} \tag{IV.15}$$

Then ℓ_g is defined as the distance over which the energy is amplified by a factor e. In analogy with the (IV.2) and (IV.10):

$$\ell_t = (\rho_s \sigma_\omega)^{-1} \tag{IV.16}$$

where σ_ω is the *gain cross section* for a radiation of frequency ω.

The latter length scale, the *amplification length* ℓ_A takes account of the diffusion property of the medium and then of the fact that the light trajectory in general does not follow a straight line. In the diffusive regime:

$$\ell_A = \sqrt{\frac{D\ell_g}{v}} \tag{IV.17}$$

where v is the average velocity of the radiation inside the medium and D the *diffusion coefficient*. Indicating as v the energy transport velocity, in a three dimensional system:

$$D = v\ell_t/3 \tag{IV.18}$$

and ℓ_A becomes:

$$\ell_A^{(3D)} = \sqrt{\frac{\ell_t \ell_g}{3}} \tag{IV.19}$$

In diffusion equation (IV.13) the amplification within the random active medium can act as source term. Thus Letokhov considered the change of flux spectral density $\Phi_\omega(\mathbf{r}, t)$ of photons of frequency ω (near to the gain resonance ω_0 of the inverted medium), in the point $\mathbf{r}$ and at the time t as described by the diffusion equation:

$$\frac{\partial \Phi_\omega(\mathbf{r}, t)}{\partial t} = D\Delta\Phi_\omega(\mathbf{r}, t) + \frac{v}{\ell_g}\Phi_\omega(\mathbf{r}, t) \tag{IV.20}$$

where ℓ_g is expressed by the (IV.16).

In contrast with conventional disordered passive medium, where an absorption length ℓ_{abs} in the place of ℓ_g implies the destruction of photons during their random path, in such material the radiation is amplified by stimulated emission. Moreover Letokhov suggests that the medium can also acts as generator, with particles that contemporaneously perform both emission and scattering.

In general σ_ω is not constant in space and time due to the dependence on the photon flux density that can induce gain saturation [23] and to decaying effects.

At the threshold, when the gain overcomes the losses, the effect of such dependence can be neglected and a general solution of the (IV.20) is the following:

$$\Phi_\omega(\mathbf{r}, t) = \sum_n a_n \phi_n(\mathbf{r}) e^{-(D{\Lambda_n}^2 - {\ell_g}^{-1} v)t} \tag{IV.21}$$

where $\phi_n(\mathbf{r})$ are the eigenfunctions and Λ the eigenvalues of the equation:

$$\Delta\phi_n(\mathbf{r}) + {\Lambda_n}^2 \phi_n(\mathbf{r}) = 0 \tag{IV.22}$$

a_n are arbitrary constants determined by the initial condition $\Phi_\omega(\mathbf{r}, 0)$. Then the general solution is an eigenfunction expansion of modes with an exponential decay rate that depends on the order n [24]. The boundary condition implies $\phi_n(\mathbf{r}) = 0$ at a distance d_e (*extrapolation length*) [25] beyond the medium boundaries, since the photon density is small outside the medium, but it can not be set as zero, because the light can diffuse outside the surface [26]. However d_e is smaller than ℓ_t and such condition can be applied in good approximation to the surface of the medium (*absorbing boundary condition*). The solutions to the spatial part of (IV.21) that satisfy the absorbing boundary condition are of the form $\sin(n\pi r/L)$, where n is a integer and L is the thickness of the medium. If the medium is a sphere of radius R, $\phi_n(\mathbf{r})$ and Λ_n are expressed as follows [25]:

$$\phi_n(\mathbf{r}) = \frac{1}{r}\sin\frac{n\pi r}{R} \quad \Lambda_n = \frac{n\pi}{R} \tag{IV.23}$$

Hence Letokhov found that the critical conditions are bounded to the dimensions of the inverted medium, its diffusive properties and the energy stored in the population inversion. From IV.21 follows the *threshold condition*:

$$D\Lambda^2 = {\ell_g}^{-1} v \tag{IV.24}$$

where Λ is the smallest eigenvalue Λ_n (π/R in the case of the spherical medium) and σ_0 the larger cross section (at resonance ω_0). Because of the exponential decay of the modes, only the

order $n = 1$ survives for a long time, experiencing the largest amplification. The presence of the cross section at the resonance in threshold condition implies that the spectrum of the output radiation undergoes narrowing around the central frequency of the spontaneous emission.

In absence of absorption or other dissipative channels within the medium, losses are localized on the surface and proportional to the total area. It is obvious that reflecting properties added at the boundaries of the pumped region decrease the threshold condition.

Reminding the equation (IV.19), the threshold condition predicts a critical volume V_{cr} for a three dimensional medium where the diffusive and gain properties are described by ℓ_t and ℓ_g respectively:

$$V_{cr} \approx \left(\frac{\ell_t \ell_g}{3}\right)^{\frac{3}{2}} = {\ell_A}^3 \tag{IV.25}$$

Then fixed ℓ_A, if the volume exceeds V_{cr} the first member in the (IV.24) becomes larger than the second one and from (IV.21) it follows that the energy flux grows exponentially:

$$\textit{Photonic bomb} \qquad [D{\Lambda_n}^2 - {\ell_g}^{-1} v] < 0 \tag{IV.26}$$

Such a condition and the exotic term *photonic bomb* mean that in average each spontaneous emitted photon generates almost one photon by stimulated emission before escaping the medium, in such a way to lead the system to become unstable and to trigger a 'chain reaction' analogous to the production of neutrons within an atomic bomb [27]. Of course no real 'explosion' occurs since the stimulated emission rapidly depletes the energy stored in the medium as population inversion.

Letokhov also predict the narrowing of the output spectrum, as in the non-resonant feedback mechanism (Sec. (4.5.2)) and a slow temporal dynamics of the emission. For the former effect he described the system as a '*stochastic resonator*', where a large number of strongly interacting modes lead to a complete overlap of their frequency spectrum. For the temporal behavior he predicted a stationary generation regime approached with relaxation oscillations.

The reference [22] is considered as the first mention about a system composed by a medium where scattering and amplifying properties are added in order to achieve an emission that share with the laser the characteristic of monochromaticity and with the thermal radiation the ones of directionality and spatial incoherence. Hence it is considered as the first prediction of the optical system called with the modern term *'random laser'*.

4.5.3 Powder laser and laser paint

The experimental realizations of a light generator similar to the one predicted by Letokhov began to appear in scientific literature in 1970s and 1980s. In 1971 Varsanyi reported the observation of stimulated emission not supported by any optical cavity [28] in powder particles of $PrCl_3$ and $PrBr_3$. He suggested that such *powder laser*, dispersed in a suitable material (solid, liquid or gaseous), could have opened up new possibilities in display technology. In 1981 it was reported that, under not to well understood conditions, stimulated emission can be induced in ZnO powders by means of N_2 laser pumping at a temperature of 80°K [29]. Five years later Briskina's group, during routine spectroscopy measurements, observed interesting effects regarding the emission spectra from powder of a $Na_5La_{1-x}Nd_x(MoO_4)_4$ composition under the influence of a strong pump pulse provided by a dye laser [30]. They reported narrowing of the

emission and shortening of the emitted pulse duration (around four orders of magnitude) and they considered as noteworthy the threshold nature and the linear dependence on the pumping intensity, in such a way to demonstrate that the phenomenon was ascribable to a stimulated emission process. Hence, reminding the ideas of Letokhov and Varsanyi, they proposed the investigation about the possibility to realize a quasi-monochromatic source with fine-grained powders of luminescent crystals, ceramics or emulsion solutions of dye. Later on other further investigations have been reported in generation of spatially incoherent short pulses by grinding crystals, usually used as laser source, in fine-grained powder [31, 32].

Since 1990s another strategy has been developed in order to achieve laser-like emission in non-conventional materials. In 1994 Lawandy *et al*. claimed to have achieved laser action in liquid sample of rhodamine 640 perchlorate dye as gain medium, where the scatterers (colloidal suspension of TiO_2 rutile particles) concentration can be easily varied. They called such kind of material *laser paint* because the suggestion of 'painting' the laser material on a surface [33]. In the scientific correspondences that followed the paper for the first time the term '*random laser*' was introduced [34, 35].

The Lawandy's paper [33] is considered a milestone in the random laser history [36], especially because the dimension of the scattering centers, smaller than the radiation wavelength, does not allow to invoke the possibility of lasing from internal resonances of single particles. The phenomenon is not attributable, according to the original Letokhov's idea, to a single-particle feature, but to an emerging property of a disordered systems, where the active part is located outside and among the scatterers. Then the emission of such disordered system with gain began to be theoretically and experimentally investigated [37–44].

It is worth to stress the fact that the scatterers have to play a decisive role in triggering the laser-like emission. A process that manifests similar characteristics is the *amplified spontaneous emission (ASE)*. The ASE phenomenon can appear in the case of large amount of population inversion established in a medium by a pumping systems [1]. In an active medium with a linear dimension larger the other ones, if the gain is large enough, the earlier spontaneously emitted photons near the pumping beam spot are strongly amplified if their initial directions correspond to ones that guarantee the largest gain. Thus the stored energy in the medium can be rapidly depleted and emitted into the solid angle subtended by the center of the spot of the pump beam as seen by the opposite face of the sample. In contrast to the spontaneous emission, ASE is characterized by laser-like features, as spectrum narrowing and directionality of the output. Of course an ASE process cannot explain *tout court* a random laser system; in fact light generator that solely exploit such process are known as *mirror-less lasers* [45]. As it will discussed in Sec. (4.5.6), in a random laser the *modes*, even if they are not well defined and understood as in the case of a conventional laser, play a decisive role: a random laser is 'mirror-less' but not 'mode-less' [9].

4.5.4 Random Laser Regimes

An operative definition of a random laser is: *a disordered material system, where population inversion is established by means of a pump, that is able to generate light and satisfy the two following criteria:*

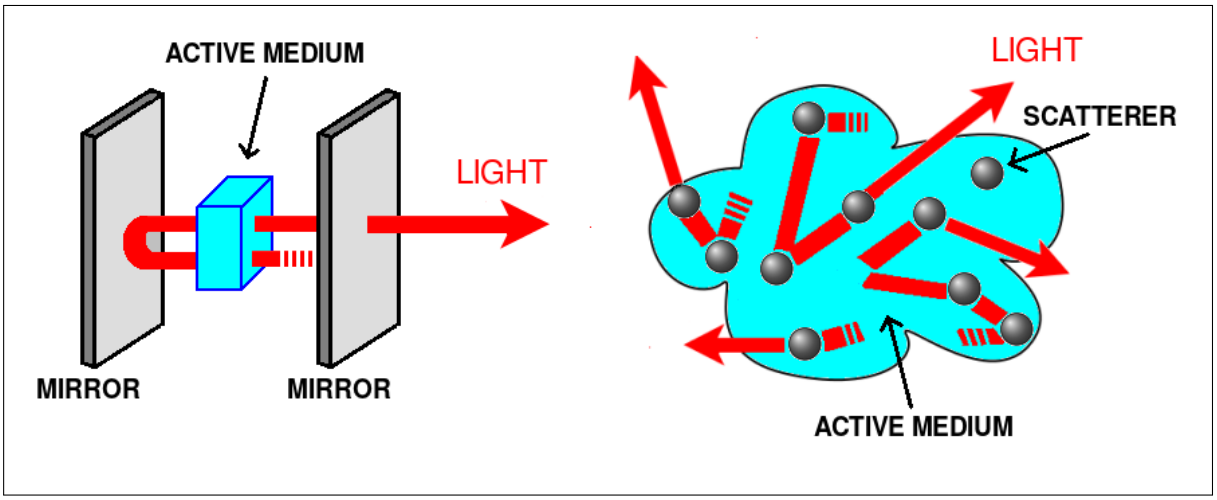

Figure IV.3: Simplified picture of a conventional laser system (on the left), provided by an optical cavity composed by two mirrors and an active medium and a random laser source (on the right), where the light is amplified along its path in a scattering active medium.

FUNDAMENTAL CRITERIA OF A RANDOM LASER SYSTEM

(1) *light is scattered and amplified by stimulated emission*

(2) *there exists a threshold induced by the scattering*

The threshold condition, in a similar way to a conventional laser, is reached when the total gain becomes greater than the losses, due to photons that leave the active medium or that are destroyed by dissipative channels. No limit exists on the maximum scattering mean free path, but its lowest possible value cannot to be larger than the sample; in fact (see Sec. (4.5.2)) the scattering has to play a critical role in the system.

According to the value of the mean free path, a further sub-classification of random laser systems is possible. Wiersma and Lagendijk proposed a model based on light diffusion and gain, considering a powder slab of a four levels system as active material, such as Ti:sapphire or Rhodamine 6G, a pump pulse and a probe pulse [44]. The pumping rises the system to the excited level $|2\rangle$, from which it rapidly dacays to the metastable level $|1\rangle$, in such a way to establish a population inversion if the level $|0'\rangle$ has a fast decay rate to the ground level $|0\rangle$. Hence the dynamics of the process is described by a set of three diffusion equations, for the pulses and the ASE, and one for the population of the level $|1\rangle$. Such system of coupled equations, once numerically solved, predicts an emission dynamics with a spiky structure under pulsed excitation. In order to characterize a random laser system, for different scattering strengths they distinguished three regimes, that can be related to the scattering regimes identified in Sec. (4.4.2):

RANDOM LASER REGIMES

Incoherent Random Laser

(1) *quasi-ballistic regime* $\Longrightarrow$ *weak scattering and gain*
the role of the scatterers is not critical and the emission is dominated by ASE emission. If ℓ_t further increases the classification as a random laser becomes no longer correct.

(2) *light diffusion regime* $\Longrightarrow$ *modest scattering and gain*
The presence of scattering increases the time spent by light inside the sample and the spectral and temporal behavior of the output emission is strongly influenced by diffusion processes. The interference effects are negligible and the amplification is provided by an intensity feedback mechanism.

Coherent Random Laser

(3) *localized regime* $\Longrightarrow$ *strong scattering and gain*
The strong scattering forces light to form closed loop paths, along which it can experience a large gain. Anderson localization can be invoked to explain such *random ring cavities*.

In the diffusive regime the pumping system creates an amplifying region from which the spontaneously emitted photons, because the absence of reflecting surfaces, can easily escape. However, after a random walk due to the scattering, they can re-enter in the active medium, experiencing additional amplification. Such energy feedback is non-resonant, because the return of the light in its starting position is not required. Hence such kind of system is called *random laser with incoherent* (or *non-resonant* or *intensity*) - *feedback*.

Although the interference effects are not required for the random laser lasing, they can become predominant in the multiple scattering regime . Such *coherent random laser* [46–49] has been reported in semiconductor nanostructures [50, 51], disordered polymers [43, 52], organic materials [53]. Closed-loop paths act as a cavity where gain can overcome losses leading to lasing oscillations at frequencies that satisfy constructive interference requirements [54, 55].

4.5.5 Random Laser Threshold

The dependence of the critical conditions threshold of the random laser emission on the concentration of active molecules and scatterers and on the pumping system energy and spatial properties has been investigated by several works [40, 56, 5, 57–68]. Since the feedback mechanism requires return of the radiation to the pumped volume, whereas missed photons cause a large loss source, the threshold is inversely proportional to the dimension of the active region.

The saturation of the active medium by the pump and its "bleaching" is desirable, because it assures a depth increment of the pumped zone. However, in order to achieve an efficient pumping, a gain volume larger than the diffusion volume is to be avoided, leading to the importance to find the optimal conditions.

Experimentally the detection of the threshold of such kind of light generator is not well defined as in the case of the conventional laser system. Generally the system appears to be in the threshold condition when the transition between an emission spectrum dominated by spontaneous emission and one characterized by the narrowing due to stimulated emission begins to occur. In analogy with the conventional laser, introduction of a $\beta-$factor has been proposed in order to quantitatively describe the response of the system subjected to a pump pulse [68, 69]. The β-factor is defined as the ratio of the rate of spontaneous emission into the lasing mode to the total rate of spontaneous emission. It ranges from 0 to the limit value $\beta \to 1$ (*thresholdless laser*), where all possible emission modes coincide to the laser mode. Since the typical emission of a random laser is non-directional the criterion based on the wavevectors is not applicable and the only possibility is to consider the spectral overlap of the spontaneous emission spectrum and the narrow spectrum of a random laser above the threshold. Such definition leads to relatively large β ($\beta \sim 0.1$).

Another definition of random laser threshold that has been proposed consists in detection of changes in statistical regimes of the spectrum [70], as it is discussed in the next section.

4.5.6 Random laser modes and fluctuations in emission spectra

A typical random laser emission is intrinsically dominated by the interplay between randomness and non-linearity and many works have been devoted to investigate the physical phenomena that underlie that behavior. In particular the debate has involved the description of light interactions in terms of interactions between 'modes', whose definition is not straightforward as in the case of a conventional laser system.

In the conventional laser the optical cavity, as the Fabry-Perot cavity, determines those *resonator eigenmodes* that characterize the spectral behavior of the emission. The resonant frequencies among the gain curve being able to spend a long time inside the cavity, via the destructive interference of the light exiting out, can experience a large amplification. The random laser emission (as discussed in Sec. (4.5.2)), in spite of its chaotic behavior, can be described in terms of *modes* too; instead of individual high-Q modes of a Fabry-Perot cavity, the emission spectrum can be viewed as a large number of low-Q modes that spectrally overlap around the central frequency of the active medium. The output spectrum appears as continuous and with no presence of individual discrete components, except for some relevant cases that will be shortly discussed.

In 1999 Cao *et al*. reported the observation of narrow spikes superimposed on the spectrum of a powder laser and they interpreted such phenomenon as the first evidence of a coherent random lasing attributable to a transition between incoherent (dominated by ASE and coherent feedback [71–73]. In such a picture the spikes are caused by the existence of *localized modes* which cause such a phase transition, with $k\ell_t \sim 5 \div 14$. In case of solid matrices, i.e. scatterers located in fixed position, the spectral position of these spikes should not change.

Successive experiments have reported the presence of fluctuations and narrow spikes in a large range of scattering strengths, even in scattering regimes where the condition (IV.14)

is not satisfied [74–80]. Such experimental evidences have promoted investigations about the theoretical framework and alternative model, in order to understand the physical origin of these spikes and their link to the interplay between the random laser modes and the experimental parameters. For instance, mechanisms that have been proposed are based on involving localized modes due to random resonators that are induced by the correlation radius of the disorder [81] or large-scale Bragg-like configurations [82, 83].

As an opposite picture, the existence of narrow spikes in random laser spectra is ascribable to an *open model*, according which *extended* or *open modes* are interpreted as possible paths within the diffusive medium [75, 6]. In experiments with ZnO powder dispersed in rhodamine 6G-methanol solution narrow peaks in conditions of $k\ell_t \sim 5800$ have been reported [75] Modes in general are mutually coupled by the competition for the available gain, but, in certain condition rare long paths of long lifetime, the so-called *lucky photons*, are able to experiment a very large amplification [84, 85]. Such a mode-uncoupling for these rare modes decreases the available energy for the other modes, giving rise to narrow spikes in the spectrum [79, 80]. Unlike as predicted for the case of localized modes, the spikes spectral positions have been found independent on the arrangement of the scatterers [84]. The principal characteristics of such kind of modes are summarized below:

EXTENDED MODES

(1) large spatial extension within the sample

(2) no phase information are required (light diffusion scattering regime)

(3) photons are modeled as particles in a random walk

(4) they compete for the available gain

Such model provided a theoretical framework and encouraged the investigation about the intensity fluctuations in random laser spectra in term of *statistical regimes* of the emission [78, 86–88].

References

[1] O. Svelto. *Principles of Lasers*. Springer, 2010. ISBN: 9781441913029 (cited in pages 52, 75).

[2] G. Zaccanti, E. Battistelli, P. Bruscaglioni, and Q. Wei. "Analytic relationships for the statistical moments of scattering point coordinates for photon migration in a scattering medium". In: *Pure and Applied Optics: Journal of the European Optical Society Part A* 3.5 (1994), p. 897. DOI: doi:10.1088/0963-9659/3/5/019 (cited in page 68).

[3] M. Kerker. *The Scattering of Light and Other Electromagnetic Radiation*. Academic Press, New York, 1969 (cited in page 69).

[4] G. Mie. "Beiträge zur Optik trüber Medien, speziell kolloidaler Metallösungen". In: *Annalen der Physik* 330.3 (1908), pp. 377–445 (cited in page 69).

[5] R. Michels, l. FoschumF, and A. Kienle. "Optical properties of fat emulsions". In: *Opt. Express* 16.8 (2008), pp. 5907–5925. DOI: 10.1364/OE.16.005907 (cited in page 69).

[6] W. L. Bond. "Measurement of the Refractive Indices of Several Crystals". In: *Journal of Applied Physics* 36.5 (1965), pp. 1674–1677. DOI: http://dx.doi.org/10.1063/1.1703106 (cited in page 69).

[7] J. R. Devore. "Refractive Indices of Rutile and Sphalerite". In: *J. Opt. Soc. Am.* 41.6 (1951), pp. 416–417. DOI: 10.1364/JOSA.41.000416 (cited in page 69).

[8] C. F. Bohren and D. R. Huffman. *Absorption and Scattering of Light by Small Particles*. Wiley (New York), 1983 (cited in page 69).

[9] D. S. Wiersma. "The physics and applications of random lasers". In: *Nat Phys* 4 (5) (2008), pp. 359–367. DOI: http://dx.doi.org/10.1038/nphys971 (cited in pages 70, 75).

[10] P. W. Anderson. "Absence of Diffusion in Certain Random Lattices". In: *Phys. Rev.* 109 (1958), pp. 1492–1505. DOI: 10.1103/PhysRev.109.1492 (cited in page 70).

[11] A. F. Ioffe. *Proceedings of the International Conference on Electron Transport*. Can. J. Phys. 34 (Ottawa, Canada), 1956 (cited in page 70).

[12] A. Ioffe and A. Rogel. In: *Prog. Semicond.* 4 (1960), p. 237 (cited in page 70).

[13] D. Wiersma, P. Bartolini, A. Lagendijk, and R. Righini. "Localization of light in disordered medium". In: *Nature* 390 (1997), pp. 671–673. DOI: doi:10.1038/37757 (cited in page 71).

[14] R. V. Ambartsumyan, N. G. Basov, P. G. Kryukov, and V. S. Letokhov. "Laser with a non-resonant feedback [*Pis'ma Zh. Eksp. i Teor. Fiz.* 3, 261-264 (1966)]". In: *JETP Lett.* 3 (1966), pp. 167–169 (cited in page 71).

[15] R. V. Ambartsumyan, N. G. Basov, P. G. Kryukov, and V. S. Letokhov. "Laser with a non-resonant feedback [*Zh. Eksp. i Teor. Fiz.* 51, 724-729 (1966)]". In: *Sov. Phys. JETP* 24.6 (1967), pp. 481–485 (cited in page 71).

[16] R. V. Ambartsumyan, S. P. Bazhulin, N. G. Basov, and V. S. Letokhov. "Emission spectrum of an He-Xe laser with nonresonant feedback [*Zh. Eksp. i Teor. Fiz.* 58, 441-455 (1970)]". In: *Sov. Phys. JETP* 31.2 (1970), pp. 234–241 (cited in page 71).

[17] R. V. Ambartsumyan, P. G. Kryukov, V. S. Letokhov, and Y. A. Metveets. "Statistical emission properties of a non resonant feedback laser [*Zh. Eksp. i Teor. Fiz.* 53, 1955-1966 (1967)]". In: *Sov. Phys. JETP* 26.6 (1968), pp. 1109–1114 (cited in page 71).

[18] H. Weaver, D. Williams, N. H. Dieter, and L. W. T. "Observation of Strong Unidentified Microwave Line and of Emission from the OH melucule". In: *Nature* 208 (1965), pp. 29–31. DOI: 10.1038/208029a0 (cited in page 71).

[19] A. E. E. Rogers, J. M. Moran, P. P. Crowther, B. F. Burke, M. L. Meeks, J. A. Ball, and G. M. Hyde. "Interferometric Study of Cosmic Line Emission at OH Frequencies". In: *Phys. Rev. Lett.* 17 (1966), pp. 450–452. DOI: 10.1103/PhysRevLett.17.450 (cited in page 71).

[20] D. A. Varshalovich. "Coherent Amplification of Radio Emission in a Cosmic Medium [*ZhETF Pis'ma* 4, 180-182 (1966)]". In: *Sov. Phys. JETP* 4 (1966), pp. 180–182 (cited in page 71).

[21] V. S. Letokhov. "Stimulated Radio Emission of the Interstellar Medium [*ZhETF Pis'ma* 4, 477-481 (1966)]". In: *Sov. Phys. JETP* 4 (1966), pp. 321–323 (cited in page 72).

[22] V. S. Letokhov. "Stimulated Radio Emission of an ensemble of scattering particles with negative absorption [*Pis'ma Zh. Eksp. i Teor. Fiz.* 5, 262-265 (1967)]". In: *JETP Lett* 5 (1967), pp. 212–215 (cited in pages 72, 74).

[23] R. Karplus and J. Schwinger. "A Note on Saturation in Microwave Spectroscopy". In: *Phys. Rev.* 73 (9) (1948), pp. 1020–1026. DOI: 10.1103/PhysRev.73.1020 (cited in page 73).

[24] S. Redner. *A Guide to First-Passage Processes*. Cambridge University Press, 2001 (cited in page 73).

[25] A. M. Weinberg and E. P. Wigner. *Physical Theory of Neutron Chain Reactor*. University of Chicago, 1958 (cited in page 73).

[26] V. S. Letokhov. "Generation of light by a scattering medium with negative resonance absorption [*Zh. Eksp. Teor. Fiz.* 53, 1442-1447 (1967)]". In: *Sov. Phys. JETP* 26 (1968), pp. 835–840 (cited in page 73).

[27] B. Davison and J. B. Sykes. *Neutron Transport Theory*. Oxford University Press, Oxford, 1958 (cited in page 74).

[28] F. Varsanyi. "Surface lasers". In: *Appl. Phys. Lett.* 19 (1971), pp. 169–171. DOI: 10.1063/1.1653870 (cited in page 74).

[29] V. A. Nikitenko, A. I. Tereschenko, I. P. Kuz'mina, and A. N. Lobachev. "Stimulated emission of ZnO at high level of single photon excitation". In: *Optika i Spektroskopiya* 50 (1981), pp. 605–607 (cited in page 74).

[30] V. M. Markushev, V. F. Zolin, and C. M. Briskina. “Luminescence and stimulated emission of neodymium in sodium lanthanum molybdate powders”. In: *Sov. J. Quantum Electron.* 16 (1986), pp. 281–282. DOI: 10.1070/QE1986v016n02ABEH005792 (cited in page 74).

[31] V. M. Markushev, N. E. Ter-Garielyan, C. Briskina, V. R. Belan, and V. F. Zolin. “Stimulated emission kinetics of neodymium powder lasers”. In: *Sov. J. Quantum Electron.* 20 (1990), pp. 773–777. DOI: doi:10.1070/QE1990v020n07ABEH006817 (cited in page 75).

[32] C. Gouedard, F. Auzel, A. Migus, D. Husson, and C. Sauteret. “Generation of spatially incoherent short pulses in laser-pumped neodymium stoichiometric crystals and powders”. In: *J. Opt. Soc. Am. B* 10.12 (1993), pp. 2358–2363. DOI: 10.1364/JOSAB.10.002358 (cited in page 75).

[33] N. M. Lawandy, R. M. Balachandran, A. S. L. Gomes, and E. Suvain. “Laser action in strongly scattering media”. In: *Nature* 368 (1995), pp. 436–437. DOI: 10.1038/368436a0 (cited in page 75).

[34] D. Wiersma, M. P. van Albada, and A. Lagendijk. “Random laser?” In: *Nature* 373 (1995), pp. 203–204 (cited in page 75).

[35] N. M. Lawandy and R. M. Balachandran. “Random laser? - Reply”. In: *Nature* 373 (1995), p. 204 (cited in page 75).

[36] H. Cao. “Random thought”. In: *Nat. Photon.* 7 (3) (2013), pp. 164–165. DOI: 10.1038/nphoton.2013.39 (cited in page 75).

[37] J. Martorell, R. M. Balachandran, and N. M. Lawandy. “Radiative coupling between photonic paint layers”. In: *Opt. Lett.* 21.4 (1996), pp. 239–241. DOI: 10.1364/OL.21.000239 (cited in page 75).

[38] R. M. Balachandran, N. M. Lawandy, and J. A. Moon. “Theory of laser action in scattering gain media”. In: *Opt. Lett.* 22.5 (1997), pp. 319–321. DOI: 10.1364/OL.22.000319 (cited in page 75).

[39] M. Noginov, H. Caulfield, N. Noginova, and P. Venkateswarlu. “Line narrowing in the dye solution with scattering centers”. In: *Optics Communications* 118.3–4 (1995), pp. 430–437. ISSN: 0030-4018. DOI: 10.1016/0030-4018(95)00177-A (cited in page 75).

[40] W. Zhang, N. Cue, and K. M. Yoo. “Emission linewidth of laser action in random gain media”. In: *Opt. Lett.* 20.9 (1995), pp. 961–963. DOI: 10.1364/OL.20.000961 (cited in pages 75, 77).

[41] S. John and G. Pang. “Theory of lasing in a multiple-scattering medium”. In: *Phys. Rev. A* 54 (1996), pp. 3642–3652. DOI: 10.1103/PhysRevA.54.3642 (cited in page 75).

[42] B. R. Prasad, H. Ramachandran, A. K. Sood, C. K. Subramanian, and N. Kumar. “Lasing in active, sub-mean-free path-sized systems with dense, random, weak scatterers”. In: *Appl. Opt.* 36.30 (1997), pp. 7718–7724. DOI: 10.1364/AO.36.007718 (cited in page 75).

[43] G. A. Berger, M. Kempe, and A. Z. Genack. "Dynamics of stimulated emission from random media". In: *Phys. Rev. E* 56 (1997), pp. 6118–6122. DOI: 10.1103/PhysRevE.56.6118 (cited in pages 75, 77).

[44] D. Wiersma and A. Lagendijk. "Light diffusion with gain and random lasers". In: *Phys. Rev. E.* 54 (1996), pp. 4256–4265. DOI: 10.1103/PhysRevE.54.4256 (cited in pages 75, 76).

[45] A. E. Siegman. *Lasers*. Univ. Science Books, Mill Valley, 1986 (cited in page 75).

[46] H. Cao, J. Xu, Y. Ling, A. Burin, E. Seeling, X. Liu, and R. P. Chang. "Random lasers with coherent feedback". In: *Selected Topics in Quantum Electronics, IEEE Journal of* 9.1 (2003), pp. 111–119 (cited in page 77).

[47] H. Cao. "Review on latest developments in random lasers with coherent feedback". In: *Journal of Physics A: Mathematical and General* 38.49 (2005), p. 10497. DOI: doi:10.1088/0305-4470/38/49/004 (cited in page 77).

[48] Y. Ling, H. Cao, A. L. Burin, M. A. Ratner, X. Liu, and R. P. H. Chang. "Investigation of random lasers with resonant feedback". In: *Phys. Rev. A* 64 (2001), p. 063808. DOI: 10.1103/PhysRevA.64.063808 (cited in page 77).

[49] H. Cao. "Random Lasers: Development, Features and Applications". In: *Opt. Photon. News* 16.1 (2005), pp. 24–29. DOI: 10.1364/OPN.16.1.000024 (cited in page 77).

[50] S. V. Frolov, Z. V. Vardeny, A. A. Zakhidov, and R. H. Baughman. "Laser-like emission in opal photonic crystals". In: *Optics Communications* 162.4–6 (1999), pp. 241 –246. DOI: 10.1016/S0030-4018(99)00089-9 (cited in page 77).

[51] K. Yoshino, S. Tatsuhara, Y. Kawagishi, M. Ozaki, A. A. Zakhidov, and Z. V. Vardeny. "Amplified spontaneous emission and lasing in conducting polymers and fluorescent dyes in opals as photonic crystals". In: *Applied Physics Letters* 74.18 (1999), pp. 2590–2592. DOI: 10.1063/1.123907 (cited in page 77).

[52] R. Polson, J. Huang, and Z. Vardeny. "Random lasers in π-conjugated polymer films". In: *Synthetic Metals* 119.1–3 (2001). Proceedings of the International Conference on Science and technology of Synthetic Metals, pp. 7 –12 (cited in page 77).

[53] S. V. Frolov, Z. V. Vardeny, K. Yoshino, A. Zakhidov, and R. H. Baughman. "Stimulated emission in high-gain organic media". In: *Phys. Rev. B* 59 (1999), R5284–R5287. DOI: 10.1103/PhysRevB.59.R5284 (cited in page 77).

[54] D. S. Wiersma, M. P. van Albada, B. A. van Tiggelen, and A. Lagendijk. "Experimental Evidence for Recurrent Multiple Scattering Events of Light in Disordered Media". In: *Phys. Rev. Lett.* 74 (1995), pp. 4193–4196. DOI: 10.1103/PhysRevLett.74.4193 (cited in page 77).

[55] P. Pradhan and N. Kumar. "Localization of light in coherently amplifying random media". In: *Phys. Rev. B* 50 (1994), pp. 9644–9647. DOI: 10.1103/PhysRevB.50.9644 (cited in page 77).

[56] J. Kitur, G. Zhu, M. Bahoura, and M. A. Noginov. "Dependence of the random laser behavior on the concentrations of dye and scatterers". In: *Journal of Optics* 12.2 (2010), p. 024009. DOI: 10.1088/2040-8978/12/2/024009 (cited in page 77).

[57] M. Siddique, G. A. Berger, M. Kempe, R. R. Alfano, and A. Z. Genack. "Time-resolved studies of stimulated emission from colloidal dye solutions". In: *Opt. Lett.* 21.7 (1996), pp. 450–452. DOI: 10.1364/OL.21.000450 (cited in page 77).

[58] G. Beckering, S. J. Zilker, and D. Haarer. "Spectral measurements of the emission from highly scattering gain media". In: *Opt. Lett.* 22.18 (1997), pp. 1427–1429. DOI: 10.1364/OL.22.001427 (cited in page 77).

[59] G. van Soest, M. Tomita, and A. Lagendijk. "Amplifying volume in scattering media". In: *Opt. Lett.* 24 (1999), pp. 306–308. DOI: 10.1364/OL.24.000306 (cited in page 77).

[60] K. Totsuka, G. van Soest, T. Ito, A. Lagendijk, and M. Tomita. "Amplification and diffusion of spontaneous emission in strongly scattering medium". In: *Journal of Applied Physics* 87.11 (2000), pp. 7623–7628. DOI: http://dx.doi.org/10.1063/1.373432 (cited in page 77).

[61] F. A. Pinheiro and L. C. Sampaio. "Lasing threshold of diffusive random lasers in three dimensions". In: *Phys. Rev. A* 73 (2006), p. 013826. DOI: 10.1103/PhysRevA.73.013826 (cited in page 77).

[62] B. R. Anderson, R. Gunawidjaja, and H. Eilers. "Low-threshold and narrow linewidth diffusive random lasing in rhodamine 6G dye-doped polyurethane with dispersed ZrO_2 nanoparticles". In: *J. Opt. Soc. Am. B* 31.10 (2014), pp. 2363–2370. DOI: 10.1364/JOSAB.31.002363 (cited in page 77).

[63] "Ultra-low threshold optically pumped random laser emission behavior of highly oriented pyrolytic graphite". In: *Materials Letters* 115.0 (2014), pp. 261 –264. ISSN: 0167-577X. DOI: http://dx.doi.org/10.1016/j.matlet.2013.10.045 (cited in page 77).

[64] S. M. Morris, D. J. Gardiner, M. M. Qasim, P. J. W. Hands, T. D. Wilkinson, and H. J. Coles. "Lowering the excitation threshold of a random laser using the dynamic scattering states of an organosiloxane smectic A liquid crystal". In: *J. Appl. Phys.* 111.3 (2012). DOI: http://dx.doi.org/10.1063/1.3681898 (cited in page 77).

[65] M. Bahoura, K. Morris, G. Zhu, and M. Noginov. "Dependence of the neodymium random laser threshold on the diameter of the pumped spot". In: *Quantum Electronics, IEEE Journal of* 41.5 (2005), pp. 677–685. ISSN: 0018-9197. DOI: 10.1109/JQE.2005.845027 (cited in page 77).

[66] L. S. Froufe-Pérez, W. Guerin, R. Carminati, and R. Kaiser. "Threshold of a Random Laser with Cold Atoms". In: *Phys. Rev. Lett.* 102 (2009), p. 173903. DOI: 10.1103/PhysRevLett.102.173903 (cited in page 77).

[67] G. van Soest, F. J. Poelwijk, R. Sprik, and A. Lagendijk. "Dynamics of a Random Laser above Threshold". In: *Phys. Rev. Lett.* 86 (2001), pp. 1522–1525. DOI: 10.1103/PhysRevLett.86.1522 (cited in page 77).

[68] G. van Soest and A. Lagendijk. "β factor in a random laser". In: *Phys. Rev. E* 65 (2002), p. 047601. DOI: 10.1103/PhysRevE.65.047601 (cited in pages 77, 78).

[69] K. L. van der Molen, A. P. Mosk, and A. Lagendijk. "Intrinsic intensity fluctuations in random lasers". In: *Phys. Rev. A* 74 (2006), p. 053808. DOI: 10.1103/PhysRevA.74.053808 (cited in page 78).

[70] R. Uppu and S. Mujumdar. "Lévy exponents as universal identifiers of threshold and criticality in random lasers". In: *Phys. Rev. A* 90 (2014), p. 025801. DOI: 10.1103/PhysRevA.90.025801 (cited in page 78).

[71] H. Cao, Y. G. Zhao, S. T. Ho, E. W. Seelig, Q. H. Wang, and R. P. H. Chang. "Random Laser Action in Semiconductor Powder". In: *Phys. Rev. Lett.* 82 (1999), pp. 2278–2281. DOI: 10.1103/PhysRevLett.82.2278 (cited in page 78).

[72] H. Cao, J. Y. Xu, S.-H. Chang, and S. T. Ho. "Transition from amplified spontaneous emission to laser action in strongly scattering media". In: *Phys. Rev. E* 61 (2000), pp. 1985–1989. DOI: 10.1103/PhysRevE.61.1985 (cited in page 78).

[73] H. Cao, Y. Ling, J. Y. Xu, C. Q. Cao, and P. Kumar. "Photon Statistics of Random Lasers with Resonant Feedback". In: *Phys. Rev. Lett.* 86 (2001), pp. 4524–4527. DOI: 10.1103/PhysRevLett.86.4524 (cited in page 78).

[74] R. C. Polson, A. Chipouline, and Z. V. Vardeny. "Random Lasing in π-Conjugated Films and Infiltrated Opals". In: *Advanced Materials* 13.10 (2001), pp. 760–764. ISSN: 1521-4095. DOI: 10.1002/1521-4095(200105)13:10<760::AID-ADMA760>3.0.CO;2-Z (cited in page 79).

[75] S. Mujumdar, M. Ricci, R. Torre, and D. S. Wiersma. "Amplified Extended Modes in Random Lasers". In: *Phys. Rev. Lett.* 93 (2004), p. 053903. DOI: 10.1103/PhysRevLett.93.053903 (cited in page 79).

[76] G. Strangi, S. Ferjani, V. Barna, A. D. Luca, C. Versace, N. Scaramuzza, and R. Bartolino. "Random lasing and weak localization of light in dye-doped nematic liquid crystals". In: *Opt. Express* 14.17 (2006), pp. 7737–7744. DOI: 10.1364/OE.14.007737 (cited in page 79).

[77] X. Wu, W. Fang, A. Yamilov, A. A. Chabanov, A. A. Asatryan, L. C. Botten, and H. Cao. "Random lasing in weakly scattering systems". In: *Phys. Rev. A* 74 (2006), p. 053812. DOI: 10.1103/PhysRevA.74.053812 (cited in page 79).

[78] R. Uppu, K. A. Tiwari, and S. Mujumdar. "Identification of statistical regimes and crossovers in coherent random laser emission". In: *Opt. Lett.* 37.4 (2012), pp. 662–664. DOI: 10.1364/OL.37.000662 (cited in page 79).

[79] R. G. S. El-Dardiry, R. Mooiweer, and A. Lagendijk. "Experimental phase diagram for random laser spectra". In: *New Journal of Physics* 14.11 (2012), p. 113031. DOI: 10.1088/1367-2630/14/11/113031 (cited in page 79).

[80] E. Ignesti, F. Tommasi, L. Fini, S. Lepri, V. Radhalakshmi, D. Wiersma, and S. Cavalieri. "Experimental and theoretical investigation of statistical regimes in random laser emission". In: *Phys. Rev. A* 88 (2013), p. 033820. DOI: 10.1103/PhysRevA.88.033820 (cited in page 79).

[81] V. M. Apalkov, M. E. Raikh, and B. Shapiro. "Random Resonators and Prelocalized Modes in Disordered Dielectric Films". In: *Phys. Rev. Lett.* 89 (2002), p. 016802. DOI: 10.1103/PhysRevLett.89.016802 (cited in page 79).

[82] J. Herrmann and B. Wilhelmi. "Mirrorless laser action by randomly distributed feedback in amplifying disordered media with scattering centers". In: *Appl. Phys. B* 66.3 (1998), pp. 305–312. DOI: 10.1007/s003400050393 (cited in page 79).

[83] B. Wilhelmi. "Laser action in resonators composed of scattering mesoscopic particles". In: *Proc. SPIE* 3573 (1998), pp. 13–16. DOI: 10.1117/12.321016 (cited in page 79).

[84] S. Mujumdar, V. Türck, R. Torre, and D. S. Wiersma. "Chaotic behavior of a random laser with static disorder". In: *Phys. Rev. A* 76 (2007), p. 033807. DOI: 10.1103/PhysRevA.76.033807 (cited in page 79).

[85] S. Mujumdar, S. Cavalieri, and D. S. Wiersma. "Temperature-tunable random lasing: numerical calculations and experiments". In: *J. Opt. Soc. Am. B* 21.1 (2004), pp. 201–207. DOI: 10.1364/JOSAB.21.000201 (cited in page 79).

[86] D. Sharma, H. Ramachandran, and N. Kumar. "Lévy statistical fluctuations from a random amplifying medium". In: *Fluctuation and Noise Letters* 06.01 (2006), pp. L95–L101. DOI: 10.1142/S0219477506003185 (cited in page 79).

[87] S. Lepri, S. Cavalieri, G.-L. Oppo, and D. S. Wiersma. "Statistical regimes of random laser fluctuations". In: *Phys. Rev. A* 75 (2007), p. 063820. DOI: 10.1103/PhysRevA.75.063820 (cited in page 79).

[88] R. Uppu and S. Mujumdar. "Dependence of the Gaussian-Lévy transition on the disorder strength in random lasers". In: *Phys. Rev. A* 87 (2013), p. 013822. DOI: 10.1103/PhysRevA.87.013822 (cited in page 79).

Further reading

[89] A. Ishimaru. *Wave Propagation and Scattering in Random Media*. IEEE/OUP series on electromagnetic wave theory v. 2. Academic Press, 1978. ISBN: 9780123747020.

[90] V. Baby, N. Bokor, H. Cao, N. Davidson, W. Gao, D. J. Gauthier, G. Gbur, I. Glesk, P. R. Prucnal, B. C. Wang, L. Xu, J. Yin, and Y. Zhu. *Progress in Optics vol. 45*. Edited by Emil Wolf (Amsterdam, Netherlands), 2006. ISBN: 04445133445.

[91] D. S. Wiersma. "Disordered photonics". In: *Nature Photonics* 7.3 (2013), pp. 188–196. DOI: 10.1038/nphoton.2013.29.

[92] F. Martelli, S. Del Bianco, A. Ismaelli, and G. Zaccanti. *Light Propagation Through Biological Tissue and Other Diffusive Media: Theory, Solutions, and Software*. Press Monographs. SPIE Press, 2010.

[93] P. Sheng. *Introduction to Wave Scattering, Localization and Mesoscopic Phenomena: Localization and Mesoscopic Phenomena*. Springer Series in Materials Science. Springer, 2006. ISBN: 9783540291565.

[94] M. Noginov and V. S. Letokhov. *Solid-State Random Lasers*. Springer Series in Optical Sciences. Springer, 2005. ISBN: 9780387239132.

[95] H. Cao. "Lasing in random media". In: *Waves in Random Media* 13.3 (2003), R1–R39. DOI: 10.1117/3.832717.ch11.

[96] H. Cao. "Review on latest developments in random lasers with coherent feedback". In: *Journal of Physics A: Mathematical and General* 38.49 (2005), p. 10497.

[97] H. Cao. "Random Lasers with Coherent Feedback". In: *Optical Properties of Nanostructured Random Media*. Ed. by V. M. Shalaev. Vol. 82. Topics in Applied Physics. Springer Berlin Heidelberg, 2002, pp. 303–330. ISBN: 978-3-540-42031-6. DOI: http://dx.doi.org/10.1007/3-540-44948-5_14.

[98] J. Andreasen, A. A. Asatryan, L. C. Botten, M. A. Byrne, H. Cao, L. Ge, L. Labonté, P. Sebbah, A. D. Stone, H. E. Türeci, and C. Vanneste. "Modes of random lasers". In: *Adv. Opt. Photon.* 3.1 (2011), pp. 88–127.

[99] O. Zaitsev and L. Deych. "Recent developments in the theory of multimode random lasers". In: *Journal of Optics* 12.2 (2010), p. 024001. DOI: http://dx.doi:10.1088/2040-8978/12/2/024001.

Chapter V

Random Laser with Non-Resonant Feedback

A random laser is a disorder system where a strong non-linear effects due to stimulated emission is added to the stochastic scattering process. In recent literature the Lévy statistics of the random laser emission has been reported [1–4] and theoretically predicted [5–7].

This chapter is devoted to describe the original theoretical and experimental work that concerns random laser investigation.

In the first section of this chapter (Sec. (5.1)), the fundamental concepts of statistics needed for statistical regimes description are reported.

Then the next two sections are devoted to discuss the theoretical (Sec. (5.2)) and experimental investigation (Sec. (5.3)) on the random laser behavior. In particular, with an extensive characterization of the statistical regimes of the emission, it is highlighted and discussed the link that emerges between an improved theoretical model based on the incoherent non-resonant feedback mechanism and the experimental data. The results reported in this work led to publication of a paper published in Physical Review A (Physical Review Highlighted article) [8].

Finally, the last part of the chapter (Sec. (5.4)) presents the theoretical and experimental investigation about the possibility of controlling the deviations, from the pure spontaneous emission case, in directionality of the random laser emission output. Such a topic is under preparation.

I worked in the experimental set-up arrangement and I wrote the software of data analysis. I improved the theoretical model and I wrote the software for numerical model and conducted the simulations. I am also the corresponding author of the scientific paper.

5.1 Lévy and Gaussian statistical regimes

5.1.1 Lévy Stable Distributions

The *Brownian motion* (classical diffusion), which concerns the chaotic motion of small particles within a medium, is a chaotic phenomenon that has been long since extensively studied for a long time. It was described by Robert Brown in 1827 and explained by Albert Einstein and Marian Smoluchowski at the beginning of the XX$^{\text{th}}$-century. It is the typical example of a process that is able to characterize many dynamical system in every different field. For a particle in Brownian motion that was in the origin $x = 0$ at time $t = 0$, the probability $P(x, t)$ for the displacement in position x at time t is given by the *diffusion equation*:

$$\frac{\partial P(x,t)}{\partial t} = D\frac{\partial^2 P(x,t)}{\partial t^2} \tag{V.1}$$

whose solution is the Gaussian:

$$P(x,t) = \frac{1}{\sqrt{4\pi Dt}} \exp\left[-x^2/4Dt\right] \tag{V.2}$$

with a second moment (variance) that linearly grows with time, whatever the characteristic of the particle:

$$\langle x^2(t)\rangle = 2Dt \tag{V.3}$$

The existence of many observable quantities that are the result of the sum of a large number of random events is a very important problem, strictly connected to the probability theory and the study of stochastic processes. Let us introduce a fundamental theorem in statistics:

Theorem 1 Central Limit Theorem (CTL)*: the sum X_N of N statistically independent and identically distributed, each with a well-defined expected value and well-defined variance, whatever the exact form x_n of the distribution that individually underlie them, approaches a Gaussian distribution with variance linearly proportional to N.*

Then the requirements on x_n are that the first $\langle x_n\rangle$ and the second moment $\langle {x_n}^2\rangle$ do not diverge. Such a restriction is easily satisfied and many distributions belong to the domain of attraction of the Gaussian, leading to an efficient description of a large number of phenomena by the CTL. Let, in sake of simplicity, $\langle x_n\rangle = 0$ and $\langle {x_n}^2\rangle = \sigma^2$:

$$X_N = \sum_{n=1}^{N} x_n \qquad \text{with} \quad N \to \infty \tag{V.4}$$

The probability density function of X_N is the following:

$$p(X_N) = \frac{1}{\sqrt{2\pi\sigma^2}} \exp\left[-x^2/2{\sigma_N}^2\right] \tag{V.5}$$

where ${\sigma_N}^2 = N{\sigma_n}^2$.

Such behavior can be altered if N is not so large or the constraint on x_n are not satisfied [9]. For the former case, corrections to the Gaussian behavior can be introduced by higher-order mode, since the tail of the distribution is strongly slowed down. However if $N \to \infty$, but

the variance diverges a non-Gaussian behavior is to be expected. The *Cauchy distribution* is a relevant example of such class:

$$p(x) = \frac{a}{\pi}\frac{1}{x^2 + a^2} \tag{V.6}$$

The problem of finding a limit distribution for a sum of random variables whose second momentum diverges was primarily worked out since 1920s and 1930s by Paul Lévy and Aleksandr Y. Khintchine, leading the the introduction of the *Lévy-stable-distributions* [10, 11]. The property of stability involves random variables and their sum:

Definition 1 Stable Distribution*: A random variable x with real values has a stable distribution if: let* $(x_1, x_2, \ldots, x_N)$ *a sequence of independent variables with the same distribution of x, then* $\exists\, a_N \in \mathbb{R}^+$ *and* $b_N \in \mathbb{R}$ *such that* $X_N = \sum_{n=1}^{N} x_n$ *has the same distribution of* $a_N x + b_N$.

A *probability density function (pdf)* $p(x)$ of a random variable is completely determined by its *characteristic function* $\phi(k)$. According the *Lévy-Khinchine Representation*, the possible form of all possible stable distribution, characterized by the parameters $\alpha, \beta, \mu, \sigma$, is specified by the logarithm of the characteristic function:

$$\phi(k, \alpha, \beta, \mu, \sigma) = \int_{-\infty}^{+\infty} p(x, \alpha, \beta, \mu, \sigma) \exp[ikx] dx \tag{V.7a}$$

$$\ln \phi(k, \alpha, \beta, \mu, \sigma) = \begin{cases} i\mu k - \sigma^{\alpha}|k|^{\alpha}\left[1 - i\beta \frac{k}{|k|} \tan(\frac{\pi\alpha}{2})\right] & \text{for} \quad \alpha \neq 1 \\ i\mu k - \sigma\,|k|\left[1 + i\beta \frac{k}{|k|} \ln|k|\right] & \text{for} \quad \alpha = 1 \end{cases} \tag{V.7b}$$

The parameters are:

- α ($\in (0, 2]$) the *index of stability* or *tail index*,
  describes the rate at which the tail of the distribution tapers off
- β ($\in [-1, 1]$) the *skewness* ,
  the measure of the asymmetry
- μ ($\in \mathbb{R}$) the *location parameter*
- σ ($\in (0, +\infty)$) the *scale parameter*

In general no closed form are known (the problem of estimation of parameters is a relevant numeric practical problem), with the following three exceptions:

(1) $\alpha = 2, \beta = 0 \quad \rightarrow \quad$ *Gaussian distribution*

(2) $\alpha = 1, \beta = 0 \quad \rightarrow \quad$ *Cauchy distribution*

(3) $\alpha = 1/2, \beta = \pm 1 \quad \rightarrow \quad$ *Lévy distribution*

Although the term 'Lévy distribution' is referred only to specific cases of stable distribution, often (and also in this text) it is essentially used for labeling a general case of stable distribution that is not Gaussian.

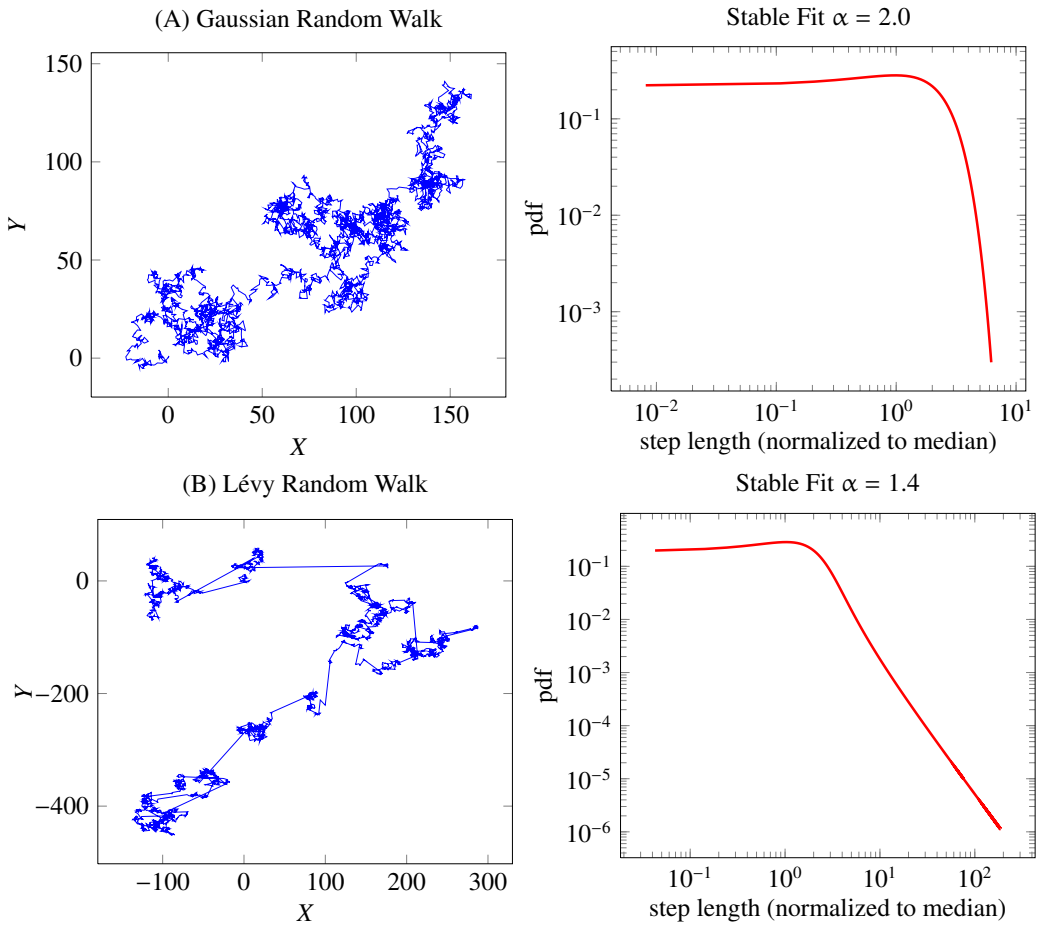

Figure V.1: Examples of numerical simulation of a random walk composed by 5000 steps, in the classical Brownian case (A) and in the Lévy flight- case (B). The walker changes its direction with uniform probability after each step. On the right the corresponding stable fit for the step lengths (normalized to the median) are shown.

For $0 < \alpha < 2$, the index of stability describes the asymptotic behavior of a class *fat-tailed* distributions that approach a inverse power-law trend:

$$p(x) \sim \frac{1}{|x|^{(1+\alpha)}} \qquad \text{for} \quad x \to +\infty \tag{V.8}$$

The works of Lévy and Khintchine led to a reformulation of the CTL:

Theorem 2 Generalized Central Limit Theorem (GCLT)*: The sum of independent identically distributed random variables belongs to domain of attraction of a stable distribution*

Hence the Gaussian distribution ($\alpha = 2$) is a special case of stable distribution with finite variance.

The fat-tail decaying of the distribution (eq. (V.8)) highlights the presence of extremely intense events, whose magnitude results stronger than their rarity regarding the weight in the overall statistics. Moreover, the divergence of the variance invokes scale-invariance properties

that are associated to the *self-similarity* and *fractals* [12]; a particular class of generalized random walk, the *Lévy flights*, describes stochastic processes characterized by extremely long and rare jumps that are interposes by clusters of short steps. Respect to the Brownian case , Lévy flights lead to *superdiffusion* [13–15] :

$$\langle x^2(t)\rangle = 2Dt^{(2/\alpha)} \qquad \text{for} \quad 0 < \alpha < 2 \tag{V.9}$$

while for $\alpha = 2$ the normal diffusive behavior holds (eq. (V.3)). Fig. (V.1) shows examples of a Gaussian random walk ($\alpha = 2.0$) and a Lévy random walk.

Stable distributions have been extensively studied because can be used to successfully fit empirical data that originate from phenomena characterized by extreme events and that are poorly or no longer described by a *Gaussian statistics*. Hence their applicability covers a large range of different fields :

- displacement patterns [16–20], animal foraging and exploration paths [21–25] highlight an innate or evolved capacity in nature to utilize Lévy flights to optimize fundamental behaviors and strategies
- distribution of human travels, mobility and search strategies [26–31] and epidemics and diseases spreading [32]
- some aspects of earthquake behavior and occurrence [33]
- materials for superdiffusive transport of light (*Lévy glass*) [34], behavior of spectral lines [35, 36], dynamics of turbulent fluids [37]
- study of financial data and price variation in markets [9, 38–41]

Because of the divergence of the variance, experimental data that follows a *Lévy statistics* are characterized by a lack of self-averaging of the fluctuations, leading to irreproducibility of the measurements. Many chaotic systems, when some non-linear mechanisms are superimposed to a stochastic behavior, show induced 'pathologies' that completely rule the dynamics of the system. Hence a random laser show, where both stochastic and non-linear mechanism are present, appears as a good candidate to manifest such tendency under suitable conditions.

5.1.2 Statistics of the emission

As discussed in Sec. (4.5.6), the peculiar characteristic of the fluctuations in random laser is the presence of narrow spikes at random frequencies. With a large number of spectra corresponding to the same experimental parameters and once fixed a narrow bandwidth of observation, one is able to characterize the system by means of the statistics of the emission.

Therefore the reference parameter becomes the α-index of the stable distribution that fits the spectral intensity histograms. Since a stable distribution has not in general an explicit form, in the fitting procedure used in this work and implemented in the Matlab software written for the data analysis, the parameters are estimated via a regression-type fitting [42, 43].

It is worth to note that in practical cases, both in numerical simulations than in the experimental case, the possible number of measures is of course finite and the procedure, utilized to label a statistical regime by means of the result of the alpha stable fit, needs a word of caution.

Since the number of available data is large but finite, the accuracy to resolve the tail of distributions is limited. In order to characterize the spectral behavior, the fundamental guide is provided by the spectra themselves: despite a Gaussian statistics exactly holds only for the value $\alpha = 2.0$, results that approaches such value are to be labeled as Gaussian if at an inspection the spectra appear smooth and spikes-less. Such situations are to be referred to spectral behavior where the emission comes back to a Gaussian regime from a fluctuations regime increasing energy. Hence it is reasonable to use a certain degree in arbitrariness in discrimination between Gaussian distribution and a Lévy one in such borderline cases, as well as it is to expected that an a further improvement of the statistics should lead to an accurate resolution of the tail of the distribution. Then, with the qualitative help provided by the inspection of the spectra, the assumed operative procedure consists in determining a reasonable threshold value of α, above which the statistical regime is to be consider Gaussian.

5.2 Theoretical Model

5.2.1 Gaussian-Lévy statistics in random laser emission

Reference [5] describes the probability distribution of the emitted intensity as (see Appendix A)):

$$p(I) = \bar{\alpha}\frac{1}{I^{(1+\bar{\alpha})}} \tag{V.10}$$

where

$$\bar{\alpha} = \frac{\ell_g}{\langle \ell \rangle} \tag{V.11}$$

Thus the asymptotic behavior of the distribution has the same heavy tail trend of the equation (V.8), with a coefficient $\bar{\alpha}$ that depends on the dimension (L) and on the properties of the sample, i.e. the available gain (ℓ_g) and the scattering strength (D). As discussed in Sec. (5.1.1), for $0 < \bar{\alpha} < 2$ the variance $\langle I^2 \rangle$ diverges and one can recognize the asymptotic Lévy behavior. Then the statistics of the emission can provide a parameter to label the emission behavior, in such a way to quantitatively characterize the fluctuation regimes. The presence of random spikes at random frequencies discussed in Sec. (4.5.6) proves the existence of rare events with large energy. In fact the presence in random laser of Lévy statistics has been reported [1–4] and theoretically predicted [5–7] and the present work reported aims to provide an extensive investigation of the statistical regimes of random laser emission and a clear link between a theoretical model and the experimental data.

For this purpose, at this stage it is worth to raise two important points that concern the gain in a real medium, respect the picture reported in the probability distribution (A.12):

(1) the total gain provided by the active medium is finite

(2) the available gain is shared by a large number of co-propagating mode

The first and inevitable point (*gain saturation*) fixes a limit to the amplification that a mode can experience, setting a cut off to the accessible value for I in equation (A.12). The second one allows to introduce the hearth of the mechanism that ruled the emission properties and behavior, once fixed the initial conditions and the characteristics of the medium: *the modes coupling in the competition for the available gain*.

Hence, in the real case, ℓ_g is not a constant parameter, but a complicate and unpredictable function of time and spatial coordinates, as well as the initial condition and the scattering strength. Moreover, also a general initial spatial inhomogeneity of the energy displacement on the medium can be exists.

In Sec. (4.5.6) the concept of mode in a random laser system has been introduced and described, as well as the detection of modes with long lifetime as possible candidates to emergence of fluctuations and random spikes in the emission spectrum. Then let us focus the attention on the diffusive case, where the extended modes are interpreted as possible paths of photons inside the medium. In such scattering regime light is pictured as particles that carry a certain amount of identical photons without considering the effect of wave superpositions. Since the model does not predict the effects due to interference between modes, the solely mechanism that allows the coupling between modes is indeed the competition for the available gain. Hence such coupling can prevent the presence of *lucky photons*, rare modes with large lifetime that be able to experience a large amplification, in particular in those cases where the available gain is shared with a large number of modes. Such a forced averaging mechanism can lead, under particular circumstances, to inhibits the presence of fluctuations and narrow spikes. A detailed theoretical and experimental investigation is discussed in the further part of the chapter.

In practical cases an estimation of α making a fit of the tail of the probability distribution can be too demanding in terms of needed data amount. Thus in this work all data are used in order to estimate α by means of a Lévy stable fit.

5.2.2 Numerical model

In order to simulate the behavior of an incoherent random laser, a numerical model has been elaborated and implemented by writing a dedicated C++ software. The simulation is based on Monte Carlo dynamics and consists in a parallel processing of a large number of *co-propagating extended modes*, in order to introduce the gain competition mechanism. The execution proceeds by a cyclic repetition of three steps, that model physical processes, for each temporal unit dt.

The stochastic behavior of the system is inserted by means of *spontaneous emission*, that, with a probability that depends on the local population, creates new modes with random frequency and initial direction, and by *diffusion*, that randomizes the photons trajectory. Then the intrinsic causality of such phenomenon plays a fundamental role in triggering the final result of the system dynamics. No non-radiative decaying processes of the population of the medium are implemented.

The output emission of each complete simulation, performed with varying the parameters that characterize the medium, as the diffusive properties and the level and the temporal behavior of the pumping system.

The goal of the Monte Carlo simulation, that aims to qualitatively reproduce the random laser system in diffusive regime, and the subsequent statistical analysis is the investigation about the detection of those parameters that determine the dynamics of the real system.

• **The Medium** The medium is pictured as a two-dimensional square lattice composed by a grid of square sites with the same length l and with a side of $L = q \cdot l$, where q is an integer. In the simulation l is the spatial length unity and in the successive text it will be omitted.

The active part of the medium is provided by filling each cell of the lattice with a certain amount of excited atoms. Such gain medium is modeled by a four-level atomic system, where a pumping system raises the population to the level $|3\rangle$, that has a rapid decay to the level $|2\rangle$, establishing a population inversion with the level $|1\rangle$, that in turn rapidly decays to the ground level $|0\rangle$. Since these two rapid decays are considered as instantaneous in the timescale of temporal steps dt of simulation, the levels $|3\rangle$ and $|1\rangle$ are always considered unpopulated. Hence the number of excited atoms injected in a site of coordinates (x, y) are counted as population inversion $N(x, y)$ and once the decay from the $|2\rangle$ via spontaneous or stimulated emission occurs, the involved atom is instantaneously eliminated from the simulation.

The initial excited state population has a two-dimensional Gaussian shape (see Fig. (V.2)); the origin setting in $(x_0, y_0) = (L/2, L/2)$, the population is:

$$N(x, y) = A \exp\left[-\frac{(x - x_0)^2 + (y - y_0)^2}{2\sigma_G^2}\right] \tag{V.12}$$

where $\sigma_G = \sigma_x = \sigma_y$ is the width of the Gaussian and A a constant assigned to have a prescribed total energy. The code of the software is able to generate other shapes for the density, but the Gaussian has been chosen because it manifests some similarities with the distribution created by absorption of a pumping beam.

Finally the diffusive properties are introduced by the assignment of a probability of scatteringper unit time $\mathcal{P}_s$. An estimation the ℓ_s of the medium is $(1/\mathcal{P}_s)l$. Considering that the model does not consider the wave interference effects, with the assumption that $l \gg \lambda$, where λ is the radiation wavelength, it is straightforward that the condition of diffusive regime ($\ell_s \gg \lambda$) is satisfied for all value of $\mathcal{P}_s \leq 1$. In theory no lower bound of $\mathcal{P}_s$ is fixed, but corresponding large value of ℓ_s should move the system from a diffusive regime to a quasi-ballistic one or to a complete ballistic behavior too. Whereas in the quasi-ballistic case the properties of the emission preserves the random laser ones, in the latter case the only possible mechanism for large energy is the ASE. If such condition occurs the definition of random laser system does not more hold, as discussed in Sec. (4.5.3).

• **The Spectrum** The spectral properties are implemented dividing the frequency window into 1000 arbitrary channels, labeled from -500 to 500 and centered on the resonance frequency ω_0 of the atomic transition $|3\rangle \rightarrow |2\rangle$ (channel 0). One channel (chs) becomes the Units of measurement for the frequency. The probability for a frequency ω in the simulated atomic transition has a Lorentzian shape of HWHM w and centered in ω_0, given by:

$$f(\omega, \omega_0, w) = \frac{1}{\pi} \frac{1}{(\omega - \omega_0)^2 + w^2} \tag{V.13}$$

• **The Modes** As the effect of interference is not consider in the diffusive regime, the modes are represented by *random walkers* that propagates,in the bidimensional lattice along four possible directions.. Since, as discussed in Sec. (4.5.6) an extended mode one of possible paths of light within the medium, a random walker is a good candidate for a simple, but useful and efficient, representation. After an unit time of the simulation dt, a walker, according its trajectory, can reach one of the four adjacent neighboring squares. Then walkers move at a speed

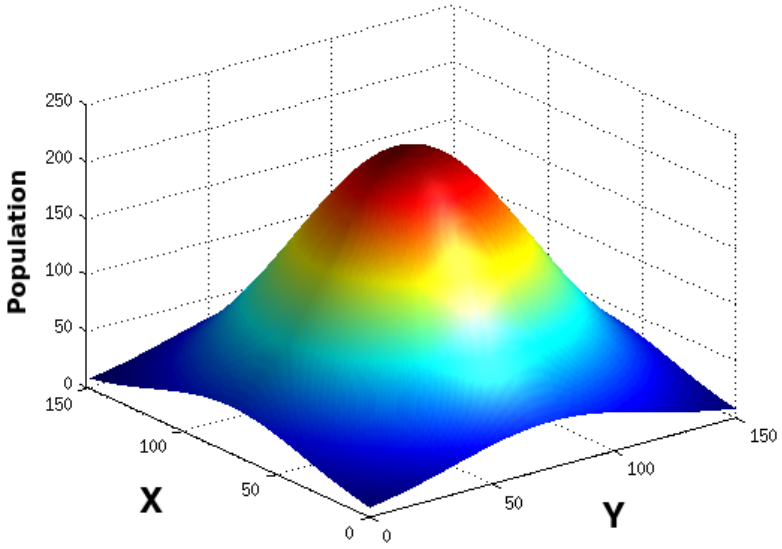

Figure V.2: Example of population distribution on the lattice

$v = l \cdot dt$ with trajectories that remain a straight line as long as a scattering event occurs or they reach a lattice boundary. The scattering process leads to randomization of the walkers propagation directions. The walker also carries energy in the form of identical photons with the same frequency.

• **The Frequency Generator** Each walker also has its own frequency that is randomly assigned in the time of creation by spontaneous emission, to reproduce the stochastic behavior of such process. The spontaneous emission of a large amount of walkers must spectrally reproduce the lineshape of the atomic transition. Then, considering the Lorentzian shape of such transition, the frequency of a walker is drawn from a Cauchy distribution of random number.

In order to generate values according to such distribution, the *inverse transform sampling method* is implemented in the C++ code of the numerical simulation. The method allows to generate random numbers from a distribution given its cumulative distribution function (cdf). The method descends from the following theorem:

Theorem 3 Probability Integral Transformation*: if X is a random variable with cdf F_X, then the random variable $Y = F_X(X)$ has a uniform distribution in the interval [0,1].*

Hence, once the software has generated a pseudo-random real number $\xi \in [0, 1]$ with uniform probability, a new pseudo-random number ω following a Cauchy distribution can be derived. Therefore, it is necessary to solve the equation:

$$F(\omega) = \frac{w}{\pi} \int_{-\infty}^{\omega} \frac{1}{(\eta - \omega_0)^2 + w^2} d\eta = \xi \tag{V.14}$$

where $F(\omega)$ is the cdf of the Cauchy distribution (V.13). Then the solution is:

$$\frac{1}{\pi} \arctan\left(\frac{\omega - \omega_0}{w}\right) + \frac{1}{2} = \xi \tag{V.15}$$

from which finally one can derive the random number ω as following:

$$\omega = \omega_0 + w \tan\left[\pi\left(\xi - \frac{1}{2}\right)\right] \tag{V.16}$$

• **The Pumping System** Once decided the total amount of population inversion, i.e. the pumping level, the excited atoms are distributed on the medium according the spatial density given by the (V.12). Expressed in term of photon energy, the total energy E_t is the following:

$$E_t = \hbar\omega_0 \int N_0(x, y)dxdy \tag{V.17}$$

where the subscript 0 means that $N_0(x, y)$ is the maximum value assigned to the site if all prearranged energy is provided and all decaying processes are inhibited. Then $\hbar\omega_0$ represents a measurement unit of the energy stored in each atom. In sake of simplicity, in this text the energy will be expressed in term of number of excited atoms.

From temporal point of view, there are two different ways to provide the energy to the medium:

(1) *impulsive pumping*
all energy of the medium is provided in a time instant $t = 0$ of the simulation, i.e. with a pumping temporal duration $T_p \ll dt$

(2) *finite time pumping*
The whole amount of energy is supplied during a time interval $T_p > dt$

In the second case, after each temporal step dt, the population of each site of coordinate (x, y) is updated according the following rule:

$$N(x, y, t) \longrightarrow N(x, y, t) + R_p(x, y, t)dt \tag{V.18}$$

where the *pumping rate* $R_p(x, y, t)$ is given by:

$$R_p(x, y, t) = \begin{cases} \frac{N_0(x,y)}{T_p} & \text{if} \quad 0 \le t \le T_p \\ 0 & \text{if} \quad t > T_p \end{cases} \tag{V.19}$$

where t is the simulation time given in units of dt. The finite pumping mode gives the same result of the instantaneous one if one sets $T_p = 1$.

• **The Simulation Steps** The steps that simulates the different involved processes in the random laser dynamics are the following:

(1) ***Spontaneous Emission***
In a lattice cell of coordinate (x, y), during each temporal step of the simulation a spontaneous emission event can occur (Fig. (V.3)) with a probability $\mathcal{P}_{sp}$ that depends the local population $N(x, y)$:

$$\mathcal{P}_{sp} = \gamma_0 N(x, y)dt \tag{V.20}$$

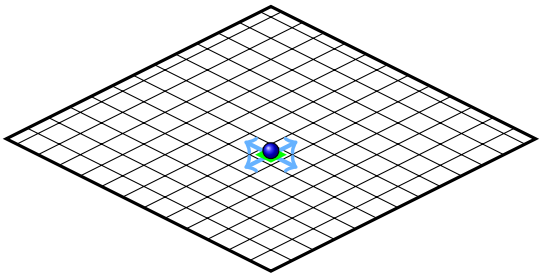

Figure V.3: *Spontaneous Emission:* During each temporal step a generation of a walker (blue sphere) can occur in a cell site (in green) with a probability that depends on the local population.

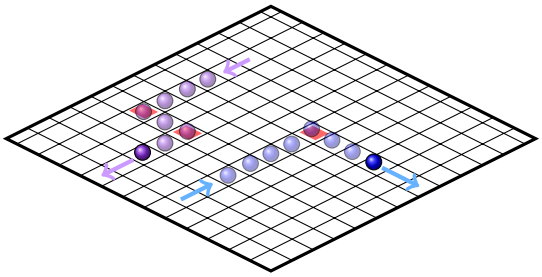

Figure V.4: *Diffusion:* After each temporal step each walker moves to a neighboring site according its trajectory. If a scattering event occurs (red cell) the direction of propagation is randomized.

where γ_0 is the *spontaneous emission rate* expressed in dt^{-1}. A number $\xi \in [0, 1]$ is drawn and if it is lower than $\mathcal{P}_{sp}$, the spontaneous emission event occurs. In this case the local population is decreased by one unit:

$$N(x, y) \longrightarrow N(x, y) - 1 \tag{V.21}$$

and a new walker is created with the following characteristics:

(i) the initial coordinate (x, y) of the generation site

(ii) a initial direction of the trajectory that is uniformly randomly assigned among one of the four possible directions

(iii) an initial energy represented by a number $n = 1$ photons

(iv) a frequency assigned by means of the random value $\xi \in [0, 1]$ inserted in the equation (V.16)

(2) ***Diffusion***

Each walker in the lattice can undergo to a *scattering event* with the probability $\mathcal{P}_s$ assigned according the desired diffusive property of the medium (Fig. (V.4)). During the time unit dt, such occurs if a random number ξ, with uniform distribution in the interval [0,1], results greater than $\mathcal{P}_s$. If a walker is scattered a new direction of trajectory is drawn, among the four available possibilities, with uniform probability.

Then, whether the scattering event is happened or not, the position of each walker is updated by moving it in a adjacent neighboring cell according its trajectory. If a walker reaches a boundary of the *emission event* occurs (Fig. (V.6)): the walker is destroyed

and eliminate from the simulation and its energy (number of carried photons) with its frequency is recorded to the output.

(3) ***Stimulated Emission***

During this step the population of each cell of the lattice and the number of photons carried by each walker are deterministically update according the following rules, devoted to simulate the stimulate emission process (Fig. (V.5)). Let n_i the number of photons carried by the i$^{\text{th}}$-walker with frequency ω_i and located in the cell of coordinates (x, y):

$$n_i \longrightarrow [1 + \gamma(\omega_i)N(x, y)dt]n_i \tag{V.22a}$$

$$N(x, y) \longrightarrow [1 - \gamma(\omega_i)n_i dt]N(x, y) \tag{V.22b}$$

where the stimulated emission coefficient γ depend on the detuning of the walker's frequency from resonance:

$$\gamma(\omega_i) = \frac{\gamma_0}{1 + (\omega_i/w)^2} \tag{V.23}$$

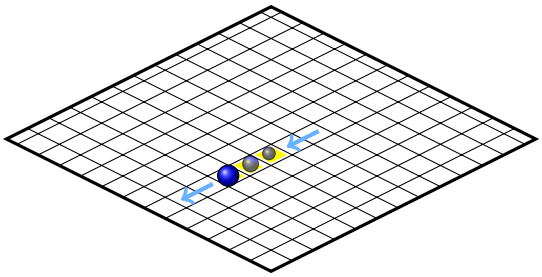

Figure V.5: *Stimulated Emission:* during each step the energy carried by the walker is deterministically amplified by stimulated emission, with depletion of population of the sites crossed (in yellow).

• **The Output Emission** The walkers that overstep the boundaries of lattice are recorded as output emission in order to provide two different statistical analysis of the emission: in time and frequency.

At each time step the energy of those walkers that has flowed out during the time interval dt are summed to create a temporal behavior of the overall emission as a function of time. Such resulting time series is binned on a time window of duration T_w, with the intent to simulate a output light pulse measured by an external photon counter with a finite time response. Then each point of the final time behavior consists in the sum of a large number of events.

From spectral point of view each the energy of each recorded walker in summed in a output spectral windows of 1000 channels according its frequency. Such sum is continued for the overall simulation, recording a total spectrum of emission without considering the exit time of individual walker.

• **Simulation Dynamics and Computational Details** From computational point of view the each step of the simulation consists in a sequential updating of every walker and site population according the corresponding process. The parallel processing of a large number of walkers

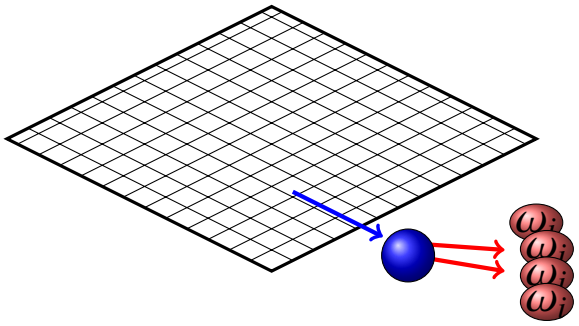

Figure V.6: *Output Emission:* if a walker reaches a lattice boundary it is destroyed and the its carried photons are recorded, taking account of the frequency ω_i.

is of course very computationally expensive, but it is necessary in order to consider the gain competition. The number of active walker during a temporal step of the simulation has a large variability and strongly depends on the evolution of the system and on the choice of experimental parameters. It can range from a few units, at low pump energy, to many thousands, at the first instants for high pump energy. In the former case, the probability (V.20) is low and the average time of generation becomes comparable to the lifetime of the walker within the lattice. In the latter one, the large population density causes a large amount of spontaneous emission events in the first instants, leading to an accumulation of co-existing walkers due to average generation time much smaller than the walker lifetime. Although, such trend relaxes to a smaller generation rate in a time comparable with exiting time of the oldest walkers, because the amplification by stimulated emission, that depletes the active medium and wherever decreases $\mathcal{P}_{sp}$.

In order to improve the execution speed of the numerical simulation, the code is written with the attempt to achieve an optimum management of the memory of the calculator. Such a execution time represents a very critical point, because, in order to achieve a statistical analysis a large number of simulation with identical initial parameters has to be performed. In fact in the corresponding experimental results the statistical analysis demand a large set of recorded data from emission with the same experimental conditions. As discussed in Sec. (5.1), the knowledge of the statistics can be solely achieved with collecting a very large set of data.

In the C++ code, only the population of the lattice cells and the spectral and temporal emission are recorded in arrays during the execution. All informations of each random walker are allocated by concatenate list, whose dimension is not predetermined and from which the occupied memory by data corresponding to destroyed walker are dynamically deallocated.

In order to guarantee the randomness, the seed of the pseudo-number generator is initialized to the execution time, in order to avoid the generation of identical sequences of random values in different simulations.

• **Parameters Choice** In choice the parameters of the simulation, one have to pay attention to remain among the range of validity of the model, which requests that the spontaneous emission lifetime is much greater than dt and the cell size of the lattice are small enough to determine less of one local event of walker generation. A spatial mapping of the medium that does not satisfy the latter requirement should lead to a complete isotropy of the diffusion mechanism and to a lack of validity of the theoretical description. Then the parameters involved in (V.20) have to be

such that $\mathcal{P}_{sp} < 1$, posing a upper limit to the energy density and in the spontaneous emission rate.

The total dimension of the sample also poses limits in the $\mathcal{P}_s$; in particular a value of ℓ_s greater than the lattice side L leads a system in a complete ballistic regime, whereas the dimension of the cell determines the lower limit to the accessible mean free path.

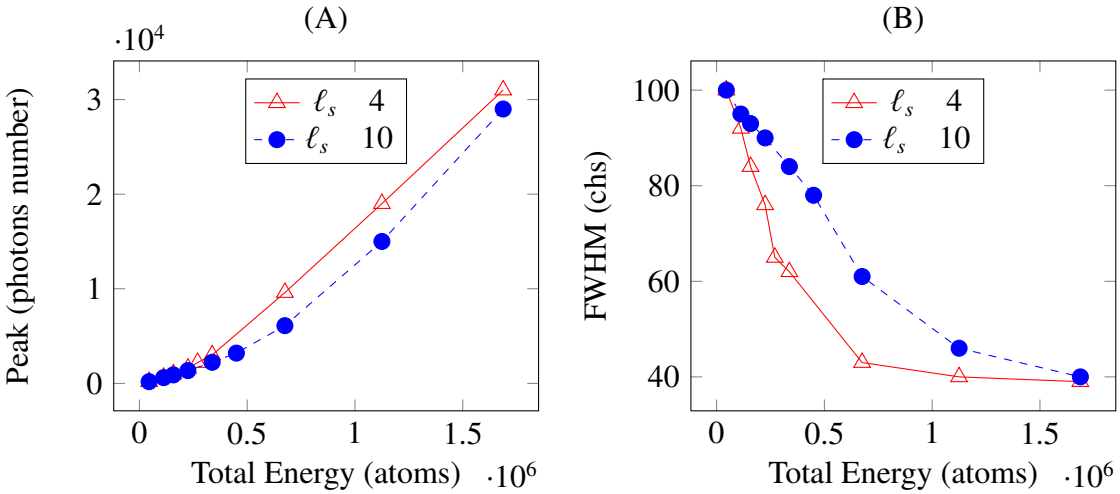

Figure V.7: On the left it is shown the peak value as a function of the total energy instantaneously provided to the lattice for $\ell_s = 4$ and $\ell_s = 10$, whereas on the right the FWHMs are reported.

Nevertheless such intrinsic limitation, such 2D numerical model is able to reproduce the behavior of a random laser system in diffusive regime, as shown in the next section.

5.2.3 Numerical results

The chosen parameters for the numerical simulation campaign are the following:

- lattice side of 150 cells
- total population N that ranges from 1.125×10^5 to 2.025×10^7, with corresponding average number of atoms per cell of 5 and 900 respectively.
- active medium of 2D-Gaussian shape with $\sigma_G = 40$
- $P_s = 0.25, 0.05, 0.025, 0.01$ ($\ell_s = 4, 20, 40, 100$)
- spontaneous emission rate $\gamma_0 = 10^{-4}$ (spontaneous emission lifetime $\tau_{sp} = 10^4$) and bandwidth of the transition of 50 chs
- simulation total duration $T_{sim} = 3\tau_{sp}$, with an output binning time $T_w = 10$

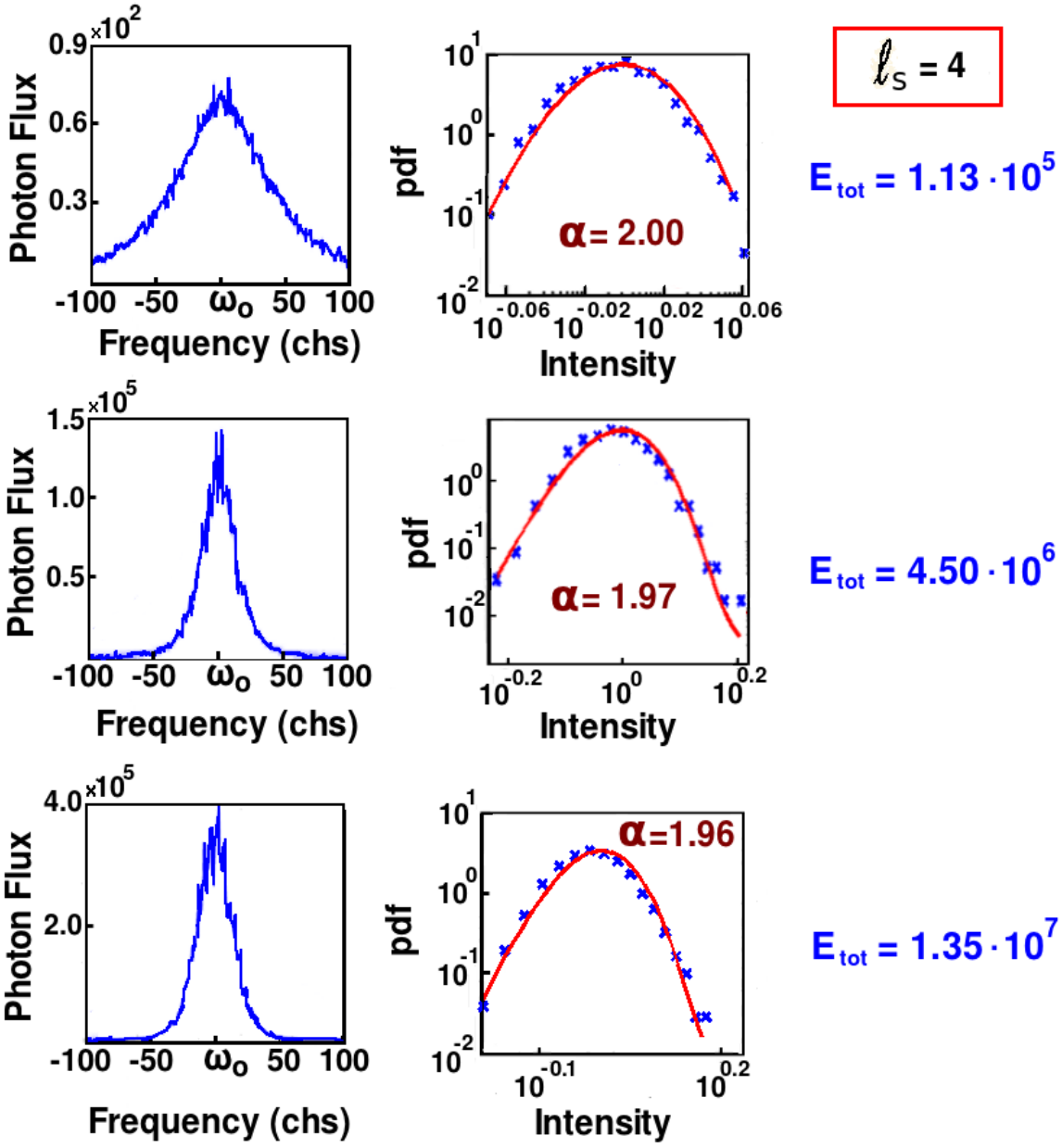

Figure V.8: Typical numerical simulation spectra (left column) at different energy for the lattice with strongest scattering ($\ell_s = 4$). On the right column the intensity histograms and the α-stable fitting of the correspondent energy are shown. The spectra manifest a larger narrowing around the central frequency of the transition as the energy increases. No random narrow spikes are detectable.

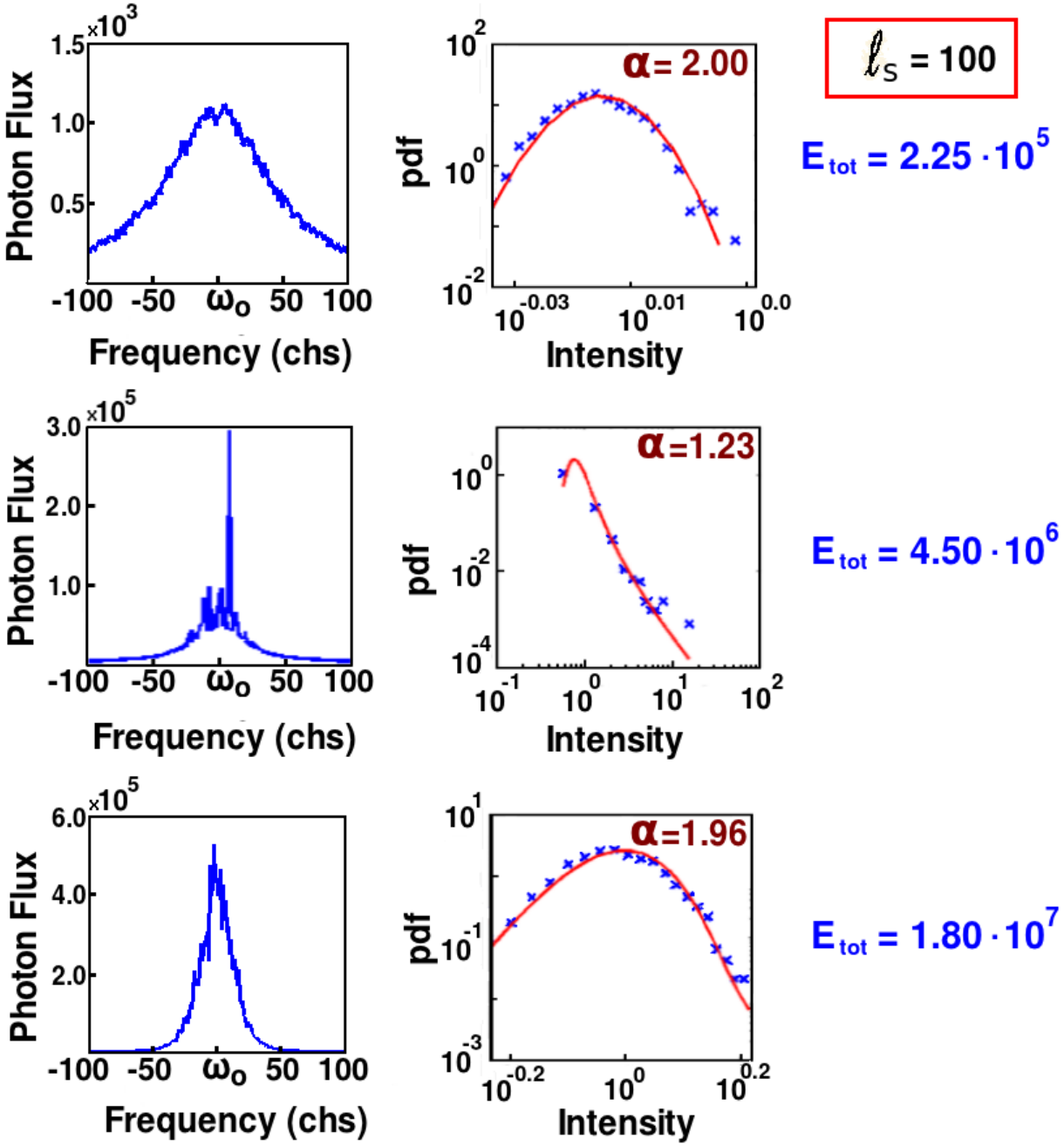

Figure V.9: Typical numerical simulation spectra (left column) at different energy for the lattice with weakest scattering ($\ell_s = 100$). On the right column the intensity histograms and the α-stable fitting of the correspondent energy are shown. The spectra manifest a larger narrowing around the central frequency of the transition as the energy increases. For the intermediate energy value the presence of random narrow spikes are evident.

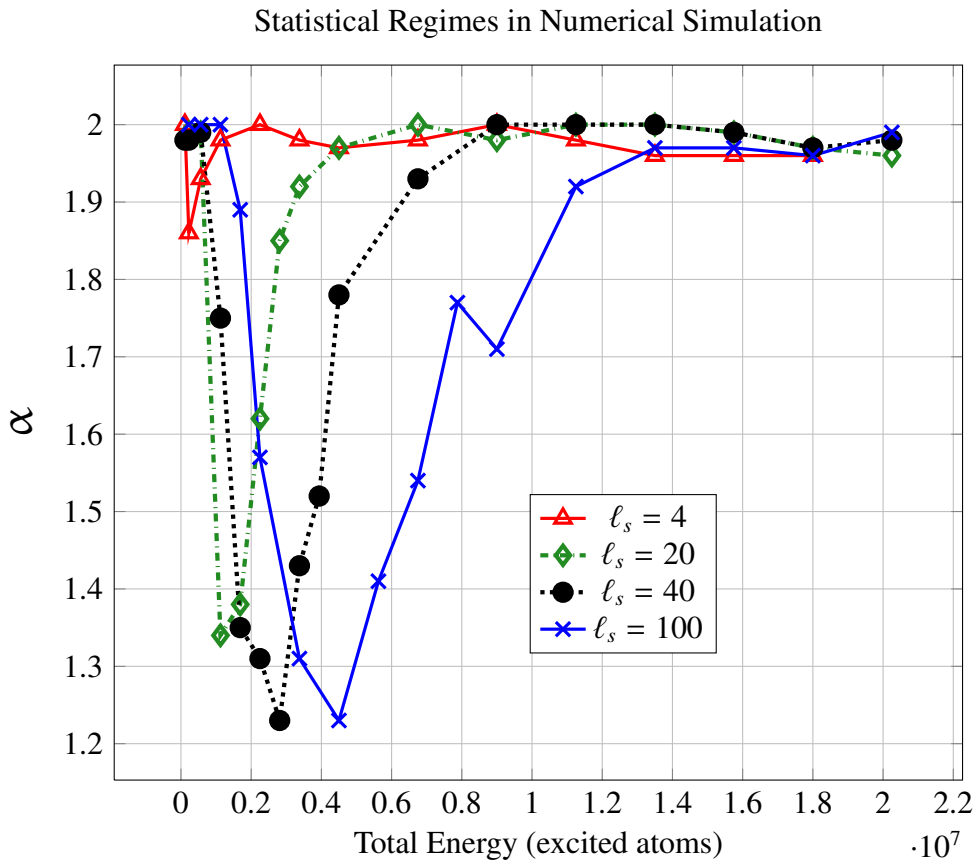

Figure V.10: Numerical simulation results: α-index as a function of energy for different scattering strengths, in the case of instantaneous pumping. The crossover to Gaussian-Lévy regime can be arbitrarily fixed to α=1.8.

With observing the numerical spectra, the simulation accurately reproduces the behavior of a random laser system in diffusive regime: with increasing the energy the spectrum of emission changes from a typical broadening of the spontaneous emission to the narrowing around the central frequency of the transition, due to the stimulated emission process (see (V.13) and (V.23)).

Therefore, a low-energy emission regime, dominated by the spontaneous emission, and a high-energy emission one, ruled by stimulated emission and with narrow spectra, are identified. Moreover, in certain range of intermediate energies a threshold condition can be detected, with observing when the narrowing due to stimulated emission mechanism begins to emerge. In Fig. (V.7)-(A) the peak value as a function of energy for two scattering strength ($\ell_s = 4$ and $\ell_s = 10$) are shown; a slope change appears localized around $0.2 \cdot 10^6$ excited atoms for $\ell_s = 4$ and around $0.5 \cdot 10^6$. As expected from the Letokhov threshold condition (eq. (IV.24)), on equal ℓ_g and sample geometry the more diffusive sample has a lower threshold energy, because the increased lifetime of the walkers inside the lattice promotes their amplification, leading to the role played by the spontaneous emission to become dominant. In Fig. (V.7)-(B) the correspondent FWHMs are reported: for low energy values the FWHM approaches the selected one $2w = 100$ chs for the linewidth of the transition, whereas after threshold the bandwidth

rapidly approaches ~ 40 chs.

For each variable initial parameters set (N, P_s, T_p) and leaving the other ones fixed, about 10^4 simulation have been performed in order to achieve a sufficient statistics, that is performed with using data recorded in a channel of frequency. The data as collected are used to produce histograms of intensities and the corresponding stable fit.

In Fig. (V.8) and Fig. (V.9) numerical results are shown for a ℓ_s of 4 and 100 respectively for 3 different level of initial energy provided with an instantaneous pumping) given in number of excited atoms of: $1.15{\cdot}10^5$, $4.50{\cdot}10^6$ and $1.35{\cdot}10^7$. In the first case, the most diffusive medium, one can find a narrowing of emission with increasing energy, showing in every case typical smooth spectra with small fluctuation in the form of a small amount of noise. The right column reports the corresponding statistics of the emission: the crosses represent the point of the intensity histogram normalized the the median and the red curve the stable fit. In every case the α-index calculated approaches the value 2.0 that identifies the Gaussian statistics. No large fluctuations with presence of narrow spikes are detectable in the whole range of pumping energy. As justified in Sec. (5.1.2), cases with a value of α lower but very near 2.0 can be considered as Gaussian.

In Fig. (V.9), where $\ell_s = 100$, a relevant different behavior emerges: for low energy the output emission regime shows the spectral property of the spontaneous emission, with smooth broad spectrum and a Gaussian statistical regimes. Further increasing energy, peaks at random frequencies appear, causing the corresponding intensity histogram to manifest a fat-tail due to rare large values that appear in the channel selected for the statistics. The α-index calculated by the fit becomes much smaller than 2 and the emission regime can be labeled as a Lévy regime. At high energy a overall narrowing of the spectrum occurs, whereas the narrow random spikes are no longer detectable and the emission statistic re-becomes Gaussian.

The Fig. (V.10) shows the detailed results of the statistics of the emission, with plotting α-index as a function of energy for different scattering strengths, in the case of instantaneous pumping. If one fixed the arbitrary value for the crossover between Gaussian to Lévy statistics, the lattice with the larger level of scattering does not reach such limit and it remains in the Gaussian regime for the whole range of provided energies. On the contrary, the other lattices show a crossover to the Lévy regime, an approach to a bottom limit of α and then, with a further increment of energy, a return to $\alpha = 2$.

Hence three different statistical regimes are present with varying energy:

(1) *First Gaussian Statistical Regime*
The value of α approaches 2 and the spectra are as broad as the bandwidth of the atomic transition, smooth and without the presence of large fluctuations and random spikes. The dominant process is the spontaneous emission one.

(2) *Lévy Statistical Regime*
The process that rules the emission behavior is still the spontaneous emission with a limited spectral narrowing, but instability effects due to amplification by stimulated emission become strongly present in the form of fluctuations and presence of narrow random spikes. The values of α typically are much below 2.

(3) *Second Gaussian Statistical Regime*
The value of α approaches 2 again, but the stimulated emission becomes the dominant mechanism. The spectrum is narrow and the presence of random spikes no longer detectable.

After the statistical investigation and characterization, the emission spectra can be labeled as ascribable to a statistical regime; in the Fig. (V.11) another example of emission spectra are shown for a lattice with an intermediate scattering level. Then fixed the diffusive properties, a tuning of the statistical regime of the emission is possible with varying energy.

Since, as seen in Fig. (V.7), the threshold value increases with the ℓ_s, such similar behavior for the first statistical crossover means that the Lévy regime should linked to an instability state experienced by the system in such range of energies. In fact the statistical crossover occurs in those ranges of energy where the spontaneous emission and the stimulated emission competes for the role of dominant mechanism. Then the second crossover is then linked to a state where the stimulated emission becomes the dominant process, leading, by means of the spectral narrowing to another Gaussian regime.

Moreover it is worth to note that the Lévy region appears deeper and broader for lattice with a large ℓ_s, whereas a decrement of such parameter can lead to the total inhibition of the Lévy behavior. Such results, in the light of the theoretical picture of extended modes, is discussed in the following section.

5.2.4 Statistical regimes crossover and gain coupling

It has been noted the clear link that emerge between the scattering and the statistical regime with varying energy; therefore the next step of theoretical discussion concerns the detection of a parameter that is able to characterize such behavior. This parameter can be find in the comparison between the active medium dimension, represented by the width $\sigma_G = 40$ of the two-dimensional Gaussian distribution of the population on the lattice, and the scattering mean free path ℓ_s:

$$\zeta = \frac{\ell_s}{2\sigma_G} \tag{V.24}$$

Then ζ spans from 0.05 (diffusive regime) for strong scattering to 1.25 (quasi-ballistic regime) for the weakest diffusive medium. The choice to consider the dimension of the active medium and not of the whole sample has two motivation: the first concerns the too large computational power requested to explore the behavior of lattice whose dimension are much larger than the active part. The second reason, in the light of the experimental data, the only parameter that should act as activator of a statistical regime is the above defined ζ.

As discussed in Sec. (5.2.1), in order to describe the fundamental mechanisms that trigger different system behavior, the attention is focused on the gain coupling between modes . In numerical simulation, walkers are "coupled" if they share their paths in the spatial-temporal domain, in such a way to exploits, for amplification purposes, the same population. It is straightforward that only the uncoupled modes may reach an anomalously large amplification.

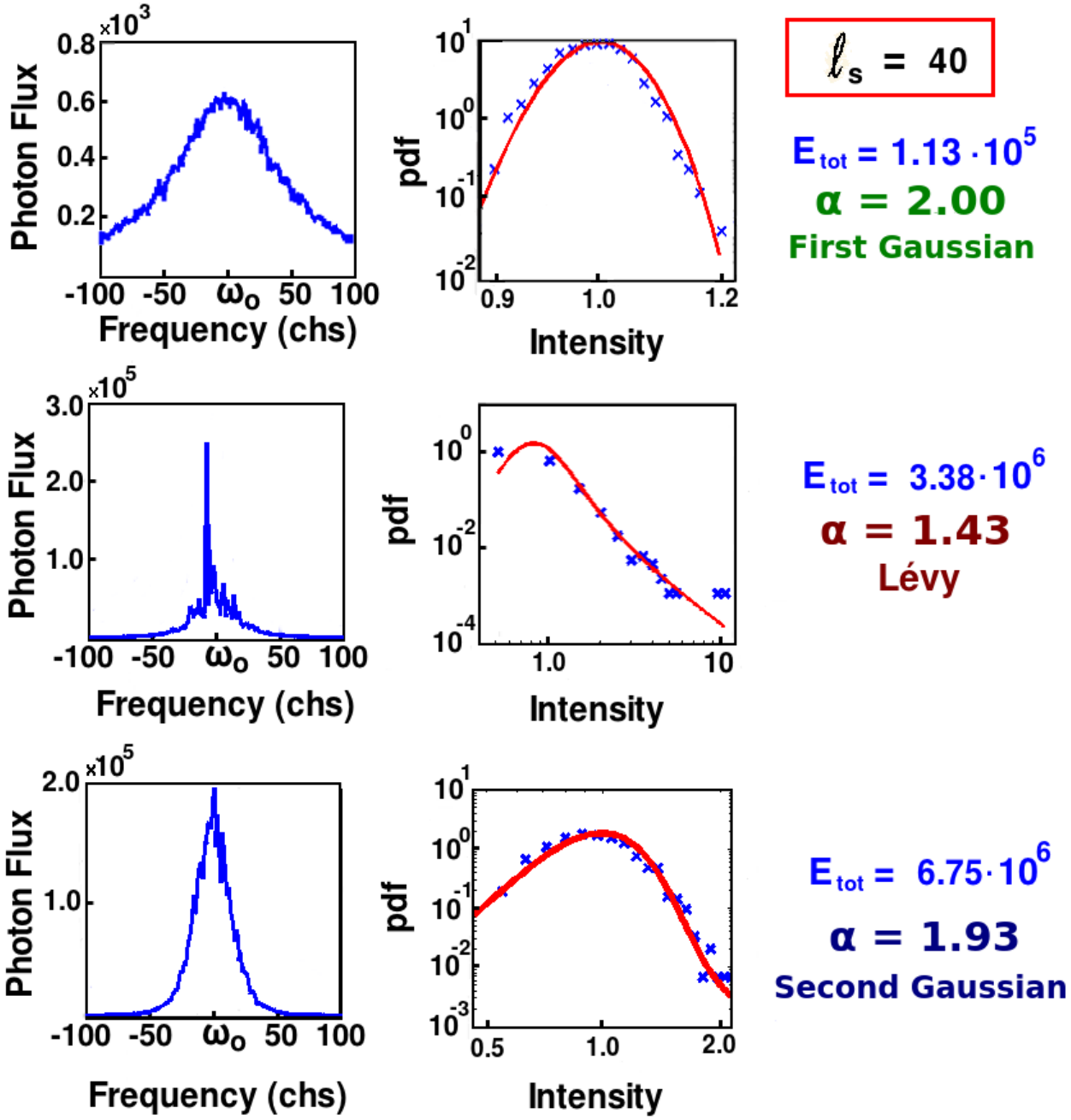

Figure V.11: Typical numerical simulation spectra (left column) at different energy for the lattice for an intermediate scattering strength ($\ell_s = 40$). On the right column the intensity histograms and the α-stable fitting of the correspondent energy are shown. The label of the statistical regime it is also shown.

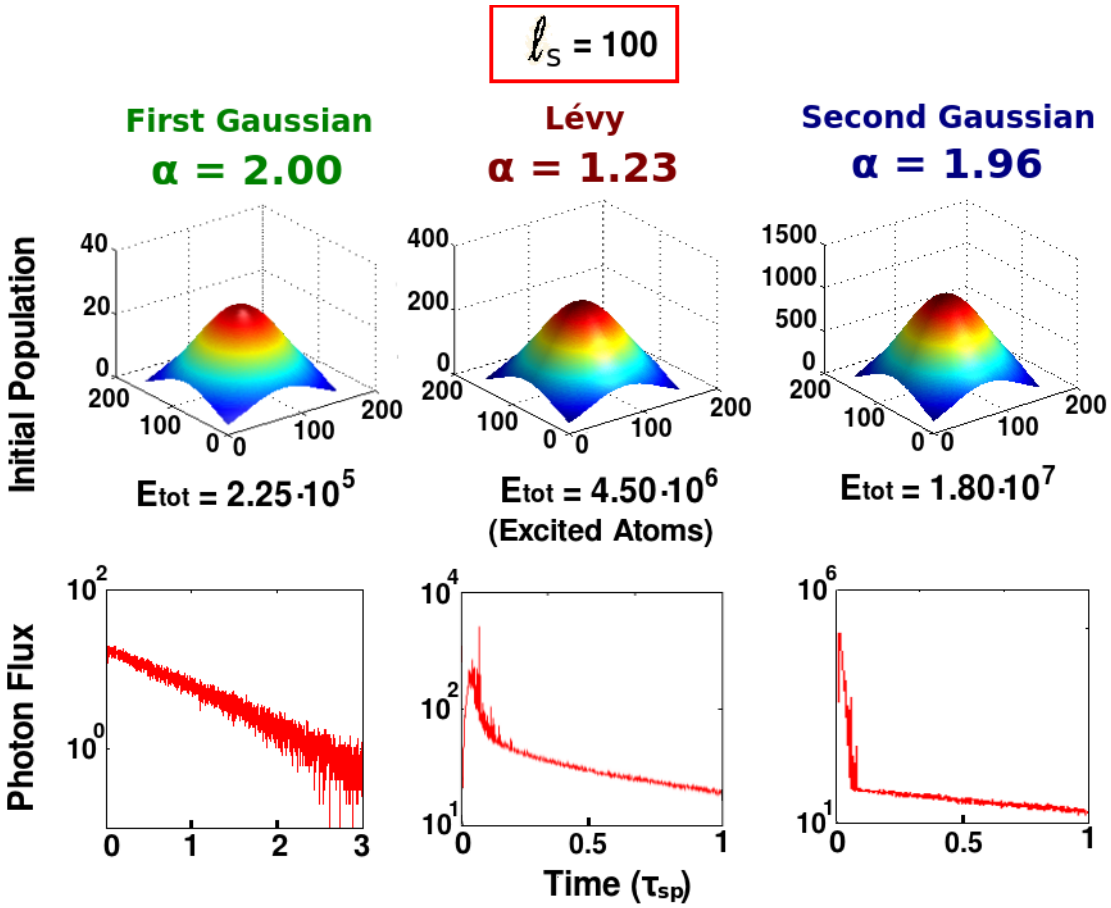

Figure V.12: Temporal behavior of the emission as a function of time, expressed in units of the spontaneous emission lifetime τ_{sp}. The time of energy releasing by the system decreases as the initial energy increases, because the stimulated emission. Since the presence of the "lucky photons", in the Lévy regime narrow temporal spikes are present.

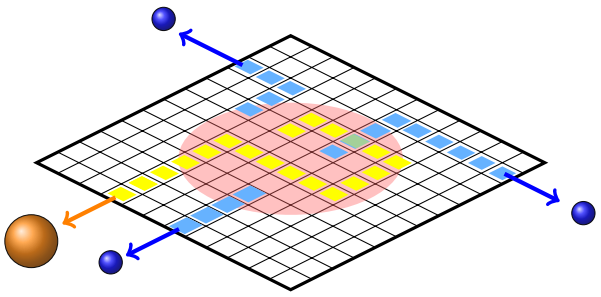

Figure V.13: Within a weakly scattering medium, a random walker ("lucky photon", in yellow), that undergoes anomalous large number of scattering events, has a lifetime much longer than the other walkers (in blue). If their path is overlapped to the active zone of the lattice (in red), it can experience a large amplification. In addition to the weak scattering condition, the other constrain for the Lévy regime is on the available energy amount, that should not be too large. If such a constrain is satisfied, the number of co-propagating walkers is small, making possible the uncoupling of the "lucky photon" from the gain competition, for example with a negligible superposition of walkers paths.

When the provided energy to the lattice is low, whichever the scattering strength, the amplification that a walker can experience during its lifetime is negligible and the system is the first Gaussian regime, with smooth spectra solely determined by the spontaneous emission. In such a case the gain competition mechanism between modes has not significance, since the available population is too low. From temporal point of view the emission duration is long and ruled by the spontaneous emission lifetime (see Fig. (V.12), left column).

With increasing energy to an intermediate level, the system approaches the threshold condition and the behavior becomes strongly dependent on ζ. For large or intermediate values of ζ (weak scattering), rare modes ("lucky photons") with a long lifetime, due to an anomalously large number of scattering events and direction of randomized trajectories that delayed the exit time from the medium, can experience a large amplification. Since the rate generation of new walker is still relatively low, the "lucky photons", during their lifetime, can exploits a portion of active medium that has not still explored by other walkers. Since the amplification is a nonlinear mechanism, small variation in path length should lead to huge difference in the number of carried photons, as it is simply pictured in the Fig. (V.13). Then an anomalously large amplification can be experiment and, once the "lucky photon" finally exits from the lattice, its frequency assumes an important weight in the output spectrum. Then, since the frequency of every walker is randomly assigned, the output spectrum shows a narrow spike at a random frequency. The other "not so lucky" walkers experience only a modest amplification, also because a large part of available energy is took away by the "lucky photons". Therefore, since the initial population is not large enough, a walker can undergo low amplification, unless it becomes uncoupled to the gain competition. The overall spectrum of the emission present a main part ruled by the spontaneous emission, with only a moderate narrowing due to the modest walkers average amplification, that, because the (V.23), is encouraged for a small detuning from the resonance. In superposition of this spectral shape, high energetic narrow spikes at random frequencies appears, highlighting a threshold situation where the stimulated emission puts its signature on the emission dynamics. In determining the statistical regime, when in a simulation run the frequency value of a random spike falls in the monitored channel, a rare event with a large value is recorded, contributing to increment the tail of the distribution and the determination of a Lévy statistical regime.

The characteristic time of emission in the Lévy regime is still long and dominated by the spontaneous emission, with a presence of temporal spikes due in correspondence of the exit time of the "lucky photons" (see Fig. (V.12), middle column).

With a further increasing of the energy, the rate of walkers generation increases too. The large available population causes a decrement of the gain length ℓ_g, with a sensible amplification that can occur also for short paths. In this scenario, the mechanism that prevents the appearance of "lucky photons" is provided by a strong gain coupling; indeed, because the high probability of walker generation per unit time in each lattice sites, a large number of walkers appears in the from the first instant of the simulation. Despite the short ℓ_g, many walkers find themselves in the condition to share the available energy that pick up along their paths with the other walkers. Hence this gain coupling prevents a situation according which a walker bears away an anomalous large value of energy, leading the system to a more "democratic" scenario where the first appeared walkers share the energy and reach a similar level of amplification.

In this case the ruled mechanism is played by the stimulated emission, that drives the system to the new equilibrium state of the Second Gaussian Regime. Therefore the global output

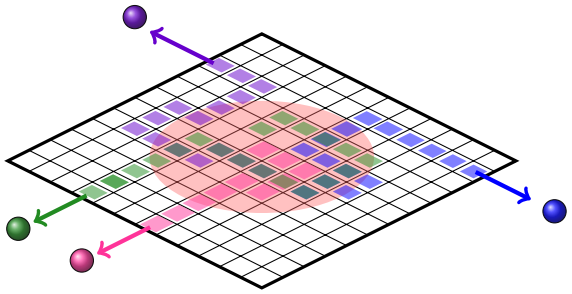

Figure V.14: In presence of strong scattering, the walkers share the same available gain (in red) along their path, leading to a strong gain coupling and then to an average mechanism that acts on the possible amount of carried energy.

spectrum appears smooth, due the average mechanism in the maximum energy that a walker can carry, and with a large narrowing around the central frequency of the transition. Then the statistics of the emission does not reveal large fluctuations and the value of α approach 2.

From temporal point of view, the emission is concentrated among the first instant of the emission; the large number of created walkers as soon as the simulation run is started causes a rapid depletion of the energy available, because the amplification by stimulated emission and the small ℓ_g. Therefore the main part of the energy stored in the medium is took away when the first walkers exit from the lattice. After that a small population is survived on the lattice, causing a abrupt increment of ℓ_g and a decrement in the new walkers generation rate. In such very long fading phase the emission becomes slow and ruled by the spontaneous emission and not able to introduce modification on the spectral shape, because the large energy emitted in the first temporal part of the overall emission. In summary the emission temporal trend is characterized by a peak of emission of duration comparable with the walker lifetime and a following long tail with modest energy (see Fig. (V.12), right column).

The last issue that remains to analyze is the lacking of a detectable Lévy regime in the most diffusive case, as shown in Fig. (V.10) for the lattice with ℓ_s=4. In this case only a small decrement of α is present and with values that are in any case grater than 1.8. Moreover the inspection of emission spectra does not reveal the presence of a fluctuations regime. In order to clarify such inhibition of the Lévy regime, let us focus the attention of the conditions that cause and stoke the instability behavior that occurs in the range of energies where the crossovers between the Gaussian and Lévy regime occurs. Indeed, one can considers the random laser in diffusive regimes the laser-like source where the threshold condition involves a large range of energy and large instability condition. With increasing ζ the entrance in the Lévy regime is at larger energies, because the threshold condition depends on the scattering strength, since the rapid exit time in weak scattering regime is a large loss factor. However for $\zeta \sim 1$ the Lévy regime is "deeper", i.e. it is characterized by very low value of α, and "broader", i.e. the return to values of $\alpha \sim 2$ occurs to large value of energy (Fig. (V.10)). The former is due to the fact that walkers that have a long lifetime are rare, since the small probability of scattering, and then become the rare energetic events that determine the fat tail of the intensity statistics. The latter is originated by the large loss factor due to the short average walker lifetime, that causes the condition "gain that overcomes losses" to occur at very large energy, whereby the stimulated emission finally prevails on the spontaneous emission in determining the spectrum shape. Then, as ζ decreases, the value of threshold energy, above which the stimulated emission begins to

compete with the stimulated emission, shifts towards lower energy, as well as the "closure" of the Lévy regime band. Hence it is to be expected a gradual fading of the range of energies involved in the Lévy regime towards a limit condition of total suppression of such statistical behavior. Therefore, on equal ℓ_g, in a strong scattering medium the longer lifetime allows to easily experience amplification meanwhile the gain coupling becomes promoted (Fig. (V.14)).

Such a scenario can also be described in the temporal domain by means of the comparison of two characteristic times: the *mean scattering time* $\tau_s = dt/P_s$ and the *gain time*, i.e. the ballistic time span T_g required to cross the active part of the medium (with estimated linear dimension $\sim 2\sigma_G$). The former is 100 in the case of the weakest scattering medium and 4 in the strongest one, whereas the latter is always 80. The Lévy statistics emergence appears favored if $\tau_s \geq T_g$.

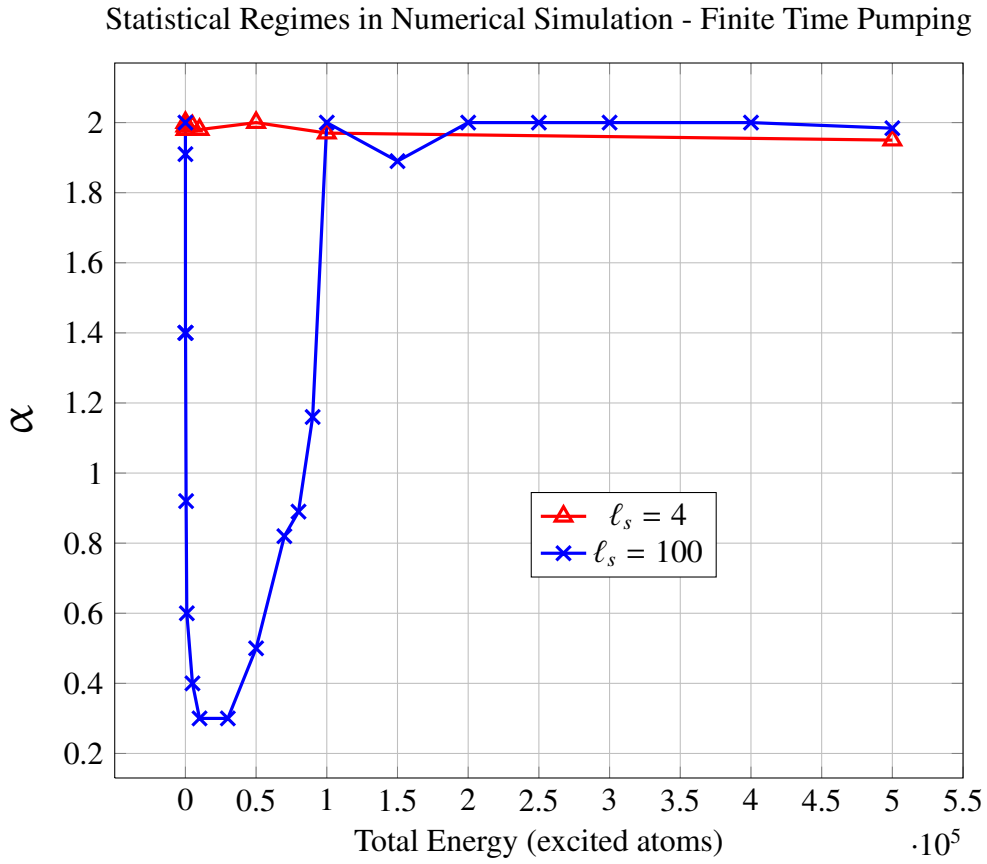

Figure V.15: Numerical simulation results: α-index as a function of energy for different scattering strengths, in the case of finite time pumping ($T_p = \tau_{sp} = 10^3$). For the most diffusive sample ($\ell_s = 4$, red triangles)the statistical regime remains Gaussian for the whole range of provided energies. In the weak scattering medium ($\ell_s = 1000$, blue crosses) a deep Lévy regime is instead present.

5.2.5 Finite time pumping

A temporal duration of the pumping comparable with the spontaneous emission lifetime has been proposed as a condition whereby an average mechanism should act between modes, leading to an inhibition of random spikes in spectrum. Hence the experimental parameters, as

well the numerical model, that have been used a presence of a pumping system with a very small temporal duration. A typical example makes use of a pump pulse about ∼25 ps long and active media whose spontaneous emission lifetime has a temporal duration about some ns. In such a condition, the pumping time can be approximated as instantaneous, because the whole amount of energy is provided to the medium in a time much short than the response time of the system.

Since, as it is shown in the Sec. (5.3), the presence of narrow spikes are detectable also when the above condition is not satisfied, from theoretical point of view it should be worth to explore such dynamics by means of numerical simulations where $T_p \sim \tau_{sp}$.

Then another set of simulations was performed in the cases of ℓ_s=100 and 4 and $T_p = \tau_{sp} = 10^3$; because the increment on computational time required for the finite time pumping, the spontaneous emission rate is raised from 10^{-4} to 10^{-3}. Since, in order to guarantee the recording of complete spectra, the output emission requests an integration time that is a multiple of τ_{sp}. Therefore such an increment on the spontaneous emission rate allows to reduce of one order the total time of each simulation run. On the other hand the downside consists in the impossibility to explore a energy range as large as in the case of instantaneous pumping, because the constrain given by the (V.20). However, the energy range investigated gives results complete enough to clarify the possible role of the pumping time on the spectrum characteristics.

The results are showed in Fig. (V.15): in the less diffusive lattice a Lévy regime zone is present in a large range of energies, whereas in the opposite case the value of α approaches 2 whatever the energy. Therefore the time duration of the pumping mechanism has not an important influence in determining the statistical regime of the emission; if the conditions described by the parameter ζ hold and the total energy stored in the medium has the appropriate value, the Lévy statistical regime appears.

5.3 Experimental results

5.3.1 Experimental set-up and samples

The experimental sample consists in a solution of 1mM concentration of Rhodamine 6G dye dissolved in methanol, as active medium, with different concentration of a TiO_2 nanopowder, whose concentration was varied from 0.1 to 3 mg/cm^3, to create disorder.

In order to estimate the scattering mean free paths that correspond to the different concentration, independent sets of measurement of attenuation according the Lambert-Beer law, at very low scatterers concentrations (0.003 to 0.03 mg/cm^3), have been performed. A He-Ne laser has been used to produce the ballistic beam, since the wavelength (633 nm) is rather near to the peak of the Rhodamine 6G dye fluorescence. Then an extrapolation at higher concentrations has been calculated. Of course an estimation of ℓ_s and ℓ_t can be numerically calculated by the Mie theory, with the approximation of identical spherical particles. However, since for particles with a size parameter around the unity, as the TiO_2 particles have, the scattering efficiency is strongly dependent on the particle radius, whose value is difficult to predict and measure. The transport free paths ℓ_t of the sample used in this work are estimate to range among 0.13 to 4 mm. A modification of such values as the wavelength of the emission changes is to expected, but the measurement described above however give a reasonable estimation of the ℓ_s. Since, considering an emission peak wavelength about 560 nm, the corresponding values of the pa-

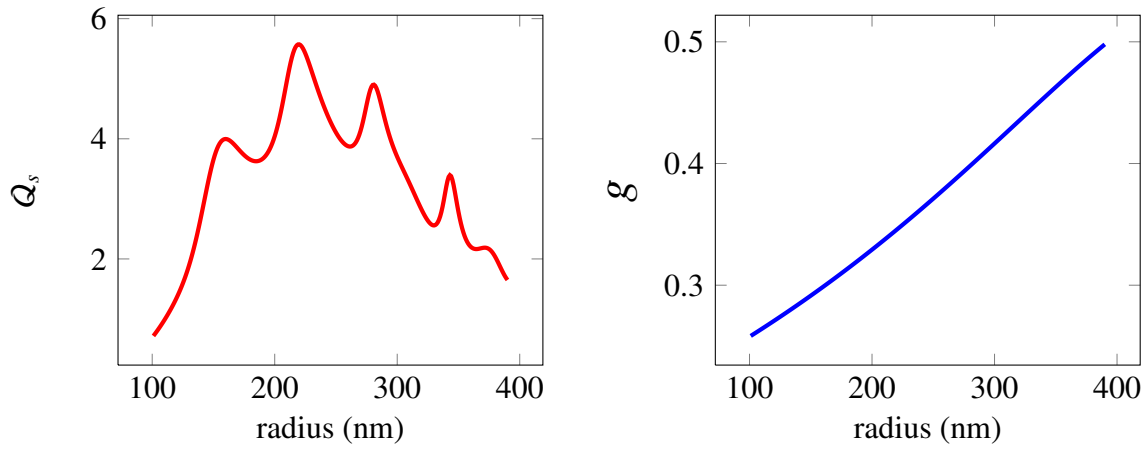

Figure V.16: Numerical calculation of the scattering efficiency Q_s and the asymmetry factor g, with spherical particles with refractive index of 2.58 (TiO_2) dispersed in water and for light with wavelength of 633 nm.

rameter $k\ell_s$ for the used samples do not fall below $\sim 10^3$, the scattering condition of diffusive regime is always satisfied during this experiment.

In order to prevent inhomogeneity and clustering of TiO_2 nanopowder, samples are subjected to ultrasonic bath before and shuffled during the measurement.

The pumping system is provided by a monomode second harmonic Nd:YAG laser (λ= 532 nm) with a 10 Hz repetition rate and a time duration of 4 ns, a time comparable to the spontaneous emission decay time of Rhodamine 6G. The pump beam is focused on a spot with diameter of 30 μm and with an energy up to 360 μJ. The cuvette that contains the liquid sample is cylindric, but, since the spot diameter is much larger than the curvature radius of the box (0.5 cm), the external side of the active medium can be considered as a flat plane.

The shot-to-shot emission from the sample is collected by an Ocean Optics Spectrometer with a spectral resolution of 0.3 nm. An optical fiber collects the emitted radiation from a tilted angle of 15° with respect the pump beam direction.

The system of data acquisition is automatic, with the spectrometer that is trigger by a signal received from the Nd:YAG control unit. The pump beam energy is tuned by means of the rotation of a polarizer. This rotation is performed during the measurement by a stepper motor that rotates in the two different direction covering the selectable angle at a selectable velocity. The stepper motor is driven by an electronic circuit connected by the parallel port of a calculator and controlled by an expressly written C++ software. As a further experimental condition during the measurement the conditions of monomode laser pulse excitation are checked, in order to assure a smooth temporal shape. This issue is also important in order to discriminate the intrinsic emission statistics of the random laser emission from strong temporal laser pulse intensity fluctuations that are present in multimode pump laser.

As shown in Fig. (V.17) typical experimental spectra are shown for three pump energy level and for two different samples. In the diffusive one (right column), the spectra manifest a progressive narrowing as the energy increase, without a detectability of large fluctuations or the presence of random spikes. As the scattering concentration decreases (left column), near random laser threshold narrow spikes at random frequencies emerges in the spectra. If

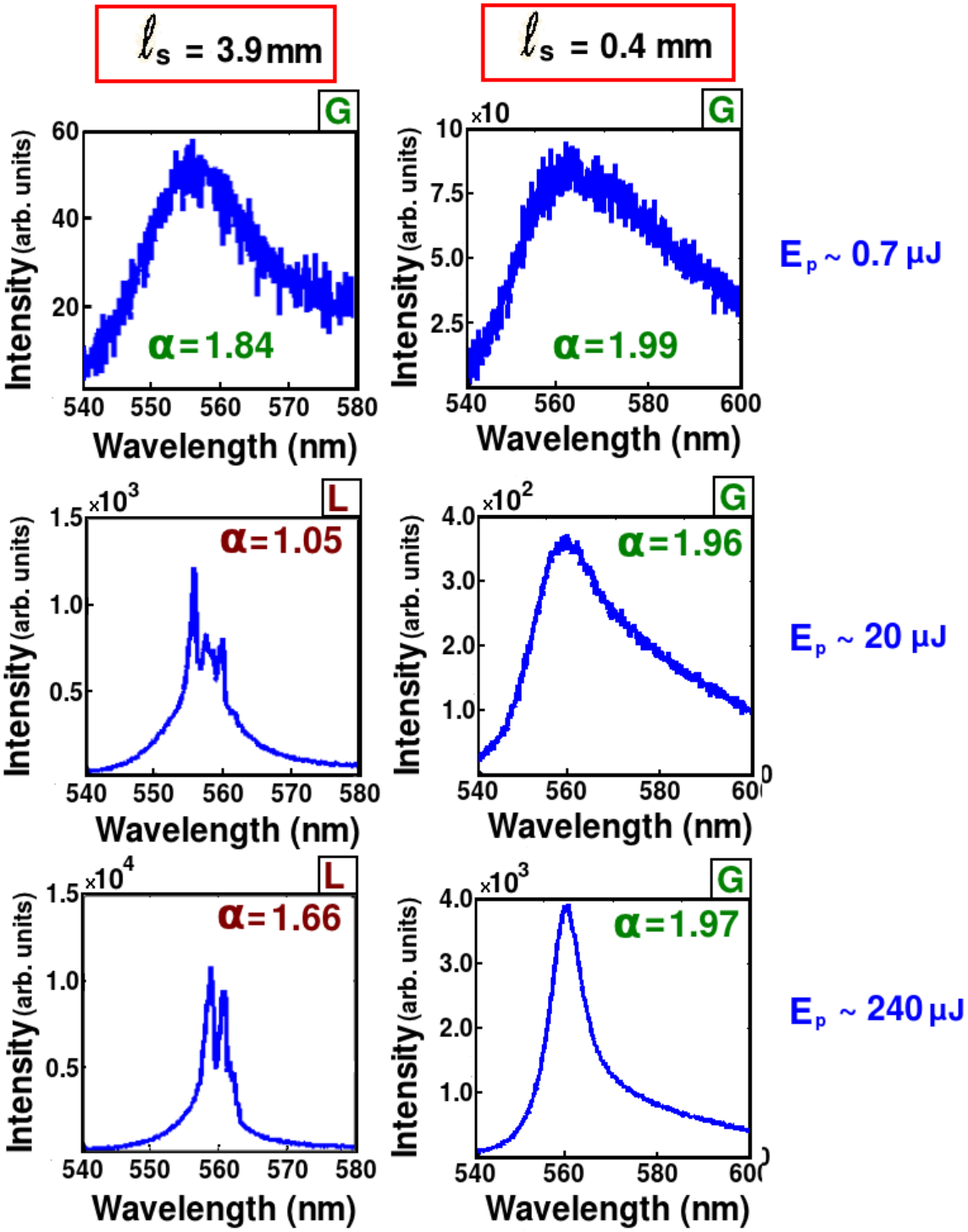

Figure V.17: Experimental spectra at different energies for a sample with different diffusive properties. Only the sample with weaker scatterers concentration shows a fluctuations regime.

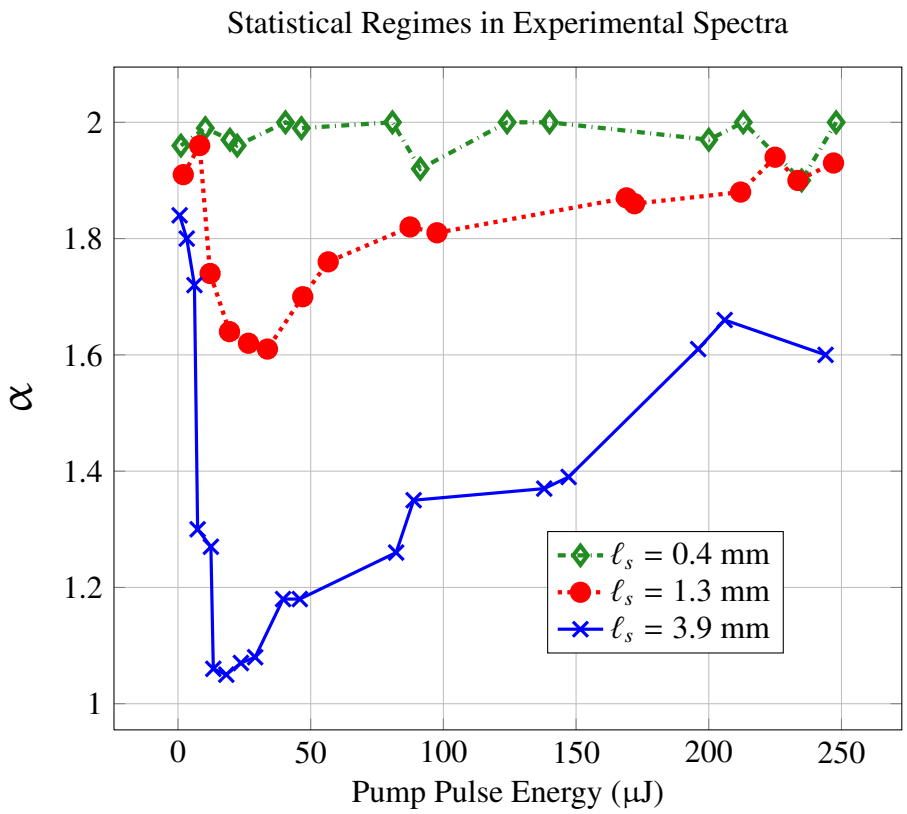

Figure V.18: Experimental results of statistics of the emission spectra: α-index as a function of energy for different scattering strengths. The crossover to Gaussian-Lévy regime can be arbitrarily fixed to α=1.8.

the spikes are isolated from each others, their bandwidth approaches the finite resolution of the spectrometer (0.3 nm), whereas in general cases the spikes are close in frequency and not singularly resolved, with appearance of broadening. Then, for high pump energy, the spectrum appears narrowing and the presence of spikes not more detectable. Therefore the behavior appears similar to that of the numerical simulation.

A intensive measurement campaign and a successive statistical analysis are needed in order to achieve a detailed comparison with the numerical simulation and then a theoretical explanation of the phenomenon. The automatic system of pumping and shot-to-shot spectra acquiring made the former procedure possible, whereas the expressly written Matlab® code for data analysis performs the statistical analysis.

For each shot 6 values of the emitted spectrum, corresponding to different frequencies spaced by 0.5 nm within a narrow bandwidth around the peak, are collected for a large number of consecutive spectra, up to 2000, for each pumping energy interval. Great care has been used to monitor the shot-by-shot pump pulse energy to measure the emission characteristics as a function of pump energy limited to a small energy interval with an *a posteriori* analysis in order to eliminate the fluctuations of the laser pump pulse as spurious causes of fluctuations in the random laser emission intensity. The energy interval is variable to 1 to 15 μJ to follow the critical behavior of the statistical fluctuations characteristics versus pump pulse energy.

5.3.2 Results and discussion

The Fig. (V.18) shows the experimental results concerning the α as a function of energy for three scattering strength. In a similar way to the numerical case showed in Fig. (V.10), three different scattering regimes are detectable.

In Fig. (V.19) different spectra at different statistical regimes are shown for the sample with intermediate diffusive properties. At low energy, in all cases, the output spectra are smooth and reproduce the shape of the fluorescence of the Rhodamine 6G (*First Gaussian Regime*). As the energy increased, beside a partial narrowing of the spectrum, in the sample with weakest scattering the presence of fluctuations and random spikes leads the system in a *Lévy Regime*. For high energy the spectrum becomes narrow and, in all cases but one of weakest scattering, the condition of absence of random narrow spikes (*Second Gaussian Regime*). As it is observed in the theoretical case, the width of the energy range of the Lévy regime, as well as the its depth, fades as the scatterer concentration increases. In the sample with strongest scattering (ℓ_s =0.4 mm) the Lévy regime is not present. The sample with lowest scatterers concentration (ℓ_s=3.9 mm) does not show a return to a Gaussian regime at the range of the highest used pump energy; however an increment of α as a function of energy is evident after 20 μJ. Then an stabilization in the Second Gaussian regime is then expected for larger energies, that have not been explored in order to avoid sample damage.

Moreover, it is worth to note that, since the pump pulse temporal duration is of the same order to that of the spontaneous emission lifetime, the finite time pumping, also in the experimental case, is not able to trigger average mechanisms that lead to inhibition of the random narrow spikes.

Therefore the experimental results allow a direct comparison with the numerical simulation, reproducing the identical behavior, and then a clear link from theory with experiment by means of an extended modes model.

In the numerical case, the parameter ζ has been used to qualitatively describe and frame the statistical behavior expected. In the experimental case, respect to the mean free path measurement, the estimation of the active medium dimension is even more difficult. As some works have reported [44, 45], the geometry of active part of the medium especially depends on two factors:

(1) the pump photons scattering, that causes an enlargement of the active medium in the transversal direction respect the direction of the beam, leading of a generation of active molecules populations also outside the zone crossed by the ballistic beam.

(2) the absorption saturation of the dye, that causes an increment of the penetration depth of the pump beam

Then the active medium geometry is expected to change both with the scattering strength and with the pump energy. However, a qualitative estimation of ζ_{exp} is possible with considering the ratio between ℓ_s and the focus beam diameter ($\sim$ 30μm). Again the Lévy regime tends to be promoted for $\zeta_{exp} \gg 1$ and inhibited as ζ_{exp} decreases.

As regards the role of the dimension of the whole sample of the system behavior, whereas in the numerical simulations such a parameter has not been investigated because computational difficulties, in the experiment it seems to not interpret a critical role. Moreover, in our experiment the output emission is directly collected from the excited medium surface and photons that

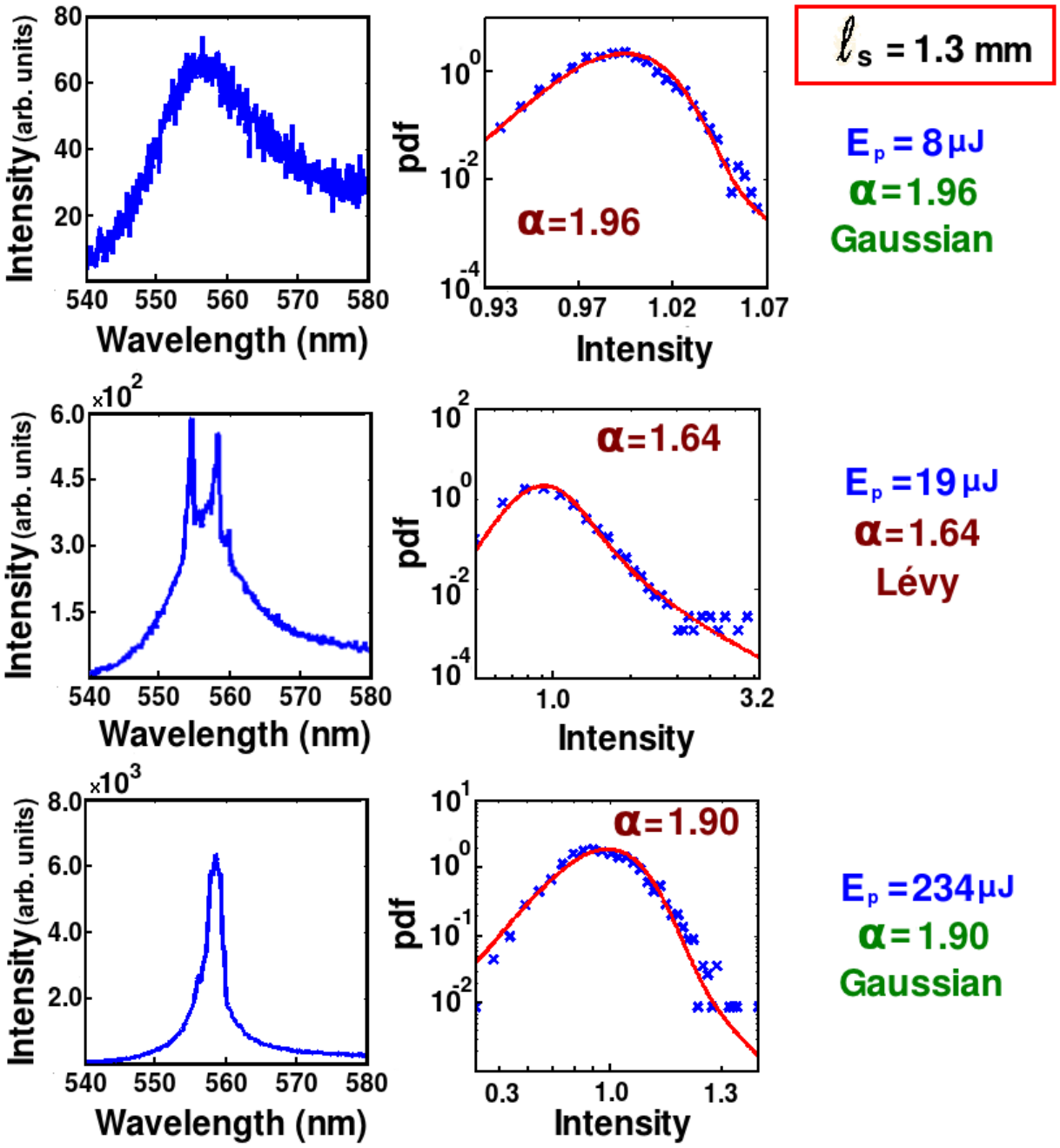

Figure V.19: Experimental spectra at different energies for a sample with intermediate diffusive properties. On the left column typical spectra are shown, whereas in the right column are present the intensity histogram and the corresponding α-stable fit for the energy range around the reported value.

propagates far away from such a region to the non-active part of the sample, whose extension is much larger, can be considered lost or with negligible effects on the overall dynamics.

The results can be summarized as it follows:

(1) Three statistical regime of the random laser spectra have been reported both in numerical simulations, based on extended mode model without considering interference effects, and in experimental data, in disordered active samples in diffusive regime

(2) In the general case and as the energy increases, the statistical regime passes from a Gaussian regime, characterized by smooth and broad spectra, to a Lévy regime, with presence of fluctuations and narrow spikes at random frequencies, to a final Gaussian regime again, with smooth and narrow spectra. The statistical parameter α is used to label and describe the spectral behavior.

(3) The first Gaussian regime is dominated by spontaneous emission, whereas the second one by the stimulated emission. The Lévy regime is detectable in energy range around the random laser threshold.

(4) The theoretical model, corroborated by the emerged link between the theory and experiment, describes the system dynamics in terms of extended mode with a non-resonant feedback mechanism in competition for the available gain. A "mode" is to be interpreted as a possible path of light inside the sample.

(5) The mode competition acts as an average mechanism on the intensity of the mode. Such a mechanism prevails for the sample with strong scattering whatever the stored energy in the active medium and no Lévy regime becomes detectable.

(6) In the energy range around the random laser threshold, in a weak scattering media few modes can become uncoupled from mode competition and experience a large amplification. The random assignment of their initial frequency, by means of the intrinsic causality of the spontaneous emission process, leads to presence of narrow spikes at random frequency in the spectrum.

(7) In order to qualitatively characterize and predict the system behavior with varying the energy, the comparison between the dimension of the active part of the medium and scattering mean free path is used as parameter.

5.4 Controlling Random Laser Directionality

5.4.1 Directionality of the random laser emission

Among characteristics that make the random laser system different from the conventional laser one, the principal can perhaps be the directionality degree. Whereas in a laser the output power is concentrated in a very small solid angle, a random laser emission, because the chaotic

nature of light propagation inside the disordered medium, generally is spatially isotropic, quite similar to the spontaneous emission from a diffusive surface.

The ideal surface of a disordered material system that emits radiation by spontaneous emission is the Lambertian surface. Such an emitter was introduced by Lambert in the XVIIth-century as property of an ideal perfect diffusely reflecting surface [46]. The radiant intensity of a radiant emitting surface follows the *Lambert's cosine law*, which stats that the intensity observed from an ideal diffusely reflecting or irradiating surface is directly proportional to the cosine of the angle θ between the observer's line of sight and the normal to the surface. From this law it follows that the radiance, i.e. the power emitted per unit solid angle and per unit of area that falls within a given solid angle around a specified direction, remains the same, whatever the angle of sight. Indeed, although the emitted power from a given area element is reduced by the cosine of the emission angle, the observed cross section area is decreased by the same amount.

Then, in a general case the emitted light from the surface of a disordered medium approaches the limit features of the Lambertian surface, unless mechanisms bounded to random laser modes and stimulated emission process divert such behavior.

In literature, the works that have been reported investigations that concern the directionality of the random laser emission are few. In 2006 an experimental measurement of variation of directionality degree associated to different scattering strengths has been reported in a system of TiO_2 nanoparticles in a Rhodamine 640 dye dissolved in diethylene glycol [47]. The measurement of the angular distribution of output emission intensity covers 6° in the backward direction around the direction of the pump beam and it evidences an increment in directionality for samples with weaker scattering properties. In 2008 directionality in random laser emission has also been reported in dye doped organic-inorganic Bragg grating structure with introduced disorder [48]. More recently, from theoretical point of view, an optimization procedure of the pump profile to select extended modes with different tuning in weak scattering systems [49].

Concerning the present work and in the light of the theoretical and experimental investigation presented in the previous sections, the raised question is: does the dynamics of extended modes within an active medium trigger, under certain conditions, a higher degree of directionality of the output emission? If the answer is affirmative, is it possible to tune the experimental parameters in order to magnify such an effect?

In the previous part of this chapter it has been discussed the dynamics of the random laser system behavior in the light of a theoretical model based on extended modes and non-resonant feedback. As a result, both experimental and theoretical, the Lévy statistical regime appears to be linked to the presence of rare extended modes with large energy. Such modes reveals their existence by means of the weight that their energy has in the overall spectrum, that leads to the detection of narrow random spikes. Then, one can expect that such a large weight is also present in other characteristics of the emission, as the directionality. Therefore the starting point of investigation consists in two hypotheses:

(1) a deviation in directionality respect the usual diffusive emitting surface can be detected in the Lévy statistical regime of the random laser emission, because the presence of few modes with large intensity

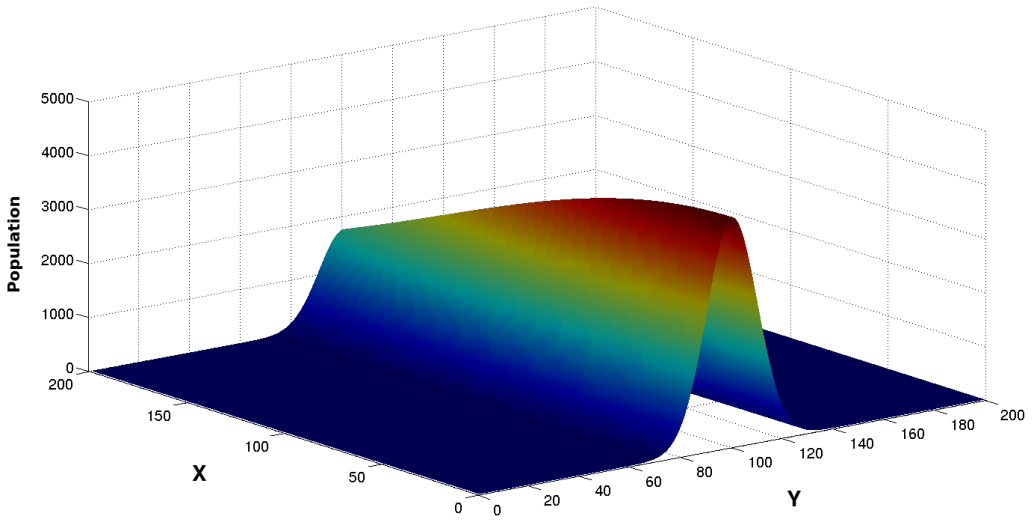

Figure V.20: Example of an asymmetric population distribution on the lattice

Figure V.21: Example of an asymmetric population distribution on a lattice. The maximum of population density is located near a side of the medium.

(2) the directionality can be tuned within the Lévy regime by means of the spatial constriction on the paths of these modes

The work presented in the next sections is devoted to a detailed experimental and theoretical characterization of the directionality with varying the statistical regime and to bring out the possibility of control the behavior of the emission by means of an external optical parameter, recognized in the pump energy, given the optical features of the sample. The followed strategy involves the arrangement of a samples with spatially asymmetric active medium in order to provide a *mode selector*, by forcing the "lucky photons" along a preferential direction.

5.4.2 Numerical simulation and results

The numerical simulation model is based on one discussed in Sec. (5.2.2), with modifications that concern the profile of the population displaced on the lattice and the output emission recording. The former consists in an active medium of e 2D Gaussian shape with different widths and centered in the center of a side of the lattice:

$$N(x,y) = A \exp\left[-\frac{(x-x_0)^2}{2\sigma_x^2} - \frac{(y-y_0)^2}{2\sigma_y^2}\right] \tag{V.25}$$

where the center of the two-dimensional Gaussian, whose only an half part effectively lies in the square lattice of side L, $(x_0, y_0) = (0, L/2)$ and with $\sigma_x \gg \sigma_y$. Then the appearance of the active medium, whose example is reported in Fig. (V.20), shows a distribution that has a maximum in

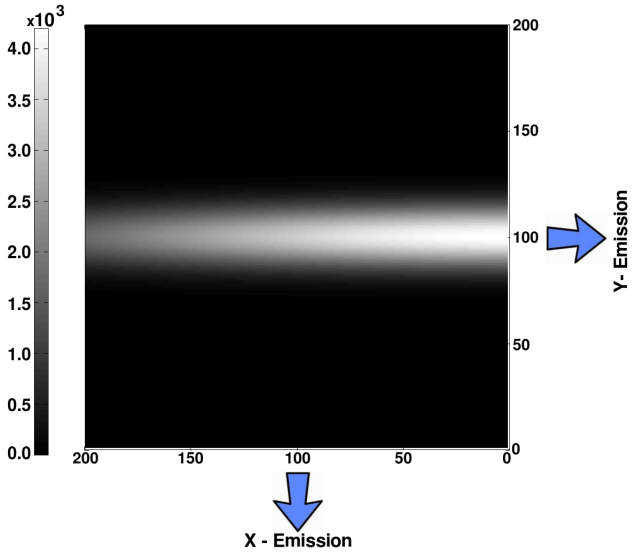

Figure V.22: Example of a greyscale image of a total initial population distribution on the lattice with dimensions 200x200 cells. The number of excited atoms for each cell follows a 2D Gaussian distribution with $\sigma_x = 150$ and $\sigma_y = 10$. Those walkers that leave the medium from the right edge are collected in the Y-Emission, while onos from the bottom edge in the X-Emission.

correspondence of a side of the sample and decreases with different trend along the coordinate x and y. Such a representation aims to qualitatively reproduce the population distribution that has been created by a pumping beam with a small focal spot, then with a small extension along the transversal direction, and a large penetration depth.

Concerning the emission recording, with reference of Fig. (V.22), the output emission is differently recorded from the side near the maximum population density (Y-Emission) and in a one of the perpendicular sides (X-Emission). The chosen parameters are: $L = 200$, $\sigma_x = 150$, $\sigma_y = 10$, $x_0 = 0$, $y_0 = 100$. The Y-Emission represents output emission collected within a small angle around the backward direction of the pump beam, whereas the X-Emission simulate the emission collected at large angle.

As for the numerical simulations described in Sec. (5.2), the comparison between the scattering mean free path ℓ_s and the dimension of the active medium triggers different dynamics of the systems with varying energy.

Fixed the variable parameters, i.e. the initial total energy and ℓ_s, the directionality $\mathcal{D}_{sim}$ is estimated as the average of the ratio Y-Emission/X-Emission upon a set of simulation runs, with identical initial conditions.

In the choice of parameters the constrain are similar to that discussed in the Sec. (5.2.2), whereas the values of ℓ_s are selected in order for describe scenarios where such length is much smaller or comparable to the dimensions of the active medium.

The chosen parameters for this numerical simulation campaign are the following:

- lattice side length L of 200 cells

- total population N that ranges from 2×10^5 to 12×10^7, with corresponding average number of atoms per cell of 5 and 3000 respectively.
- active medium of 2D-Gaussian shape with $\sigma_x = 150$ and $\sigma_y = 10$ and peak located in (x_0, y_0)=(0,100)
- $P_s = 1, 0.1, 0.02, 0.01$ ($\ell_s = 1, 10, 50, 100$)
- spontaneous emission rate $\gamma_0 = 10^{-5}$ (spontaneous emission lifetime $\tau_{sp} = 10^5$) and bandwidth of the transition of 50 chs
- simulation total duration $T_{sim} = 3\tau_{sp}$, with an output binning time $T_w = 10$
- instantaneous pumping ($T_p = 1$)

In order to highlight the divergence from the pure spontaneous emission case, as the Lambertian surface in the real case, one needs an ideal isotropic sample as comparison. In the numerical case such a sample is explicated by the pure spontaneous emission case for various scattering strength. Then simulation runs have been performed for each ℓ_s, with the constrain of inhibition of the stimulated emission process, leading to different value $\mathcal{D}_{sim}^{SP}$, calculated as (Y-Emission)/(X-Emission). The values are reported in Table (V.1). Lacking the stimulated

Table V.1: Pure Spontaneous Emission Case

ℓ_s	$\mathcal{D}_{sim}^{SP}$
1	2.37
10	2.06
50	1.40
100	1.19

emission process, the value of $\mathcal{D}_{sim}^{SP}$ does not depend on the energy, but only by the scattering strength. A much diffusive sample easily leads to a complete randomization of the walkers direction, giving to each edge of the medium the same probability as exit boundary if the starting point of the propagation should be the center of the lattice. In the medium used for the simulation the peak of population density, and then the origin of the main part of generated walker (see the equation (V.20)), is located close a side of the lattice, i.e. the edge from which the Y-Emission is collected. Therefore, such a side becomes the preferential boundary of exit, because a small amount of steps are enough for the largest number of the walkers to approach it. On the contrary, a decrement of $\mathcal{D}_{sim}^{SP}$ is expected for weakly scattering medium. When the scattering regime becomes quasi-ballistic, many walkers escape from the lattice without undergo scattering event. If this case the side of exit is selected by the initial direction, provided to the walker, with uniform probability among the four possible directions, by the process of spontaneous emission. Then, because the structure of the numerical model, $\mathcal{D}_{sim}^{SP} \to 1$ as ℓ_s increases.

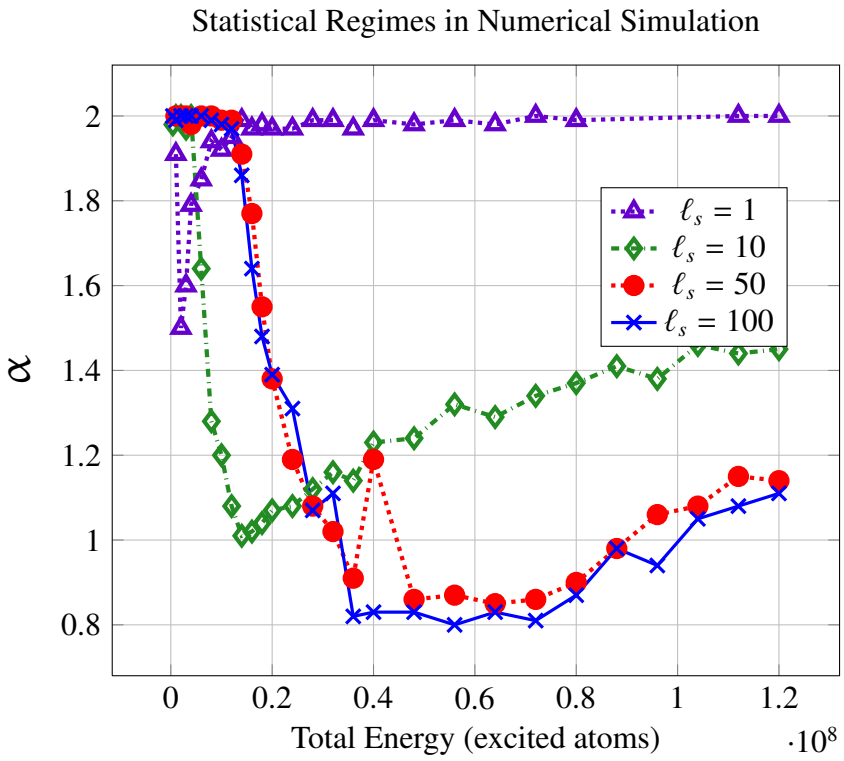

Figure V.23: Numerical simulation results: α-index as a function of energy for different scattering strengths, in the case of instantaneous pumping. As in the case of symmetric active medium, the Lévy region tends to fade as the scattering mean free path decreases.

By re-activation of the stimulated emission, the system undergo to the similar dynamics presented in Sec. (5.2.3). The value of directionality, for each ℓ_s, initial energy E and as average among a set of simulation about $\sim 10^2$ runs, is calculated as normalized to the pure spontaneous emission case:

$$\mathcal{D}_{sim}(\ell_s, E) = \frac{(Y\text{-Emission})}{(X\text{-Emission})} \times (\mathcal{D}^{SP}_{sim}(\ell_s))^{-1} \tag{V.26}$$

In Fig. (V.23) α-index as a function of the pumping energy is shown. Since the particular geometry of the active part of the medium, a Lévy statistical regime is present whatever the scattering strength. However, the fading trend as ℓ_s decreases is confirmed, insomuch as in the most diffusive case ($\ell_s = 1$) the Lévy zone covers a small energy range and with α values much greater than in other case. Such a case it is also the solely case in which the approaching to the Second Gaussian regime becomes complete within the energy r35ange explored. The behavior at high energy of the other values of ℓ_s allows to consider a complete approaching of the Second Gaussian regime at higher unexplored energies.

Fig. (V.24) reports the value of directionality defined by the (V.26) and the behavior of such parameter can be correlated to the statistical regimes as the energy changes.

Concerning the most diffusive medium ($\ell_s = 1$), whereas the α is close to 2, but a small energy range around the threshold, the directionality behavior remains identical to the case of pure spontaneous emission ($\mathcal{D}_{sim} \simeq 1$). In the small range of fluctuations there are many modes weakly coupled to the gain competition, with a small presence of "lucky photons". Whatever

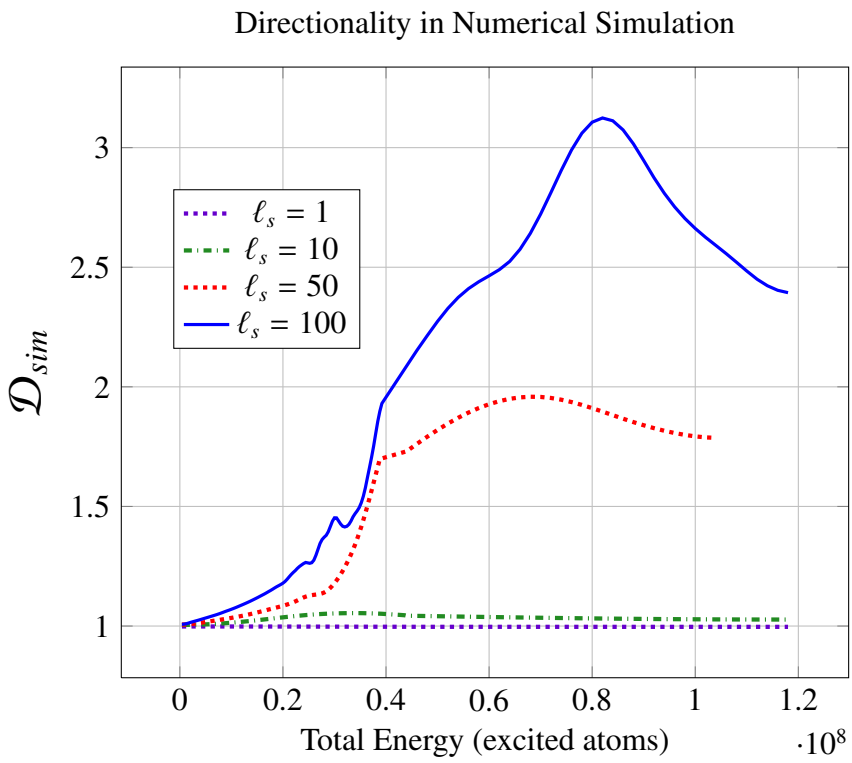

Figure V.24: Smoothing of the collected data.

the energy, whether or not the stimulated emission prevails on the spontaneous emission, the strong scattering leads to a randomization of the walker propagation, causing the directionality locked to the pure spontaneous case.

The situation begins to change if ℓ_s becomes 10; α falls significantly below 2 for a large range of energy, while $\mathcal{D}_{sim}$ deviates for a small amount respect 2. Hence in the Lévy region of this system the spatial asymmetry of the active medium acts as a weak selector for the preferential direction of the "lucky photons". competition among other modes. In it is worth to note the directionality begins to grow starting from energies ($\sim 3.5 \times 10^7$) larger than the minimum of α ($\sim 1.5 \times 10^7$), i.e. when the "lucky photons" are not yet completely uncoupled by the gain

The behavior appears more evident in the case of weak scattering media ($\ell_s = 50$ and $\ell_s = 100$). For low values of energy (less than 2×10^7) Fig. (V.23) shows a Gaussian behavior, while in Fig. (V.24) the increment of directionality remains modest (below ~ 1.2). When the energy further increases (up to $\sim 4 \times 10^7$), α rapidly drops to its lowest values and $\mathcal{D}_{sim}$ slowly, but pointedly grows. This situation marks a break in the spatial emission, due to the amplification mechanism of the stimulated emission and the asymmetry of the population distribution. Since the "lucky photons" are still few, in this energy range α significantly deviates from 2, because these rare events are localized in the tail of the probability distribution, and their contribute have still a small weight in determining the $\mathcal{D}_{sim}$, that is averaged upon many emissions. Increasing further the pump energy, because the spatial asymmetry, the possibility for the "lucky photons" to escape from the lattice after experiencing a large gain due to preferential path is increased. The also $\mathcal{D}_{sim}$ reaches its peak, with a large amount of energy carried away by those walkers that have a direction such that to cross the the largest population density. The statistics of the

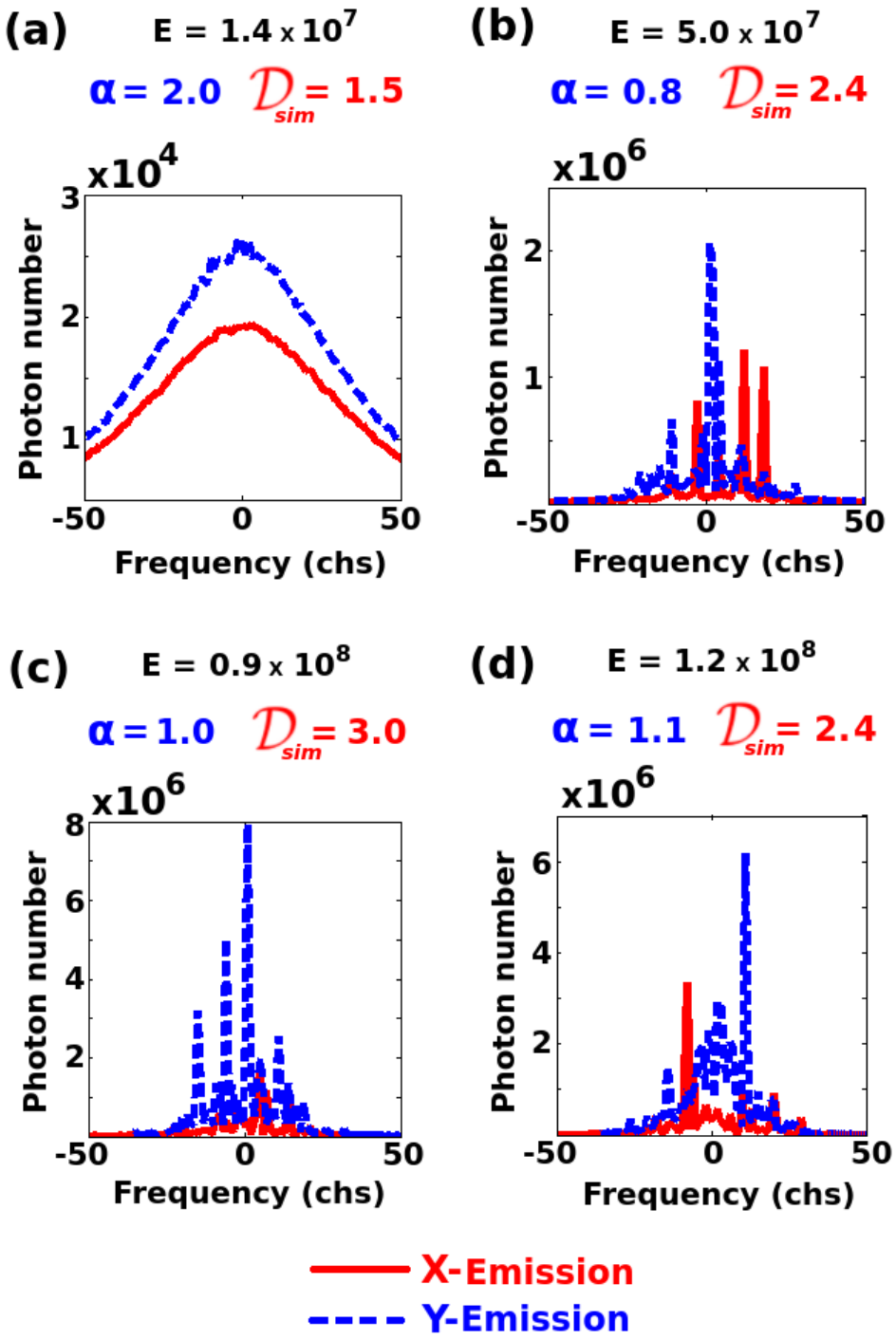

Figure V.25: Typical emission spectra for the lattice with $\ell_s = 100$ and different energies: 1.4×10^7 (a), 5.0×10^7 (b), 0.9×10^8 (c) and 1.2×10^8 (d). The dashed blue line and the red continuous line are the spectrum collected from the Y-edge and X-edge respectively.

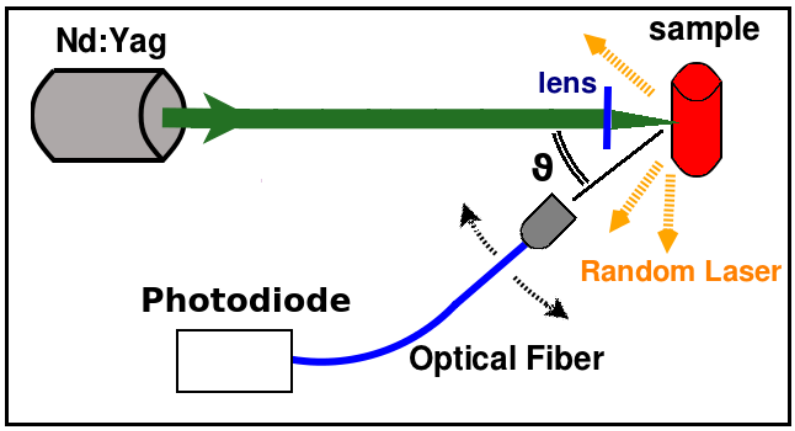

Figure V.26: Diagram of the experimental set-up. The pump beam is focalized onto the sample by a lens, producing o focal spot diameter about 30 μm. The signal is collected by an optical fiber head that forms a selectable angle θ centered on the focal spot.

emission still is in the Lévy regime, but α has larger value, because the random spikes in the spectrum are more numerous. Finally, increasing the energy of the lattice towards the largest possible values, α increases to 2, whereas the mode coupling causes a decrement of $\mathcal{D}_{sim}$. A final approach for the former parameter to 2 and to 1 for the latter is predictable, even if not investigable because the time needed for computation.

Fig. (V.25) shows typical spectra with varying energy for the sample with $\ell_s = 100$. The dashed blue spectra are collected from the Y-edge and the continuous red ones from the X-edge. The spectra in the Fig. (V.25)-(a) are smooth and the directionality weakly differs from the pure spontaneous emission case. In (b), the Lévy regime is near its peak and the directionality is larger. However, the spikes are distributed in both spectra; these "lucky photons" may be the modes that undergo an anomalously large number of scattering events, leading to trajectory direction and then the side of exit completely randomized. A prevalence of the Y-emission is attributable to the spatial asymmetry. In (c), α is lower and the directionality reaches its peak. The X-emission appears to weaken and the main part of the emission concentrated in the Y-emission peaks, originated by walkers that have started their propagation deep inside the medium and have experienced a large gain during a scattering less propagation towards the Y-edge. Finally, in (d), the gain competition is more important and the emission merges in a central Y-emission "bulge", inhibiting the presence of narrow spikes and leading to a decrement of $\mathcal{D}_{sim}$.

5.4.3 Experimental investigation

In the experimental setup, the sample have identical characteristic of ones described in Sec. (5.3.2).

As discussed in Sec. (5.3.2), no detailed experimental image of the gain medium has been performed, although the attempt to ensure a small as possible focal spot of the pump beam has been carefully done, in order to induce an asymmetry in the gain medium. A lens provides a focal spot of the pump beam of diameter of 30 μm on the surface of the random laser medium, contained in a transparent cylindrical cuvette. The signal is collected by an optical fiber, whose

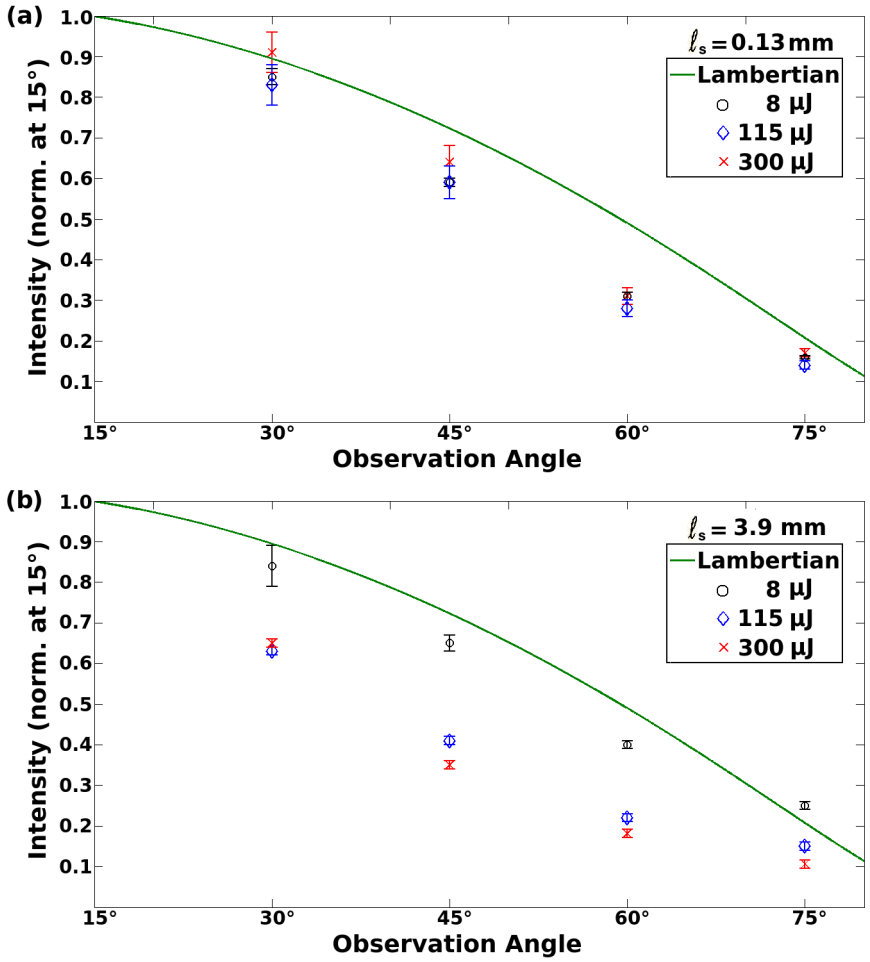

Figure V.27: Angular distribution of the random laser emission for various pump energy values. In the case (a), the strongest diffusive sample is shown, while in (b) the weakest one. For comparison the angular emission profile for an ideal Lambertian source is also reported (green continuous line), corrected for Fresnel reflections. The Lambertian emission curve and the experimental data are normalized at the corresponding 15°emission.

head can rotate to a selectable angle around the direction of the pump beam, and sent to a photodiode, in order to measure the radiation intensity. The angles have been measured by means of a red laser diode bounded to the head of the fiber and that creates a luminous spot in the experimental table, where the angles of measurement (30°, 45°, 60°and 75°) have been drawn. The resolution of angle of observation is given by the acceptance angle of the fiber and it is about 2°.

Fig. (V.27) shows measurement of the random laser emission for different observation angles and the angular profile of the ideal Lambertial curve for comparison. Such a profile has been also corrected for Fresnel reflection losses, due to the interfaces methanol-glasses and glass-air. Both the measurements and the Lambertian profile has been normalized to the corresponding 15°value. In Fig. (V.27)-(a) the results for the most diffusive medium are shown; the angular profile differs from the ideal Lambertian curve, but in such a way independent on pump energy. Hence in this medium, despite the contribute of stimulated emission, the emission

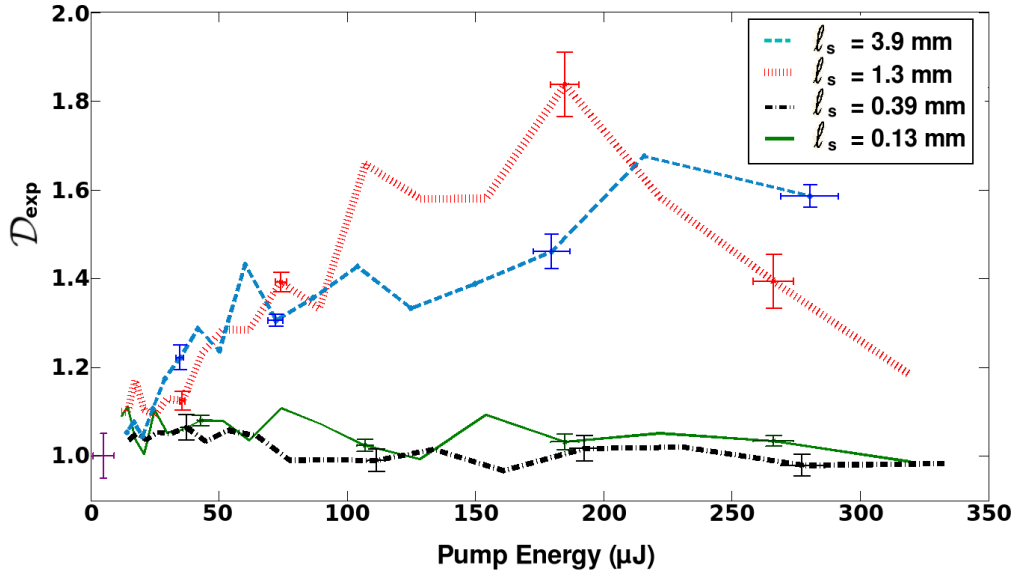

Figure V.28: Experimental results of directionality normalized to the corresponding spontaneous emission value. Same experimental bars are also reported in order to show the measurement accuracy, whereas the purple error bars represent $\mathcal{D}_{exp}^{SP}$ (used for $\mathcal{D}_{exp}$ normalization), measured in the pure spontaneous emission regime at very low energy. The directionality appreciably differs from 1 only for the weakly scattering samples.

maintains the same degree of directionality. In the weakly scattering medium (case (b)), when the pump energy increases (115 μJ and 300 μJ), the fraction of the emission intensity released at large angles decreases, leading to a larger amount of energy radiated at small angles.

In Fig. (V.28) the directionality $\mathcal{D}_{exp}$ measured as a function of energy for four samples with different ℓ_s are shown. In analogy with the (V.26):

$$\mathcal{D}_{exp}(\ell_s, E) = \frac{(15°\text{-Emission})}{(45°\text{-Emission})} \times (\mathcal{D}_{exp}^{SP}(\ell_s))^{-1} \tag{V.27}$$

where $\mathcal{D}_{exp}^{SP}$ are defined as the (15°-Emission) ratio at the lowest measurable pump energies, i.e. when the dye de-excites only by spontaneous emission. In Fig. (V.29) α as a function of energy is reported again in order to allow to follow the directionality evolution with one of the statistical emission regimes.

In the cases of strong scattering, as Fig. (V.27) has suggested, the value of $\mathcal{D}_{exp}$ remains independent on pump energy and close to 1, whereas α remains close to 2 (Gaussian regime). For weakly scattering samples, Fig. (V.28) and Fig. (V.29) show that $\mathcal{D}_{exp}$ grows after the onset of the statistical Lévy regime. The point that strongly deviates from the Lambertian profile in Fig. (V.27) both lies in the Lévy statistical regime. For the sample with $\ell_s = 1.3$, the directionality decreases when the system falls in the second Gaussian regime.

5.4.4 Experimental Results and Directionality Regimes

Both experimental data and numerical simulation show a clear link between the directionality and the Lévy statistical regime of the emission. Secondly, in both cases the peak of directionality appears shifted in energy respect the Lévy one. The enhancement in directionality

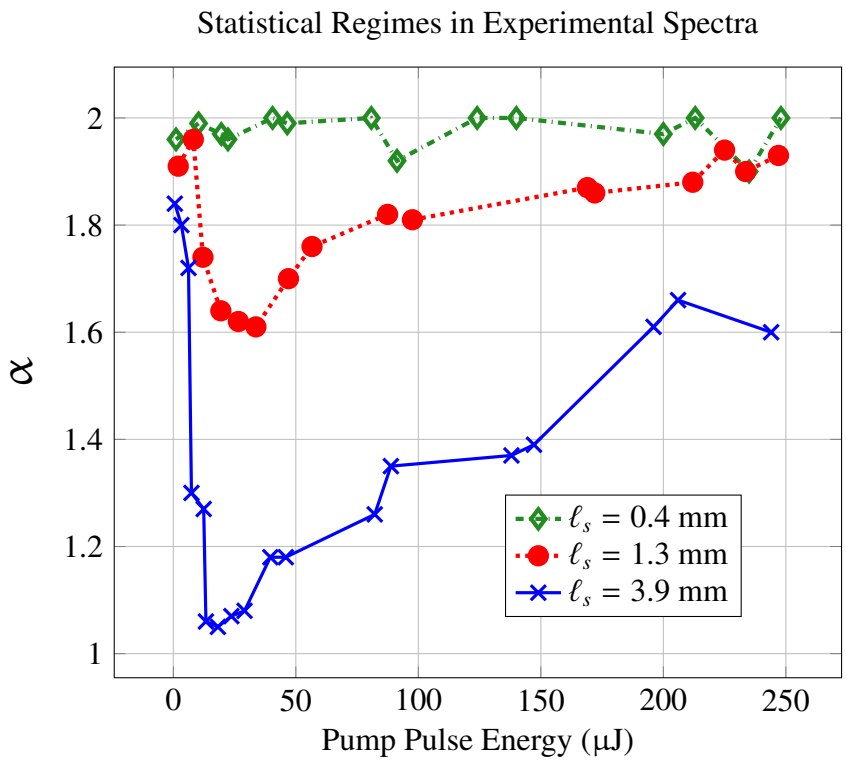

Figure V.29: Experimental results of statistics of the emission spectra: α-index as a function of energy for different scattering strengths.

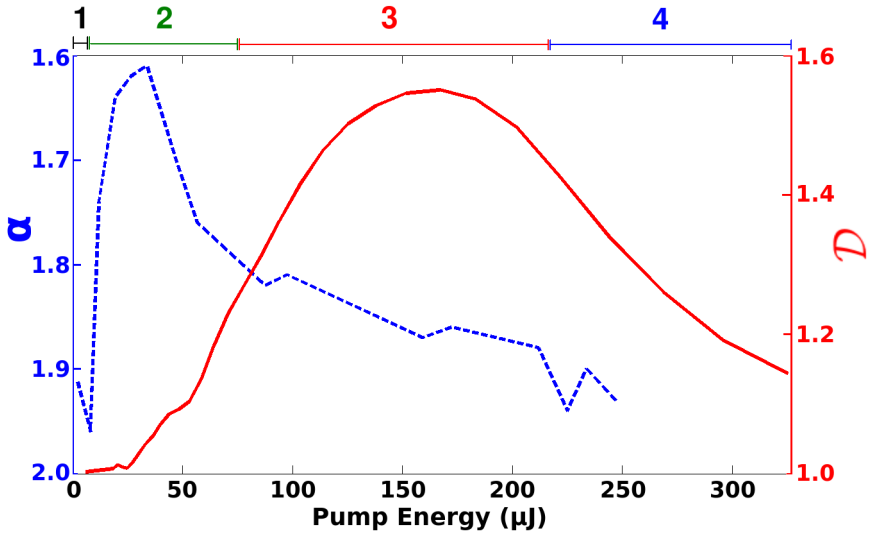

Figure V.30: Comparison between the trend of α (dashed blue) and $\mathcal{D}_{exp}$ (red) for the sample with ℓ_s=1.3 mm. Data are smoothed to highlight the results. Above qualitative extensions of the different regimes are also shown: 1) *First Gaussian Regime* (α ∼ 2 $\mathcal{D}_{exp}$ ∼ 1), 2) *Deep Lévy Regime* (α below 2 and growing $\mathcal{D}_{exp}$), 3) *Directional Regime* (α below 2 and large values of $\mathcal{D}_{exp}$) and 4) *Second Gaussian Regime* (α ∼ 2 $\mathcal{D}_{exp}$ ∼ 1).

is not straightforwardly triggered by the emergence of the Lévy regime, that can be considered sub-divided in two Lévy sub-regimes.

In Fig. (V.30) is shown the smoothed trend of α and $\mathcal{D}_{exp}$ for $\ell_s = 1.3$ mm. The peak of α is reached for ~ 50 µJ, whereas the $\mathcal{D}_{exp}$ approaches its maximum value for ~ 170 µJ. For the energy range where $\mathcal{D}_{exp}$ reaches its largest values, the Lévy regime is strongly reduced respect the peak value, but substantially still different from the Gaussian regime value of 2. A return of α to 2 and $\mathcal{D}_{exp}$ to 2 is expected.

In summary by increasing energy the spectral and directional characterization of the emission for a weakly scattering medium can be described as following regimes:

(1) ***First Gaussian Regime***
Spectra are smooth and emission is dominated by spontaneous emission (α close to 2). Energy is radiated outside the sample with an angular distribution similar to that of an ideal Lambertian source. This energy range is the narrowest one because a small amount of energy is needed to trigger a random laser emission in such kind of material systems.

(2) ***Deep Lévy Regime***
Near above threshold narrow energetic spikes at random frequencies due to rare extended amplified modes superimpose to the typical spontaneous emission profile. The α parameter reaches its lower value within this regime because these *lucky photons* are statistically located at the tail of the probability distribution. $\mathcal{D}_{exp}$ begins to grow, suggesting that these modes have a preferential path, but the weight of the *lucky photons* is still too weak.

(3) ***Directional Lévy Regime***
Spectra become narrower with numerous random spikes, whose probability increase causes α-parameter to grow. $\mathcal{D}_{exp}$ raises to its peak value within this regime. As numerical simulations suggested, the increase of the pump energy causes a larger extension of the gain volume inside the sample, in such the way to determine, given the geometric asymmetry, a preferential path for the *lucky photons*.

(4) ***Second Gaussian Regime***
At high energy the spectra become smooth and narrow and the spikes completely disappear. As the theoretical model and numerical simulations show, within such regime modes are coupled by gain competition and the presence of strongly amplified modes with high directionality is inhibited. Then the directionality value returns to approach the spontaneous emission one.

Fig. (V.31) show typical spectra that belong to these different regimes. In the case (a) (*First Gaussian Regime*), the spectrum dominated by spontaneous emission. In (b) (*Deep Lévy Regime*) the spectrum is broad, but with the presence of rare and energetic random spikes. In (c) (*Directional Lévy Regime*) the spectrum becomes narrower and random spikes more numerous. The case (b) and (c) allow to highlight the difference between the two Lévy sub-regimes: in the Deep Lévy-case the rarity of the energetic narrow spikes does not allow a crucial weight in that

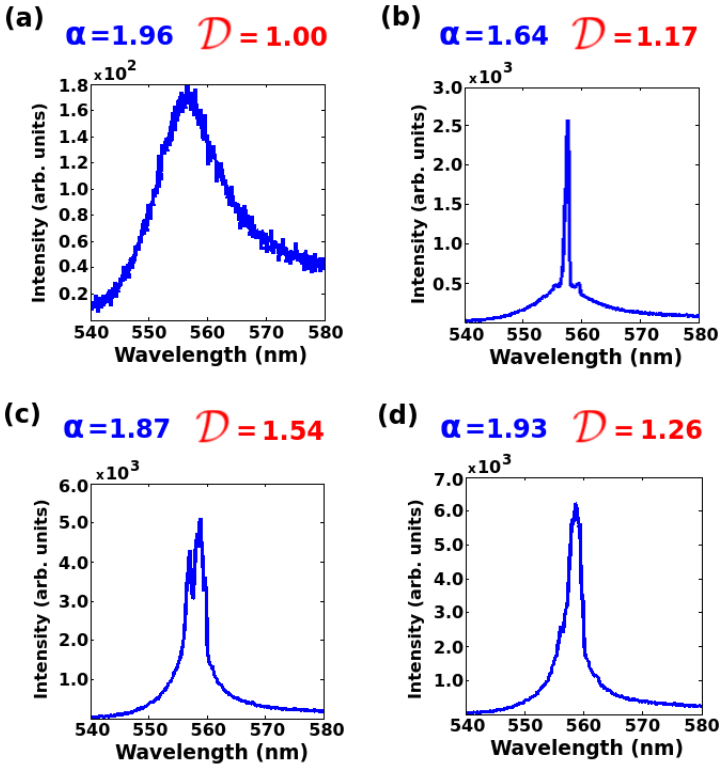

Figure V.31: Typical examples of spectra for the sample with $\ell_s = 1.3$ m: (a) *First Gaussian*, (b) *Deep Lévy*, (c) *Directional Lévy* and (d) *Second Gaussian*.

of the whole emission, while in the Directional Lévy-case many contemporaneously present directional spikes cause a large value of $\mathcal{D}_{exp}$. Finally in (d) (*Second Gaussian Regime*) the spectrum is smooth and narrow, with α that approaches 2 and a reduced value of $\mathcal{D}_{exp}$.

In sample with strong scattering properties, the small scattering mean free path leads to an increment of gain competition between modes, with a passage between the 2 Gaussian regime without showing a detectable presence of the two Lévy sub-regimes.

5.4.5 Conclusions

A theoretical and experimental investigation about the directionality of the random laser output emission in diffusive regime has been performed. The theoretical model, based on a non-resonant feedback mechanism of extended modes, is corroborated by numerical simulations based on random walkers propagation in lattice. The starting hypothesis involves a spatially asymmetric active medium as *mode selector*, by means of the "lucky photons" paths along a preferential direction.

Such numerical simulations are qualitative representation of the structure of the real gain medium and they are not devoted to provide quantitative results. In sake of simplicity, a fixed asymmetric geometry of the population distribution is assumed, whatever the scattering level and the pumping energy. Moreover the directionality has been estimated by the recording of the output emission from only two directions, one near the maximum of the asymmetric population distribution profile and the other in the perpendicular direction. In the experimental case the

population distribution spatial profile actually depends on the scattering, because the diffusion of the pump photons, and by the absorption saturation of the Dye molecules. Although, despite its simplicity, it is able to provide important indications on the physical mechanism of the emission: *the asymmetry of the gain medium is a necessary but not sufficient condition for the enhancement of directionality respect the pure spontaneous emission case*.

Both experimental and numerical data show that the directionality trend not only is bounded to the Lévy regime, but, more precisely, to the fine structure of such a fluctuations zone as the initial energy is increased. Where the diffusive property of sample and the pump energy do not allow a Lévy regime of the output emission, the gain medium profile is not able to act as mode selector for extended modes with high energy and directionality.

Finally, let talk about the possibility of controlling the behavior of the emission. Fixed the experimental condition, i.e. the active molecules and scatterers concentrations and the focal spot diameter of the pump beam, and as a consequence of the detailed characterization and the theoretical investigation, one is able to use the energy as a tuning parameter in controlling the directionality. Then, besides different statistical regimes, also a control of directionality of the output emission can be achieved.

References

[1] D. Sharma, H. Ramachandran, and N. Kumar. "Lévy statistical fluctuations from a random amplifying medium". In: *Fluctuation and Noise Letters* 06.01 (2006), pp. L95–L101. DOI: 10.1142/S0219477506003185 (cited in pages 89, 94).

[2] R. Uppu, K. A. Tiwari, and S. Mujumdar. "Identification of statistical regimes and crossovers in coherent random laser emission". In: *Opt. Lett.* 37.4 (2012), pp. 662–664. DOI: 10.1364/OL.37.000662 (cited in pages 89, 94).

[3] X. Wu and H. Cao. "Statistical studies of random-lasing modes and amplified spontaneous-emission spikes in weakly scattering systems". In: *Phys. Rev. A* 77 (2008), p. 013832. DOI: 10.1103/PhysRevA.77.013832 (cited in pages 89, 94).

[4] G. Zhu, L. Gu, and M. A. Noginov. "Experimental study of instability in a random laser with immobile scatterers". In: *Phys. Rev. A* 85 (2012), p. 043801. DOI: 10.1103/PhysRevA.85.043801 (cited in pages 89, 94).

[5] S. Lepri, S. Cavalieri, G.-L. Oppo, and D. S. Wiersma. "Statistical regimes of random laser fluctuations". In: *Phys. Rev. A* 75 (2007), p. 063820. DOI: 10.1103/PhysRevA.75.063820 (cited in pages 89, 94).

[6] O. Zaitsev, L. Deych, and V. Shuvayev. "Statistical Properties of One-Dimensional Random Lasers". In: *Phys. Rev. Lett.* 102 (2009), p. 043906. DOI: 10.1103/PhysRevLett.102.043906 (cited in pages 89, 94).

[7] S. Lepri. "Fluctuations in a Diffusive Medium with Gain". In: *Phys. Rev. Lett.* 110 (2013), p. 230603. DOI: 10.1103/PhysRevLett.110.230603 (cited in pages 89, 94).

[8] E. Ignesti, F. Tommasi, L. Fini, S. Lepri, V. Radhalakshmi, D. Wiersma, and S. Cavalieri. "Experimental and theoretical investigation of statistical regimes in random laser emission". In: *Phys. Rev. A* 88 (2013), p. 033820. DOI: 10.1103/PhysRevA.88.033820 (cited in page 89).

[9] W. Paul and J. Baschnagel. *Stochastic Processes: From Physics to Finance*. Springer, 1999. ISBN: 9783540665601 (cited in pages 90, 93).

[10] P. Lévy. "Théorie de l'addition des variables aléatoires". In: *Gauthier-Villars (Paris)* (1937) (cited in page 91).

[11] P. Lévy. *Théorie de l'addition des variables aléatoires*. Monographies des probabilités ; calcul des probabilités et ses applications v. 60. Jacques Gabay, 1954 (cited in page 91).

[12] B. Mandelbrot. *The Fractal Geometry of Nature*. Henry Holt and Company, 1983. ISBN: 9780716711865 (cited in page 93).

[13] M. F. Shlesinger, G. M. Zaslavsky, and J. Klafter. "Strange kinetics". In: *Nature* 363.6424 (1993), pp. 31–37. ISSN: 0028-0836. DOI: 10.1038/363031a0 (cited in page 93).

[14] J.-P. Bouchaud and G. A. "Anomalous diffusion in disordered media: Statistical mechanisms, models and physical applications". In: *Physics Reports* 195.4–5 (1990), pp. 127 –293. ISSN: 0370-1573. DOI: http://dx.doi.org/10.1016/0370-1573(90)90099-N (cited in page 93).

[15] M. F. Shlesinger, J. Klafter, and G. Zumofen. "Above, below and beyond Brownian motion". In: *American Journal of Physics* 67.12 (1999), pp. 1253–1259. DOI: 10.1119/1.19112 (cited in page 93).

[16] T. H. Harris, E. J. Banigan, D. A. Christian, C. Konradt, E. D. Tait Wojno, K. Norose, E. H. Wilson, B. John, W. Weninger, A. D. Luster, A. J. Liu, and C. A. Hunter. "Generalized Levy walks and the role of chemokines in migration of effector CD8+ T cells". In: *Nature* 486 (2012), pp. 545–548. DOI: 10.1007/s100510050276 (cited in page 93).

[17] G. M. a. Viswanathan. "Ecology: Fish in Lévy-flight foraging". In: *Nature* 465 (2012), pp. 1018–1019. DOI: 10.1007/s100510050276 (cited in page 93).

[18] A. M. Reynolds. "Mussels realize Weierstrassian Lévy walks as composite correlated random walks". In: *Sci Rep* 4 (2014), p. 4409. ISSN: 2045-2322 (cited in page 93).

[19] A. M. Reynolds and C. J. Rhodes. "The Lévy flight paradigm: random search patterns and mechanisms". In: *Ecology* 90.4 (Apr. 2009), pp. 877–887. DOI: 10.1890/08-0153.1 (cited in page 93).

[20] A. Ferreira, E. Raposo, G. Viswanathan, and M. da Luz. "The influence of the environment on Lévy random search efficiency: Fractality and memory effects". In: *Physica A: Statistical Mechanics and its Applications* 391.11 (2012), pp. 3234 –3246. ISSN: 0378-4371. DOI: http://dx.doi.org/10.1016/j.physa.2012.01.028 (cited in page 93).

[21] N. E. Humphries, N. Queiroz, J. R. Dyer, N. G. Pade, M. K. Musyl, K. M. Schaefer, D. W. Fuller, J. M. Brunnschweiler, T. K. Doyle, J. D. Houghton, G. C. Hays, C. S. Jones, L. R. Noble, V. J. Wearmouth, E. J. Southall, and D. W. Sims. "Environmental context explains Lévy and Brownian movement patterns of marine predators". In: *Nature* 465.7301 (2010), pp. 1066–1069 (cited in page 93).

[22] G. M. Viswanathan, V. Afanasyev, S. V. Buldyrev, E. J. Murphy, P. A. Prince, and H. E. Stanley. "Lévy flight search patterns of wandering albatrosses". In: *Nature* 381.6581 (May 1996), pp. 413–415. DOI: 10.1038/381413a0 (cited in page 93).

[23] F. Bartumeus, M. Da Luz, G. Viswanathan, and J. Catalan. "Animal search strategies: A quantitative random-walk analysis". In: *ECOLOGY* 86.11 (2005), pp. 3078–3087. ISSN: 0012-9658. DOI: 10.1890/04-1806 (cited in page 93).

[24] R. P. D. Atkinson, C. J. Rhodes, D. W. MacDonald, and R. M. Anderson. "Scale-Free Dynamics in the Movement Patterns of Jackals". In: *Oikos* 98.1 (2002), pp. 134–140 (cited in page 93).

[25] G. Viswanathan, E. Raposo, and M. da Luz. "Lévy flights and superdiffusion in the context of biological encounters and random searches". In: *Physics of Life Reviews* 5.3 (2008), pp. 133 –150. ISSN: 1571-0645. DOI: http://dx.doi.org/10.1016/j.plrev.2008.03.002 (cited in page 93).

[26] D. Brockmann, L. Hufnagel, and T. Geisel. *The scaling laws of human travel*. 2006 (cited in page 93).

[27] X.-P. Han and B.-H. Wang. "Impacts of distance and memory in the emergence of scaling mobility pattern of human". In: *Physics Procedia* 3.5 (2010), pp. 1907 –1911. DOI: http://dx.doi.org/10.1016/j.phpro.2010.07.035 (cited in page 93).

[28] D. Volchenkov, J. Helbach, M. Tscherepanow, and S. Küheel. "Exploration-exploitation Trade-off in a Treasure Hunting Game". In: *Electronic Notes in Theoretical Computer Science* 299.0 (2013). Proceedings of the fourth International Workshop on Interactions between Computer Science and Biology (CS2Bio'13), pp. 101 –121. ISSN: 1571-0661. DOI: http://dx.doi.org/10.1016/j.entcs.2013.11.009 (cited in page 93).

[29] I. Rhee, M. Shin, S. Hong, K. Lee, S. J. Kim, and S. Chong. "On the Levy-walk Nature of Human Mobility". In: *IEEE/ACM Trans. Netw.* 19.3 (June 2011), pp. 630–643. ISSN: 1063-6692. DOI: 10.1109/TNET.2011.2120618 (cited in page 93).

[30] C. Brown, L. Liebovitch, and R. Glendon. "Lévy Flights in Dobe Ju/'hoansi Foraging Patterns". In: *Human Ecology* 35.1 (2007), pp. 129–138. ISSN: 0300-7839. DOI: 10.1007/s10745-006-9083-4 (cited in page 93).

[31] F. Radicchi and A. Baronchelli. "Evolution of optimal Lévy-flight strategies in human mental searches". In: *Phys. Rev. E* 85 (2012), p. 061121. DOI: 10.1103/PhysRevE.85.061121 (cited in page 93).

[32] H. Janssen, K. Oerding, F. van Wijland, and H. Hilhorst. "Lévy-flight spreading of epidemic processes leading to percolating clusters". In: *The European Physical Journal B - Condensed Matter and Complex Systems* 7.1 (1999), pp. 137–145. ISSN: 1434-6028. DOI: 10.1007/s100510050596 (cited in page 93).

[33] A. Corral. "Universal Earthquake-Occurrence Jumps, Correlations with Time, and Anomalous Diffusion". In: *Phys. Rev. Lett.* 97 (2006), p. 178501. DOI: 10.1103/PhysRevLett.97.178501 (cited in page 93).

[34] P. Barthelemy, J. Bertolotti, and D. S. Wiersma. "A Lévy flight for light". In: *Nature* 453.7194 (2008), pp. 495–498. DOI: 10.1038/nature06948 (cited in page 93).

[35] G. Peach. "Theory of the pressure broadening and shift of spectral lines". In: *Advances in Physics* 30.3 (1981), pp. 367–474. DOI: 10.1080/00018738100101467 (cited in page 93).

[36] M. Orrit and J. Bernard. "Single pentacene molecules detected by fluorescence excitation in a p-terphenyl crystal". In: *Phys. Rev. Lett.* 65 (1990), pp. 2716–2719. DOI: 10.1103/PhysRevLett.65.2716 (cited in page 93).

[37] T. H. Solomon, E. R. Weeks, and H. L. Swinney. "Observation of anomalous diffusion and Lévy flights in a two-dimensional rotating flow". In: *Phys. Rev. Lett.* 71 (1993), pp. 3975–3978. DOI: 10.1103/PhysRevLett.71.3975 (cited in page 93).

[38] B. Mandelbrot. "The Pareto-Lévy Law and the Distribution of Income". English. In: *International Economic Review* 1.2 (1960), pp. 79–106. ISSN: 00206598 (cited in page 93).

[39] J. Voit. *The Statistical Mechanics of Financial Markets*. Theoretical and Mathematical Physics. Springer, 2006. ISBN: 9783540262893 (cited in page 93).

[40] B. B. Mandelbrot. “The Variation of Certain Speculative Prices”. In: *The Journal of Business* 36 (1963) (cited in page 93).

[41] B. B. Mandelbrot. ““New Methods of Statistical Economics,” revisited: Short versus long tails and Gaussian versus power-law distributions”. In: *Complexity* 14.3 (2009), pp. 55–65. ISSN: 1099-0526. DOI: 10.1002/cplx.20264 (cited in page 93).

[42] I. A. Koutrovelis. In: *JASA* 75 (1980), p. 918 (cited in page 93).

[43] I. A. Koutrovelis. In: *Commun. Stat.-Simul. Comput.* 10 (1981), p. 17 (cited in page 93).

[44] X. Wu, W. Fang, A. Yamilov, A. A. Chabanov, A. A. Asatryan, L. C. Botten, and H. Cao. “Random lasing in weakly scattering systems”. In: *Phys. Rev. A* 74 (2006), p. 053812. DOI: 10.1103/PhysRevA.74.053812 (cited in page 117).

[45] R. Uppu and S. Mujumdar. “Dependence of the Gaussian-Lévy transition on the disorder strength in random lasers”. In: *Phys. Rev. A* 87 (2013), p. 013822. DOI: 10.1103/PhysRevA.87.013822 (cited in page 117).

[46] J. Lambert. *Photometria*. 1760 (cited in page 120).

[47] X. Wu, W. Fang, A. Yamilov, A. A. Chabanov, A. A. Asatryan, L. C. Botten, and H. Cao. “Random lasing in weakly scattering systems”. In: *Phys. Rev. A* 74 (2006), p. 053812. DOI: 10.1103/PhysRevA.74.053812 (cited in page 120).

[48] Q. Song, L. Liu, and L. Xu. “Directional random-laser emission from Bragg gratings with irregular perturbation”. In: *Opt. Lett.* 34.3 (2009), pp. 344–346. DOI: 10.1364/OL.34.000344 (cited in page 120).

[49] T. Hisch, M. Liertzer, D. Pogany, F. Mintert, and S. Rotter. “Pump-Controlled Directional Light Emission from Random Lasers”. In: *Phys. Rev. Lett.* 111 (2013), p. 023902. DOI: 10.1103/PhysRevLett.111.023902 (cited in page 120).

Further reading

[50] B. Gnedenko and A. Kolmogorov. *Limit distributions for sums of independent random variables*. Addison-Wesley series in statistics. Addison-Wesley, 1968.

[51] S. Chandrasekhar. “Stochastic Problems in Physics and Astronomy”. In: *Rev. Mod. Phys.* 15 (1943), pp. 1–89. DOI: 10.1103/RevModPhys.15.1.

[52] J. Nolan. *Stable Distributions: Models for Heavy-Tailed Data*. Birkhauser Boston, 2007. ISBN: 9780817641597.

[53] A. V. Chechkin, V. Y. Gonchar, J. Klafter, and R. Metzler. “Fundamentals of Lévy flight processes”. In: *Advances in chemical physics* 133.B (2006), p. 439.

[54] J. Lahèrrere and D. Sornette. “Stretched exponential distributions in nature and economy: fat tails with characteristic scales”. In: *European Physical Journal B* 2 (1998), pp. 525–539. DOI: 10.1007/s100510050276.

Conclusions

The work presented in this thesis has as central topic the propagation of light in atomic and diffusive media. The link between the two experimental frameworks is provided by the response that a conveniently arranged material exhibits to an optical disturbance.

In the first part of this thesis the original work about the control of the propagation dynamics of optical pulses has been described.

We have developed an experimental apparatus that is able, by using a control optical pulse, to convert a rarefied hot sodium vapor in a passive or an active medium, depending on the atomic resonances involved in the interactions. Then we have studied the effects of the induced dispersion properties on the propagation of a probe pulse. Such a scheme, that has been used to produce both slow and fast light propagation, does not require temporal superposition between the two pulses or the exploitation of coherent effects, making the requirements for the realization of a propagation control less demanding. In a first experiment the control pulse frequency was resonant with the transition between the ground level and the $^2P_{3/2}$ level of sodium. The frequency of the probe pulse was quasi resonant with the transition between the latter level and the *D*-doublet of closely spaced resonances. Therefore, by varying the detuning of the probe pulse frequency, a large spectral region of a normal dispersive zone could be explored. In this case we have obtained a slow light regime, with group velocity significantly smaller than the speed of light in vacuum. We have demonstrated the possibility of controlling the induced delay and other features of the probe pulse by means of three optical parameters: the energy of the control pulse, the control-probe separation time at the entrance of the medium and the detuning of the probe central frequency from the transition resonance. Moreover, the experimental data are in good agreement with the analytic model that describes the process in term of the atomic parameters. Extra induced delays up to 13 ns and compression factors up to 3 have been achieved on pulses of 3 ns duration, without severe absorption, and the results has been reported in an article published in Physical Review A.

The same experimental scheme has been utilized, changing the involved atomic interactions, to achieve fast light propagation. In this case the control pulse excites, by a two photons transition, the D-doublet of sodium, creating a population inversion with the level $^2P_{3/2}$. The sub-sequent co-propagating probe pulse finds an inverted medium and experiences amplification and modification of group velocity, in a way dependent on the explored anomalous dispersion zones. The experimental results, in good agreement with numerical simulations based on atomic parameters and published in a paper in Physical Review A, show advances respect to the vacuum propagation up to 400 ps, without severe distortions. The temporal duration of the probe pulses is of some order smaller than other cases of fast light propagation reported in literature.

The two experiments described above suggested the idea to include, in the same experimen-

tal set-up, both propagation modes. Therefore, the probe pulse was previously delayed in a slow light stage and then such a delay was recovered in a fast light stage. Besides a complete recover of the delay, the second stage, by increasing the pump energy, is also able to induce an extra advance respect to the vacuum propagation. The arrival time of the pulse on the detector has been measured both when the slow light stage is switched on and when it is switched off: as a result we have observed that, increasing energy, the overall advance approaches a limit value that is independent on the history of the pulse before the entrance in the fast light stage. Then, as a remarkable effect, the probe pulse appears to move faster when it has been previously delayed. These results, reported in a paper in Optics Express, can open new perspectives in the field of optical data processing and communication via optical signals.

The topic of the second part of this thesis is the propagation of light through disordered media when gain is added. Such kind of optical systems, called random laser, exhibits a laser-like emission without the requirement of an optical cavity. The light is amplified along random paths inside the disordered active medium and, if the gain overcomes the losses, the output exhibits a narrowing of the spectrum but not a clear spatial directionality. Also in this case the work has been both experimental than theoretical.

In the experiment, the sample used to achieve random laser emission was Rhodamine 6G dye dissolved in methanol with added TiO_2 nanoparticles in order to create disorder. We have studied the spectral properties of the emission, and in particular the transition from the typical broad shape due to spontaneous emission at low pump energy, to the narrow shape caused by stimulated emission that becomes the leading process at higher energies, and found under which circumstances the random laser emission exhibits the peculiar features of fluctuations and presence of random spikes at random frequencies. The emission spectra have been described in terms of statistical regimes, labeled by the α-indexes that emerge from a Lévy-stable distribution fit of the spectral intensity histograms, for various experimental parameters and samples characteristics. The α-index values of the Lévy stable fit allowed the identification of two Gaussian regimes with smooth emission spectra: one at low pump energies, where the spontaneous emission is the leading process, and one at high energies, where stimulated emission dominates. On the contrary, random spikes occurs at the pumping energy range around the random laser threshold, i.e. if, for a certain amount of available energy and scattering level, the system dynamics is in the middle between regimes dominated by spontaneous or stimulated emission (Lévy regime).

A model based on a non-resonant feedback mechanism, where the extended modes are treated as possible paths inside the medium, has provided the framework for the interpretation of experimental data. Assuming a diffusive scattering regime, with a scattering mean free path much larger than the radiation wavelength, we have neglected wave interference effects and pictured the system as a medium where random walkers are created by spontaneous emission events and amplified by stimulated emission. Then, we have performed a numerical simulation based on such a model by parallel processing a large number of random walkers, that represent possible extended modes competing for the available gain. These modes share the available energy in the sample and the output emission spectrum becomes marked by such a gain competition. The results draw a scenario in which the random spikes are due to rare energetic modes that, under certain conditions, are uncoupled by the mode competition for the available gain, in such a way to experience a large amplification and get a large weight in the overall spectrum. Therefore, the gain uncoupling between modes in competition for the available energy stored

in the medium, has been detected as the key mechanism that can trigger the presence of random spikes at random frequencies in the output spectrum. The situation that occurs in samples with short scattering mean free paths, where the gain coupling leads to a complete inhibition of the Lévy regime is also discussed and observed both in numerical simulation and in experimental data. Then, the results, reported in a an article in Physical Review A (Highlighted Article), reveal a remarkable clear link between theory and experiment.

Moreover, a theoretical and experimental investigation about the possibility of controlling on certain degree the random laser emission is discussed as topic in preparation. The issue is how the statistical regime influences the directionality degree of the random laser emission, respect to the case of pure spontaneous emission. The directionality, both in experiment and in numerical simulation, shows a maximum when the system is in a Lévy regime, because of the correlation between the presence of random spikes in the spectrum and rare energetic extended modes that exhibit preferential paths due to an asymmetric active medium.

In conclusions, during this thesis work two topics concerning the light propagation through material systems have been investigated. In both cases the experimental data are in good agreement with the theoretical predictions. In the different realized experimental set-ups and measurement methods and strategies, the synchronization of signals generation and data acquisition have been able, besides an ad-hoc written software, to collect and analyze a large amount of data. Then the theoretical models have provided the basis for numerical simulations that have allowed a comparison between theory and experiment.

Finally, besides the topics under development, different intriguing perspectives can be recognized in both fields of propagation of optical signals and random lasers.

In the former, as a present field of research, an investigation (not discussed in this text) about the temporal response of the medium by varying the pulse temporal width is under development. Concerning the recovering of induced delays, fascinating perspectives arise in the framework of telecommunication; indeed, any transmission line is affected by unavoidable losses and one can suggest to add a fast light stage to the necessary amplification system in order to recover delays in propagation.

Concerning the random laser field, very interesting perspectives can be find in development of devices and optical sensors, useful in real-life purposes; indeed, albeit the random laser system has been studied since about almost decades, a clear practical application lacks to date. The principal basic idea is to realize a random laser based sensor, that, exploiting the sensitivity of an active device, could be able to detect small scale perturbations in intrinsically disordered systems, like, for instance, biological tissues.

Publications

[1] E. Ignesti, F. Tommasi, R. Buffa, L. Fini, E. Sali, M. V. Tognetti, and S. Cavalieri. "Incoherent optical control of pulse propagation and compression". In: *Phys. Rev. A* 86 (2012), p. 063818. DOI: 10.1103/PhysRevA.86.063818.

[2] E. Ignesti, F. Tommasi, R. Buffa, L. Fini, E. Sali, and S. Cavalieri. "Optical control of superluminal propagation of nanosecond laser pulses". In: *Phys. Rev. A* 87 (2013), p. 033828. DOI: 10.1103/PhysRevA.87.033828.

[3] E. Ignesti, F. Tommasi, L. Fini, S. Lepri, V. Radhalakshmi, D. Wiersma, and S. Cavalieri. "Experimental and theoretical investigation of statistical regimes in random laser emission". In: *Phys. Rev. A* 88 (2013), p. 033820. DOI: 10.1103/PhysRevA.88.033820.

[4] F. Tommasi, E. Ignesti, L. Fini, and S. Cavalieri. "Recovering the propagation delay of an optical pulse". In: *Opt. Express* 22.23 (2014), pp. 28566–28571. DOI: 10.1364/OE.22.028566.

Conferences

- Fotonica 2012 - Firenze (2012)
  E. Ignesti, F. Tommasi, E. Sali, M.V. Tognetti, L. Fini, S. Cavalieri
  Optical Control of Slow and Fast Light in Atomic Media
  ISBN:9788887237146

- XCVIII Congresso Nazionale Società Italiana di Fisica - Napoli (2012)
  E. Ignesti, F. Tommasi, R. Buffa, L. Fini, E. Sali, S. Cavalieri
  Control of slow and fast light by inchorent interaction in sodium vapour
  ISBN:9788874380732

- 11TH European Conference on Atoms, Molecules and Photons ECAMP - Aarhus (Denmark) (2013)
  F. Tommasi, E.Ignesti, L.Fini, S.Cavalieri
  Slow/Fast-Light Scheme for achieving propagation at "true" c-velocity for an optical pulse

- XCIX Congresso Nazionale Società Italiana di Fisica - Trieste (2013)
  F. Tommasi, E. Ignesti, L. Fini, S. Lepri, S. Cavalieri

Statistical regimes in random laser emission
ISBN:9788874380817

- FISMAT 2013 - Milano (2013)
F. Tommasi, E. Ignesti, L. Fini, S. Cavalieri
Recovering propagation delay of an optical pulse to achieve a "true" c-velocity

- LPHYS'14 - Sofia (Bulgaria) (2014)
F. Tommasi, E. Ignesti, L. Fini, S. Cavalieri
Recovering the delay acquired by a light pulse in propagation

Other conferences

- June 2011, Toronto (Canada): 2011 OSA OPTICS & PHOTONICS CONGRESS
Control of Slow and Fast Light by Incoherent Interactions in Atomic Schemes
Stefano Cavalieri, Emilio Ignesti, Marco Tognetti, Roberto Buffa, Lorenzo Fini, Emiliano Sali, Federico Tommasi.

- Conference of the European Group of Atomic System EGAS 46th - Lille (Francia) (2014)
F. Tommasi, E. Ignesti, L. Fini, S. Cavalieri
Vanishing the delay of a light pulse induced by propagation in matter
ISBN:9788887237146

Acknowledgements

I would like to thank my supervisor prof. Stefano Cavalieri, that supported my work in these three years of PhD course and helped me in developing all aspects of the theoretical and experimental studies.

I would like to thank Dr. Lorenzo Fini for his indispensable and precious contribute in realizing this work.

I would like to thank Dr. Emilio Ignesti, who has worked with me in the experimental set-up, giving a irreplaceable contribute in achieving the results.

I also would like to thank prof. Roberto Buffa, Dr. Emiliano Sali and Dr. Marco Valerio Tognetti for the contribute in the theoretical model discussed in Cap. II, Dr. Stefano Lepri and prof. Diederik Wiersma for the theoretical model discussed in Cap. V and Dr. Vivekananthan Radhalakshmi for the help in random laser samples making.

I would also thank prof. Jon Marangos and prof. Anna Vinattieri who read this thesis and contributed, with their suggestion, to improve the presentation of my work.

A thanks to my friends Dr. Sandro Gonzi, Dr. Alessio Gnerucci, Dr. Andrea Barucci, Dr. Valentina Quercioli, Dr. Filippo Pratesi, Dr. Gianluca Di Natale, Dr. Antonio Tropiano, Dr. Tommaso Brazzini, Dr. Paola Di Ninni, Dr. Anna Brucalassi, Carlo Bencini, Paolo Dottori, Emanuele e Francesco Benucci, Luca e Carlotta Innocenti, Massimiliano Benucci, Enrico Marioni, Gianluca Salvi, Gregorio Bartolucci, Filippo Gherardelli, Alessandro Lapi, Luca Poggesi, Daniele Giannelli, Claudio Nardi, Alessio Sorelli, Matteo Galigani, Monica Rubino, Francesco Ricci and the P.G.F. Libertas Judo. A thanks also to the PhD students Niccolò Caselli, Valentina Gori, Lucio Anderlini and Eduardo Grossi.

A special thanks is addressed to my family, my grandmother Santa Benucci, my parents Rosalba Orlandi and Marcello Tommasi, my sister Francesca Tommasi and her husband Stefano Buzzaffini, and to my girlfriend Camilla Marchiani.

Finally, I would like to dearly thank and remember my grandparents Orlando Orlandi, Marino Tommasi e Rita Bonini and my uncle father Vittorio Benucci.

Appendix A

Probability distribution of random laser emission

Let us consider an incoherent system in diffusive scattering regime, composed by an active medium of thickness L, and an extended mode that undergoes amplification due to stimulated emission during its lifetime [1]. Such an extended mode consists in a scattered path whose total length ℓ can be expressed as a random variable with exponential probability distribution:

$$p(\ell) = \frac{\exp\left[-\ell/\langle\ell\rangle\right]}{\langle\ell\rangle} \tag{A.1}$$

where $\langle\ell\rangle$ is the average distance traveled by the mode within the medium during its lifetime. Considering the mode as a path of a random walker and setting the absorbing condition to the boundaries 0 and L, in a diffusive process $\langle\ell\rangle$ can be estimated by the *mean first-passage time* [2]. The *first-passage probability* is the probability that a random walker at a specific time first reaches a site, for example the boundary of the medium. Let $c(x, t = 0)$ be the normalized initial random walker concentration:

$$\int_0^L c(x, 0)dx = 1 \tag{A.2}$$

In a generic time t, the concentration is solution of the diffusion equation:

$$\frac{\partial c(x,t)}{\partial t} = D\frac{\partial^2 c(x,t)}{\partial x^2} \tag{A.3}$$

Due to the diffusion process, once $c(x, t)$ spread becomes comparable to the size of the whole medium a rapid density decay occurs. Then the 'survival probability', i.e. the probability that at a time t the random walker is still inside the medium, is simply the following:

$$S(t) \equiv \int_0^L c(x, t)dx \tag{A.4}$$

Only the trajectories that do not reach the boundaries contribute to $S(t)$. In a similar way to the case discussed in Sec. (4.5.2), the solution of (A.3) can be written as the eigenfunction expansion:

$$c(x, t) = \sum_{n=1}^{\infty} a_n \sin\left(\frac{n\pi x}{L}\right) e^{-(\frac{n\pi}{L})^2 Dt} \tag{A.5}$$

Hence each eigenmode decays exponentially in time with a characteristic time that depends on n:

$$\tau_n = \frac{L^2}{n^2\pi^2 D} \tag{A.6}$$

Because the modes of large order decay more rapidly with time, for longs t only the $n = 1$-mode becomes not negligible and determines the asymptotic behavior of the survival probability:

$$S(t) \propto e^{-t/\tau_1} \tag{A.7}$$

where

$$\tau_1 = \frac{L^2}{D\pi^2} \tag{A.8}$$

Hence $\tau_1 = L^2/D\pi^2$ characterizes the diffusive dynamics of a mode within a medium with absorbing boundaries.

Coming back to the estimation of $\langle \ell \rangle$, indicating with v the speed of the photons and with the help of (A.9):

$$\langle \ell \rangle = v\tau_1 = \frac{vL^2}{D\pi^2} \tag{A.9}$$

Since the mode, that carries an initial intensity I_0, propagates within an active medium, during its lifetime it experiences an exponential amplification (see eq. (IV.15)) for each step ℓ:

$$I(\ell) = I_0 e^{\ell/\ell_g} \tag{A.10}$$

By combining of the (A.1), (A.9) and (A.10), the probability distribution of the emitted intensity can be derived:

$$p(I) = \bar{\alpha}\frac{1}{I^{(1+\bar{\alpha})}} \tag{A.11}$$

where

$$\bar{\alpha} = \frac{\ell_g}{\langle \ell \rangle} = \frac{\ell_g D\pi^2}{vL^2} \tag{A.12}$$

[1] S. Lepri, S. Cavalieri, G. L. Oppo, D. S. Wiersma, “Statistical regimes of random laser fluctuations ”. In: *Phys. Rev. A* 75, 063820 (2007), doi10.1103/PhysRevA.75.063820

[2] S. Redner, *A Guide to First-Passage Processes*, Cambridge University Press (2001)

Index